

**BIOLOGICAL NITRIFICATION-DENITRIFICATION AND
SULFATE REDUCTION OF REVERSE OSMOSIS
BRINE REJECTS**

by

Ilknur Ersever

A Dissertation Presented to the
FACULTY OF THE GRADUATE SCHOOL
UNIVERSITY OF SOUTHERN CALIFORNIA
In Partial Fulfillment of the
Requirements for the Degree
DOCTOR OF PHILOSOPHY
ENGINEERING (ENVIRONMENTAL ENGINEERING)

May 2003

Copyright 2003

Ilknur Ersever

UMI Number: 3103884

UMI[®]

UMI Microform 3103884

Copyright 2003 by ProQuest Information and Learning Company.

All rights reserved. This microform edition is protected against
unauthorized copying under Title 17, United States Code.

ProQuest Information and Learning Company
300 North Zeeb Road
P.O. Box 1346
Ann Arbor, MI 48106-1346

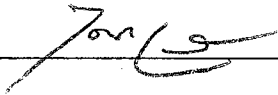
UNIVERSITY OF SOUTHERN CALIFORNIA
THE GRADUATE SCHOOL
UNIVERSITY PARK
LOS ANGELES, CALIFORNIA 90089-1695

This dissertation, written by

Ilknur Ersever

*under the direction of his dissertation committee, and
approved by all its members, has been presented to and
accepted by the Director of Graduate and Professional
Programs, in partial fulfillment of the requirements for the
degree of*

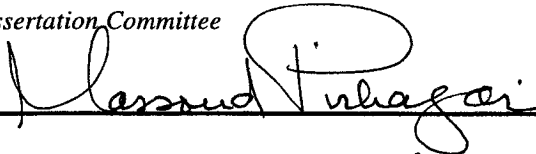
DOCTOR OF PHILOSOPHY



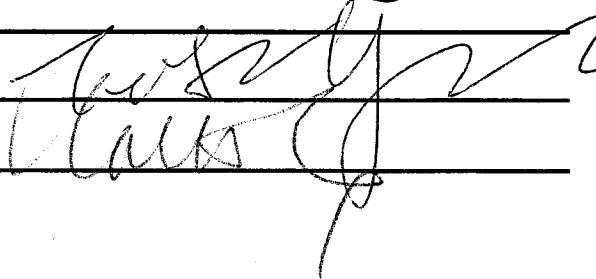
Director

Date May 16, 2003

Dissertation Committee



Chair



DEDICATION

I would like to dedicate this dissertation to my mother, Inci, who lives half the world away, and whose encouragement and sacrifice was instrumental in completing this challenging task. I would also like to dedicate this disseration to environmental engineers and scientists all over the world who work hard to make this planet a healthy place to live in.

ACKNOWLEDGEMENTS

I received assistance from many people in conducting this research and preparation of this dissertation. I gratefully acknowledge my advisor, Professor Massoud Pirbazari, for his invaluable support, direction and encouragement during the course of this study. I will never forget his support when I became ill and my work suffered due to long ailment period, as not so many people would have shown the immense patience he showed me. I would like to thank my dissertation committee members Professor Teh Fu Yen and Professor Katherine Shing for their constructive comments.

My special credit is also due to Dr. Varadarajan Ravindran, my colleague, who made professional suggestions and to Jeff Tsai who dedicated his precious time to help me on the modeling portion of this research.

This research was a collaborative effort between the Civil and Environmental Engineering Department at the University of Southern California and the Orange County Water District (OCWD), Fountain Valley, CA. My sincere thanks should especially go to Dr. Greg Leslie from OCWD for his kind heart, generosity and enthusiasm in this research. I also appreciate the assistance of Mehul Patel and Shivaji Deshmukh, both engineers at OCWD, in conducting the laboratory- and pilot-scale experiments. They all kindly undertook my duty and kept the experiments running when I could not make it there. I am also indebted to the personnel at the Water Factory-21. Tom McCormack shared his practical knowledge and gave me

advice and ideas on experimental setups, Betsy Martin maintained the the reverse osmosis unit running, the maintenance personnel provided assistance in instrumentation for the pilot units, and finally the laboratory personnel dedicated their time to help me use the laboratory instruments and run the analyses.

I would like to express my deepest gratitude to the Turkish Ministry of Education for providing the scholarship that I needed to come to the United States and finish my graduate studies. Without this scholarship, this graduate study and dissertation could never have been even initiated.

I also would like to thank my company, CH2M HILL, for giving me the time and opportunity that I needed to complete this dissertation, even though I was a new employee and the projects were pouring in.

Finally, my heartfelt love and respect should go to my family, for their emotional support and encouragement in this long journey of academic success. They have always believed in me and made me believe in myself and my abilities.

TABLE OF CONTENTS

	Page
DEDICATION	ii
ACKNOWLEDGEMENTS	iii
LIST OF TABLES	xi
LIST OF FIGURES	xvi
NOMENCLATURE	xxi
ACRONYMS	xxvi
ABSTRACT	xxvii
CHAPTER 1 INTRODUCTION AND STATEMENT OF THE PROBLEM	
1.1 Overall Review of Water Recycling	1
1.1.1 Need for Water Recycling	1
1.1.2 Laws and Regulations	4
1.1.3 Advanced Treatment Technologies in Water Recycling	5
1.2 Residue Management in Membrane Processes: Reverse Osmosis Brine Rejects	8
1.2.1 Generation of Brine Rejects and Current Disposal Practices	8
1.2.2 Regulatory Aspects Pertaining to Brine Rejects	10
1.2.3 Characteristics of Brine Rejects and Associated Health and Environmental Concerns	12
1.2.4 Other Sources of High Salt Brines	17
1.3 Statement of the Problem: Necessity for the Treatment of Brine Rejects	18
1.4 Rationale for This Research	20
CHAPTER 2 RESEARCH OBJECTIVES AND SCOPE	
2.1 Research Objectives	23
2.2 Research Scope	26
CHAPTER 3 THEORY AND PRINCIPLES OF BIOLOGICAL PROCESSES	
3.1 Theory and Principles of Biological Nitrification Process	28
3.1.1 Theory of Nitrification	28

3.1.2	Effects of Various Environmental Factors on Nitrification	30
3.1.3	Limitations of Nitrification as a Biological Process	32
3.1.4	Enhancing Nitrification Process with Powdered Activated Carbon	36
3.2	Theory and Principles of Biological Denitrification Process	39
3.2.1	Theory of Denitrification	39
3.2.2	Environmental Parameters Influencing Denitrification	43
3.2.2.1	Effect of Temperature	43
3.2.2.2	Effect of pH	46
3.2.2.3	Effect of Different Carbon Sources and Carbon-to-Nitrogen Ratios	48
3.2.2.4	Effect of Total Dissolved Solids	52
3.2.3	Biokinetic Modeling of Denitrification Process	54
3.2.3.1	Assumptions and Formulation of the Biokinetic Model	56
3.2.4	Nitrite Accumulation	61
3.3	Biological Sulfate Reduction Process	63
3.3.1	Theory and Principles of Sulfate Reduction	63
3.3.2	Factors Influencing Sulfate Reduction	65
3.3.3	Effect of Sulfate Loading and Hydraulic Retention Time	70
3.3.4	Simultaneous Nitrate and Sulfate Reduction in the Same Reactor	72
3.3.5	Coupling Sulfate Reduction with Metal Removal	74
3.4	Removal of Hydrogen Sulfide Gas Using Biofiltration Process	77
3.4.1	Definition and Principles of Biofilters	77
3.4.2	Importance of Moisture Content, Nutrient and pH Control	79
3.4.3	Hydrogen Sulfide Removal Using Biofilters	81

CHAPTER 4 PRINCIPLES AND MODELING OF FLUIDIZED BIOADSORBER REACTORS FOR BIOLOGICAL DENITRIFICATION PROCESS

4.1	Theory and Advantages of Fluidized Bioreactors	84
4.2	Design Criteria and Operational Dynamics of Fluidized Bioreactors	88
4.2.1	General Design Criteria for Fluidized Bioreactors	89
4.2.1.1	Support Medium Characteristics	89
4.2.1.2	Correlation Between Substrate Loading and Biomass Concentration	89
4.2.1.3	Correlation Between Biofilm Density, Biofilm Thickness and Media Bed Expansion	90

4.2.1.4	Correlation Between Biofilm Thickness and Superficial Velocity	92
4.2.2	Operations Dynamics and Correlation Techniques for Fluidized Bioreactors	93
4.3	Different Approaches of Biofilm Modeling and Dynamic Fluidized Bioreactors Modeling	94
4.3.1	Biofilm Modeling Approach with GAC as the Support Medium	94
4.3.1.1	Advantages of using GAC as the Support Medium for Biofilms	94
4.3.1.2	A Historical Perspective of Biofilm Modeling with GAC	96
4.3.2	Biofilm Modeling Approach of Denitrification Process for Fluidized Bioreactors with Different Support Media	98
4.4	Modeling of FBAR with GAC for Biological Denitrification Process	100
4.4.1	Significance of Modeling Approach	100
4.4.2	Model Milieu and Assumptions	101
4.4.3	Formulation of FBAR Denitrification Process with Recycle	103
4.4.3.1	Liquid Phase Material Balance	104
4.4.3.2	Diffusion and Reaction in Biofilm	108
4.4.3.3	Growth of Biofilm	109
4.4.3.4	Suspended Biomass in Bulk Liquid Solution	110
4.4.4	Non-Dimensionalization and Numerical Solution to the Model	111
4.5	Model Parameters Estimations	112
4.5.1	Biofilm Parameter Estimation	112
4.5.2	Substrate Mass Transfer Coefficient and Free Liquid Diffusivity Estimation	114
4.5.3	Biofilm Diffusion Coefficient Estimation	115
4.5.4	Axial Substrate Dispersion Coefficient Estimation	116
4.6	Protocol for Biological FBAR Modeling and Design	117
CHAPTER 5 MATERIALS AND METHODS		
5.1	Materials	121
5.1.1	Source of Brine Reject	121
5.1.2	Characteristics of Support Media	122
5.1.3	Sources of Microbial Cultures	122
5.1.4	Chemicals	123
5.2	Experimental Methods	124
5.2.1	Nitrification Studies	124
5.2.1.1	Fluidized Bioreactor for Nitrification Process	125

5.2.1.2	Rotating Biological Contactors for Nitrification Process	128
5.2.2	Batch Denitrification Studies for Environmental Parameter Optimization	132
5.2.3	Continuous Flow Chemostat Studies for Biokinetic Parameter Determination	135
5.2.4	FBAR Denitrification Studies with GAC or Sand	137
5.2.5	Simultaneous Nitrate and Sulfate Reduction Studies	141
5.2.6	Biofiltration Column Studies	142
5.3	Analytical Methods	144
5.3.1	Analysis of Ammonia	144
5.3.2	Analysis of Anions	145
5.3.3	Analysis of Total Organic Carbon	146
5.3.4	Analysis of Ethanol	146
5.3.5	Analysis of Organic Nitrogen	147
5.3.6	Analysis of Total Dissolved Solids	147
5.3.7	Analysis of Total Alkalinity	148
5.3.8	Analysis of Hydrogen Sulfide	148
5.3.9	Analysis of Metals	149
5.3.10	Biomass Assay	150
5.3.11	Scanning Electron Microscopy	151
 CHAPTER 6 NITRIFICATION OPTIMIZATION STUDIES WITH FLUIDIZED BIOREACTOR AND ROTATING BIOLOGICAL CONTACTORS		
6.1	Results and Discussions	153
6.1.1	Nitrification Optimization Studies with Fluidized Bioreactor	153
6.1.2	Nitrification Optimization Studies with Rotating Biological Contactors	156
6.2	Summary and Conclusions	159
 CHAPTER 7 BATCH BIOKINETIC STUDIES: ENVIRONMENTAL PARAMETER OPTIMIZATION FOR DENITRIFICATION PROCESS		
7.1	Results and Discussions	161
7.1.1	Batch Studies for Environmental Optimization of Denitrification Process	161
7.1.1.1	Effect of Temperature	162
7.1.1.2	Effect of pH	170
7.1.1.3	Optimum Carbon-to-Nitrogen Ratio	173
7.1.1.4	Effect of Total Dissolved Solids	176
7.2	Summary and Conclusions	179

CHAPTER 8 CONTINUOUS FLOW CHEMOSTAT STUDIES: BIOKINETIC PARAMETERS DETERMINATION

8.1	Results and Discussions	181
8.1.1	Nitrogen-Limiting Chemostat Studies	183
8.1.1.1	Nitrite-Limiting Chemostat	183
8.1.1.2	Nitrate-Limiting Chemostat	186
8.1.1.3	Comparison of Nitrite- and Nitrate- Limiting Chemostats	189
8.1.2	Ethanol-Limiting Chemostat Studies	191
8.1.2.1	Ethanol-Limiting Chemostat with Nitrite in Excess	191
8.1.2.2	Ethanol-Limiting Chemostat with Nitrate in Excess	194
8.1.2.3	Comparison of Ethanol- and Nitrogen- Limiting Chemostats	197
8.2	Summary and Conclusions	200

CHAPTER 9 FLUIDIZED BIOADSORBER REACTOR DENITRIFICATION STUDIES: MODEL PREDICTION, SIMULATION AND VERIFICATION

9.1	Results and Discussions	202
9.1.1	Experimental Results of FBAR Denitrification Studies with GAC	202
9.1.1.1	Evaluation and Comparison of Experimental Results	202
9.1.1.2	Evaluation of FBAR Operational Parameters	209
9.1.2	Experimental Results of FBAR Denitrification Studies with Sand	215
9.1.3	Prediction/Simulation of the FBAR Denitrification Model	220
9.1.3.1	Results of Model Parameter Estimation Studies	220
9.1.3.2	Model Prediction, Verification and Sensitivity Analyses	222
9.1.3.2.1	Predictive Capability of the FBAR Model	222
9.1.3.2.2	Model Sensitivity Analyses	232
9.2	Summary and Conclusions	237

CHAPTER 10 FBAR PROCESS FOR SULFATE REDUCTION FOLLOWED BY BIOFILTRATION

10.1	Results and Discussions	239
------	-------------------------	-----

10.1.1	FBAR Process for Simultaneous Denitrification and Sulfate Reduction	239
10.1.2	FBAR Process for Sulfate Reduction Alone	245
10.1.3	Sulfate Reduction and Metal Removal in FBAR	247
10.1.4	Biofiltration for the Removal of Hydrogen Sulfide Gas	250
10.2	Summary and Conclusions	252
CHAPTER 11 GRAND SUMMARY, CONCLUSIONS AND RECOMMENDATIONS FOR FUTURE RESEARCH		
11.1	Grand Summary and Conclusions	254
11.1.1	Optimization of Biological Nitrification Process	254
11.1.2	Batch Denitrification Studies	256
11.1.3	Continuous Flow Chemostat Studies	257
11.1.4	FBAR Denitrification Studies	258
11.1.5	FBAR Modeling	259
11.1.6	FBAR Sulfate Reduction Studies	259
11.1.7	FBAR Metal Removal	260
11.1.8	Biofiltration Study	261
11.2	Cost-Benefit Analysis	262
11.3	Future Research Recommendations	263
REFERENCES		265
APPENDICES		283
A	Experimental Data for Batch Studies	284
B	Experimental Data for Continuous Flow Chemostat Studies	289
C	Experimental Data for Fluidized Bioadsorber Reactor Studies	294
D	Experimental Data for FBAR Studies with Sand	308
E	Experimental Data for Sulfate Reduction Studies	311
F	FBAR Biofilm Model Simulation Data	314
G	FBAR Biofilm Model Sensitivity Analyses Data	323

LIST OF TABLES

	Page
Table 1.1. Characteristics of reverse osmosis brine reject	14
Table 5.1. Constituents and their approximate concentrations of synthetically prepared nitrified brine	136
Table 6.1. Average characteristics of nitrified brine reject effluent from RBC-PAC system	159
Table 7.1. Experimental matrix used in batch studies	162
Table 8.1. Summary of biokinetic parameters and net biomass production rates obtained from nitrogen- and ethanol-limiting chemostat studies	199
Table 8.2. Biokinetic parameters to be used in FBAR studies	200
Table 9.1. Experimental matrix for the mini pilot-scale FBAR studies with GAC (T = 30°C and pH = 7.5 for all experiments)	204
Table 9.2. Average characteristics of denitrified brine reject effluent from FBAR experiments with GAC	209
Table 9.3. Experimental matrix and biomass density for the mini pilot-scale FBAR studies with GAC (T = 30°C and pH = 7.5 for all experiments)	212
Table 9.4. Experimental matrix for the mini pilot-scale FBAR studies with sand (T = 30°C and pH = 7.5 for all experiments)	215
Table 9.5. Average characteristics of influent and effluent denitrified brine reject from FBAR experiments with sand	219

Table 9.6.	Operational parameters used in the proposed FBAR denitrification model	221
Table 10.1.	Biological oxidation-reduction reactions, their potentials and Gibbs free energies (pH = 7 and Temperature = 25°C)	243
Table 10.2.	Characteristics of brine reject effluent at steady state after denitrification in the first FBAR and after complete sulfate reduction in the second FBAR	248
Table A.1.	Data obtained from batch experiments at various temperatures (pH = 7.5, Ethanol = Excess, TDS = 4,000 mg/l)	285
Table A.2.	Data obtained from batch experiments at various pH values (Temperature = 30°C, Ethanol = Excess, TDS = 4,000 mg/l)	286
Table A.3.	Data obtained from batch experiments at various C:N ratios (Temperature = 30°C, pH = 7.5, TDS = 4,000 mg/l)	287
Table A.4.	Data obtained from batch experiments at various TDS concentrations (Temperature = 30°C, pH = 7.5, C:N = Excess)	288
Table B.1.	Data obtained from the nitrite-limited chemostat at 30°C and pH 7.5 (Initial concentrations: Nitrite = 119.3 mg N/l, Nitrate = 0 mg N/l, Ethanol = 550 mg/l)	290
Table B.2.	Data of nitrate-limited chemostat at 30°C and pH 7.5 (Initial concentrations: Nitrate = 75.2 mg N/l, Ethanol = 650 mg/l)	291
Table B.3.	Data of ethanol-limited (nitrite in excess) chemostat at 30°C and pH 7.5 (Initial concentrations: Nitrite = 121.7 mg N/l, Nitrate = 0 mg N/l, Ethanol = 325 mg/l)	292
Table B.4.	Data of ethanol-limited (nitrate in excess) chemostat at 30°C and pH 7.5 (Initial concentrations: Nitrate = 79 mg N/l, Ethanol = 280 mg/l)	293

Table C.1.	Data for FBAR denitrification experiment no 1 (Steady State Biofilm Density = 288 mg AVS/g GAC)	295
Table C.2.	Data for FBAR denitrification experiment no 2 (Steady State Biofilm Density = 227 mg AVS/g GAC)	296
Table C.3.	Data for FBAR denitrification experiment no 3 (Steady State Biofilm Density = 205 mg AVS/g GAC)	297
Table C.4.	Data for FBAR denitrification experiment no 4 (Steady State Biofilm Density = 234 mg AVS/g GAC)	298
Table C.5.	Data for FBAR denitrification experiment no 5 (Steady State Biofilm Density = 206 mg AVS/g GAC)	299
Table C.6.	Data for FBAR denitrification experiment no 6 (Steady State Biofilm Density = 163 mg AVS/g GAC)	300
Table C.7.	Data for FBAR denitrification experiment no 7 (Steady State Biofilm Density = 428 mg AVS/g GAC)	301
Table C.8.	Data for FBAR denitrification experiment no 8 (Steady State Biofilm Density = 625 mg AVS/g GAC)	302
Table C.9.	Data for FBAR denitrification experiment no 9 (Steady State Biofilm Density = 389 mg AVS/g GAC)	303
Table C.10.	Data for FBAR denitrification experiment no 10 (Steady State Biofilm Density = 217 mg AVS/g GAC)	304
Table C.11.	Data for FBAR denitrification experiment no 11 (Steady State Biofilm Density = 252 mg AVS/g GAC)	305
Table C.12.	Data for FBAR denitrification experiment no 12 (Steady State Biofilm Density = 148 mg AVS/g GAC)	306
Table C.13.	Data for FBAR denitrification experiment no 13 (Steady State Biofilm Density = 195 mg AVS/g GAC)	307
Table D.1.	Data for FBAR denitrification experiment with 300 g sand (Steady State Biofilm Density = 166 mg AVS/g GAC)	309

Table D.2.	Data for FBAR denitrification experiment with 150 g sand (Steady State Biofilm Density = 93 mg AVS/g GAC)	310
Table E.1.	Data for FBAR simultaneous nitrate and sulfate reduction experiment	312
Table E.2.	Data for (second) FBAR sulfate reduction experiment	313
Table F.1.	Model prediction data for FBAR denitrification experiment no 1	315
Table F.2.	Model prediction data for FBAR denitrification experiment no 2	316
Table F.3.	Model prediction data for FBAR denitrification experiment no 3	317
Table F.4.	Model prediction data for FBAR denitrification experiment no 4	318
Table F.5.	Model prediction data for FBAR denitrification experiment no 5	319
Table F.6.	Model prediction data for FBAR denitrification experiment no 6	320
Table F.7.	Model prediction data for FBAR denitrification experiment no 7	321
Table F.8.	Model prediction data for FBAR denitrification experiment no 8	322
Table G.1.	Model sensitivity analysis data for influent nitrate concentration	324
Table G.2.	Model sensitivity analysis data for biofilm thickness	329
Table G.3.	Model sensitivity analysis data for growth yield coefficient	334
Table G.4.	Model sensitivity analysis data for maximum specific growth rate	339

Table G.5.	Model sensitivity analysis data for Monod half saturation constant
------------	--

344

LIST OF FIGURES

	Page
Figure 1.1. Schematic representation of osmosis and reverse osmosis processes	7
Figure 4.1. General schematic of a fluidized bioreactor treatment system	85
Figure 4.2. Mathematical model formulation for the FBAR denitrification process	105
Figure 4.3. Schematic representation of a single bioparticle in FBAR model conceptualization	106
Figure 4.4. Protocol for modeling and design of FBAR process for biological denitrification	119
Figure 5.1. Schematic representation of laboratory-scale fluidized bioreactor used for nitrification process	126
Figure 5.2. Photograph of the fluidized bioreactor used in nitrification studies	127
Figure 5.3. Pilot-scale rotating biological contactor unit used for nitrification process	129
Figure 5.4. Photograph of the RBC unit and the rotating disks used in nitrification studies	130
Figure 5.5. Schematic of the fermentor used for batch and continuous flow chemostat studies	133
Figure 5.6. Photograph of the fermentor employed in batch and continuous flow chemostat studies	134
Figure 5.7. Experimental schematic of the mini pilot-scale FBAR denitrification system	138
Figure 5.8. Photograph of the mini pilot-scale FBAR	139

Figure 5.9.	Photograph of the biofiltration unit	143
Figure 7.1.	Variations of nitrate-nitrogen, nitrite-nitrogen and biomass concentration in the batch experiment at 30°C temperature	163
Figure 7.2.	Specific denitrification rates at different temperatures	164
Figure 7.3.	Natural logarithms of specific denitrification rates with respect to temperatures between 10°C and 35°C at which the linearity could be established (correlation coefficient = 0.979)	167
Figure 7.4.	Arrhenius plot at the temperatures at which linearity with respect to specific denitrification rates were established (correlation coefficient = 0.984)	169
Figure 7.5.	Experimental and theoretical specific denitrification rates at different pH values	171
Figure 7.6.	Variations of nitrate-nitrogen, nitrite-nitrogen and biomass concentrations in batch experiment with C:N ratio of 1.8:1	174
Figure 7.7.	Change in specific denitrification rates with respect to different C:N ratios	175
Figure 7.8.	Variations of nitrate-nitrogen, nitrite-nitrogen and biomass concentrations in batch experiment with 8,000 mg/l TDS concentration	177
Figure 7.9.	Change in specific denitrification rates as a function of TDS concentrations	178
Figure 8.1.	Variations in nitrite, ethanol and biomass concentration profiles with respect to time in nitrite-limiting chemostat (Initial concentrations: Nitrite = 119.3 mg N/l, Nitrate = 0 mg N/l, Ethanol = 550 mg/l)	184
Figure 8.2.	Relationship between specific denitrification rate and maximum specific growth rate with respect to nitrite and ethanol utilization in nitrite-limiting chemostat	185

Figure 8.3.	Lineweaver-Burke plot to determine the Monod biokinetic constants for nitrite-limiting chemostat according to equation (3.14)	186
Figure 8.4.	Variations in nitrate, nitrite, ethanol and biomass concentration profiles in nitrate-limiting chemostat (Initial concentrations: Nitrate = 75.3 mg N/l, Nitrite = 0 mg N/l, Ethanol = 650 mg/l)	187
Figure 8.5.	Relationship between specific denitrification rate and maximum specific growth rate with respect to nitrate and ethanol utilization in nitrate-limiting chemostat	188
Figure 8.6.	Lineweaver-Burke plot of the data obtained from nitrate-limiting chemostat to determine the Monod biokinetic constants according to equation (3.17); Overall, the maximum specific growth rate for this chemostat ($\mu_{m,a}$) is equal to the sum of maximum specific growth rates for nitrite- and nitrate-limiting chemostats, which is 1.35 hr^{-1}	189
Figure 8.7.	Variations in nitrite, ethanol and biomass concentration profiles in ethanol-limiting (nitrite in excess) chemostat (Initial concentrations: Nitrite = 121.7 mg N/l, Nitrate = 0 mg N/l, Ethanol = 325 mg/l)	192
Figure 8.8.	Relationship between specific denitrification rate and maximum specific growth rate with respect to nitrite and ethanol utilization in ethanol-limiting (nitrite excess) chemostat	193
Figure 8.9.	Lineweaver-Burke plot for to determine the Monod biokinetic constants for ethanol-limiting (nitrite excess) chemostat	194
Figure 8.10.	Variations in nitrate, nitrite, ethanol and biomass concentration profiles in ethanol-limiting (nitrate excess) chemostat (Initial concentrations: Nitrate = 79 mg N/l, Nitrite = 0 mg N/l, Ethanol = 280 mg/l)	195

Figure 8.11.	Relationship between specific denitrification rate and maximum specific growth rate with respect to nitrate and ethanol utilization in ethanol-limiting (nitrate excess) chemostat	196
Figure 8.12.	Lineweaver-Burke plot of the data to determine the Monod biokinetic constants obtained from ethanol-limiting (nitrate excess) chemostat	197
Figure 9.1.	Effect of GAC quantities on the FBAR denitrification efficiency (Temperature = 30°C, pH = 7.5 and C:N = 1.8:1)	205
Figure 9.2.	Effect of hydraulic retention time on the FBAR denitrification efficiency (Temperature = 30°C, pH = 7.5 and C:N = 1.8:1)	206
Figure 9.3.	Effect of influent nitrate concentration on the FBAR denitrification efficiency (Temperature = 30°C, pH = 7.5 and C:N = 1.8:1)	208
Figure 9.4.	Micrograph of a biofilm at the final stages of growth	214
Figure 9.5.	Comparison of FBAR denitrification profile with 150 g of sand and GAC (Temperature = 30°C, pH = 7.5 and C:N = 1.8:1)	216
Figure 9.6.	Comparison of FBAR denitrification profile with 300 g of sand and GAC (Temperature = 30°C, pH = 7.5 and C:N = 1.8:1)	217
Figure 9.7.	Experimental data and predicted profile for the FBAR with GAC = 300 g, HRT = 60 min and Nitrate = 362 mg/l	223
Figure 9.8.	Experimental data and predicted profile for the FBAR with GAC = 300 g, HRT = 120 min and Nitrate = 287 mg/l	224
Figure 9.9.	Experimental data and predicted profile for the FBAR with GAC = 300 g, HRT = 180 min and Nitrate = 386 mg/l	225
Figure 9.10.	Experimental data and predicted profile for the FBAR with GAC = 150 g, HRT = 60 min and Nitrate = 416 mg/l	226

Figure 9.11.	Experimental data and predicted profile for the FBAR with GAC = 150 g, HRT = 120 min and Nitrate = 396 mg/l	227
Figure 9.12.	Experimental data and predicted profile for the FBAR with GAC= 150 g, HRT = 180 min and Nitrate = 396 mg/l	228
Figure 9.13.	Experimental data and predicted profile for the FBAR with GAC = 150 g, HRT = 90 min and Nitrate = 1,368 mg/l	229
Figure 9.14.	Experimental data and predicted profile for the FBAR with GAC = 150 g, HRT = 60 min and Nitrate = 1,000 mg/l	230
Figure 9.15.	Experimental data and predicted profile for the FBAR with GAC = 300 g, HRT = 90 min and Nitrate = 1,400 mg/l	231
Figure 9.16.	Sensitivity analysis for changes in influent nitrate concentration	233
Figure 9.17.	Sensitivity analysis for changes in biofilm density	234
Figure 9.18.	Sensitivity analysis for changes in growth yield coefficient	235
Figure 9.19.	Sensitivity analysis for changes in maximum specific growth rate	236
Figure 9.20.	Sensitivity analysis for changes in Monod half saturation constant	237
Figure 10.1.	Simultaneous nitrate and sulfate reduction in the first FBAR	241
Figure 10.2.	Sulfate reduction profile in the second FBAR unit	246

NOMENCLATURE

a_p	total surface area available for mass transfer on GAC particle (L^2)
A	Arrhenius constant (dimensionless)
B_w	cell weight (M_x)
d	bioadsorber reactor diameter (L)
d_p	GAC particle diameter (L)
D	dilution rate (1/T)
D_x	axial (hydrodynamic) substrate dispersion coefficient (L^2/T)
D_f	biofilm substrate diffusion coefficient (L^2/T)
D_l	molecular liquid diffusivity (L^2/T)
E_a	activation energy (cal.g/mol)
g	gravitational acceleration (L^2/T)
Ga	Galileo number (dimensionless)
I	inhibition concentration (M/L^3)
k	temperature constant ($^{\circ}K^{-1}$)
$k_{d,a}$	endogenous decay coefficient for nitrate-limiting chemostat (1/T)
$k_{d,b}$	endogenous decay coefficient for nitrite-limiting chemostat (1/T)
k_i	constant (dimensionless)
k_{fc}	substrate mass transfer coefficient (L/T)
K_s	half saturation constant (M/L^3)
$K_{s,a}$	half saturation constant for nitrate reduction (M/L^3)

$K_{s,a}$	half saturation constant for nitrate reduction in ethanol-limiting chemostat (M/L^3)
$K_{s,b}$	half saturation constant for nitrite reduction (M/L^3)
$K_{s,b'}$	half saturation constant for nitrite reduction in ethanol-limiting chemostat (M/L^3)
L	length of FBAR (L)
L_f	biofilm thickness at any time (L)
$L_{f,0}$	initial biofilm thickness (L)
$L_{f,max}$	maximum biofilm thickness (L)
N	bulk substrate concentration at any time (M/L^3)
N_0	initial substrate concentration (M/L^3)
N_a	nitrate concentration (M/L^3)
N_b	nitrite concentration (M/L^3)
N_e	effluent substrate concentration (M/L^3)
N_f	biofilm substrate concentration (M/L^3)
$N_{f,0}$	initial biofilm substrate concentration (M/L^3)
$N_{f,s}$	substrate concentration at bulk liquid-biofilm interface (M/L^3)
N_s	substrate concentration at biofilm-adsorbent interface (M/L^3)
P_n	number of GAC particles (dimensionless)
Q	fluid flowrate (L^3/T)
Q_a	temperature quotient (dimensionless)
Q_r	recycle flowrate (L^3/T)
r	carbon particle radius

r_f	radial direction normal to surface of the biofilm (L)
R	universal gas constant (cal.g [°] K.mol)
Re	Reynolds number (dimensionless)
Re_{mdf}	modified Reynolds number (dimensionless)
Sc	Schmidt number (dimensionless)
Sh	Sherwood number (dimensionless)
SDR_{max}	specific denitrification rate (M/M.T)
SDR_T	specific denitrification rate at any temperature (M/M.T)
SDR_{20}	specific denitrification rate at 20°C (M/M.T)
t	time (T)
t_{max}	time at which biofilm thickness is maximum (T)
T	Temperature (°K)
v_s	superficial fluid velocity (L/T)
v_x	interstitial fluid velocity (L/T)
ΔV	volume of bed expansion due to growth of biomass (L ³)
W	total dry weight of activated carbon in the reactor (M)
W_{ev}	weight of evaporated water (M)
x	axial coordinate (L)
X	biomass concentration in chemostat (M _x /L ³)
X_o	influent biomass concentration (M _x /L ³)
X_f	biomass density (M _x /L ³)
X_l	biomass concentration in bulk liquid phase (M _x /L ³)

$X_{i,o}$	initial biomass concentration in bulk liquid phase (M_x/L^3)
$X_{l,f}$	biomass concentration lost from biofilm to bulk liquid phase (M_x/L^3)
Y	growth yield coefficient (M_x/M_s)
Y_a	growth yield coefficient for biomass consuming nitrate (M_x/M_s)
$Y_{a,N}$	growth yield coefficient with respect to nitrate utilization in nitrate-limiting chemostat (M_x/M_s)
$Y_{a,N'}$	growth yield coefficient with respect to nitrate utilization in nitrate-limiting chemostat (M_x/M_s)
$Y_{a,E}$	growth yield coefficient with respect to ethanol utilization in nitrate-limiting chemostat (M_x/M_s)
$Y_{a,E'}$	growth yield coefficient with respect to ethanol utilization in nitrate-limiting chemostat (M_x/M_s)
Y_b	growth yield coefficient for biomass consuming nitrite (M_x/M_s)
$Y_{b,N}$	growth yield coefficient with respect to nitrite utilization in nitrite-limiting chemostat (M_x/M_s)
$Y_{b,N'}$	growth yield coefficient with respect to nitrite utilization in nitrite-limiting chemostat (M_x/M_s)
$Y_{b,E}$	growth yield coefficient with respect to ethanol utilization in nitrite-limiting chemostat (M_x/M_s)
$Y_{b,E'}$	growth yield coefficient with respect to ethanol utilization in nitrite-limiting chemostat (M_x/M_s)
ε	bed porosity (dimensionless)
ε°	potential
μ	specific growth rate ($1/T$)
μ_m	maximum specific growth rate ($1/T$)

$\mu_{m,a}$	maximum specific growth rate for the biomass consuming NO_3 (1/T)
$\mu_{m,a'}$	maximum specific growth rate for the biomass consuming NO_3 in ethanol-limiting chemostat (1/T)
$\mu_{m,b}$	maximum specific growth rate for the biomass consuming NO_2 (1/T)
$\mu_{m,b'}$	maximum specific growth rate for the biomass consuming NO_2 in ethanol-limiting chemostat (1/T)
ρ_a	apparent GAC density (M/L^3)
ρ_l	fluid density (M/L^3)
ρ_s	bioparticle density (M/L^3)
ΔG^0	Gibbs free energy

ACRONYMS

AVS	attached volatile solids
C:N	carbon-to-nitrogen ratio
EPA	Environmental Protection Agency
FBAR	fluidized bioadsorber reactor
GAC	granular activated carbon
HRT	hydraulic retention time
MLVSS	mixed liquor volatile suspended solids
OCWD	Orange County Water District
PAC	powdered activated carbon
RBC	rotating biological contactors
RO	reverse osmosis
SDR	specific denitrification rate
TDS	total dissolved solids

ABSTRACT

RO membrane process is a viable and cost-effective advanced treatment technology mostly used in water recycling facilities to reclaim the secondary treated wastewater. However, similar to the conventional treatment technologies, RO membranes also produce a toxic and non-recyclable treatment by-product often referred to as brine reject. The high ammonia, TDS, sulfate and heavy metal content of RO brine rejects render them hazardous to the environment into which they are discharged. As the RO membrane technology becomes widely used by the water recycling facilities, the brine reject streams will likely become a serious issue and a significant barrier in the application and full-scale implementation of this technology due to their toxic residue status. In addition, stringent future environmental regulations may restrict or fully prevent the direct disposal without toxicity reduction. This research employed various biotechnology processes to remove ammonia, nitrate and sulfate from such RO brine rejects.

The research was conducted in five stages. The first stage involved converting the toxic ammonia into nitrate through the biological nitrification process using (i) a laboratory-scale fluidized bioreactor with GAC and (ii) a pilot-scale RBC with PAC. The nitrification process was optimized to achieve maximum ammonia removal efficiencies. The fluidized bioreactor with GAC achieved nitrification efficiency of about 95 percent with a minimum hydraulic retention time of 180 minutes. Similarly, the RBC-PAC process achieved steady state nitrification

efficiencies well above 95 percent during the entire operational period. For both processes, the most influential factor appeared to be a strict control over the system pH.

In the second stage of this research, a series of laboratory-scale batch studies were conducted to determine the effects of various environmental parameters on the denitrification process. The environmental factors tested included temperature, pH, TDS and C:N ratio. For each environmental parameter, only the parameter tested was varied within a pre-determined range and all other factors were maintained constant. The maximum specific denitrification rates were obtained at a temperature of 35°C, pH of 8.0 and C:N of 1.8:1. Experimental results showed little or no effect of TDS on the denitrification rate, should the TDS concentration fluctuate.

In the third stage of this research, a series of continuous flow chemostat tests were conducted to determine the kinetic parameters including the maximum specific growth rate, Monod half saturation constant, growth yield coefficient and decay coefficient. These parameters were determined using modified Monod equations under nitrogen- and carbon-limiting conditions to assess the feasibility of denitrification process for the RO brine rejects and used as the inputs for the mathematical model developed for the denitrification process. Experimental results demonstrated that nitrate was far more favorable as the main substrate for the denitrifying culture used in the study than nitrite, and that insufficient carbon source caused instability of the system due to inhibitory effect of nitrate and/or nitrite accumulation.

The fourth stage of this research focused on the denitrification process using an FBAR with GAC. The experiments were conducted at different GAC quantities, hydraulic retention times and influent nitrate concentrations. The FBAR studies demonstrated nitrate removal efficiencies as high as 96 to 100 percent even at shorter hydraulic retention times of 40 minutes. The quantity of GAC played an important role in maintaining higher biomass in the bioadsorber, and higher influent nitrate concentrations resulted in prolific biomass growth. Nitrite build-up was insignificant at steady state operation. Therefore, it was suggested that FBAR denitrification system be considered as a single-step treatment process in design considerations.

The results of the FBAR experiments were also used to develop and refine a mathematical model for the FBAR denitrification process. The most important feature of the model was that it assumed biodegradation to occur not only in the biofilm immobilized on the GAC particles but also in the liquid phase suspension. The biodegradation phenomenon in the biofilm and bulk liquid phase was effectively represented by the modified Monod biokinetics determined previously from the continuous flow experiments. The model simulation results demonstrated good agreement between the experimental data and model predictions. Sensitivity analyses of the model indicated that growth yield coefficient and maximum specific growth rate had the utmost influence on the FBAR denitrification process.

Similar FBAR experiments under the same operational conditions were also conducted with sand for comparison purposes. Completion of denitrification process with sand took much longer time than with GAC (2,350 minutes vs. 500 minutes)

with substantial nitrite accumulation. Sand supported relatively lower biomass concentration than GAC.

During the last stage of the research, simultaneous denitrification and sulfate removal process were investigated using a similar FBAR process at hydraulic retention time of 180 minutes. Denitrification process was completed in 400 minutes of operation, while sulfate reduction from 1,300 mg/l to 712 mg/l occurred in 585 hours. The zoning in the bioadsorber bed became visible in that denitrification took place in the lower portion of the bed while sulfate reduction took place in the upper portion. A second FBAR employed to remove the remaining sulfate from the first FBAR successfully reduced sulfate in 412 hours of operation. During this process, the reactor walls were covered with well-separated black spots, an indication of ferric sulfide precipitation. The FBAR also removed a number of other metals including arsenic, copper, manganese, selenium, silver and zinc in the range of 24 to 100 percent.

A biofilter column was employed to remove the hydrogen sulfide gas generated by the FBAR sulfate reduction process. The column was very effective in complete removal of hydrogen sulfide.

Results from this research demonstrated that FBAR using GAC is an effective and reliable technology in removing nitrates, sulfates and metals from the RO brine rejects. The model developed successfully predicted the FBAR denitrification process performance under a variety of conditions.

CHAPTER 1

INTRODUCTION AND STATEMENT OF THE PROBLEM

1.1 Overall Review of Water Recycling

1.1.1 Need for Water Recycling

In the near future, it is likely that many nations will face serious water shortages due to pollution or limited quantity of water resources. Even with the available water sources of high quality as to provide potable water, the increase in population necessitates the production of sufficient water that can be safely used by millions of people. This enormous demand for fresh water supplies is growing at a rapid rate, and may eventually outgrow the existing supplies. For example, California is among the states recently facing serious water shortages, which is expected to worsen unless some timely preventive measures are taken. It is estimated that by the year 2010, the net demand for water will be 35.6 million acre-feet with an annual deficit of about 2.3 million acre-feet, by which time the state's population is anticipated to rise to 41 million (California State Water Resources Control Board, 1990; WaterReuse Association, 1993). It is for this reason that water and wastewater districts in California have received early lessons on the importance of a well-organized and comprehensive approach to explore other reliable water sources.

Recycled water is defined in California Water Code as "the water, which, as a result of treatment of wastewater, is suitable for a direct beneficial use or a controlled

use that would not otherwise occur" (U.S. EPA Guideline, 1992). Replacing the potable water used for non-potable purposes with used water, where feasible, after treating it to the extent not to pose any health risks to the users, would preserve millions of gallons of water for potable use. In this respect, water recycling is regarded as a new, reliable and economically viable alternative to the existing options including water conservation, desalination, import from other states, etc.

In recycling practices, wastewater is the source water that can be recovered through a series of treatment processes. After receiving treatment, the secondary effluent or a blend of primary and secondary effluents from the wastewater treatment plant is taken to the recycling plant. Here, it is provided with an advanced tertiary treatment so that the final effluent quality is high enough to be safely used by urban, agricultural and industrial water customers for beneficial uses that include practices such as agricultural and landscape irrigations, groundwater recharge, surface water augmentation and industrial cooling water. A survey found that, among these beneficial uses, groundwater recharge was in the lead by 47 percent (WateReuse Association, 1993). Over the decades, aquifers have become over-pumped, resulting in reaching for greater depths to extract water, which, in turn, has resulted in higher pumping costs. In addition to this, saline water intrusion from the sea or ocean to these aquifers bearing clean water has become a major issue. Large quantities of recycled water, therefore, can be spread onto the basins and let percolate, or discharged directly into the aquifers that provide an inexpensive reservoir and distribution system for conveying the water from the source to the destination.

In the light of above reasons, the advantages of water recycling and its benefits to meet non-potable water demands can be summarized as follows:

- Many countries face rapid population growth, which makes the water conservation efforts meet the current needs only. More effort needs to be directed towards conservation of existing potable water supplies. Water recycling is one of the best few alternatives that could save the potable quality water sources.
- Some cities may lack water sources simply because of their location or over-consumption of their existing water resources. Importing water would be a solution, but it is capital intensive and politically tenuous. Instead, the existing limited sources could be augmented with recycled water, and this water could be used as a substitute for the potable quality water for irrigation, industry and groundwater recharge.
- Recycling could be a main incentive for economic growth in small communities with limited water supplies. It can provide reliable and affordable quantity of water to attract new industries that would create new job opportunities for the community, and contribute to its development (Filteau, 1995).
- For some inland cities, wastewater treatment costs could be high because of the regulatory requirements to protect the downstream water quality. At this point, water recycling proves to achieve downstream water quality criteria for such cities (Okun, 1991).
- Over-pumping of groundwater resources is a short-term solution to water shortage problems, as it may deplete the aquifers. Recharging these aquifers with

recycled water not only would keep the groundwater basin replenished, but also prevent saline water intrusion into the aquifers.

- Seawater desalination has been in practice in many countries to obtain drinking water. However, it is an expensive potential water source with yet undefined environmental constraints and considerations. Water recycling, in most cases, is proven to be more cost-effective than desalination.

1.1.2 Laws and Regulations

In water recycling practices, the secondary treated effluent from a wastewater treatment plant requires further purification to ensure proper contaminant removal and compliance with the current water quality standards. There are no U.S. EPA set standards for recycled water. However, the regulations in California, for instance, are very strict regarding the quality of the recycled water and for unrestricted uses only, i.e., recycled water is suitable for all applications except drinking (Myers, 1996).

The basic principle underlying water quality regulations pertaining to the recycled water is to assure that health protection is not compromised through its use. Where the human exposure is likely in a reuse application, regulations state that the recycled water should be treated to the highest degree possible prior to the reuse. It must be free of pathogens that could spread disease. Conversely, where public access to a reuse site can be restricted so that the exposure is unlikely, a lower level of treatment may be satisfactory (U.S. EPA Guidelines, 1992).

Direct reuse applications such as discharging the recycled water directly into the distribution system is prohibited by the regulations on the grounds that there are no real time microbiological quality assessment studies (U.S. EPA Guidelines, 1992). In other words, the consequences of direct discharge on public health are still under investigation. However, surface water augmentation and groundwater recharge are strongly encouraged since no negative health effects have been reported.

1.1.3 Advanced Treatment Technologies in Water Recycling

In order to accomplish the high quality standards set by regulatory agencies for recycled water, water utilities are forced to use the best available technologies available in the market. Recently, much attention has been given to the pressure-driven membrane processes such as microfiltration, ultrafiltration, nanofiltration and reverse osmosis. According to Duranceau (2001), these technologies have been proven to be cost-effective due to recent advances in the membrane materials and construction, and easy to operate and maintain. They are also reliable in the sense that unlike the conventional treatment processes, the finished water quality does not vary significantly from day to day with the fluctuations in the raw water or wastewater quality. He also emphasized that the current trend indicates that membrane processes will play a major role in the treatment market in the near future due to the increasingly stringent water quality regulations and safe discharge requirements.

Among the different membrane technologies, reverse osmosis is probably the oldest technology, and has been in use to remove salts from brackish and seawater for several decades. It is considered highly effective in achieving the effluent discharge goals. The basic principle of reverse osmosis membrane filtration is a semi-permeable cellulose acetate or thin film composite membrane through which the treated wastewater is passed under high osmotic pressure. Osmosis occurs when solutions of two different concentrations are separated by a semi-solid membrane; pure water molecules diffuse through the membrane to the side with more concentrated total dissolved solids until each side has equal total dissolved solids concentrations, or until the pressure differential becomes equal to the osmotic pressure. In the case of reverse osmosis, this process is reversed by applying pressure on the concentrated side of the membrane until the flow changes its direction. Figure 1.1 illustrates the concept of osmosis and reverse osmosis. Pure water molecules diffuse through the membrane and are released as clean water. Salts, minerals and other total dissolved solids can not penetrate the membrane and are discharged as brine rejects (Cappor, 1995). The quality improvement achieved by the reverse osmosis membrane process is outstanding; almost all contaminants that are within 5-20 Angstroms range and have about 200 molecular break-off points are removed virtually completely (Caetano et al., 1995).

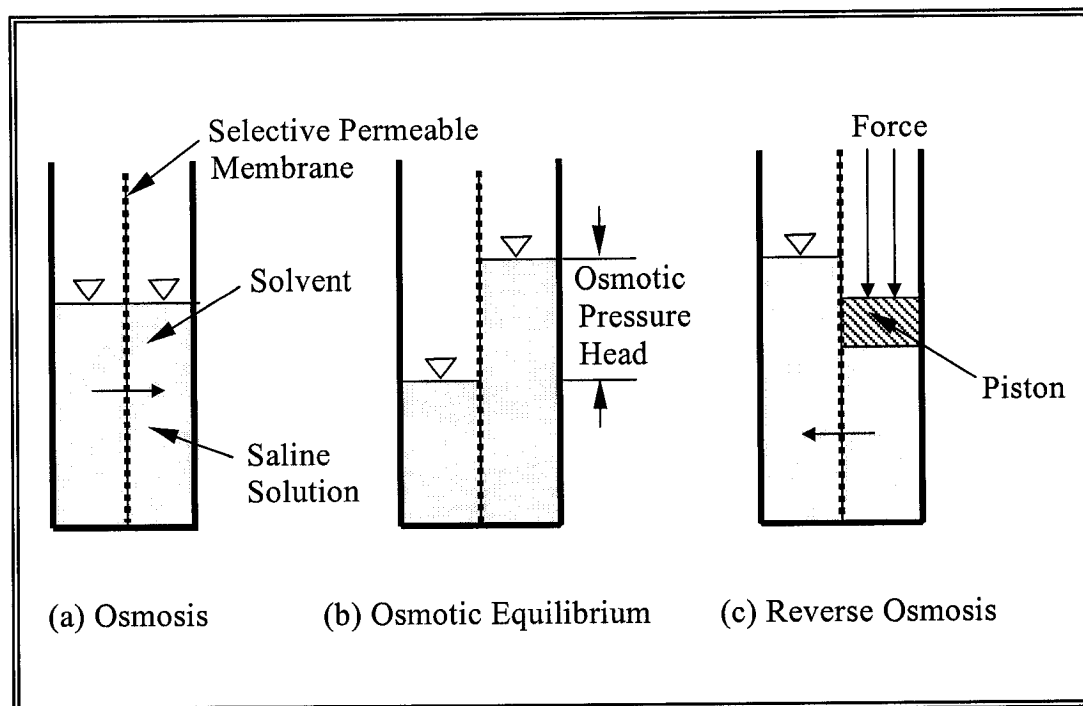


Figure 1.1. Schematic representation of osmosis and reverse osmosis processes

Reverse osmosis membrane technology has recently developed into a more reliable and economical unit operation that outperforms many conventional water treatment technologies employed by water utilities. Multi-contaminant compliance problems could be solved using such membranes. Furthermore, the utilities could allocate relatively smaller plant blueprint to build a reverse osmosis unit, while conventional technologies could occupy enormous plant area. This is especially an important advantage for the utility companies that have limited plant area but still need extension in order to provide water for a constantly growing population. However, research is still on the way to prove that a reverse osmosis unit could

successfully replace an entire conventional water treatment unit, or could be employed in water recycling facilities and would still prove to be cost-effective.

As the membrane processes become widely used technologies in the water recycling practices, their by-products or waste streams are likely to become a problematic issue with respect to their disposal and/or treatment. With the upcoming water quality requirements, it is quite possible that the regulatory agencies would require proper pre-treatment prior to disposal of these residues.

1.2 Residue Management in Membrane Processes: Reverse Osmosis Brine Rejects

1.2.1 Generation of Brine Rejects and Current Disposal Practices

As mentioned above, reverse osmosis (RO) is by far one of the most commonly used membrane processes that is capable of producing potable quality water from non-potable sources and, therefore, referred to as best available technology (BAT) in the market. Similar to most treatment technologies, RO membrane process also produces residues that require handling either by various disposal methods or by separate treatment processes. The waste product of RO membrane process referred to as “brine reject” (brine, reject or concentrate), is comprised of materials rejected by the membrane filter, and regarded as non-recyclable. RO systems can remove up to 97 percent of dissolved minerals, and more than 95 percent of most dissolved organics (Rorech & Bond, 1993). Overall, total dissolved solids rejection of RO membranes is in the range of 85-98 percent for all

ions (Dietrich, 1995). The contaminants in the feed source are generally concentrated by a factor that is determined by the hydraulic ratios established by system design (Comb, 1994).

Ocean dump, stream discharge, dilution, deep-well injection, evaporation ponds, mechanical evaporation and spreading on an arid land area are among the current trends for disposal of brine rejects. A recent survey has shown that 60 percent of the RO plants have been discharging their brine rejects into a nearby surface water (Kenna & Zander, 2001). However, many recycling facilities that employ or plan to employ RO technology are often not situated near an available surface water for the ultimate disposal. Such facilities will need to find their own ways to handle or treat the brine reject prior to disposal. Furthermore, when a new treatment technology is introduced to the market, its operational practicality and cost effectiveness have to be established ahead of time not only for the technology itself, but also for its residues so that it could be integrated into the initial planning stage. For instance, Turner et al. (1997) conducted a study for a two-stage low pressure RO pilot plant in a small, underdeveloped community to provide potable water from the groundwater that was highly saline due to salt water intrusion into the aquifer. The RO plant constructed provided exceptionally high quality water. However, the disposal of the brine reject became a major problem. After having considered many options such as self-sealing infiltration basins, salinity gradient solar ponds and saline vegetative wetlands, they decided to construct enhanced evaporation ponds favored by the availability of ample and inexpensive land areas. In conclusion, these researchers stated that

disposal of highly saline brine rejects in semi-arid regions posed a considerable challenge in so far as contaminating the surface water or groundwater resources. This was not only environmentally unacceptable, but also economically and socially detrimental to those communities that relied on those water resources. Therefore, the most glaring barrier to the implementation of RO membrane projects is the issue surrounding the disposal or treatment of the brine reject streams produced as the natural process residues.

1.2.2 Regulatory Aspects Pertaining to Brine Rejects

Since membrane processes are fairly new, there are no established regulations pertaining to the handling of brine rejects. Depending on the disposal alternative selected, proper permits must be obtained from the regulatory agencies. For example, discharge of brine rejects to a receiving water body requires a National Pollutant Discharge Elimination System (NPDES) permit, which is authorized under the Clean Water Act (CWA). For those utilities that discharge into the local wastewater treatment plant *via* the sewer system or a direct pipeline, some type of local permit or agreement with the local Publically Operated Treatment Works (POTW) is necessary. On the other hand, if deep well injection method is chosen as the disposal alternative, a permit for well operation and underground injection with the appropriate state agency must be obtained. In this case, extensive monitoring is required under the permit (Kenna & Zander, 2001).

In the near future, new regulations may be enforced to preserve and protect the marine water (ocean) or non-marine surface water (lake, river, etc.) environment from the adversities of improper disposal of brine rejects, as the disposal alternative chosen by the water authorities could be responsible for high concentrations of contaminants in such waters, and could pose serious health risks and environmental problems. The regulatory agencies may force the treatment plants to implement treatment techniques to treat their brine reject streams. Determining the treatment alternative and testing the feasibility of the RO membrane process for the waste residues, therefore, would avoid problems down the line with the regulatory agencies regarding their handling and disposal. For example, the RO brine reject handled by Squire et al. (1996) was high in alkalinity, sulfate, chloride, total dissolved solids, and trace and heavy metals. These contaminant species in the brine reject were approximately concentrated by five times during the RO membrane process. After considering different disposal alternatives, they finally decided on surface water discharge due to proximity of the treatment facility to a near river, and contacted the local environmental agency in order to obtain approval for river disposal. Since this disposal was the first of its kind in the region, the agency showed great concern about the disposal due to the characteristics of the brine reject. Finally, it was concluded that the brine reject could only be discharged to the river after being diluted with the backwash water generated from the filtration unit. Since there were no established regulations pertaining to the RO brine reject and no data on

pre-established water quality, the facility was required to extensively monitor the river water quality for evaluating the long-term impacts of the disposal.

Later, Acquaviva et al. (1997) emphasized that brine reject handling and disposal must be an integral part of RO treatment plant design, permitting, and operational considerations. Strict regulations pertaining to disposal can potentially present substantial economic burden for small and medium-sized systems. These burdens apply to both the planning of new systems and the continuing operation of existing systems.

Kenna and Zander (2001) stated that the impurities contained in RO brine rejects are those initially contained in the wastewater stream treated using the membranes, and emphasized the regulatory restrictions surrounding the disposal and reuse of the brine rejects as one of the major barriers preventing the implementation of membrane technology.

1.2.3 Characteristics of Brine Rejects and Associated Health and Environmental Concerns

In general, membrane brine rejects are classified as an industrial waste, which is the result of a simple process elimination rather than the result of any sound fact or judgement (American Desalting Association, 1995). The basic environmental concern with the brine reject streams is the high concentration levels of the contaminants in spite of their small volume. Contaminants that are initially in the feed water stream and have been removed by the RO membranes, eventually end up

in the system brine reject. For example, if the RO membrane recovery is 85 percent, 15 percent of the water or wastewater treated is discarded as the brine reject with a wide array of contaminants, rendering them non-recyclable by-products of the process. The RO membranes are highly selective to the inorganic constituents depending on their pore size. Table 1.1 presents the characteristics of the RO brine reject generated by the Water Factory-21 at the Orange County Water District (OCWD), CA with reference to the constituents and their minimum and maximum concentrations. It is evident that it contains high concentrations of ammonia, sulfate, total dissolved solids and a wide variety of heavy metals besides a number of other contaminants. Most of these constituents are toxic to human, animal and plant life. For instance, ammonia causes general deoxygenation and is, therefore, toxic to marine life, especially during the summer months when dilution factors are at their lowest. Furthermore, its presence in fresh water supplies increases the chlorine demand required for disinfection, as it forms chloramines with chlorine. Another adverse effect of ammonia is that it causes corrosion of industrial structures.

Nitrates, the oxidation product of ammonia, on the other hand, cause eutrophication in receiving bodies, as nitrate serves as one of the inorganic nutrients required along with phosphate. Eutrophication leads to severe water quality deterioration problems caused by increase in the algal growth and the concomitant oxygen depletion. In addition to this, transformations of nitrogen compounds by microorganisms lead to the production of gaseous intermediates such as nitric and

nitrous oxides which are considered major contributors to ozone depletion in the stratosphere (Tabazadeh et al., 2000).

Table 1.1. Characteristics of reverse osmosis brine reject*

Constituent	Unit	Concentration	
		Min.	Max.
Total Organic Carbon	mg/l	31.4	48.8
Total Dissolved Solids	mg/l	3,380	4,550
Total Alkalinity	mg CaCO ₃ /l	521	1,490
Coliform	(MPN/100 ml)	--	--
Organic Nitrogen	mg/l	1.7	14.7
Ammonia Nitrogen	mg/l	62.1	97.8
Sulfate	mg/l	999	1,480
Phosphate	mg/l	15	25
Chloride	mg/l	800	1,000
Fluoride	mg/l	0.5	1.0
Cyanide	µg/l	--	40
Calcium	mg/l	--	500
Magnesium	mg/l	--	50
Silver	µg/l	<1	5.2
Arsenic	µg/l	<2	19
Barium	µg/l	89	120
Cadmium	µg/l	<1	3.8
Cobalt	µg/l	<1	5.2
Copper	µg/l	13	49
Iron	µg/l	260	710
Mercury	µg/l	<0.5	1.4
Manganese	µg/l	120	250
Lead	µg/l	<1	4.3
Selenium	µg/l	<5	7.3
Zinc	µg/l	74	180

* Minimum and maximum values are taken from the OCWD brine reject analysis reports between August 1998 and March 2001

In addition to their environmental damages, nitrates pose severe health hazards to humans in that, although the exact nature of the toxicity to humans is not entirely understood, ingestion of water containing high nitrate and its consequent reduction to nitrite in the gastrointestinal tract produce methemoglobinemia (blue baby syndrome) in infants (McCleaf & Schroeder, 1995). Also, ingested nitrate is endogeneously reduced to nitrite and subsequently to N-nitroso compounds through nitrosation reactions in the stomach. These compounds have been found to induce cancer in a variety of organs in human beings. In a most recent cohort study by Weyer and his coworkers (2001) on 21,977 Iowa women, who were 55-59 years of age in 1986 through 1998, and had used the same water supply more than 10 years, there was a positive association between increased nitrate levels and bladder and ovarian cancer. Compared with women drinking water with less than 0.36 mg N/l, women drinking water with greater than 2.46 mg N/l were at increased risk of bladder cancer. In another population-based case-control study conducted in California between June 1989 and May 1992, Croen et al. (2001) concluded that exposure to nitrate in drinking water at concentrations above the 45 mg/l maximum contaminant level (MCL) was associated with increased risk for anencephaly. They observed a doubling in anencephaly risk for maternal exposure to groundwater containing nitrate at 5-15 and 6-35 mg/l ranges as compared to the groundwater containing less than 5 mg/l nitrate. They also supported their findings by a previous study conducted by Arbuckle et al. (1988) which reported a two-fold risk for central

nervous system anomalies associated with exposure to nitrate in groundwater containing 26 mg/l nitrate relative to the baseline of 0.1 mg/l.

The health problems associated with consumption of high-nitrate waters have forced regulatory agencies to establish MCLs. The EPA established the MCL for nitrate as 10 mg/l for drinking water. Due to public health concern explained above, water streams contaminated with nitrate require adequate treatment prior to usage or ultimate disposal. The conversion or discharge of nitrate is usually governed by the environmental regulations pertaining to its allowed concentration level and by the technologies chosen for treatment.

Similarly, sulfates in high concentrations could be toxic to the environment into which they are discharged. They impart bitter taste and odor, and may have laxative effect that could lead to dehydration in humans and, therefore, of special concern for infants. The EPA established (secondary) standard for sulfates in drinking water is 250 mg/l.

High total dissolved solids, another content in RO brine rejects, could yield complexation reactions with metals or change the physiological reactions of marine organisms (OCWD Final Feasibility Study, 1995). High electrical conductivity of the brine reject is attributed to its high total dissolved solids content. The total dissolved solids standard is established at 500 mg/l level by the EPA.

Heavy metals found in the RO brine reject streams, on the other hand, tend to accumulate in the tissues of aquatic species. They can contribute to physiological well-being at extremely low concentrations, and at the same time can be quite toxic

at very low concentrations. It appears that heavy metals in low extracellular concentrations can exert very destructive influences on the integrity of the so-called tight junction between the cells of aquatic species. As heavy metal concentrations increase, osmo-regulation can be interfered with by impairing the salt accumulation and enlarging leak pathways through which solutes are lost to the environment (Mickly et al., 1997).

1.2.4 Other Sources of High Salt Brines

Other membrane processes such as microfiltration, ultrafiltration, nanofiltration and desalting *via* ion exchange process are also highly effective in removing turbidity, organic compounds, dissolved solids and microorganisms, and produce side waste streams that require proper handling and disposal. The waste stream from a microfilter is mostly wash water, which is usually high in turbidity and microorganisms. The waste stream from an ultrafiltration unit is usually rich in turbidity, organic compounds, microorganisms and iron and manganese. The nanofiltration process produces a reject stream that contains mostly anions, metals, total dissolved solids and microorganisms and shows similar characteristics with the RO brine rejects. In this case, the same disposal methods as RO brine rejects have been employed by the water agencies. The ion exchange process, on the other hand, is aimed to remove the target pollutants such as salt, nitrate, sulfate, etc. through the use of an ion exchange medium. Although the process is cheaper than the RO

process, the treatment efficiency with regard to the multi-contaminant removal is not as satisfactory as the RO membranes (Kenna & Zander, 2001).

1.3 Statement of the Problem: Necessity for the Treatment of Brine Rejects

The demand for potable water by the increasing population has placed a substantial burden on the water utilities to look for alternative solutions to the water shortages. The use of recycled water to supplement the existing local water supplies has relieved this burden with the progress made in the advanced water/wastewater treatment field. The membrane processes, especially the RO membranes, have produced high quality water beyond expectations, and have been employed in recycling facilities extensively. Although the finished water is not yet allowed by the regulatory agencies to be used as drinking water, it is widely used to augment the existing surface water and groundwater supplies and for irrigation.

However, very few studies have focused on the management of residuals produced by the membranes during the processing of treated wastewater. This could be attributed to the fact that the volume of brine rejects is relatively smaller than the treated wastewater streams, and could easily be discharged to the sanitary sewer system. Currently, extensive research on the advanced membrane technologies is being conducted to expand the capacity of recycling plants in order to provide recycled water for the beneficial uses other than drinking. As the capacity of these plants is increased in the near future, substantial quantity of brine rejects will be

generated. The concentrations of the salts, metals, various anions and nutrients in the brine rejects will be approximately 8.5 times the influent concentration of the raw wastewater when the recycling plants are operated at 85 percent recovery (Patel et al., 2001).

The main concern associated with disposal of brine rejects containing all the above contaminants into ocean or surface waters is its adverse impact on the beneficial uses and existing marine environment. Mandrup-Poulsen (1995) provided an overview of the existing Florida Department of Environmental Protection rules and options for proper disposal of brine rejects in Florida. He stated that many of the facilities that dispose of their brine rejects to surface waters have shown persistent acute toxicity to the mysid shrimp. Two types of potential impacts to marine biota possibly as a result of exposure to elevated contaminant levels in brine reject streams are: (i) physiological and toxic impacts resulting from intermittent exposure to increased total dissolved solids and heavy metal content, and (ii) stresses that lower resistance of the endogenous organisms to other environmental factors that would otherwise not occur (OCWD Final Feasibility Study, 1995). Consequently, the disposal of membrane residuals can be deleterious to the marine environment, and this can result in violation of water quality standards triggering a need for source treatment. On the other hand, disposal in the sanitary sewer system could be expensive, and require approval and permit from the local environmental agency. Similarly, deep well injection, self-sealing infiltration ponds or evaporation ponds as

alternatives to the surface water disposal in arid areas may also have adverse impacts on the environment besides being costly.

As mentioned before, the disposal of the brine reject streams generated as the natural residue of the RO membranes could be the major barrier to the implementation of large membrane plants. For instance, a water reuse project in Virginia was cancelled because of the lack of acceptable brine reject disposal options (Freeman et al., 2002). Therefore, decisions regarding the strategies to handle brine rejects in the realm of residue management must be made in the initial design stage. The feasibility evaluations should (i) address future regulatory issues, (ii) include proper disposal alternatives, and (iii) should compare the disposal with or without treatment.

1.4 Rationale for This Research

The brine rejects generated by the membrane processes can be post-treated to increase the dissolved oxygen concentration or to remove toxic constituents prior to discharging. Current post-treatment practices commonly include aeration and static mixing in order to increase the dissolved oxygen concentration. Additional post-treatment may include appropriate processes to remove any constituents that may be harmful to the receiving body of water.

In light of the issues mentioned above, this research project was primarily directed at developing a post-treatment strategy for the removal of nitrate, the oxidation product of ammonia, from the RO brine rejects containing high

concentrations of ammonia, total dissolved solids, sulfate, a wide array of metals and other contaminants. Treatment technologies employed in nitrate removal (known as denitrification process) can be divided into two groups. The first group includes those technologies which do not require the addition of an exogenous organic carbon source. Suspended growth system such as conventional activated sludge reactors with an anoxic zone or modifications to this process, such as the four- or five- stage Bardenpho process, oxidation ditches and sequencing batch reactors with anoxic cycles are among this group in which the soluble organic matter that is already present in the feed water is utilized as the electron donor. The second group consists of those technologies that require an exogenous carbon source for the biological denitrification to occur. In these systems, denitrification takes place within the biofilms formed on the surfaces of a support media. Anaerobic submerged fixed bed reactors, rotating biological reactors, membrane bioreactors and fluidized bioreactors can be used for denitrification if they are supplemented with an organic carbon source (Rittmann & McCarty, 2001; Tchobanoglous & Burton, 1991).

In the first part, this research employed a laboratory-scale aerobic fluidized bioreactor with granular activated carbon, as well as a pilot-scale rotating aerobic biological contactor unit supplemented with powdered activated carbon for oxidation of ammonia (known as nitrification process) present in RO brine reject. Both technologies were optimized for maximum nitrification performance. In the second part, the research employed a mini pilot-scale anaerobic fluidized bioadsorber reactor with granular activated carbon for biological denitrification of RO brine reject. The

feasibility and efficiency of fluidized bioadsorber reactor process were assessed with respect to hydraulic retention times, quantity of carbon and substrate (nitrate) concentration. The effects of temperature, pH, total dissolved solids and organic carbon concentrations on denitrification process were also studied to optimize process performance and economy. Biokinetic studies were conducted to determine the biological parameters including maximum specific growth rate, Monod half saturation constant, growth yield coefficient and decay coefficient. The magnitude of these constants influences the feasibility of the denitrification process for the RO brine rejects as well as allows comparisons with the literature values for different wastewater streams. A mathematical model was employed to predict the process efficiency under various operating conditions, and to provide the basic design tools for up-scaling the process. Sensitivity analyses were performed out to evaluate the qualitative influence of various parameters on the model performance. Furthermore, the research investigated the potential of the fluidized bioadsorber reactor process for simultaneous removal of nitrate and sulfate. Finally, gas-phase biofiltration technology was employed to remove the resultant hydrogen sulfide gas produced by the sulfate reduction process in the fluidized bioadsorber reactor.

CHAPTER 2

RESEARCH OBJECTIVES AND SCOPE

2.1 Research Objectives

The main objective of this research is the removal of nitrogen compounds including ammonia, nitrate, nitrite and sulfates from the RO brine rejects using various bio-physicochemical processes. For example, ammonia removal is an aerobic process achieved through biological nitrification, whereas nitrate (oxidation products of ammonia) is removed through an anaerobic process called biological denitrification. Biological sulfate removal is accomplished through anaerobic sulfate reduction process, which may occur simultaneously in the same biological environment as the denitrification process under optimal conditions. In the same way, hydrogen sulfide, a toxic off-gas generated by the sulfate reduction process, could effectively be removed using biofiltration process.

This research is focused on: (i) optimization of two different aerobic biological nitrification processes including fluidized bioreactor and rotating biological contactors for the removal of ammonia, (ii) assessment of feasibility and efficacy of anaerobic fluidized bioadsorber reactor technique for biological denitrification and sulfate reduction, and (iii) removal of hydrogen sulfide gas generated by sulfate reduction process employing gas-phase biofilters.

The first part of the research will include the nitrification studies using two techniques, namely a laboratory-scale aerobic fluidized bioreactor employing granular activated carbon (GAC) and a pilot-scale aerobic rotating biological contactors unit employing powdered activated carbon (PAC). Both techniques will be initiated and optimized with respect to hydraulic retention time and process efficiency to be able to nitrify the RO brine reject, and provide feed for the following denitrification and sulfate reduction studies.

The second part of the research will include the application of a mathematical model to predict the performance of anaerobic fluidized bioadsorber reactor (FBAR) denitrification process. The predictive model will provide the basic design tools for up-scaling the process. The first step towards the FBAR studies will be to assess the effects of various environmental parameters including temperature, pH, carbon-to-nitrogen ratio, and high total dissolved solids concentrations on the denitrification process through bench-scale batch experiments. This investigation will aid in optimizing the denitrification process efficiency in order to maximize the efficiency and cost-effectiveness of the FBAR treatment system. The second step will be to determine several model input parameters. The biokinetic parameters will be determined employing a continuous flow chemostat technique. A number of continuous flow chemostat experiments will be conducted under nutrient-limiting (nitrate or nitrite) and carbon-limiting (ethanol) conditions, and the data obtained will be used in modified Monod equations in order to estimate the maximum specific

growth rate, Monod half saturation constant, growth yield coefficient and decay coefficient. Other necessary parameters, such as substrate mass transfer coefficient, axial substrate dispersion coefficient, free liquid diffusivity, biofilm diffusion coefficient, initial and maximum biofilm thickness, biofilm density will be estimated by correlation techniques or direct measurements. The predictability of the model will then be verified by comparing the model outputs with the experimental results from mini pilot-scale FBAR studies with GAC. These studies will be used to evaluate the influence of the GAC quantity, hydraulic retention time and influent nitrate concentration on the FBAR denitrification performance. Sensitivity analyses will be performed to predict the efficiency of the FBAR denitrification process under varying conditions. A set of FBAR experiments will also be carried out employing sand as the support medium in order to compare the system efficiency with that of FBAR with GAC.

The final part of this research will investigate the removal of sulfate from the nitrified RO brine reject simultaneously with the nitrate removal. The optimal parameters to achieve highest possible sulfate reduction will be investigated. Moreover, removal capacity of the system with respect to heavy metals will be studied. The biofiltration technique will be employed to remove the noxious hydrogen sulfide gas generated during the sulfate reduction process.

2.2 Research Scope

1. Optimize the two biological nitrification processes, namely laboratory-scale fluidized bioreactor and pilot-scale rotating biological contactor unit in order to effectively nitrify the RO brine reject for the subsequent denitrification studies.
2. Conduct batch studies to determine the effects of temperature, pH, carbon-to-nitrogen ratio and high total dissolved solids concentration on the biological denitrification process.
3. Choose the optimum parameters from (2) to conduct a series of continuous flow chemostat studies under nitrogen- and carbon-limited conditions to determine Monod biokinetic parameters including maximum specific growth rate, half saturation constant, growth yield coefficient and decay coefficient.
4. Conduct mini-pilot scale anaerobic FBAR denitrification studies with GAC as the support medium under a variety of operating conditions to determine the process performance in removing nitrate.
5. Perform mini-pilot scale anaerobic FBAR denitrification studies with sand as the support medium, and compare the results with the FBAR experiments employing GAC.
6. Conceptualize and apply a mathematical model for the design and up-scaling of the FBAR concept for biological denitrification of RO brine reject.
7. Conduct mini-pilot scale anaerobic FBAR studies under various operational conditions to verify the applicability and predictive capability of the FBAR model.

8. Perform model sensitivity analyses to assess the influence of various parameters including biokinetic constants, biofilm density and influent nitrate concentration on the FBAR model performance.

9. Conduct anaerobic FBAR studies to investigate the process efficiency in removing nitrate and sulfate simultaneously.

10. Conduct gas-phase biofiltration studies for the removal hydrogen sulfide gas generated by the sulfate reduction process.

CHAPTER 3

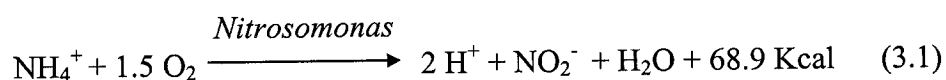
THEORY AND PRINCIPLES OF BIOLOGICAL PROCESSES

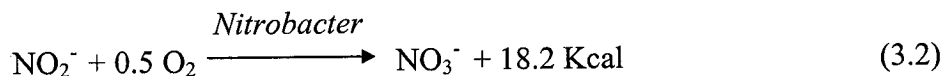
This chapter is divided into four major sections that present the theory and principles of the biological processes and techniques used in this research, namely the nitrification process for ammonia oxidation, denitrification process for nitrate removal, sulfate reduction process for sulfate removal and biofiltration technique for hydrogen sulfide removal. Each section includes fundamentals of the respective process, biological aspects, and environmental and operational factors affecting the process performance.

3.1 Theory and Principles of Biological Nitrification Process

3.1.1 Theory of Nitrification

Biological nitrification process is a two-step process, which involves the oxidation of ammonia sequentially into nitrite and nitrate by chemoautotrophic bacteria under strict aerobic conditions. The process does not remove nitrogen compounds from the system, but converts them into another chemical form (nitrate) as shown below (Ng, 1985):





The first step of the nitrification process is quite complex, and not only carried out by *Nitrosomonas*, but also *Nitrosococcus*, *Nitrosopira*, *Nitrosovibrio* and *Nitrosolobus* are involved (Teske et al., 1994). However, the *Nitrosomonas* genus is more diverse than the others, and none of these subdivisions could dominate over the other in a given system. In this step, ammonia is first oxidized to hydroxylamine, and then hydroxylamine is oxidized to nitrate. The subsequent oxidation of hydroxylamine to nitrate is the major energy-yielding source for *Nitrosomonas* ($\Delta G^\circ = -68.89 \text{ Kcal/mole N}$) (Ng, 1985). The second step is relatively simple compared to the first step, and carried out by *Nitrobacter*, which is the most famous genus among others including *Nitrospina*, *Nitrospira*, *Nitrococcus* and *Nitrocystis* (Teske et al., 1994). In this step, nitrite is oxidized to nitrate, and the process nets 18.18 Kcal/mole N (Ng, 1985).

Gee et al. (1990) reported the possibility to achieve nitrification consistently in almost any system, and produce an effluent containing less than 1 mg $\text{NH}_3\text{-N/l}$, provided that prevailing environmental conditions are adequate to maintain the population of the nitrifying bacteria. Sharma and Ahlert (1977) indicated in their comprehensive review on nitrification process that phosphate, sodium, calcium, magnesium, copper and iron are absolute nutrients required by both *Nitrosomonas* and *Nitrobacter*. Of these, sodium is specifically required by *Nitrosomonas*, while *Nitrobacter* requires calcium. Besides nutritional requirements, Rittman and

McCarty (2001) reported nitrifiers as to be highly sensitive to chemical inhibition and toxic substances, low dissolved oxygen concentration, low temperature and low carbonate alkalinity. The effects of these factors on the nitrification process are briefly explained in the following section, as they make the process highly sensitive and susceptible to adverse conditions.

3.1.2 Effects of Various Environmental Factors on Nitrification

It is a general consensus that nitrifiers are extremely sensitive to prevailing environmental conditions and operating variables in any given nitrification systems. Deviations from optimal environmental conditions may result in slow growth rates and low process efficiencies resulting in higher ammonia concentrations in the system effluent.

As one of the most important environmental condition, a minimal dissolved oxygen concentration must be maintained in any nitrification system to achieve a sustained degree of nitrification rate, since oxygen can be the limiting substrate at low concentrations. Especially, the presence of organic matter in the wastewater to be treated can directly inhibit nitrifiers by virtue of the competition for available dissolved oxygen at such low concentrations (Ng, 1985). The lowest limiting oxygen concentration was reported as 0.5 mg/l for suspended growth systems, whereas the dissolved oxygen concentrations below 3 mg/l were reported to inhibit the

nitrification process in attached growth biofilm systems (Kang, 1978; Rittmann & McCarty, 2001).

The rate of nitrification may also be profoundly altered by temperature, as the magnitude of maximum specific growth rate and the half saturation constant greatly vary with temperature. Scientists have used various empirical equations to determine the effect of temperature. However, such correlations should be determined for each system through experimentation, or else must be used with caution. The optimum temperature for suspended culture nitrification systems was reported by the U.S. EPA to fall in the range of 28 and 32°C (Kang, 1978). The same agency also reported optimum temperature for activated sludge nitrification to be in the range of 30 to 35°C.

As mentioned earlier, nitrifying bacteria have a relatively low growth rate that generally prevents significant nitrifying populations from occurring in treatment systems with short solids retention times. Since the low growth rate of the nitrifying bacteria is further decreased with decreased temperature in many conventional treatment environments, the minimum hydraulic retention time required to maintain a sufficient nitrifying population will increase as temperature decreases. Contrary to suspended growth systems, attached growth systems exhibit the ability to withstand much lower temperatures as compared to suspended growth systems without any significant decline in the nitrification activity.

Similarly, the biochemical activity of nitrifying bacteria is also influenced by pH on the enzymatic level (Kang, 1978). Although the optimum range of pH is generally between 7 and 9, nitrifiers have been shown to acclimate to new pH values outside this limit. They can retain similar maximum growth rates and nitrification efficiencies once they have been acclimated to lower pH values (Haug & McCarty, 1972). The effect of carbon dioxide produced from the degradation of organic matter that exists in the wastewater to be treated does not constitute a problem since carbon dioxide is in equilibrium with the atmosphere. Although the optimal pH for nitrification process may be greater than 8, it was recommended by Wang et al. (1978) to operate the process at 7.6 to 7.8 in order to allow carbon dioxide to escape to the atmosphere.

Inadequate buffering capacity in a nitrification system may impair the process by depressing the nitrification rates. Large amounts of alkalinity are consumed during nitrification to neutralize the production of free acid in context of the carbonic acid system. The U.S. EPA reported approximately 7.1 mg/l (as CaCO_3) alkalinity is destroyed per milligram of ammonia oxidized (Kang, 1978). Therefore, pH control must be an integral part of any nitrification system.

3.1.3 Limitations of Nitrification as a Biological Process

One of the major limitations of the nitrification process is that nitrifiers possess much smaller growth rate and cellular yield per mass of ammonia oxidized

as compared to other aerobic heterotrophs that reduce inorganic carbon. Their electron donors (ammonia) release less energy per electron equivalent than organic electron donors, hydrogen or reduced sulfur. Low yield coefficients translate into a small maximum specific growth rate and larger solids retention times, which make nitrifiers slow growers and the nitrification process an energy expensive process (Shammas, 1986). Thus long cell residence times are required to maintain a viable nitrifying mass in order to prevent bacterial washout with the effluent. Another disadvantage granted by the slow growth rate is the decrease in the ability of the nitrification systems to recover from system shocks, such as pH or temperature excursions, low dissolved oxygen levels and the presence of toxic materials.

Another important drawback of the process is to be aware of inhibitory effects of some chemical compounds found in waters and wastewaters on the nitrification activity. Knowledge on the types and concentrations of the inhibitory compounds, and duration and circumstances of the exposure to them may make it possible to predict and, if necessary, to modify the existing operating conditions under which the nitrification process can take place effectively. Among the organic and inorganic compounds mentioned by Rittmann and McCarty (2001) that could inhibit the growth and metabolism of nitrifiers are unionized ammonia, undissociated nitrous acid, anionic surfactants, heavy metals and chlorinated organic chemicals. The inhibitions are generally in the form of disruption of enzyme production and/or action, and inhibition of cell wall synthesis or damage to the cell wall itself. The

inhibition is manifested with decreased specific growth rates and maximum substrate utilization rates of the nitrifying bacteria.

There are conflicting reports about the effects of organic compound content of a water or wastewater on the nitrification process. Although some research done before 1900s reported some adverse effects of organic compounds even when at low concentrations, the research done after this period has reported little or no general toxic effect for a number of organic matter, unless they are found in large concentrations (Buswell et al., 1954; Delwiche & Finstein, 1965; Ida & Alexander, 1965). Downing et al. (1964) reported that the microorganisms were able to slowly adapt to many of the inhibitory organic compounds that they had included in their study. The current belief is that, even though there are several organic compounds toxic to the nitrifiers, the biological nitrification process is generally not affected by the presence of most organic compounds.

Heavy metals, on the other hand, have considerable inhibitory effect on *Nitrosomonas* especially due to its relatively complicated enzyme system as compared to that of *Nitrobacter*. For instance, in an early work conducted by Skinner and Walker (1961) reported the inhibitory effect of chromium and nickel on the growth of *Nitrosomonas* at concentrations less than 250 $\mu\text{g/l}$. Similarly, Painter and Loveless (1968) found that copper, zinc and cobalt at concentration ranges of 50-560 $\mu\text{g/l}$, 80-500 $\mu\text{g/l}$, and 80-500 $\mu\text{g/l}$, respectively, inhibited the growth of *Nitrosomonas*. Among these metals, copper, being the essential growth element for

Nitrosomonas at a concentration range of 5-30 $\mu\text{g/l}$, exhibited an inhibition at such high concentrations. At a later date, Braam and Klapwijk (1981) demonstrated that the free copper concentration had more adverse effect on the efficiency of their nitrification system than the total copper concentration, and that the free copper concentration increased with decreasing pH. They suggested that these findings could explain the effects of pH on the nitrification process with respect to heavy metal concentration, and solve the mystery behind the reported tolerances of nitrifiers to heavy metal inhibition.

In the same way, nitrite accumulation may present another drawback for any nitrification system. The accumulation in the start-up of the nitrification process is unavoidable, and may even occur under optimal nitrifying conditions due to the reason that the yield coefficient for *Nitrosomonas* is higher than that for *Nitrobacter*, while the decay rate of *Nitrobacter* appears to be higher than that of *Nitrosomonas* (Kang, 1978). Moreover, *Nitrosomonas* obtains more energy per mole of nitrogen oxidized than does *Nitrobacter*, which is a fact reflected in their relative cell yields, that is, 0.06 for *Nitrosomonas* and 0.02 for *Nitrobacter* as weight of cells formed per mole of nitrogen oxidized (Painter, 1977). Consequently, the length of lag period for *Nitrobacter* becomes longer. However, once the population of *Nitrobacter* becomes established, the accumulation of nitrite decreases to a very minimal value due mainly to the higher rate of growth.

3.1.4 Enhancing Nitrification Process with Powdered Activated Carbon

It is essential to first convert all the ammonia into nitrate through the nitrification process so that complete nitrogen removal could be achieved in the denitrification step through the reduction of nitrate into nitrogen gas. It is a well-known fact that the efficiency of nitrogen removal from a treatment system is strictly correlated with the degree of nitrification achieved, rather than the degree of denitrification. In other words, since denitrification process is a highly effective process, the nitrification phase becomes the limiting step in determining the efficiency of overall nitrogen removal (Shammas, 1971). Since nitrifiers and denitrifiers are kinetically very different from each other (nitrifiers being slow growers and, therefore, requiring much longer retention times as compared to denitrifiers), the design of nitrification and denitrification must reconcile the conflicting physiological characteristics between these two genera (Rittman & McCarty, 2001).

The increase in the efficiency of nitrification-denitrification process depends on the improvement of nitrification phase. There are a few techniques that have been in use over the last few decades to enhance the nitrification process such as improving the oxygen transfer efficiencies, bioaugmenting the existing system with cultures with specific degradative abilities and use of special media such as beads, synthetic materials or PAC floating inside the nitrification reactors. Among these

techniques, addition of a biologically inert adsorbent such as PAC into the content of the nitrification tank is worth consideration.

The initial motivation behind PAC enhancement was to remove biologically resistant chemical compounds from the waste streams. Later, PAC enhanced nitrification processes were employed in the treatment processes operated under the conditions that were not favorable to microorganisms such as low temperature, high organic concentrations, etc. For example, Ng (1985) provided convincing evidence in support of the theory that PAC can adsorb inhibitory compounds, thereby, enhancing nitrification rates substantially. The plausibility of the use of PAC to enhance the nitrification process in activated sludge tanks was also demonstrated by a number of other researchers (Bettens, 1979; Leipzig, 1980; Specchia & Gianetto, 1984; Stenstrom & Grieves, 1977). In short, the overall benefits realized by the addition of PAC into a treatment system are (i) the improved nitrification through organics and toxic constituents removal *via* adsorption, (ii) enhanced growth of nitrifiers on the carbon particles, (iii) higher active biomass in the system, (iv) higher oxygen transfer efficiencies, and (v) higher concentration of trace nutrients at the carbon surfaces.

Biological nitrification process can be achieved employing various technologies which include conventional aeration tanks, sequencing batch reactors, packed bed towers, trickling filters and rotating biological contactors. Among these, rotating biological contactors (RBC) consist of a single or series of circular disks usually made of polystyrene or polyethylene that are half-submerged in the

wastewater and rotated slowly. As they rotate, biological growth becomes attached onto the surfaces of the disks, and form a slime layer where the nitrification process occurs. Rotation of the disks maximizes the oxygen transfer to the system and maintains aerobic conditions in the RBC tank. As an attached growth system, RBC are known to be resistant to shock loads (Tchobanoglous & Burton, 1991).

The application of RBC technology enhanced with PAC (RBC-PAC) for the nitrification process results in a number of advantages not afforded by the use of PAC or RBC alone. The main goal is to more effectively treat the wastewaters by combining the desirable features of a RBC unit with that of PAC (Ng, 1985). For instance, the biofilm layer formed on the surface of the rotating discs of the RBC not only will consist of a mixture of biomass, but also will contain PAC as an adsorbent. The biofilm layer has the unusual property of accumulating the PAC particles into its structure, thereby, carrying the adsorbent on the disc surface along with the biomass. The ratio of biomass amount to PAC will depend essentially upon the solids residence time of the system and the composition of the feed wastewater stream. It can be said that PAC not only aids in removing adsorbable material from the wastewater, but also has the property of substantially increasing the residence time of adsorbable and slowly biodegradable substances. In general, it has been found that the addition of PAC as a suspended adsorbent to the nitrification system and maintaining its concentration at a high level permits the accumulation of very large

masses of active nitrifying organisms in the mixture, thereby improving the overall rate of nitrification process (Knopp & Burant, 1981; Knopp & Gitchel).

A further advantage of adding PAC to the RBC unit is its positive effect on the overall mass transfer rate of oxygen. The improved mass transfer rate has a direct dual impact upon the performance of the contactor. First, higher oxygen transfer rates permit slower rotational speeds and hence lower power costs, and second, the oxygen profile across the film on the rotating discs is improved providing deeper penetration through the biofilm layer with a greater resultant active aerobic biological mass. This effect is particularly important for those nitrifying systems where the nitrifying organisms must be exposed to dissolved oxygen concentrations in excess of 0.5 mg/l to be efficient (Ng, 1985).

3.2 Theory and Principles of Biological Denitrification Process

3.2.1 Theory of Denitrification

Denitrification is an anoxic biological process carried out by essentially facultative anaerobic microorganisms in which nitrate is reduced to nitrogen gas in the presence of an organic substrate. Nitrate serves as the terminal electron acceptor, whereas organic substrate serves as the electron donor. The end-product is the inert nitrogen gas that can safely be allowed to escape to the atmosphere.

In many denitrification systems, after the conversion of nitrate into nitrite, some intermediate steps occur between the reduction of nitrite into nitrogen gas.

First, nitrite is converted into nitric oxide, then into nitrous oxide, and finally into nitrogen gas. The overall reaction is (Payne, 1973):



Nevertheless, in practical applications, a commonly made assumption is the lumping of the four actual steps of the reduction sequence shown above to only two:



This kind of lumping is necessary in many mathematical denitrification models if they are to be used to predict the performance of the system over a wide range of operating conditions. The lumping is valid if the reduction rates of the nitric oxide and nitrous oxide are sufficiently faster than the reduction rates of nitrate and nitrite so as not to accumulate in the system. In many systems, nitric oxide is rarely detected during denitrification either in batch or continuous cultures. One of the reasons is that bacteria tend to reduce any free nitric oxide in an effort to avoid the toxicity attributed to its reactivity with heme and non-heme iron-containing proteins (Kornaros et al., 1996). In fact, a research conducted by Kornaros and Lybertos (1998) with *Pseudomonas* to address the plausibility of low steady state levels of nitric oxide showed that the nitric oxide reductase was active in much lower apparent half saturation constant (K_s) and higher specific growth rate (μ_{\max}) than the nitrite reductase, and the reduction of nitrous oxide was faster than that of nitrite. In consequence, little or no nitrous oxide evolved during the denitrification of nitrite.

Nitrate reduction is of two distinct types; assimilatory and dissimilatory nitrate reductions, which are quite different with respect to their functions. In assimilatory nitrate reduction, nitrate is reduced to ammonia for the synthesis of protein. This process is generally not included in denitrification because the end products remain in the system. However, true denitrification includes the “dissimilatory nitrate reduction” process, and results in removal of nitrate to nitrogen as the gaseous end-product (Moore & Schroeder, 1970). In the dissimilatory nitrate reduction, nitrate serves as the terminal exogenous hydrogen acceptor for the oxidation of an organic substrate, whereas assimilatory nitrate reduction is closely related to the use of oxygen as the hydrogen acceptor (Focht & Chang, 1975). Since the requirement of a microbial cell is greater for oxygen than for nitrogen, dissimilation proceeds at a faster rate than assimilation. Throughout this research, the term “denitrification” represents the “dissimilatory” denitrification process.

Denitrification is carried out by a number of biochemically and taxonomically diverse heterotrophic bacteria that form a specific biocenosis during the process. The denitrifying genera include *Achromobacter*, *Alcaligenes*, *Bacillus*, *Chromobacter*, *Corynebacterium*, *Halobacterium*, *Methanomonas*, *Micrococcus*, *Moraxella*, *Paracoccus*, *Propionibacterium*, *Pseudomonas*, *Spirillum*, *Thiobacillus*, and *Xanthomonas* (Gayle et al., 1989). Among these, the *Pseudomonas* genus represents the most active bacteria in natural environments and, therefore, includes the most commonly isolated denitrifiers.

The denitrifying bacteria are capable of reducing nitrate when dissolved oxygen is limited or absent in the system. According to Payne (1981), denitrification could clearly be a “second choice” mechanism for even the most active denitrifiers since oxygen has a clear precedence over any of the nitrogen oxides as terminal electron acceptor. When there is dissolved oxygen in the system, bacteria prefer to use it as the electron acceptor over nitrate. Consequently, nitrate-reducing enzymes are not produced and denitrification does not occur. Wang et al. (1995) reported that the presence of oxygen exerted an inhibition on the denitrification in two main modes: (i) repression of the formation of denitrifying enzymes, and (ii) exertion of inhibition of pre-existing enzymes on the denitrifying activity. However, according to Simpkin and Boyle (1988), the synthesis of denitrifying enzymes is either repressed little or not repressed at all even under aerobic conditions. They assumed that there were substantial numbers of denitrifiers in activated sludge that would produce the denitrifying enzymes even in the presence of oxygen. Denitrifying enzymes could still be synthesized to at least 50 percent of their maximum level, which suggested the inhibition of enzyme activity by oxygen, and not the repression of enzyme synthesis by oxygen.

Aside from anoxic conditions and essential nutrients, there are many factors that affect the performance and economics of a denitrification system such as temperature, pH, type and amount of carbon substrate, salt concentration, etc. Without knowing the influence of these parameters on the process performance,

optimum design and operation of any denitrification treatment system could not be effectively achieved.

3.2.2 Environmental Parameters Influencing Denitrification

The following sections present a detailed discussion on the influence of various environmental parameters including temperature, pH, C:N ratio and total dissolved solids on the biological denitrification process. These parameters are of importance not only from the viewpoint of understanding the denitrification process dynamics, but also because they affect the economy of the denitrification treatment system.

Most often, batch chemostat studies are carried out to determine the effects of these parameters on the specific denitrification rate and system dynamics due to their simplicity. Furthermore, it is easier to observe the response of a denitrification system to changes in the parameters of concern in batch reactors.

3.2.2.1 Effect of Temperature

One of the most significant factors that have influence on the thermodynamical and economical aspects of the denitrification process is the temperature. Considerable amount of research has been done to investigate the change of specific denitrification rates with respect to temperature. Lewandowski (1982) performed a series of experiments within a temperature range of 25 to 35°C, and concluded that

the relationship between specific denitrification rate and temperature was linear between 5 and 35°C. Delanghe et al. (1994) obtained a slightly different result. The specific denitrification rate was linear within the temperature range of 10°C to 40°C, and the denitrification activity dropped substantially outside this range. A 10°C decrease caused the activity to drop by a factor of 1.9. Later, Wang et al. (1995) studied the effect of temperature on *Pseudomonas denitrificans*, and found that the net specific growth rate increased within the temperature range of 30 to 38°C, whereas no reaction occurred at and above 40°C. They concluded that the optimum temperature for their denitrification system was around 38°C.

The reduced biological activity associated with the decrease in temperature is a particularly important parameter in denitrification process where wastewater temperatures decrease during the winter season. For example, Dawson and Murphy (1972) observed that specific denitrification rate at 5°C was one fifth of the rate determined at 20°C in their denitrification system with *Ps. denitrificans*.

Denitrification rates usually respond to changes in temperature in a manner typical of biological systems - a doubling in the denitrification rate for a 10°C rise in temperature. Mechalias et al. (1970) reported a 2.3 times increase in denitrification rate for an 11°C temperature increase. Similarly, Timmermans and Van Haute (1983) reported a temperature quotient of 3.3, indicating that the denitrification rate decreased by a factor of 3.3 when a temperature change of 10°C occurred in their system employing *Hyphomicrobium sp.*, and proving that *Hyphomicrobium sp.* was

temperature sensitive since the temperature quotient was quite high compared to other reported values.

The following expression stating that “the net specific denitrification rate at any substrate concentration could be described with the Arrhenius equation” has been followed by many researchers (Dawson & Murphy, 1972; Delanghe et al., 1994; Lewandoski, 1982) :

$$SDR = A \exp^{(-E_a / RT)} \quad (3.5)$$

where

SDR = Specific denitrification rate (mg N/mg MLVSS.hr)

A = Arrhenius constant

E_a = Activation energy (cal.g/mol)

R = Universal gas constant (cal.g^oK.mol)

T = Temperature (°K)

According to this equation, the values of the specific denitrification rate at a given concentration, when plotted semi-logarithmically versus inverse of absolute temperature, should yield a straight line. The activation energy that must be overcome by the microorganisms in order to produce the denitrification reactions could then be calculated from the slope of this line. Lewandowski (1982) reported an activation energy range of 10.9-12.3 Kcal/mol corresponding to a temperature range of 5 to 35°C for their denitrification system with varying carbon source, while Delanghe et al. (1994) reported an activation energy of 9.16 Kcal/mol within the

temperature range 10-40°C with ethanol as the sole carbon source. Similarly, Wang et al. (1995) observed an activation energy of 8.59 Kcal/mol for nitrate reduction and 7.21 Kcal/mol for nitrite reduction within the temperature range of 30 to 38°C.

3.2.2.2 *Effect of pH*

The second important factor that has influence on the denitrification process is the pH. Reactions involved in denitrification process produce alkalinity which, in turn, cause an increase in the pH of the system. Any substantial pH deviation from the optimal established value could impair the process unless a pH control unit is provided. Glass and Silverstein (1998) reported that net 0.375 equivalents of acidity were consumed for every mole of nitrate reduced to nitrogen gas in the presence of acetic acid as the carbon source. According to them, this was the main reason as to why pH increased in an “inadequately” buffered system.

The research revealed closer pH values at which the denitrification rate was maximum. Knowles (1982) reported that biological denitrification could occur in a pH range of 5 to 11, with the optimum being in the range of 7 to 8. Timmermans and Van Haute (1983) performed a series of batch tests at different pH values ranging from 6 to 10 at a constant temperature of 25°C. The optimum pH for their system was 8.3, and the change in the denitrification activity with respect to pH resulted in a bell-shaped curve. The methanol-to-nitrate ratio increased when the system deviated

from the optimum pH in order to obtain the same specific denitrification activity.

They used a mathematical expression given below to define the effect of pH:

$$SDR = \frac{SDR_{\max}}{(1 + k_i I)} \quad (3.6)$$

where

SDR_{\max} = Specific denitrification rate at maximum pH value (mg N/mg MLVSS.hr)

k_i = Constant (dimensionless)

I = Inhibitor concentration ($I = 10^{(pH_{\max} - pH)} - 1$)

Delanghe et al. (1994) conducted several batch tests to investigate the short-term effects of pH on the specific denitrification activity for their system. The optimum pH was found to be 8.1, representing the peak in their bell-shaped pH curve, and the constant (k_i) value was obtained as 0.03. Denitrification was still achieved at lower pH values of 5 and 6, but at very slower rates, whereas pH values higher than 8.5 had negative effects on the system performance. In a similar manner, Wang et al. (1995) determined that the best pH for nitrate reduction with *Ps. denitrificans* was 7.45 for their denitrification system.

In general, the reported pH values for high efficiency denitrification reactors range from 7 to 8. At low pH ranging from 2.5 to 6, the denitrification activity is inhibited severely in wastewaters with high nitrate concentration. Glass and Silverstein (1998) reported that, at pH values less than or equal to 7, denitrification

with an initial nitrate concentration of 1,350 mg N/l was completely inhibited. As pH increased from 7.5 to 8.5, and finally 9, there was a substantial increase in nitrite accumulation. The rate of nitrite reduction in the same activated sludge in the absence of nitrate increased significantly between pH 8.5 and 9. Also, the suppression of nitrite reduction in the presence of nitrate increased from 33 to 63 percent as the pH increased from 8.5 to 9. In conclusion, pH change was shown to be a clear indicator of the progress of the denitrification reactions. Thus, monitoring and control of pH was found to be necessary to enhance the performance of the system. It was also acknowledged by the same researchers that pH monitoring and control may enhance the denitrification performance of high-strength nitrate containing wastewater.

3.2.2.3 Effect of Different Carbon Sources and Carbon-to-Nitrogen Ratios

Denitrifying bacteria use a variety of organic carbon sources such as methanol, ethanol, acetic acid, lactic acid, molasses, glucose, glycerol, etc., which serve as electron donor. Therefore, the nature and quantity of carbon source is another factor that affect the performance and cost-effectiveness of the process.

A research conducted by Martiensen and Schops (1999) investigated the influence of substrate (nitrate) concentration and growth conditions on the composition of denitrifying bacteria through a series of batch studies. They concluded that the carbon supply determined the efficiency of the denitrification

process rather than the individual microbial enzyme activities. This conclusion is of prime importance in determining the type of carbon source to be used when the primary target is to achieve high denitrification efficiencies.

A number of researchers have investigated the denitrification performance of different treatment systems using different sources of organic carbon and their respective ratios. Narkis et al. (1979) studied denitrification at various carbon-to-nitrogen (C:N) ratios by using methanol, sodium acetate and residual dissolved organic matter from a chemically treated raw sewage as the carbon source, and compared the denitrification efficiencies. The critical ratios were 2.38:1, 2.3:1 and 2.3:1 BOD/N for methanol, sodium acetate and raw sewage, respectively. Complete denitrification was achieved above a ratio of 2.3:1, while a sharp decline in the process efficiency was experienced below this value. Later, Grabinska-Loniewska et al. (1985) used an upflow anaerobic sludge blanket reactor to investigate the feasibility of glycerol as the carbon source. The optimum C:N ratio was 1:1 at 600 mg N/l. Similarly, Akunna et al. (1993) determined the potentials of digested sludge to reduce nitrate and nitrite in the presence of five different carbon sources, namely, glucose, glycerol, acetic acid, lactic acid and methanol. Ammonium accumulated in glucose and glycerol media. Nitrate and nitrite reduction in acetic acid and lactic acid media was essentially a denitrification activity. However, methanol culture media showed very small nitrogen reduction rate, indicating the absence (or presence in very small amount) of the bacteria capable of denitrifying with this substrate. Later,

Sison et al. (1996) incorporated the adsorption-desorption capability of GAC into their denitrification system using sucrose in continuous, intermittent and injection modes. The results showed that both intermittent and injection modes provided possible effective alternatives to continuous mode. Activated carbon was found to be more effective in storing the carbon source than anthracite during the feeding stage. The carbon source that was stored on activated carbon was used in the starvation period.

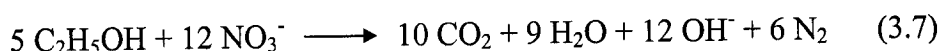
Ethanol, as the main carbon source in the denitrification process, has recently been used by many researchers, and its effectiveness has been compared to other carbon sources. In a study conducted by Constantin and Fick (1997), the system performance with ethanol and acetic acid was compared. The acclimation and growth of microorganisms and the overall denitrification was higher with ethanol, whereas the specific denitrification rate was higher with acetic acid. This was explained by the fact that acetic acid was directly assimilable whereas ethanol first had to be converted into acetaldehyde and then acetate to be assimilated. In another study, Aesoy et al. (1998) investigated the denitrification efficiency in a packed bed reactor using hydrolysed sludge (hydrolysate) and solid organic waste as a carbon source, and compared it to the cases where ethanol and acetic acid were employed as carbon sources. It was observed that the maximum as well as the most stable denitrification rate was achieved with ethanol. Acetic acid produced lower and more variable rates, whereas hydrolysate and solid organic waste produced the same maximum

denitrification rate as ethanol at much higher COD:N ratios as compared to ethanol. Another investigation conducted by Hallin and Pell (1998) on the metabolic properties of the denitrifying community that adapted to methanol and ethanol in single-sludge systems, also favored ethanol. The denitrifying population adapted slowly to methanol, whereas their adaptation to ethanol was rapid. The rapid increase in the capacity to denitrify with ethanol suggested that bacteria present in the sludge had induced enzymatic activity.

In general, a C:N ratio of 1.38:1 mol/mol is required for the denitrification process with ethanol as the main carbon source (Constantin & Fick, 1997). However, the real value is higher than the theory because some carbon is used towards the formation of new biomass. The reported C:N ratios for the denitrification process are in the range of 1.5:1 to 2.5:1, depending on the type of waste stream being treated and the treatment technique used. However, if the ratio is kept too high, the total organic carbon residual in the effluent may increase, resulting in an undesirable situation.

This research employed ethanol as opposed to methanol for several reasons. First, methanol has been the subject of many research efforts; its efficiency as carbon source has been well proven, and its popularity is attributable to its low expense. However, its toxicity makes its usage unsafe. Second, although ethanol is proven to be about 25 percent more expensive than methanol (Clifford & Liu, 1993), its safety renders it more favorable. Third, in addition to the safety concern, ethanol produces

the maximum specific denitrification activity as mentioned above. Last, the system employing ethanol is more stable than those employing other carbon sources as far as shock load handling and biomass concentration are concerned. The C:N ratio used in this research for the denitrification studies are based on the following stoichiometric relationship (Gayle et al.,1989):



3.2.2.4 *Effect of Total Dissolved Solids*

For a wastewater stream such as brine reject that is high in salt content, it is necessary to consider the effects of total dissolved solids (TDS) concentrations on the denitrification efficiency. There is an inconsistency in the reported effects of TDS on the denitrification activity in the literature. Some studies demonstrated substantial decline in the denitrification activity as the TDS concentration increased, while others reported no significant impact at all. Clifford and Liu (1993) studied biological denitrification of a spent ion exchange regenerant brine using a sequencing batch reactor. The source brine contained 0.5 N NaCl and about 835 mg N/l. They found that the denitrification rate at 0.25 N NaCl level was almost equal to that in the control reactor that did not have any salt, while the rate declined about 10 percent at 0.5 N NaCl concentration, although acclimation was provided. The C:N ratio was higher than the maximum literature value, which was 2.5 at pH 8.3. On the other hand, Van der Hoek et al. (1987) determined that 25,000 mg/l TDS only slightly

inhibited the denitrification activity. Similarly, Duncan (1995) and Denton (1996) observed complete denitrification of high salinity brines up to 18 percent of TDS concentration without significant reduction in the denitrification rate.

It is necessary to realize the importance of acclimating the denitrifiers to hypersaline brine rejects. A study by Woolard and Irvine (1994) aimed to remove phenol from a hypersaline waste brine *via* a sequencing batch biofilm reactor. The halophilic bacteria that these investigators cultivated showed tolerance to 15 percent salt concentration, and were capable of achieving 99 percent phenol removal. In another study, Yang et al. (1995) examined a mixed-culture entrapped microbial cell immobilization (EMCI) process for nitrate removal from brine waste stream that contained high salt and bicarbonate. The process was shown to be unaffected by the presence of sodium chloride and bicarbonate at concentration levels up to 20,000 mg/l. The researchers claimed that the EMCI process was better than other biological denitrification techniques with respect to tolerance to high salt conditions, process stability and performance. They hypothesized that microbial cells were capable of gradually acclimating themselves to elevated salt concentrations, which resulted in the reduction of nitrite production over an extended experimental period. Similarly, Glass and Silverstein (1999) acclimated an activated sludge sample for denitrifiers by increasing the initial nitrate concentration from 2,700 mg N/l to 8,200 mg N/l and TDS concentration from 5 to 18 percent TDS and maintaining the mixed liquor pH at 9. Their attempt for acclimation at pH 7.5 was unsuccessful. At pH 9, although

denitrification was complete, the maximum specific nitrate reduction rate declined as the nitrate and salinity concentrations increased. The maximum nitrite reduction rate also declined, resulting in substantial nitrite accumulation.

3.2.3 Biokinetic Modeling of Denitrification Process

Biokinetic studies provide information on to what extent the contaminated wastewater is amenable to the biological process employed. The information on biodegradability of the wastewater also provides a basis for the performance of the process under different operating conditions (Chiue et al., 1972). The biodegradability is based on the rate and the extent of biodegradation of the given contaminant. The rate is dependent on biochemical kinetics represented by (modified or unmodified) Monod coefficients, while the extent is determined by biochemical thermodynamics based on the contaminant degraded (Pirbazari et al., 1996).

Biokinetic parameters for the denitrification process including maximum specific growth rate (μ_m), half-saturation constant (K_s), yield coefficient (Y), and decay coefficient (k_d) could be determined through a series of batch tests or continuous flow chemostat studies (Kornaros et al., 1996; Shimizu et al., 1978). Continuous flow chemostats operated at a number of specific growth rates are generally considered the best despite being time-consuming and labor-intensive (Templeton & Grady, 1988). Furthermore, batch tests do not possess the capability of adequately modeling a continuous flow system (Moore & Schroeder, 1970). In this

research, continuous flow chemostat technique was used to determine the biokinetic parameters.

The estimation of biokinetic parameters for the FBAR denitrification process using continuous flow chemostat technique is important from the viewpoint of (i) evaluating the feasibility of the biological denitrification process for the RO brine rejects, and comparing the values obtained from these studies with the literature values, (ii) modeling the denitrification process using the Monod parameters that provide the basic inputs to predict the process dynamics under variety of operating conditions, and (iii) designing and up-scaling the process in an efficient and cost-effective way.

The widely-used steady state Monod rate expression states that there is a particular substrate concentration that is the driving force for a given microbial growth rate (Stensel et al., 1973). Since denitrification is assumed to take place in two reduction steps, nitrogen-limiting experiments - namely nitrate and nitrite limiting - in which ethanol is abundant, are used to determine the Monod biokinetic constants.

Due to economic and regulatory considerations, the concentration of nitrogen compounds in the effluent may be kept as low as possible, which may result in both nitrate and organic substrate source to become rate-limiting. If the nitrate concentration is taken as the rate-limiting substrate, which is the usual case in denitrification studies, its removal efficiency can be evaluated by varying the

operational parameters of the system. On the other hand, the dosing of organic carbon source should be maintained on such a level that it is sufficient for the denitrification process to take place, while it should not be flushed out of the system unused and violate the effluent regulations or become a major expense. Therefore, it is also necessary to conduct ethanol-limiting studies to evaluate the biokinetic parameters and the process stability.

3.2.3.1 Assumptions and Formulation of the Biokinetic Model

The assumptions made for the biokinetic model of this study are as follows (i) denitrification proceeds in two consecutive steps as explained earlier, (ii) Monod kinetics which relate the rates of bacterial growth and substrate removal to the concentration of the substrate being removed, is applicable to each step, (iii) denitrifying bacteria grow only when nitrate and/or nitrite is abundant, provided that all other nutrients and carbon source are present in sufficient quantities, and (iv) nitrate is the rate-limiting variable with respect to microbial growth. The last assumption is of significance because determination of the rate-limiting variables is considered necessary before experimental studies and process design could be initiated (Engberg & Schroeder, 1975).

Generalized Monod equation is:

$$\mu = \frac{\mu_m N}{K_s + N} \quad (3.8)$$

where

μ = Specific growth rate (hr^{-1})

μ_m = Maximum specific growth rate at saturation concentrations of growth limiting substrate (hr^{-1})

N = Residual growth limiting substrate concentration (mg/l)

K_s = Saturation constant numerically equal to the substrate concentration at which $\mu = \mu_m/2$ (mg/l)

Even though the Monod equation was originally developed using pure cultures, it has been widely and successfully applied to mixed microbial culture systems as well (Beltrame et al., 1984; Curi & Eckenfelder, 1980; Namkung, 1985). Several researchers stated that the maximum substrate utilization rate and the half velocity constant obtained using continuous cultures were, in reality, average values resulting from many predominant species found in the microbial culture (Chiu et al., 1972; Ghosh & Pohland, 1971). Therefore, biokinetic parameters for mixed microbial culture systems are characterized by a range of values rather than single ones. Nevertheless, it is well agreed that Monod equation best describes the biokinetic dynamics of wastewater treatment systems, and therefore is widely used.

However, since most treatment systems for which the Monod equation has been employed to describe are suspended systems, the question whether or not Monod equation could be applicable to attached biomass systems arise. Williamson (1973) suggested that the biokinetic values for surface-grown bacteria would be close

to those values for suspended bacteria as long as the same growth-limiting substrate is utilized in both cases.

Including all the assumptions mentioned above, the rate equations for a two-step denitrification process can simply be expressed as follows (Kornaros et al., 1996; Shimizu et al., 1978):

Cell growth:

$$\frac{dX}{dt} = \mu_{m,a} \left(\frac{N_a X}{K_{s,a} + N_a} \right) + \mu_{m,b} \left(\frac{N_b X}{K_{s,b} + N_b} \right) \quad (3.9)$$

Nitrate consumption:

$$\frac{dN_a}{dt} = - \frac{\mu_{m,a} N_a X}{Y_a (K_{s,a} + N_a)} \quad (3.10)$$

Nitrite consumption:

$$\frac{dN_b}{dt} = \frac{\mu_{m,a} N_a X}{Y_a (K_{s,a} + N_a)} - \frac{\mu_{m,b} N_b X}{Y_b (K_{s,b} + N_b)} \quad (3.11)$$

where:

X = Biomass concentration in the chemostat (mg/l)

N_a = Nitrate concentration in the chemostat (mg/l)

N_b = Nitrite concentration in the chemostat (mg/l)

$\mu_{m,a}$ = Maximum specific growth rate for the biomass consuming nitrate (hr^{-1})

$\mu_{m,b}$ = Maximum specific growth rate for the biomass consuming nitrite (hr^{-1})

$K_{s,a}$ = Half saturation constant for nitrate reduction (mg/l)

$K_{s,b}$ = Half saturation constant for nitrite reduction (mg/l)

Y_a = Growth yield coefficient for the biomass consuming nitrate (mg MLVSS/mg N)

Y_b = Growth yield coefficient for the biomass consuming nitrite (mg MLVSS/mg N)

In general, the biomass yield per unit mass of nitrogen consumed (Y) in both nitrate- and nitrite-limiting steps is determined from a plot of the specific substrate utilization rate (SDR) versus specific growth rate (μ) according to the general relation:

$$SDR = \frac{1}{Y} \mu + k_d \quad (3.12)$$

The Monod equation given in equation (3.8) could be re-written for nitrite-limiting condition as follows:

$$\mu_b = \frac{\mu_{m,b} N_b}{K_{s,b} + N_b} \quad (3.13)$$

Transforming the above equation into reciprocal form shown below, and plotting ($1/\mu_b$) as a function of ($1/N_b$) could be used for estimating the maximum specific growth rate ($\mu_{m,b}$) and the half-saturation constant ($K_{s,b}$) for the nitrite-limiting condition as follows:

$$\frac{1}{\mu_b} = \frac{1}{\mu_{m,b}} + \frac{K_{s,b}}{\mu_{m,b}} \frac{1}{N_b} \quad (3.14)$$

The Monod equation could be transformed into appropriate form for estimating the maximum specific growth rate ($\mu_{m,a}$) and half saturation constant ($K_{s,a}$) for the nitrate-limiting condition. Another differential equation could be formulated by applying the kinetic equations (3.9), (3.10) and (3.11) to the mass balance relation as follows:

$$\frac{dX}{dt} = -DX + \frac{\mu_{m,a} N_a X}{K_{s,a} + N_a} + \frac{\mu_{m,b} N_b X}{K_{s,b} + N_b} \quad (3.15)$$

where

$$D = \text{Dilution rate (hr}^{-1}\text{)}$$

Under steady state conditions, dX/dt is set to zero, and the dilution rate is set to the specific growth rate so that D could be replaced by μ :

$$-\mu X + \frac{\mu_{m,a} N_a X}{K_{s,a} + N_a} + \frac{\mu_{m,b} N_b X}{K_{s,b} + N_b} = 0 \quad (3.16)$$

where

$$\mu = \text{Overall specific growth rate (hr}^{-1}\text{)}$$

Dividing both sides by X , and then taking the reciprocal, the following equation is obtained:

$$\frac{1}{\mu - \left(\frac{\mu_{m,b} N_b}{K_{s,b} + N_b} \right)} = \frac{K_{s,a}}{\mu_{m,a}} \frac{1}{N_a} + \frac{1}{\mu_{m,a}} \quad (3.17)$$

The Lineweaver-Burke plot of $(1/[\mu - (\mu_{m,b}N_b/K_{s,b} + N_b)])$ versus $1/N_a$ yields maximum specific growth rate ($\mu_{m,a}$) from the intercept, and half saturation constant ($K_{s,a}$) from the slope for the nitrate-limiting condition.

3.2.4 Nitrite Accumulation

A number of mechanisms may be responsible for transient nitrite accumulation in many denitrification systems. In their research with different pure cultures, Betlach and Tiedje (1981) reported that different rates of reduction of the denitrification intermediates caused their accumulation, rather than any specific inhibitory mechanism. One mechanism for such an accumulation with especially pure cultures, as reported by Glass and Silverstein (1997), is a competitive advantage for electrons of nitrate reductase over nitrite reductase. Nitrite is temporarily transported out of the cells by an unknown mechanism, and then taken in for further reduction. In a second mechanism, nitrite may accumulate as a result of an imbalance between the populations of bacteria that are capable of reducing nitrate and those that are capable of reducing nitrite, rather than as a result of competition between nitrate reductase and nitrite reductase. This mechanisms could be seen in activated sludge systems hosting different types of denitrifying bacteria. Another mechanism may be the lag in the synthesis of nitrite reductase due to unfavorable environmental conditions such as presence of oxygen, and a pH that is out of the optimal range.

Wilderer et al. (1987) hypothesized that two kinds of denitrifying bacteria existed in the mixed cultures: (1) denitrifiers that are capable of reducing nitrate to nitrite only (nitrate respiring bacteria), and (2) “true” denitrifiers that are capable of reducing nitrate to either nitrous oxide or nitrogen gas. They reported that nitrite accumulation took place when glucose was consumed before the denitrification process reached completeness, which suggested that nitrate respiring denitrifiers were favored over true denitrifiers. On the other hand, the samples receiving acetate showed transient nitrite accumulation, and denitrification was complete at the end, which suggested the existence of true denitrifiers.

Lazarova et al. (1994) investigated the influence of choice of inoculum and seeding conditions on the performance of fluidized bed reactor denitrification, particularly on the residual nitrite accumulation. Even at the oxygen levels as high as 8.8 mg/l, the nitrite concentration in the biofilm of *Pseudomonas stutzeri* remained lower than the nitrite accumulated at complete anoxic conditions in the biofilm of *Pseudomonas aeruginosa*. Also, *P. stutzeri* biofilm appeared to be more insensitive to the decrease in C:N ratio than the *P. aeruginosa* biofilm with respect to nitrite accumulation. They concluded that the quantity of residual nitrite observed in biofilm reactors depended mostly on the physiological characteristics of the preponderant microorganisms rather than on the operating and environmental conditions.

In an effort to better understand the effects of C:N ratio on nitrite accumulation, a research of Oh and Silverstein (1999) investigated the effect of C:N

ratio on the exogenous denitrification in the primary anoxic denitrification basin. These investigators found that, with acetate supplied at a C:N ratio of 2:1, complete denitrification occurred in less than couple of hours with negligible concentrations of nitrite detected in the mixed liquor. On the other hand, acetate limitation resulted in either aerobic respiration during the process or partial denitrification with significant nitrite accumulation. The implication of these results is that limitation of carbon source could trigger nitrite accumulation in any denitrification system.

Despite the accumulation of nitrite, nitrate is the rate-limiting substrate for the denitrification processes operated to produce effluents with low nitrogen concentrations (Engberg & Schroeder, 1975). This conclusion is very important for both designers and researchers, as determination of rate-limiting variable is necessary before the commencement of any experimental study and process design.

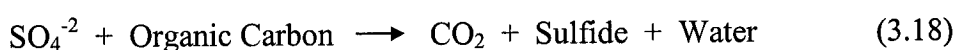
3.3 Biological Sulfate Reduction Process

3.3.1 Theory and Principles of Sulfate Reduction

The release of wastewaters from various industrial processes and by-product waste streams from treatment plants with high sulfate content is one of the major sources of pollution in receiving waters. When sulfates are present in a water system, they may cause the water to have bitter taste and odor have a laxative effect that can lead to dehydration. Currently, the only regulation limiting the sulfate levels in drinking water is a secondary standard of 250 mg/l.

Several chemical and physicochemical methods that are available today for sulfate removal are either expensive or unsuitable for large applications due to their by-products. Therefore, sulfate reduction through the use of microorganisms is potentially a valuable process that has gained much attention as an alternative treatment process to chemical treatment methods.

Dissimilatory sulfate reduction or “sulfate respiration” is the process in which sulfate ion acts as an oxidizing agent and a terminal electron acceptor for the dissimilation of an organic compound (electron donor) by sulfate-reducing microorganisms. Microbial sulfate reduction produces toxic hydrogen sulfide gas which is the hydraulization product of sulfide ion, and primarily responsible for the nuisance caused by the “noxious rotten egg odor.” However, only a small amount of reduced sulfur is assimilated by sulfate-reducing bacteria, almost all of it is released into the environment as sulfide ion. A general stoichiometric equation for sulfate reduction expressed by Postgate (1979) is as follows:



In general, sulfate-reducing bacteria are obligately anaerobic heterotrophs. However, they can survive remarkably well in aerobic terrestrial and aquatic environments by remaining dormant, and become active when the local conditions become anaerobic. They grow slowly as compared to other soil or water microorganisms partly because the growth of cultures exhibits a non-exponential trend (Postgate, 1979).

Initially, sulfate-reducing bacteria were classified according to salt tolerance and ability to use different organic carbon substrates. However, fresh water strains have been adapted to saline environments, and organic carbon classifications did not hold for all strains. Therefore, recent classification schemes use two main groups: spore formers and non-spore formers. Among all bacteria, due to the ease of isolation, the genus *Desulfovibrio* is the most commonly encountered sulfate-reducing bacteria. They are known to be mesophilic, and at the same time, can be halophilic (salt-tolerant up to 6 to 10 percent TDS) or non-halophilic (Postgate, 1979).

3.3.2 Factors Influencing Sulfate Reduction

Mixed cultures containing sulfate-reducing bacteria usually used in the treatment of wastewaters with high sulfate concentrations require an organic energy and carbon source for extensive growth and higher sulfate reduction activity. Low molecular weight organic compounds, such as acetate, propionate, ethanol, glucose, glycerol, malate, lactate, sucrose, hydrogen etc., are all known electron donors for sulfate reduction (Middleton, 1975).

Okabe et al. (1992) studied the specific growth rate and cell yield for *Desulfovibrio desulfuricans* under sulfate-limiting and lactate-limiting (carbon source) conditions. The specific growth rate and yield coefficient under sulfate-limiting conditions were lower than those obtained under lactate-limiting conditions,

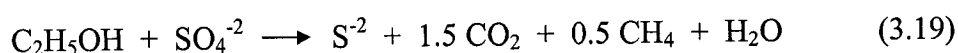
mainly due to the increase in the maintenance energy requirement. The limiting carbon-to-sulfur ratio was in the range of 45:1-120:1.

Dovark et al. (1992) reported that rates of sulfate reduction and metal retention increased by a factor of 10 when lactate was added to the nickel-contaminated influent to a reactor filled with spent mushroom compost. This suggested that the type and quantity of organic compound released by the decomposition of compost substantially limited the maximum sulfate reduction rate.

Matsui et al. (1993) conducted fluidized bioreactor experiments with mixed culture of sulfate-reducing bacteria on glucose decomposition with and without sulfate reduction. Glucose in the reactor was mainly decomposed into lactate and ethanol which, in turn, were decomposed into acetate and propionate. Sulfate reduction occurred with propionate and acetate decomposition. With sulfate reduction, propionate was decomposed into acetate, while accumulation of propionate was observed without sulfate reduction. Later, Nagpal et al. (2000) stated that some species of sulfate-reducing bacteria are capable of complete oxidation of the organic compound molecules into carbon dioxide, while others can oxidize the C2-C4 compounds to only acetate.

Among the carbon sources mentioned above, although ethanol permits poor bacterial growth, its yield of sulfide is relatively high (Postgate, 1979). Barnes et al. (1991a) employed upflow anaerobic sludge blanket (UASB) process called "Pacques Process" for sulfate reduction utilizing ethanol as the electron donor. A mixed culture

of anaerobic sulfate reducers and methanogens obtained from various natural sites and industrial waste effluents was used in the start-up of the process. The laboratory-scale reactor was able to achieve sulfate reduction rates of 7.8 g/l.day at a 4 hours hydraulic retention time, while the pilot-scale reactor achieved 10 g/l.day at a hydraulic retention time of 5 hours. They reported the overall stoichiometry of sulfate reduction in their system for the growth on ethanol as:



Temperature and nutrients are the other important factors affecting the sulfate reduction process. Postgate (1979) reported that bacterial rates of sulfide production decreased substantially at temperatures 7 to 15°C. Therefore, most of the sulfate reduction studies were conducted between 30 and 37°C. Dovark et al. (1992) suggested for their simple anaerobic reactors installed to achieve sulfate reduction coupled with heavy metal removal, that sulfate reduction rates could be increased by raising the reactor temperature into the range of 25-35°C to stimulate bacterial activity. In another study conducted by Okabe and Characklis (1992), it was reported that the maximum substrate utilization rate of *Desulfovibrio desulfuricans* was relatively constant between 25°C and 43°C, and dramatically decreased outside this temperature range. However, the stoichiometry of microbial sulfate reduction was not temperature dependent.

In addition to these, *Desulfovibrio*, the most predominant sulfate-reducing bacteria, shows an exceptionally high requirement for inorganic iron to be used as

cell constituent. For instance, addition of metallic iron to a growing *Desulfovibrio vulgaris* culture in a medium containing organic carbon causes more extensive hydrogen sulfide production than its omission (Somlev & Tishkov, 1994). Since soluble iron ions are fairly common in soil and aquatic environments, blackening due to ferric sulfide (FeS) formation is a characteristic of activity of such sulfate-reducing bacteria (Postgate, 1979). The precipitation of FeS also aids in detoxifying the growth environment of the sulfate-reducing bacteria. However, they do not require any addition of excess iron to the system when grown in wastewater or sewage sludge, as reported by Middleton (1975).

Chen et al. (1994) employed an anaerobic upflow porous media biofilm reactor with sand as the support medium, lactate as the carbon source and *Desulfovibrio desulfuricans* as the sulfate-reducing strain for sulfate removal. The appearance of well-separated black spots was the initial indication of sulfate reduction and hydrogen sulfide generation (souring). Black spots were caused by the precipitation of iron present in the medium as FeS. After seven days, the blackened zones were expanded radially indicating bacterial growth.

The same investigators also reported that biofilm accumulation in porous media is the net result of microbial cell adsorption, desorption, growth on media surfaces, detachment and filtration. The sulfate-reducing bacteria attached to a solid surface were entrapped in polysaccharide gels produced by themselves or “slime-forming” bacteria. Within these biofilms, the bacteria find themselves in a somewhat

protected environment. They also observed that, in such biofilm reactors, bacterial cells attached to the entry part of the column grew faster than those attached to the upper parts of the reactors because most of the substrate was depleted at the inlet part of the reactor. This observation is supported by an earlier work by another group of researchers (Taylor et al., 1990) who reported high permeability reduction and much thicker biofilm formation at the inlet of their reactor attributable to high substrate utilization and biofilm growth in this part.

Another factor influencing the sulfate reduction is the salt content of the wastewater. Postgate (1979) expressed that above 2 percent salinity levels, the microbial population almost always consists of *Desulfovibrio*. In a recent study, Muthumbi et al. (2001) investigated the extent to which the process of sulfate reduction with acetate as the carbon source in an upflow anaerobic sludge blanket reactor depended on the level of salinity. They further investigated whether the composition of the microbial communities in the reactor was related to the process performance at various salinity levels. They found that the salinity level in the influent had a strong influence on the reactor performance which was indicated by the sulfate conversion rate and efficiency. Optimal sulfate reduction of 14 g S /l.day (corresponding to a conversion efficiency of more than 90 percent) by acetate utilizing sulfate-reducing bacteria was achieved after raising the salinity level to between 1.26 and 1.39 percent. Raising the concentration of chloride, potassium and magnesium ions only helped to enhance the sulfate removal rate and efficiency. They

concluded that the initial increase observed in the reactor performance was due to the enhanced biological activity of the acetate utilizing sulfate reducers as a result of increased concentrations of potassium, magnesium and chloride ions in the influent. They further concluded that salinity level had an impact on the composition of the microbial communities in the anaerobic reactor.

3.3.3 Effect of Sulfate Loading and Hydraulic Retention Time

According to Dovark et al. (1992) hydraulic flowrate strongly affects the sulfate reduction performance because it determines the residence time in the reactor. Short hydraulic retention times may not allow sufficient time for the microbial activity to remove sulfate, precipitate metals and neutralize acidity formed during the process. Very short hydraulic retention times may also overcome the capacity of a reactor to generate alkalinity, which may result in the reactor interior being acidified to the point where bacterial activity is severely inhibited. On the other hand, excessively long residence times may subject a reactor to such small influent loads of acidity and metals that much of the hydrogen sulfide and alkalinity produced will exit the reactor without having been used.

Stucki et al. (1993) employed glass beads, porous lava beads and polyurethane foam in their fixed bed reactors with recycle for sulfate removal. Acetic acid was their preferred carbon source for the pure cultures of *Desulfotomaculum acetooxidans*, *Desulfobacter postgatei*, and mixed biomass from a digester that had

been loaded with sulfate. A medium containing high salt concentration was used. Sulfate reduction rates up to 60 g/l.day was reported at conversion efficiencies equal to approximately 60-75 percent. However, the process was reported to be unstable at high sulfate loading rates.

Similarly, Van Houten et al. (1994) reported employing gas-lift reactor to conduct sulfate reduction studies using hydrogen/carbon dioxide as the electron donor. Pumice and basalt particles charged into each reactor for microbial immobilization were inoculated with anaerobic granular sludge biomass that had previously been grown on volatile fatty acids and sulfate. They reported biofilm formation on pumice particles, while no biofilm formation was reported on basalt particles. Sulfate reduction rates up to 30 g/l.day at the conversion efficiencies of 50 percent were attained at a hydraulic retention time of 2.25 hours. However, higher sulfate conversion efficiencies (> 95 percent) were reported to be possible at loading rates of 18 g/l.day.

Later, Nagpal et al. (2000) employed a fluidized bed reactor to carry out sulfate reduction using ethanol as the carbon source. The mixed culture of sulfate-reducing bacteria was immobilized on porous glass beads. The process achieved sulfate reduction rates up to 6.33 g/l.day at a hydraulic retention time of 5.1 hours. They emphasized the advantage of using fluidized bed reactors over packed bed or upflow anaerobic sludge blanket reactors as the enhancement in mass transfer rates for both substrates (sulfate and carbon source) and product gas (hydrogen sulfide).

They compared the peak capacities reported by Stucki et al. (1993) at 18 hours to those reported by Van Houten et al. (1994) at 4.5 hours and their own study at 5.1 hours. From this, the researchers concluded that fluidized bed process could be used to achieve high rates of sulfate reduction at high liquid throughputs, and that the overall sulfate reduction capacity of the system depends on the feed sulfate concentration, hydraulic retention time and efficiency of the reduction capacity.

3.3.4 Simultaneous Nitrate and Sulfate Reduction in the Same Reactor

Sulfate reduction or “sulfate respiration” is somewhat analogous to “nitrate respiration.” Microbial sulfate reduction produces toxic hydrogen sulfide gas which is the hydraulization product of sulfide ion, while denitrification process produces nitrogen gas that could be released into the atmosphere (Postgate, 1979, 1984).

Denitrification process somewhat resembles the dissimilatory sulfate reduction process, but differs in significant ways. In sulfate reduction, sulfate-reducing bacteria are forced to use sulfate as their only terminal, growth supporting oxidant because they have neither the aerobic nor the fermentative alternatives that denitrifiers exhibit. Furthermore, sulfate must be first activated by the reaction with ATP to form Adenosine -5'- phosphosulfate (ATS). Then only sulfate could be reduced to sulfite. The energy yield from this reaction is actually confined to the reduction of sulfite to sulfide. Nitrate reduction or any other nitrogen oxides reduction requires no such activation by ATP or any other energizer (Payne, 1981).

Sulfate reduction also decreases the availability of the organic carbon source for the denitrification process, as sulfate ion acts as an oxidizing agent for the dissimilation of organic matter (Postgate, 1979).

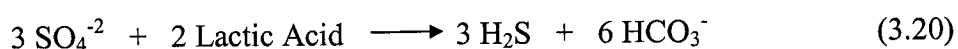
Sison et al. (1995) conducted a denitrification study with high salt regeneration brines containing 80 mg N/l employing an up-flow packed-bed GAC reactor operated at different empty bed contact times (EBCT). Sucrose solution was employed as the main organic carbon source at a C:N ratio of 1.88, and injected only once a day into the denitrification reactor. Higher denitrification efficiencies in the order of 84-89 percent were obtained from the experimental runs with 80 minutes EBCT. However, nitrate removal declined to 29 percent when EBCT was reduced to 20 minutes. The results indicated that once per day sucrose injection mode could handle 80 mg N/l loading when EBCT was kept at 80 minutes, and that EBCT was a critical factor in nitrogen removal. They concluded that, at shorter EBCT, denitrification was poor due to the unavailability of the organic carbon, as insufficient adsorption of the injected sucrose by the GAC particles took place. The same investigators also reported that sulfate reduction occurred along with denitrification in the reactors. Sulfate reduction was significant during the initial stages of the treatment cycle when adsorbed organic material level on the GAC particles was high, while it became almost negligible towards the end of the cycle. In the second set of experiments, in spite of the same influent sulfate concentrations as the first set of experiments, the columns operated at longer EBCT exhibited higher

sulfate reduction than those operated at shorter empty bed contact times. Sulfate reduction occurred mostly when nitrate was reduced to less than 5 mg/l, and took place only after the 40 cm zone from the bottom of the reactor.

Yamamoto et al. (1994) examined the effects of anoxic-oxic conditions on the growth of sulfate reducing bacteria and denitrifying bacteria in laboratory-scale sequential batch reactors. They observed that denitrifying bacteria were dominant in the anoxic-oxic conditions in which the growth of sulfate reducing bacteria was completely suppressed. However, in the anaerobic-oxic conditions, sulfate-reducing bacteria grew predominantly. Their model suggested a strong competition between denitrification bacteria and sulfate-reducing bacteria.

3.3.5 Coupling Sulfate Reduction with Metal Removal

The use of sulfate-reducing bacteria for the removal of toxic dissolved metals from the sulfate containing wastewaters by precipitation as insoluble sulfides has been widely studied (Cooney et al., 1996; Maree & Hill, 1989; Postgate, 1984; Rowley et al., 1997; Tucker et al., 1998). The general consensus has been that the reduction of sulfate into sulfide by the sulfate-reducing bacteria can effectively precipitate out the heavy metals as metal sulfides. Sulfate reducing bacteria reduce sulfate in the presence of a carbon supply such as lactic acid as follows (Dovark et al., 1992):



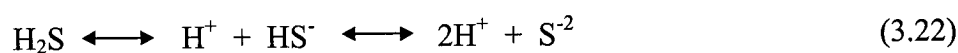
Hydrogen sulfide (H₂S) reacts with the dissolved metal content of the wastewater to form insoluble metal sulfides as follows:



where M represents heavy metals, and MS represents metal sulfides in precipitated form.

Sulfides can alleviate and prevent the toxicity resulting from heavy metals such as copper, cadmium, mercury, nickel, chromium, lead and zinc by keeping them at very low soluble concentrations in waters. This is of great importance at present because of the concern about the fate of heavy metals deposited in natural waters through waste disposal activity (Middleton, 1975). An anaerobic pilot-scale study conducted by Dovark et al. (1992) lowered the concentrations of aluminum, cadmium, manganese, zinc, nickel and iron by over 95 percent. Cadmium, iron, nickel and some zinc were retained as insoluble metal sulfides following their reaction with bacterially generated hydrogen sulfide gas. Aluminum, manganese and some zinc hydrolyzed and were retained as insoluble hydroxides or carbonates. Moreover, very little iron was ever leached from their system due to the retention within the reactor. The effluent contained high concentrations of H₂S and HS⁻, which coupled with the lowering of sulfate concentrations, indicated that microbial sulfate reduction was taking place.

Because total sulfide exists as three species, H_2S , HS^- and S^{2-} , the dissolution of H_2S in water forms the following equilibrium system (Annachhatre & Suktrakoolvatt, 2001):



The chemical equilibrium of these species is pH dependent. At pH 8, most of the total sulfides are in HS^- form, whereas at pH 6, most are in H_2S form. Low pH (< 5-6) inhibits sulfate reduction activity, and increases the solubility of metal sulfides already formed. Sulfate-reducing bacteria tend to make the environment alkaline due to the high volatility of hydrogen sulfide gas generated as a result of sulfate reduction. However, the environment tends to become acidic when there are compensating metabolic reactions leading to acid formation, or when the sulfide generated from sulfate reduction is trapped as insoluble derivatives of heavy metals (Postgate, 1979). The degree of acidity, therefore, depends on the concentrations and precipitation of heavy metals that exist in the system. When metals present in the system do not precipitate as metal sulfides, sulfate reduction alone may not be able to completely neutralize the acidity, and simultaneously produce an effluent free of hydrogen sulfide. Therefore, it is necessary to neutralize the acidity in most cases by incorporating limestone into the support medium.

3.4 Removal of Hydrogen Sulfide Gas Using Biofiltration Process

3.4.1 Definition and Principles of Biofilters

Biofiltration is a natural process in which immobilized microorganisms on a porous medium break down pollutants in a contaminated air stream. The microbial population grow in biofilms on the surfaces of the support medium. As the air is forced through the media bed in either upflow or downflow mode, the target contaminants in the gas phase absorb onto the biofilms, and either biodegraded into end products of water, carbon dioxide and biomass, or transported near the solid surface where they are eventually absorbed onto the media surfaces.

Biofiltration technology is widely used due to its practicality and affordability. In general, biofilter technology (i) has low operating cost due to low consumption of chemicals and, therefore, can be considered environmentally friendly, (ii) has high cleaning efficiency with respect to hydrogen sulfide and organic sulfur compounds of dilute to moderate concentration ranges, (iii) small space requirements at larger air flows due to relatively high velocity of the contaminated air stream, and (iv) requires low maintenance as process can be widely automated (Hansen et al., 1999). Moreover, it does not produce undesirable end-products as in chemical processes. The resultant by-product is very low in volume and easy to handle or dispose of.

The effectiveness of a biofilter is largely governed by the quality and properties of the support medium employed and the ability of the host microbial

populations. The support medium, which is the heart of a biofilter, provides optimal environment for the microbial attachment and growth. The ideal biofiltration medium should have large surface area, should be relatively homogeneous with high porosity to allow uniform air distribution with low pressure drop across the filter bed. Furthermore, the medium should preserve its structural integrity throughout the biofilter operation, and minimize the need for maintenance and replacement (Leson & Winer, 1991; Sorial et al., 1995).

Many different types of biofilter media have been used by the investigators. The media used in biofiltration practices are categorized as either natural or synthetic (Den et al., 1998). Natural media are comprised of predominantly composts, wood bark, peat and different soils, while synthetic media include ceramic and activated carbon. Compost, being the most popular natural medium usually in commercial applications, carries indigenous microorganisms and provides a natural reservoir of nutrients. However, its poor structural stability, high susceptibility to compaction and self-degradation issue makes periodical replacements necessary. Soils possess the advantages in low cost, long-term stability and strong buffering capacity, and they are easily rewetted due to their hydrophilic nature. On the other hand, synthetic media such as GAC possess excellent stability, provide large surface areas and irregular pore structures and, therefore, have become increasingly popular in recent years. Generally, GAC has the most adsorptive capacity among others. This could be the main reason as to why it could adjust to the shock loads and adapt to higher influent

contaminant concentrations in a very short period of time without any offset in the process efficiency. Unlike organic natural media, GAC is not self-degraded by the microorganisms during the waste gas elimination process. GAC also manifests a high buffering capacity in addition to its beneficial structural characteristics (Den et al., 1998). However, on a cost basis, GAC is more expensive than others. A balance should be established between the cost of the media to be employed and the targeted efficiency levels desired.

Another key element in the biofilter operation is the microbial population growing on the medium surfaces as biofilms formed generally by microbial polysaccharides production. The thickness of the biofilm is a critical parameter because of its close association with the efficiency and pressure drop across the biofilter bed. The thickness of the biofilms is determined by the rate of biomass growth and decay, accumulation of inert organic material from decayed biomass and biopolymers from substrate degradation, and erosion and transport of biomass.

3.4.2 Importance of Moisture Content, Nutrient and pH Control

Critical biofilter operational and performance parameters include moisture content, nutrient content and medium pH. Better performance in a biofilter greatly depends on the optimization of these parameters. Among these, moisture content maintained across the biofilter bed is the most important operating parameter. Biofilters usually incorporate the addition of water required for the survival and

activity of the biofilms. Insufficient moisture content across the biofilter bed results in the diminished microbial activity and poor biofilter performance. It also creates shrinkage and channeling problems in which the waste air escapes through the channels prior to having enough contact time for complete biodegradation. On the other hand, excessive moisture may cause problems such as medium compaction, further increase in the pressure drop, prevention of oxygen penetration and subsequent formation of anoxic zones across the filter bed (Devinny, 1998a, b).

Nutrient content is also an essential parameter for the growth and survival of the filter biomass and the efficiency of the biofilter operation. Natural filter media contain nutrients in sufficient quantities that no extra addition is necessary, whereas nutrients must be supplied on a regular basis if synthetic media are used. Adequate amounts of organic and inorganic nutrients such as nitrogen, phosphorous, sulfur, potassium, calcium, iron, and other trace elements must be sprayed onto the filter bed. However, these nutrients should be fed to the biofilters at optimal levels as overabundance may cause excessive biomass growth and consequent filter clogging (Den et al., 1998).

The last important parameter affecting the biofilter performance is the pH maintenance within the biofilter bed. Microorganisms attached onto the filter medium require an optimal pH range of 6 to 8 in order to function effectively. The pH in a biofilter usually changes during the operation because of the metabolic reactions of the aerobic microorganisms which evolve carbon dioxide or acidic

metabolic intermediates that lower the medium pH beyond the tolerance level of the biomass. Materials such as dolomitic limestone or crushed oyster shells are added to the medium before the operation to provide sufficient buffering capacity (Webster, 1996).

3.4.3 Hydrogen Sulfide Removal Using Biofilters

Hydrogen sulfide is generally considered to be the most important inorganic malodorant in treatment works due to its high concentration and low odor threshold. It is oxidized by chemotrophic microorganisms ordinarily involved in the sulfur cycle. *Thiobacillus* species including *Beggiatoa*, *Hyphomicrobium* and *Thiothrix* genera, could be used in different packing materials to eliminate hydrogen sulfide. These bacteria are capable of oxidizing hydrogen sulfide to elemental sulfur (S^0) and storing it in their cells. The elemental sulfur is further oxidized to sulfate (SO_4^{-2}) if the concentration of hydrogen sulfide is low (Chung et al., 1996). In this cycle, hydrogen sulfide passes sequentially through the pyrite, elemental sulfur, and polythionate intermediate stages before eventually being converted to sulfuric acid (Bohn & Bohn, 1988). The simplistic representative equation for hydrogen sulfide removal is:



There has also been quite a number of biofiltration research conducted on the removal of hydrogen sulfide and the parameter matrix affecting the process

performance. For instance, Dombroski et al. (1995) conducted a series of pilot tests at a kraft pulp mill, and reported efficiencies of well over 99 percent for hydrogen sulfide up to a concentration of 350 ppmv. The improvement in the removal efficiency was remarkable within a short period of time when *Thiobacillus thiooxidans* strain was used to inoculate the filter medium. Van Langenhove et al. (1996) conducted a biofiltration study using wood bark as the filter medium instead of compost to eliminate hydrogen sulfide of approximately 10 ppmv. The process achieved full success in converting nearly all hydrogen sulfide to sulfate under optimal conditions. However, moisture content less than 60 percent severely lowered the removal efficiency. Chung et al. (1996) used a heterotrophic strain, *Pseudomonas putida* CH11, immobilized onto Ca-alginate that provided the packing material in their biofilter used to control the hydrogen sulfide from POTWs. The process was able to attain 97 percent removal of hydrogen sulfide of 5 ppmv to 100 ppmv at hydraulic retention time of 28 seconds. Similarly, Torres et al. (1996) and Webster et al. (1996) conducted several pilot-scale studies for a wastewater treatment facility, and observed complete oxidation of hydrogen sulfide in a waste gas stream that contained approximately 3 ppmv of hydrogen sulfide and a mixture of volatile organic compounds (VOCs). They reported that the removal actually took place within the inlet portion of the filter bed at hydraulic retention time of 70 seconds. At lower hydraulic retention times, the bed efficiency decreased slightly because of deeper penetration of sulfides and subsequent filter bed acidification.

There is a great need to develop a process for the removal of this gas because of its toxicity, noxious odor and corrosive properties. Cork and Casanovich (1978) stated that accumulation of hydrogen sulfide in sulfate containing wastewater treatment by bacterial sulfate reduction is a potential problem because in excess of several millimoles per liter of hydrogen sulfide can inhibit the growth of sulfate-reducing bacteria. They suggested two schemes to remove it from the wastewater. One is to strip it by passing an inert gas through the fluid, and trapping it in ferric chloride solution where it is oxidized to elemental sulfur. Another is to strip it from the fluid, and to introduce it into a culture of photosynthetic sulfur bacteria for oxidation into sulfur.

This research employed the second method, referred to as biofiltration process, in an effort to remove the odor caused by hydrogen sulfide in the laboratory where all the experiments had been conducted.

CHAPTER 4

PRINCIPLES AND MODELING OF FLUIDIZED BIOADSORBER REACTORS FOR BIOLOGICAL DENITRIFICATION PROCESS

This chapter presents the theory of fluidized bioreactors, their advantages over other conventional processes, working principles and design criteria. A brief historical perspective is presented on the application of fluidized bioreactors for the denitrification process. The advantages of granular activated carbon used as the support medium is explained, and a brief literature review on the past biofilm modeling efforts is included. The formulation and components of the mathematical model for the fluidized bioadsorber reactors with recycle employing granular activated carbon for denitrification process are introduced along with the basics of the numerical solution to the model and the theory on the estimations of the model parameters.

4.1 Theory and Advantages of Fluidized Bioreactors

Fluidized bioreactors are up-flow reactors designed on the principle that a support medium provides an appropriate microenvironment and growth of biofilms to enhance the effectiveness of substrate degradation. The major fraction of the system microorganisms is attached to the support media, while a small fraction is

still present as suspended in the bulk solution. The feed is passed upward through the bed at a velocity sufficiently high to expand or fluidize the reactor bed beyond the point at which the frictional drag force is balanced by the net downward force exerted by the gravity. The fluidized condition is achieved by either high influent flowrates, or by high recycle ratios, which make them approach completely mixed regime. Figure 4.1 illustrates a general schematic of a fluidized bed bioreactor used in denitrification processes.

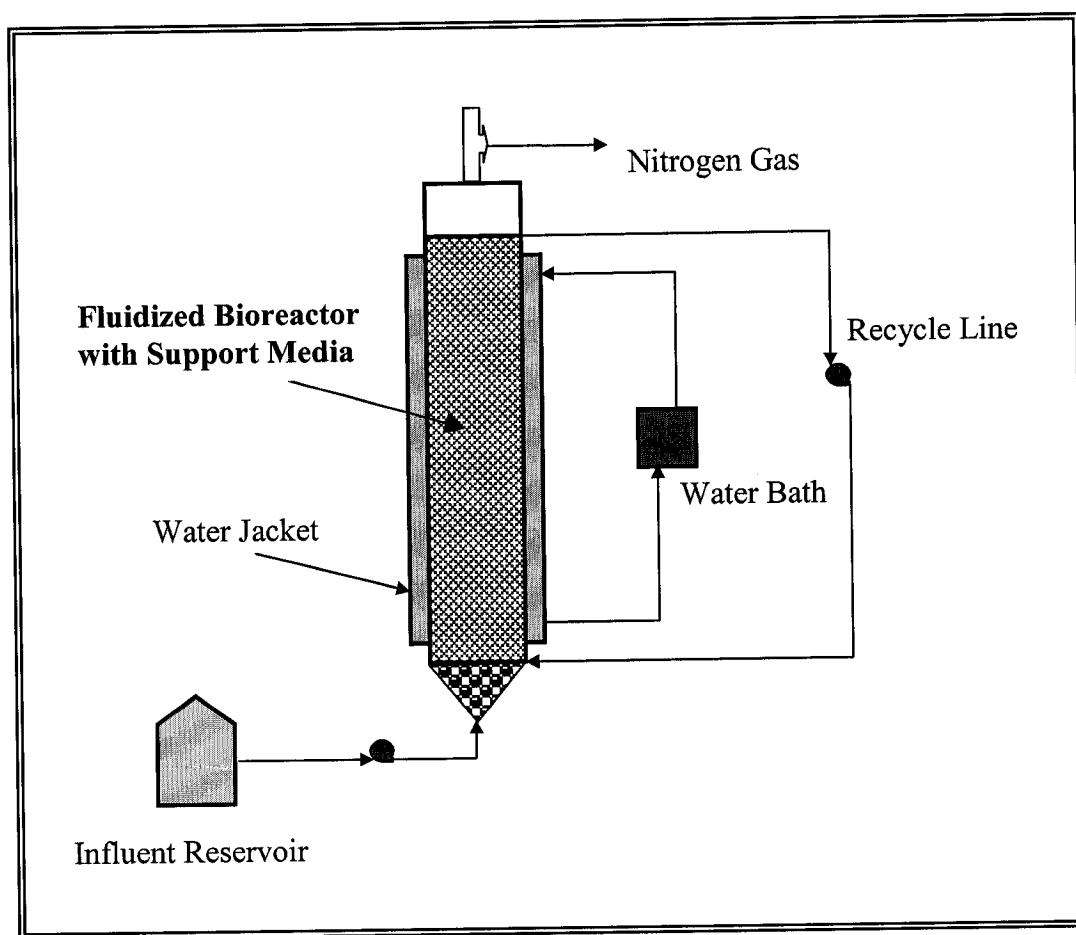


Figure 4.1. General schematic of a fluidized bioreactor treatment system

The history of fluidized bioreactors dates back to 1970s, as mentioned by Mulcahy (1978). Beer (1970) suggested the potential application of a biological fixed-film reactor for biological denitrification process in which granular material such as sand, glass beads or activated carbon could be used as the support medium for the microorganisms. Upon this suggestion, Jeris et al. (1974) initiated the research on fluidized bioreactor denitrification utilizing sand and activated carbon. They reported that poor biological growth was achieved in the fluidized bioreactor with sand particles, while excellent biomass growth and nitrate reduction was obtained in the fluidized bioreactor charged with fresh activated carbon after two weeks from startup. The same researchers also noted that an empty bed contact time of 15 to 20 minutes required for the fluidized bioreactor with activated carbon was significantly less than that required by conventional biological systems. These researchers concluded that the fluidized bioreactor technique had the capacity to handle extremely high hydraulic and nitrate loadings with very low hydraulic detention times.

Although the fluidized bioreactor concept and its advantages over other conventional technologies have been realized for quite a long time since 1974, and studied extensively on the laboratory- and pilot-scale, there were no known full-scale fluidized bioreactor plants in operation until 1980s (Heijnen et al., 1989). After overcoming the operational constraints such as unstable process, low reactor capacity, small substrate spectrum, etc., fluidized bioreactors have become more widespread, and constructed and operated successfully in full-scale systems since 1984 (Godia &

Sola, 1995). The results of these studies and operations have been that fluidized bioreactor technology has proven to be a suitable process for water and wastewater treatment.

The fluidized bioreactors are usually preferred in biological denitrification processes over other available conventional biological denitrification technologies such as activated sludge process, trickling filters and fixed-bed systems mainly for two reasons: (i) nitrate concentration of wastewater streams is suitable to be removed by biological denitrification process, and (ii) nitrate is actually removed rather than being concentrated or converted into another form, and large amounts of undesirable waste by-products such as regeneration brines are not produced. Several other potential advantages can be summarized as follows:

- The fluidized bioreactors with recycle can provide over 5 to 10 times the microorganism concentrations as compared to suspended growth processes, which is an important aspect for meeting the low-level nitrogen removal objective (Sadick et al., 1996).
- The microorganisms in the fluidized bioreactors appear to be relatively resilient to shutdowns and are capable of handling shock loadings (Heijnen et al., 1989).
- Fluidized bioreactor process with recycle has a reduced reactor size (Sutton & Mishra, 1991). Therefore, it holds promise for meeting space requirements of those treatment plants located in densely populated areas, and those who are trying to

meet the current or predicted effluent nitrogen requirements with conventional fixed-film or suspended growth technologies (Sadick et al., 1996).

- The fluidized bioreactor process is relatively simple to operate and maintain, and entails lower operational problems arising from clogging or head loss (Mulcahy et al., 1980).
- Fluidized bioreactors generate minimal quantity of bio-sludge and high quality effluent in addition to being cost-effective in terms of low capital cost.

4.2 Design Criteria and Operational Dynamics of Fluidized Bioreactors

There has been considerable amount of research to investigate different aspects of the fluidized bioreactor technology that would greatly aid the process modeling and design. Yoder et al. (1995) summarized the most important parameters in the modeling and design of fluidized bioreactors as: (i) size of the bioreactor, (ii) type, size and density of the support media employed, (iii) the quantity of biomass and thickness of biofilm, (iv) expansion in bed height due to biofilm growth and hydraulic flow, and (v) superficial velocity. These variables are closely interrelated to each other and, therefore, a one-by-one discussion is almost impossible. The following sections present a detailed discussion on these parameters and the operational dynamics and correlations among them.

4.2.1 General Design Criteria for Fluidized Bioreactors

4.2.1.1 Support Medium Characteristics

The size of a fluidized bioreactor is usually determined by the applied flowrates, the influent substrate concentration and the temperature provided across the bioreactor (Yoder et al., 1995). The selection of support media type and volume, on the other hand, is an important means by which biomass concentration and biofilm thickness in a fluidized bioreactor is controlled. In general, increasing the support media volume gives rise to the increased biomass concentration. Mulcahy and Shieh (1987) emphasized that the use of larger and denser support media, while maintaining the superficial velocity and support media volume constant throughout the operation, results in increased equilibrium biofilm thickness. However, Jeris et al. (1982) determined that process start-up using sand of 0.35 mm in diameter is much faster than that of using sand of 0.75 mm in diameter, attributing it to the lower liquid shear with smaller particles.

4.2.1.2 Correlation Between Substrate Loading and Biomass Concentration

The general operating rationale for optimization of fluidized bioreactors is to introduce the feed to the reactor without any pre-treatment, and have a near-zero substrate discharge. In order to accomplish this, the desired operating strategy for the fluidized bioreactors could be either to minimize the biomass production or to maximize the substrate removal rate. Requa and Schroeder (1973) stated that the nitrate removal rate in a fluidized bioreactor depends on nitrate and biomass

concentrations present in the system. Thus, any effluent nitrate concentration is theoretically possible at any hydraulic retention time. The choice between using nitrate and biomass concentration for controlling the removal efficiencies of nitrate is usually handled by maximizing the biomass concentration. As the mass-loading rate of nitrate increases, the biomass production also increases. As long as the cells are not washed out from the bioreactor, the biomass concentration keeps increasing.

According to Safferman and Bishop (1997), the two most important design parameters for a fluidized bioreactor are the substrate loading per unit of biomass and the biomass per unit of support medium. The greater the biomass concentration, the greater is the rate of substrate removal up to the point where diffusion into the biofilm layer becomes limiting. In the same way, biomass growth is directly related to the substrate loading; the higher the loading, the more biomass is produced. In short, the biomass control of the fluidized bioreactors is governed by the control of the substrate loading into the system or vice versa.

4.2.1.3 Correlation Between Biofilm Density, Biofilm Thickness and Media Bed Expansion

There is a strict correlation between biofilm density and biofilm thickness in a fluidized bioreactor. As indicated by Ro and Neethling (1991), the biofilm density in a fluidized bioreactor is not constant, but decreases as the biofilm thickness increases. Therefore, a thicker biofilm will form a larger but less dense particle. This finding is important in order to understand the interactions between the particle

characteristics and particle settling velocity, a critical parameter in designing and operating fluidized bioreactors. The less dense bioparticles will cause excessive bed expansion and move to the upper part of the reactor. With a high superficial velocity, these bioparticles may leave the bioreactor with the effluent or recycle flow, which could cause operational problems, such as clogging in the pipes and pumps, poor treatment efficiency and unstable effluent quality. To prevent this, most fluidized bioreactors are designed with mechanical equipment that sloughs off the excessive biomass from the support media.

Blanco et al. (1995) determined that the extent of biofilm growth on the bed expansion was significant and that it was necessary to reduce the recirculation ratio to maintain a proper set of expansion as the attached biomass in the reactor increased. In their bioreactor, the biofilm growth was accompanied by an increase in the bed segregation in that the attached biomass concentration was always greater at the top of the reactor than at the lower levels. At the lower levels, the microbial growth was slower, reaching only half or third of that at the top. They also concluded that the biofilm development had much higher effect on the hydrodynamic behavior in fluidized bioreactors than the formation of a gas phase produced as a result of microbial activity.

Lazarova and Manem (1995) reported that biofilm activity in a fluidized bioreactor was not proportional to the quantity of fixed biomass, but it increased with the thickness of the biofilm up to a pre-determined level termed as the “active thickness.” The diffusion of substrate into the biofilm became a limiting factor above

this level, thus differentiating an “active biofilm” from an “inactive biofilm.” They further stated that a stable, thin and active biofilm on a support medium thus offers numerous advantages in wastewater treatment systems.

4.2.1.4 Correlation Between Biofilm Thickness and Superficial Velocity

A study conducted by Narjari et al. (1984) investigated the effect of superficial velocity on the removal of nitrate as well as on the growth of biomass in a fluidized bioreactor that utilized sand particles. Initially, there was a steep decline in the effluent nitrate concentration with time, but eventually the concentration approached steady state. Nitrate removal reached a maximum at a specific superficial velocity, and at this velocity the biofilm thickness also reached a maximum. When the superficial velocity was increased, the biofilm thickness decreased due to increased drag and shear on the bioparticles as well as sloughing between them.

Unlike these researchers, Lazarova and Manem (1995) determined that more rigid and homogeneous biofilms were obtained in the presence of strong shear stress between the media particles in a fluidized bioreactor due to the ability of some bacterial strains to form homogeneous layers of micro-colonies. Similarly, Shieh et al. (1996) concluded that the mechanical attrition caused by intraparticle collision was unlikely to alter the balance established between bacterial growth and maintenance mechanism under the fluidization conditions commonly maintained in steady state anaerobic fluidized bioreactors. This conclusion was reached because the

biomass loss rate in the reactor remained constant when the degree of media bed expansion varied from 10 to 120 percent.

4.2.2 Operations Dynamics and Correlation Techniques for Fluidized Bioreactors

The factors affecting fluidization biomass concentration in a fluidized bioreactor including biofilm thickness, superficial velocity and expanded bed height, as mentioned above, have historically been calculated by using correlation equations or by laboratory- or pilot-scale experiments. Many research efforts have been focused on finding correlations among these parameters through mathematical models that serve as a basis for system optimization (Mulcahy et al., 1980; Richardson & Zaki, 1954; Shieh, 1980).

Ngian and Martin (1980) operated a fluidized bioreactor with char particles coated with denitrifiers. They observed the correlation developed by Richardson-Zaki (Richardson & Zaki, 1954) for homogenous spherical particles produced satisfactory results in the estimation of bed expansion index, but only under limited conditions. At a later date, Mulcahy and Shieh (1987) reported that the Richardson-Zaki's correlation (Richardson & Zaki, 1954) provided an excellent description of fluidization mechanics in their fluidized bioreactor denitrification studies. They emphasized that the correlations for computing drag coefficient and bed expansion index should be specific to fluidized bioreactor particles. They developed correlations to predict the bioparticle terminal settling velocity and

biomass concentration. However, it must be noted here that these correlations could “only” be used for fluidized bioreactors that operate under operating conditions similar to theirs.

4.3 Different Approaches of Biofilm Modeling and Dynamic Fluidized Bioreactors Modeling

4.3.1 Biofilm Modeling Approach with GAC as the Support Medium

4.3.1.1 Advantages of Using GAC as the Support Medium for Biofilms

Of all the media, GAC is an excellent adsorber, which is attributable to its large surface area (in the order of 800-1500 m²/gr), high degree of surface reactivity, universal adsorption affinity, and favorable pore size and structure (Bansal et al., 1988). Furthermore, GAC has lighter density compared to, for example, sand, another widely used support medium (Coelhoso et al., 1992). This could be considered a significant property as far as the cost-effectiveness in terms of energy of the operation is considered.

Different types of support media have been used, and the system performances have been compared. In their study, Pirbazari et al. (1990) compared various natural and synthetic media including ion exchange and carbonaceous resins, sand and activated carbon under similar environmental conditions. It was shown that GAC supported a richer biological growth than any of the other media. They pointed out that the adsorptive and morphological features of GAC provide favorable conditions in terms of substrate and nutrient concentrations and that the adsorptive

capacity of activated carbon is higher than the other support media due to its surface characteristics.

In another study, Coelho et al. (1992) compared the denitrification results in fluidized bioreactor with GAC and sand. They reported that the average cell residence time for GAC particles was much lower than that for sand particles. Moreover, the quantity of nitrate consumed per quantity of biomass in the fluidized bioreactor with GAC was substantially larger than that of with sand particles. Lastly, the biomass yield was three times greater in fluidized bioreactor with activated carbon than the bioreactor with sand. They concluded that fluidized bioreactors utilizing GAC as the support for the biomass growth had much more homogeneous biomass spatial distribution than those using sand as the support. This observation was of utmost importance in their modeling of the fluidized bioreactor process.

The study reported herein employed activated carbon because of its marked advantages over other media (Kim & Pirbazari, 1989; Pirbazari et al., 1990). First, activated carbon has an adsorption affinity for the removal of biologically resistant compounds that may be toxic to the biofilm microbial community. Second, the principal partitioning factor or driving force in a non-activated support media such as sand is the free energy for “biological adsorption.” In a system in which the support medium is activated carbon, the partitioning factor for most chemical constituents is that of “adsorption,” which has a substantially higher free energy. Third, the rough surface and the pits and crevices on the surface of activated carbon particle provide shelter for the microorganisms from high fluid shear. Fourth, the high adsorption

capacity of activated carbon renders the biofilm resistant to shock loads and fluctuating substrate concentrations. This observation is of utmost significance for biofilm reactor systems.

4.3.1.2 A Historical Perspective of Biofilm Modeling with GAC

Several mathematical models have been developed to incorporate biological activity in biological reactors that employ GAC. These models have emphasized the importance of transport of substrate in the liquid phase, intra-particle transport kinetics, bacterial growth kinetics and microbial biodegradation, and adsorption onto the solid phase as the parameters influencing the biodegradation and adsorption onto the GAC particles.

Ying and Weber (1979) developed a model that included liquid film transfer, intra-particle diffusion, Monod kinetics for substrate utilization and biomass build-up. The biofilm thickness was considered to be a function of both time and distance into the bed, and it kept growing until it reached a certain thickness, which was maintained the same by washing the media and air scouring. Their model was applicable to both completely mixed and plug flow fluidized bioreactors, and had good predictive capability for glucose and sucrose.

Andrews and Tien (1981) presented a model for the biological activity based on completely mixed tank assumption. The model included the following phenomenological assumptions: (i) liquid film and solid phase mass transfer resistance were considered negligible, (ii) organic material was assumed to be

present in low concentrations to limit the biomass growth, and (iii) organic material consumption by biofilm was assumed to follow first-order kinetics. Their model exhibited satisfactory predictive capability with respect to the dilute concentration of organic substrate (valeric acid).

Subsequently, Speitel et al. (1987) and Chang and Rittmann (1987) proposed similar models as Andrews and Tien (1981) based on the fundamental mechanisms of film transport, biodegradation within the biofilm, adsorption within GAC and growth of the biofilm. The Chang and Rittmann (1987) model was for completely mixed stirred tank reactors, while the model of Speitel et al. (1987) was for plug-flow fixed bed configurations. In essence, both models were efficient in predicting the effluent substrate concentration profile of a single substrate (phenol) in low concentrations.

The mathematical model used in this research was first introduced by Pirbazari et al. (1989), and Kim and Pirbazari (1989), and it effectively predicted the adsorption and biodegradation phenomena in their fluidized bioreactor employing GAC as the support medium. In this research and modeling approach, however, since GAC has been known with its adsorptive features, the term “fluidized bioreactors” will be replaced by a new term “fluidized bioadsorber reactors (FBAR)” from this point forward of this research. The model will be updated to provide the fundamental approach to the modeling of the FBAR denitrification process for the RO brine rejects.

4.3.2 Biofilm Modeling Approach of Denitrification Process for Fluidized Bioreactors with Different Support Media

Models for fluidized bioreactor denitrification process have been proposed by many researchers (Boaventura & Rodrigues, 1988; Hancher & Perona, 1982; Kim & Pirbazari, 1989, LaMotta & Cascante, 1996; Mulcahy et al., 1980; Shieh, 1980; Williamson & McCarty, 1976). In all these models, the substrate conversion reactions and the biofilm kinetics were assumed to be either zero- or first-order, or based on Monod equation.

A simplified mathematical model developed by Mulcahy et al. (1980) for a fluidized bioreactor denitrification process assumed both zero-and first-order kinetics and a three-step model: (i) transport of substrate from bulk-liquid to liquid-biofilm interface (external mass transfer), (ii) transport of substrate within the biofilm (internal mass transport), and (iii) substrate conversion reaction within the biofilm (biodegradation). Similarly, Shieh (1980) investigated various parameters affecting the denitrification performance in fluidized bioreactors to verify his proposed mathematical model. He assumed that the substrate conversion reactions followed intrinsic zero-order kinetics, and were limited by the diffusion of the substrate within the biofilm. He also assumed that the internal mass transfer resistances were such that the substrate penetrated only partially into the biofilm. He concluded that biofilm thickness and media size were the two most important parameters affecting the fluidized bioreactor performance, and an optimal value existed for each of these

parameters under a given set of operating conditions that maximized the substrate conversion rate.

Later, Boaventura and Rodrigues (1988) developed their models for fluidized bioreactor denitrification based on the reaction scheme of two consecutive zero-order reactions. This enabled them to distinguish three regimes arising from the competition between the reaction and transport of nitrate and nitrite species inside the biofilm. Their model also incorporated mass transport of nitrates and nitrites by diffusion into the biofilm.

Similarly, LaMotta and Cascante (1996) showed that zero-order approximation provided adequate description of anaerobic substrate consumption in an experimental fluidized bioreactor denitrification operating under a wide range of effluent concentrations. They proposed a simple correlation between influent and effluent substrate concentrations and suggested that complete penetration model for nitrate proved better than the partial penetration model.

In an earlier work, however, Williamson and McCarty (1976) reported that the substrate utilization is a process of molecular diffusion and simultaneous biochemical reaction governed by Monod kinetics. Later, Kim (1989) applied Monod kinetics to his fluidized bed bioreactor model by using the one-point orthogonal collocation method.

4.4 Modeling of FBAR with GAC for Biological Denitrification Process

4.4.1 Significance of Modeling Approach

The optimal design of FBARs with GAC for the biological denitrification process necessitates prior modeling efforts in order to estimate the feasibility, performance and cost of the process. In other words, the efficiency evaluation and cost-effective design of FBARs for denitrification process are essentially predicated upon the application of such phenomenological models. Usually, a great deal of time, effort and finance are invested in predicting the operational dynamics of bioadsorber reactors. Traditionally, the planning and design stage of bioadsorber reactors require extensive and costly pilot-scale testing. However, a robust model can considerably decrease, if not eliminate, the amount of intensive experimentation and the need for expensive as well as time-consuming pilot-scale studies. Moreover, the model can smoothen the transition from pilot-scale to full-scale implementation of the bioadsorber reactors. Well-designed laboratory-scale studies may be sufficient for model verification and validation as well as model refinement.

A functional mathematical model incorporates the estimation of overall adsorption, biodegradation and any other mechanisms of removal of nitrogen compounds in a FBAR, and predicts the influence of changing operating conditions on the reactor performance. Furthermore, a mathematical model that has been proven to be successful also facilitates a better understanding of various phenomena occurring in the reactor and associated interaction mechanisms among

microorganisms, substrate and support particles. Finally, a good model makes it possible to determine the size of the process reactor of interest, and would be a useful tool for the design engineers in up-scaling the process from bench-scale to pilot-scale and eventually full-scale.

In this research, a feedback modeling approach was used. In other words, the results from mini-pilot scale studies were employed as a feedback to verify the predictive capability of the mathematical model, and to introduce model refinement whenever necessary (Ravindran et al., 1997).

4.4.2 Model Milieu and Assumptions

The first step in developing a conceptual model involves understanding of the system fundamentals and its essential components. Microorganisms introduced in the FBAR attach themselves onto the external surfaces of the activated carbon particles, and form biofilms as they consume the substrate in the feed and begin to grow. Initially, the biofilm is very thin, and much of the substrate becomes adsorbed by the particle surface, if the substrate is adsorbable. As time progresses, the biofilms grow in thickness, the extent of which depending on the substrate concentration until the substrate diffusion is no longer possible through the most inner layers of the biofilms. At this point, shear/sloughing effects of the moving fluid at the outer layers of biofilms and decay within the biofilms become effective. The biofilm thickness is stabilized by new growth, and the effluent substrate concentration reaches a steady value, all indicating that steady state operation is reached.

It is of prime importance to maintain a steady state in the FBAR to achieve high reactor performance. At a steady state, the active biofilm volume in the column reaches a constant value even if the biofilm thickness increases with time. This is experimentally justifiable since a biofilm reactor operated under constant conditions reaches a steady state at some point of the operation where the rate of substrate removal is constant with respect to time (Skowland, 1990). This would justify the use of a steady state mathematical model to describe the system operation and performance.

The model described herein considers recycling. Fluid recycling has been taken into account in this research since high recycle ratios may be used in many FBAR operations in order to: (i) alleviate the bed clogging and pressure drop problems, (ii) increase the extent of mixing, and (iii) prevent the bioparticle agglomeration and to increase the shear in between the particles.

In addition to recycling, adsorption and degradation phenomenon in biofilm and bulk liquid phase have also been considered (Kim, 1987; Kim & Pirbazari, 1989; Ravindran et al., 1997). However, the preliminary laboratory-scale adsorption studies showed that nitrate was marginally adsorbed onto the GAC particles. This necessitated a modification in the model by excluding the adsorption phenomenon, and changing the boundary conditions for the related equations. The model incorporated substrate transport from bulk liquid to biofilm through an external liquid film, mass transfer and degradation within the biofilm and bulk liquid phase,

and growth of biofilm. Based on these mechanisms, the important assumptions made during the development of the model are as follows:

- The FBAR has uniform cross sectional area, and mixing and fluidization are achieved by high up-flow velocities and/or recycle ratios.
- Activated carbon particles are spherical, and support biofilm formation.
- Biodegradation occurs in both the biofilm layer and bulk liquid phase (none occurs in the carbon particle), and biodegradation kinetics can be represented by Monod equation.
- The biofilm is homogeneous with respect to porosity, composition and density.
- The biofilm growth does not substantially affect the porosity of the fluidized bed nor affects the flow pattern of the liquid.
- The biofilm thickness increases as a function of time, and will eventually reach a maximum value. At this point, loss of biomass due to shear and decay is balanced by the formation of new biomass. The biomass loss from the activated carbon surface is directly transferred to the bulk liquid phase in suspended form.

4.4.3 Formulation of FBAR Denitrification Process with Recycle

For the substrate uptake by a biofilm formed on the surfaces of the support medium in a reactor, substrate must first be transported from the bulk fluid into the biofilm. This process may occur in three steps: (i) transport of substrate from the bulk fluid to the fluid-biofilm interface (external mass transfer), (ii) transport of

substrate within the biofilm (internal mass transfer), and (iii) substrate consumption reaction (biodegradation) within the biofilm. Figure 4.2 shows the general schematic for the FBAR formulation, and Figure 4.3 demonstrates the schematic representation of a single bioparticle in FBAR.

The following section describes each of these steps with respect to their phases.

4.4.3.1 Liquid Phase Material Balance

The material balance on the substrate N (nitrate) for any differential segment of the FBAR is represented by the following equation:

$$\frac{\partial N(x,t)}{\partial t} = D_x \frac{\partial^2 N(x,t)}{\partial x^2} - v_x \frac{\partial N(x,t)}{\partial x} - \frac{3k_{fc}(r+L_f)^2}{r^3} \frac{(1-\varepsilon)}{\varepsilon} [N(x,t) - N_{f,s}(x,t)] - \frac{\mu_{m,a}N(x,t)}{Y_a[K_{s,a} + N(x,t)]} X_l(x,t) \quad (4.1)$$

where

N = Bulk substrate concentration at any time t in the FBAR (M/L^3)

$N_{f,s}$ = Substrate concentration at biofilm-hydrodynamic layer interface (M/L^3)

t = Reaction time (T)

x = Axial coordinate (L)

r = Activated carbon particle radius (L)

v_x = Interstitial fluid velocity (L/T)

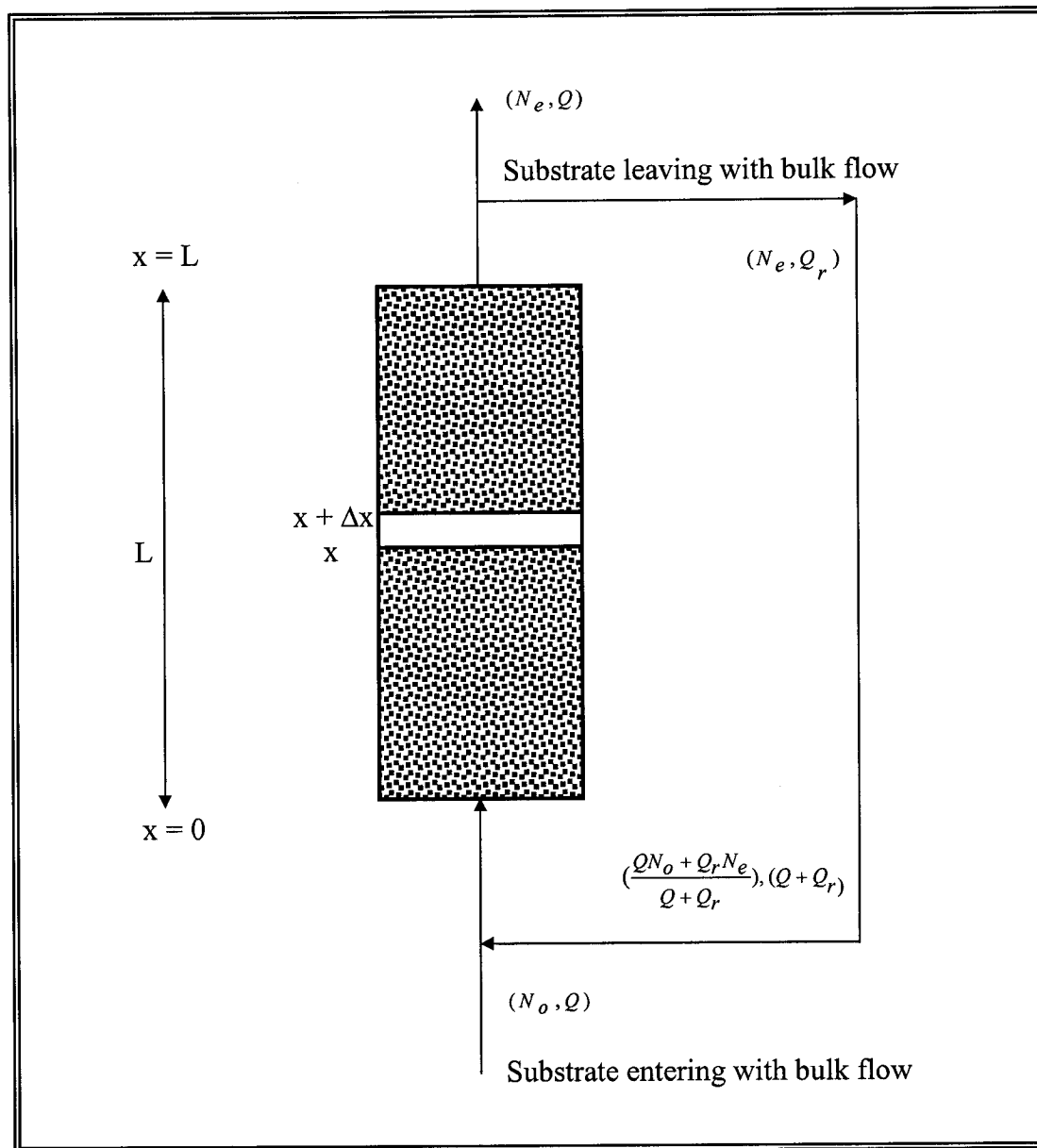


Figure 4.2. Mathematical model formulation for the FBAR denitrification process

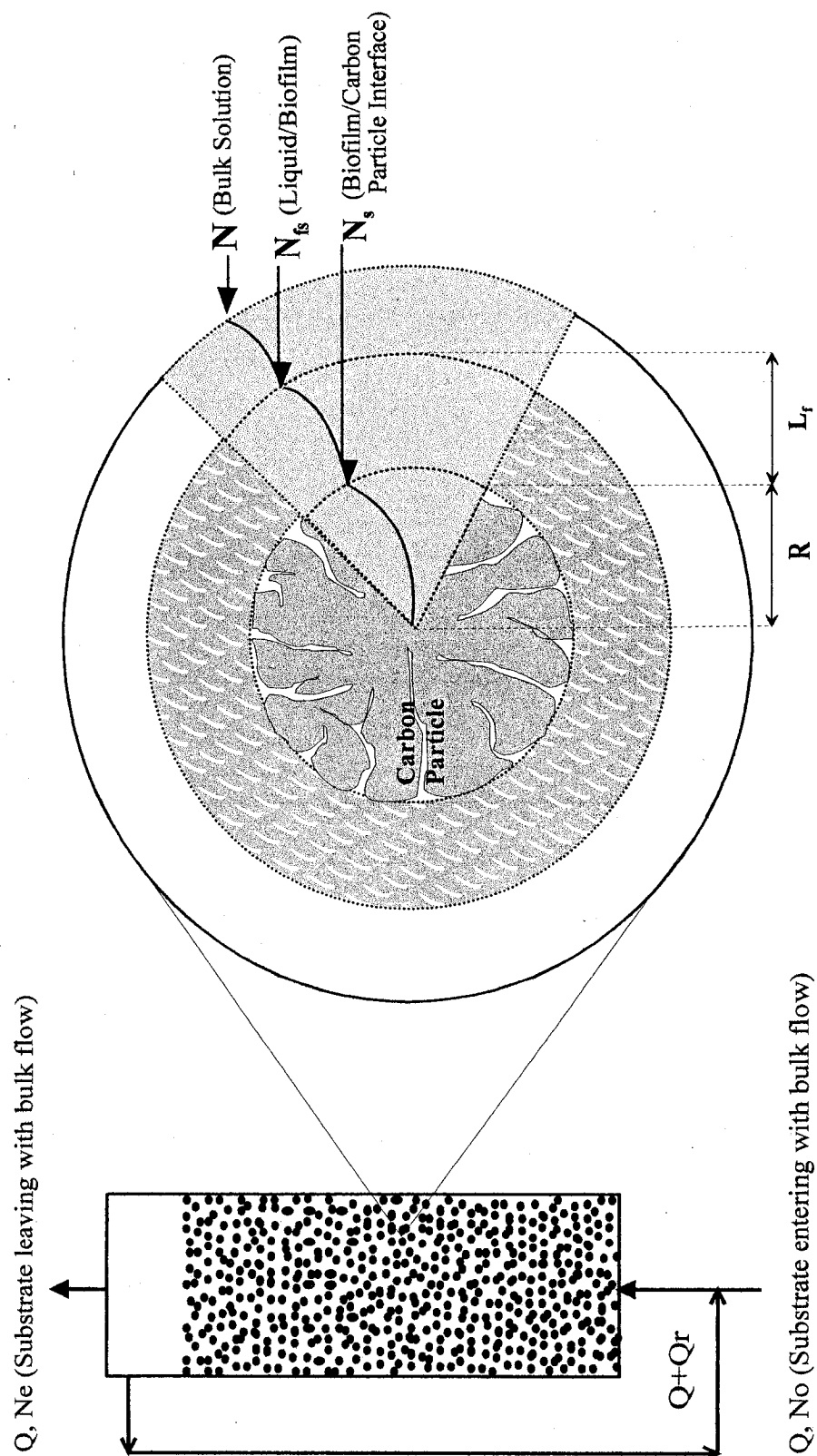


Figure 4.3. Schematic representation of a single bioparticle in FBAR model conceptualization

k_{fc} = Substrate mass transfer coefficient (L/T)

D_x = Axial (hydrodynamic) substrate dispersion coefficient (L²/T)

L_f = Biofilm thickness at any time t (L)

$\mu_{m,a}$ = Maximum specific growth rate (1/T)

$K_{s,a}$ = Half saturation constant (M/L³)

Y_a = Yield coefficient (M/M)

X_l = Biomass concentration in liquid bulk phase (M/L³)

ϵ = Bed porosity (dimensionless)

The biomass concentration in the bulk liquid phase (X_l) in equation (4.1) should be corrected for each time step calculation at the point at which the biofilm thickness exceeds the maximum biofilm thickness. At this point, the portion of the biofilm ($X_{l,r}$) will be lost into to bulk liquid phase due to shear. The term X_l will then be the sum of the biomass already present in the bulk liquid phase and the biomass that has sheared off from the biofilm. This phenomenon is formulated in equation (4.10).

The initial and boundary conditions for the above equation (4.1) are as follows:

$$N(x, t=0) = N_o \quad (4.2)$$

$$N(x=0, t) = \frac{Q N_o + Q_r N_e(x=L, t)}{Q + Q_r} \quad (4.3)$$

$$\left. \frac{\partial N(x, t)}{\partial x} \right|_{x=L} = 0 \quad (4.4)$$

where

N_o = Influent substrate concentration (M/L³)

N_e = Substrate concentration in the recycle flow (M/L³)

Q = Fluid flowrate (L³/T)

Q_r = Recycled fluid flowrate (L³/T)

L = Length of FBAR (L)

4.4.3.2 Diffusion and Reaction in Biofilm

The following equation assumes that the substrate concentration within the biofilm layer changes only in the direction normal to the surface of the biofilm (represented by r_f):

$$\frac{\partial N_f(x, r_f, t)}{\partial t} = D_f \frac{\partial^2 N_f(x, r_f, t)}{\partial r_f^2} - \frac{\mu_{m,a} N_f(x, r_f, t)}{Y_a [K_{s,a} + N_f(x, r_f, t)]} X_f \quad (4.5)$$

where

N_f = Substrate concentration within biofilm (M/L³)

r_f = Radial direction normal to the surface of the biofilm (L)

X_f = Biomass density within the biofilm (M/L³)

D_f = Biofilm substrate diffusion coefficient (L²/T)

The initial and boundary conditions are as follows:

$$N_f(x, r_f, t = 0) = N_{f,o} \quad (4.6)$$

$$k_{fc} [N(x, t) - N_{f,s}(x, t)] = D_f \left. \frac{\partial N_f(x, r_f, t)}{\partial r_f} \right|_{r_f=L_f} \quad (4.7)$$

$$\frac{\partial N_f(x, r_f = 0, t)}{\partial r_f} = 0 \quad (4.8)$$

where

$N_{f,0}$ = Initial biofilm concentration (M/L³)

4.4.3.3 Growth of Biofilm

The variation of the biofilm thickness with respect to time and position could be represented by the following equation in which Monod biokinetics is applied to describe the biofilm growth and decay:

$$\frac{\partial L_f(x, t)}{\partial t} = \int_0^{L_f} \left(\frac{\mu_{m,a} N_f(x, r_f, t)}{K_{s,a} + N_f(x, r_f, t)} - k_{d,a} \right) dr_f \quad (4.9)$$

where

$k_{d,a}$ = Endogenous decay coefficient (1/T)

The biomass lost to the bulk liquid phase can be expressed by the following equation:

$$X_{l,f}(x, t \geq t_{\max}) = \frac{3(1 - \varepsilon)}{\varepsilon} \frac{(L_f(x, t) - L_{f,\max})(r + L_{f,\max})^2}{r^3} X_f \quad (4.10)$$

when

$$L_f(x, t \geq t_{\max}) = L_{f,\max} \quad (4.11)$$

where

$X_{l,f}$ = Biomass concentration that is lost from biofilm to liquid bulk phase (M/L³)

Equation (4.10) implies that the biofilm will grow up to a certain thickness referred to as maximum biofilm thickness with time. Any further growth in the biofilm thickness will be sloughed off due to high shear and end up in the bulk liquid stream.

The initial condition for equation (4.9) is as follows:

$$L_f(x, t = 0) = L_{f,o}(x) \quad (4.12)$$

where

$L_{f,o}$ = Initial biofilm thickness (L)

t_{\max} = Time at which the biofilm thickness is maximum (T)

$L_{f,\max}$ = Maximum biofilm thickness (L)

4.4.3.4 *Suspended Biomass in Bulk Liquid Solution*

The biomass that is lost from the biofilm due to shear will become suspended in the fluid, a portion of which will leave the bioadsorber with the effluent.

$$\begin{aligned} \frac{\partial X_l(x, t)}{\partial t} = & D_x \frac{\partial^2 X_l(x, t)}{\partial x^2} - v_x \frac{\partial X_l(x, t)}{\partial x} + \\ & \left(\frac{\mu_{m,a} N(x, t)}{K_{s,a} + N(x, t)} - k_{d,a} \right) [X_l(x, t) + X_{l,f}(x, t)] \end{aligned} \quad (4.13)$$

The initial and boundary conditions are:

$$X_l(x, t = 0) = X_{l,o} \quad (4.14)$$

$$X_l(x = 0, t) = \frac{QX_o + Q_r X_l(x = L, t)}{Q + Q_r} \quad (4.15)$$

$$\left. \frac{\partial X_l(x,t)}{\partial x} \right|_{x=L} = 0 \quad (4.16)$$

where

$X_{l,0}$ = Initial bulk liquid phase biomass concentration at time zero
(M/L³)

X_0 = Influent biomass concentration (M/L³)

4.4.4 Non-Dimensionalization and Numerical Solution to the Model

Non-dimensionalization is essential in order to be able to solve the mathematical model equations given above, and is usually the first step towards the application of numerical techniques. By non-dimensionalization, the equations not only become easy to handle, but also more information is generated on the convergence conditions, numerical consistency and computational accuracy and stability of the numerical methods used. It is, therefore, convenient to normalize the domains of variables between zero and unity, and express all the differential equations as well as their initial and boundary conditions in a systematized and compact form (Badriyha, 1997).

Nevertheless, the non-dimensionalized equations describing the overall phenomena that take place in the FBAR denitrification with GAC are too complicated to be solved analytically. Therefore, it is necessary to use appropriate numerical methods to solve them. The FBAR denitrification model used in this research was solved by employing a hybrid technique that combines orthogonal

collocation and Crank-Nicholson finite differences method. This combination has been proven very efficient as observed by Pirbazari and coworkers (Kim & Pirbazari, 1989; Ravindran et al., 1996). In this technique, the FBAR and adsorption equations are approximated by orthogonal collocation grids. The biofilm degradation and diffusion phenomena are computed by the Crank-Nicholson finite differences scheme. Two different numerical techniques are combined because of the fact that orthogonal collocation method works best for spatial approximations when the solution to the problem does not have steep gradients, while finite differences method is more appropriate for the functions with steep gradients. The partial differential equations in the model are first transformed into ordinary differential equations, and then solved by using the GEAR software (Gear, 1971, 1976). The theory of orthogonal collocation method and its applications to solving the diffusion and reaction equations could be found elsewhere (Finlayson, 1972; Jain, 1985; Kim, 1987; Villadsen & Stewart, 1967).

4.5 Model Parameter Estimations

4.5.1 Biofilm Parameter Estimation

The important biofilm parameters to be determined are the maximum biofilm thickness, $L_{f,max}$ and the biofilm density, X_f . Both parameters can be estimated from the measurements of attached biomass. Two different methods have been used by researchers to approximate $L_{f,max}$. In the first method, it is estimated from the bed expansion due to biofilm growth using the following relationship:

$$L_{f,\max} = \frac{\Delta V}{\pi d_p^2 P_n} \quad (4.17)$$

where

ΔV = Volume of bed expansion due to growth of biomass (cm^3)

d_p = GAC particle diameter (cm)

P_n = Number of GAC particles (dimensionless)

The second method (Law et al., 1976) estimates $L_{f,\max}$ by using the water content of the biofilm. Carbon particles are removed from randomly selected segments of the fluidized bed, weighed, dried at 103°C , and re-weighed. Since biofilm comprises of 99 percent of water, the average value of $L_{f,\max}$ is calculated by using the following equation:

$$L_{f,\max} = \frac{W_{ev}}{0.99 \rho_a P_n a_p} \quad (4.18)$$

where

W_{ev} = Weight of evaporated water (gr)

a_p = Total surface area available for mass transfer on the GAC particle (cm^2)

ρ_a = Apparent GAC density (gr/cm^3)

The weight of evaporated water can be found by the technique described by Namkung (1985). The biofilm density, X_f could then be calculated by using the following equation (Kim, 1987):

$$X_f = \frac{B_w}{L_{f,\max} P_n a_p} \quad (4.19)$$

where

B_w = Cell weight in grams (weight of GAC with biofilm before drying – weight of virgin GAC)

4.5.2 Substrate Mass Transfer Coefficient and Free Liquid Diffusivity Estimation

Reactor substrate mass transfer coefficient, k_{fc} , relates to the hydrodynamic characteristics of a fluid particle system, and it is usually calculated from the hydrodynamic characteristics of the fluid-particle system. Similarly, free liquid diffusivity, D_l , is best estimated by using an empirical formula approach since it is impractical to find the D_l of any wastewater due to the complex nature of its composition.

The following correlation was suggested by Wakao and Funazkri (1978) to determine the values of k_{fc} and D_l :

$$Sh = 2 + 1.1 Re^{0.5} Sc^{0.33} \quad (4.20)$$

where

Sh = Sherwood number (dimensionless)

Re = Reynolds number (dimensionless)

Sc = Schmidt number (dimensionless)

This equation relates Sherwood number to both Reynold Number and Schmidt Number, and holds for Reynolds Number between 20 and 2,000, a range usually found in FBARs. These numbers are dimensionless, and defined as follows:

$$Sh = \frac{d_p k_{fc}}{D_l} \quad (4.21)$$

$$Re = \frac{d_p \rho_l v_s \varepsilon}{\mu} = \frac{d_p \rho_l v_s}{\mu} \quad (4.22)$$

$$Sc = \frac{\mu}{\rho_l D_l} \quad (4.23)$$

where

D_l = Free liquid diffusivity (cm²/sec)

ρ_l = Fluid density (gr/cm³)

v_s = Superficial fluid velocity (cm/sec)

μ = Fluid viscosity (gr/cm.sec)

Incorporating equation (4.21) into equation (4.20) the following equation is obtained:

$$\frac{d_p k_{fc}}{D_l} = 2 + 1.1 Re^{0.5} Sc^{0.33} \quad (4.24)$$

The values of k_{fc} and D_l could then be estimated *via* trial and error method.

4.5.3 Biofilm Diffusion Coefficient Estimation

The biofilm diffusion coefficient, D_f , is calculated from the D_l , whose value is estimated above, by using the ratio proposed by Williamson and McCarty (1976):

$$\frac{D_f}{D_l} = 0.8 \quad (4.25)$$

4.5.4 Axial Substrate Dispersion Coefficient Estimation

Axial substrate dispersion coefficient, D_x , is calculated by using the following empirical equations developed by Chung and Wen (1968).

$$\frac{D_x \rho_l X}{\mu} = \frac{\text{Re}}{0.2 + 0.01 \text{Re}^{0.48}} \quad (4.26)$$

where

D_x = Axial (hydrodynamic) substrate dispersion coefficient (cm^2/sec)

The terms in equation (4.26) can be calculated using the following equations:

$$X = \frac{\text{Re}_{\text{mdf}}}{\text{Re}} \quad (4.27)$$

$$\text{Re}_{\text{mdf}} = (33.7^2 + 0.048 \text{Ga})^{0.5} - 33.7 \quad (4.28)$$

$$\text{Ga} = \frac{d_p \rho_l g (\rho_s - \rho_l)}{\mu^2} \quad (4.29)$$

where

Re_{mdf} = Modified Reynolds number (dimensionless)

Ga = Galileo number (dimensionless)

g = Gravitational acceleration (cm^2/sec)

ρ_s = Density of bioparticle (gr/cm^3)

For fluidized bioadsorber reactors, the value of D_x could be neglected in the reactor mass balance equations (4.1) and (4.13) because of its very small value due to higher degree of mixing.

4.6 Protocol for Biological FBAR Modeling and Design

The traditional approach for the design of FBAR involves feasibility studies with the specific wastewater, followed by pilot-scale studies and eventually full-scale design. However, this procedure has proven expensive in view of the time, effort and cost associated with pilot-scale studies. The modeling and design protocol outlined for FBAR in Figure 4.4 would be a useful approach in economizing time, effort and costs.

The different steps delineated in the protocol are briefly summarized as follows. Batch reactor biokinetic studies are conducted to obtain temperature, pH, C:N ratio for denitrification of RO brine rejects (Step 1). Simultaneously, laboratory-scale continuous flow chemostat experiments are conducted to evaluate the biodegradation parameters including Monod constants $K_{s,a}$ and $\mu_{m,a}$, the growth yield coefficient Y_a and the decay coefficient k_d (Step 2). The axial substrate dispersion coefficient D_x , the biofilm diffusion coefficient D_f , the free liquid diffusivity D_l and the substrate mass transfer coefficient k_{fc} are estimated using correlation techniques (Step 3). In the same way, the biofilm density X_f , the initial biofilm thickness $L_{f,0}$ and the maximum biofilm thickness $L_{f,max}$ are determined using appropriate

correlations (Step 4). The FBAR model with the biodegradation parameters and flow conditions as inputs are employed to predict the FBAR dynamics under a variety of operating conditions. This “feed-forward” approach provides the means for proper design of mini pilot-scale FBARs. Subsequently, the results from mini pilot-scale FBAR experiments provide the feed-back to evaluate the predictive capability of the model and to implement any potential model refinement, if necessary.

The next few steps in the protocol involve the up-scaling of the process from mini pilot-scale to pilot-scale and eventually to full-scale. The concepts of dimensional analysis and similitude are employed in the up-scaling procedure, and these aspects are elaborately discussed by Pirbazari and coworkers (Pirbazari et al., 1993; Ravindran et al., 1996). The pilot-scale design conventionally requires verification by limited experimental testing prior to full-scale implementation. The figure addresses the steps in the protocol leading to modeling for predicting the FBAR dynamics and model verification by laboratory-scale FBAR experiments. Subsequent steps leading to pilot-scale testing and full-scale design (Steps 5 through 11) are beyond the scope of this research.

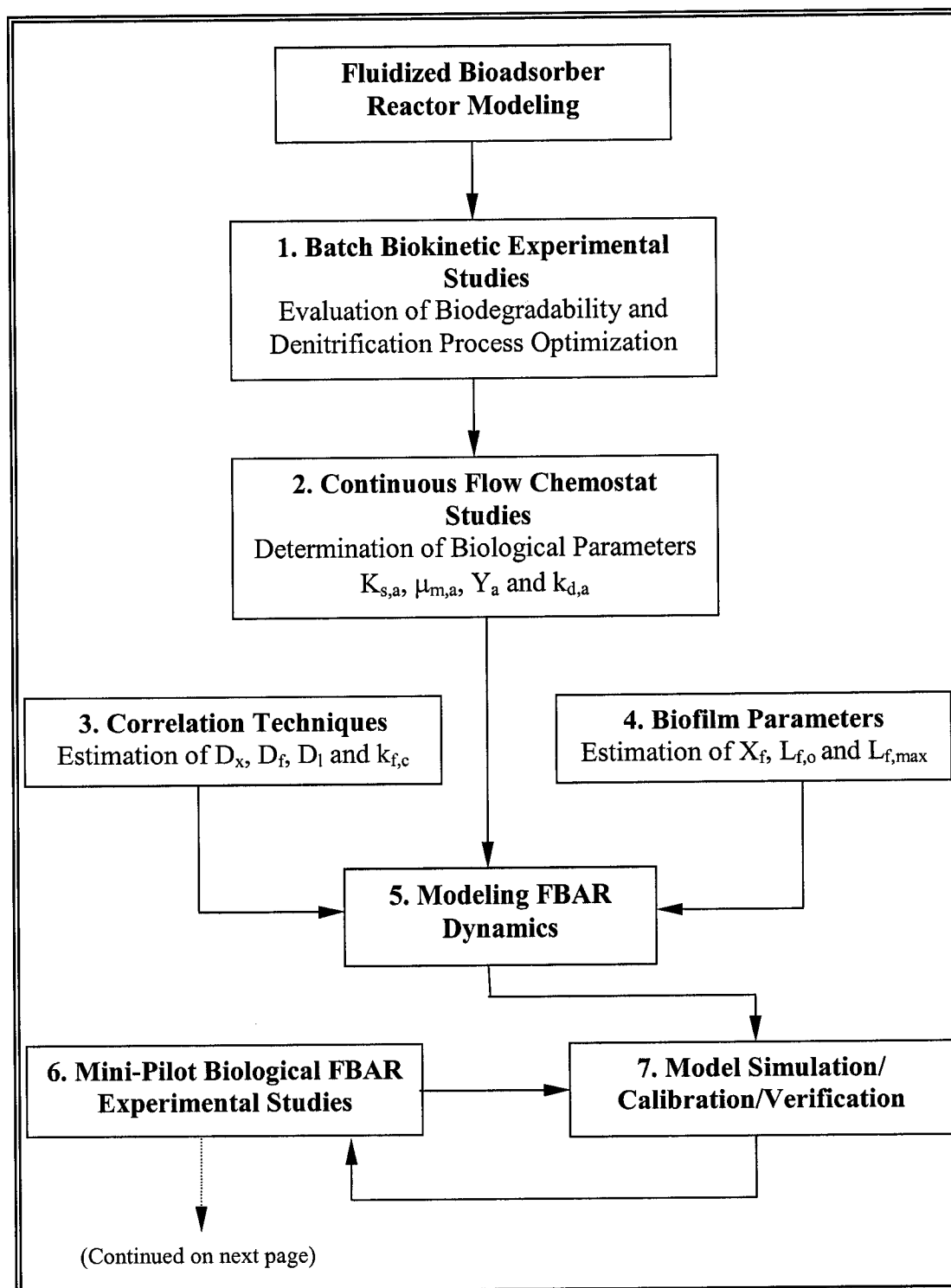


Figure 4.4 Protocol for modeling and design of FBAR process for biological denitrification

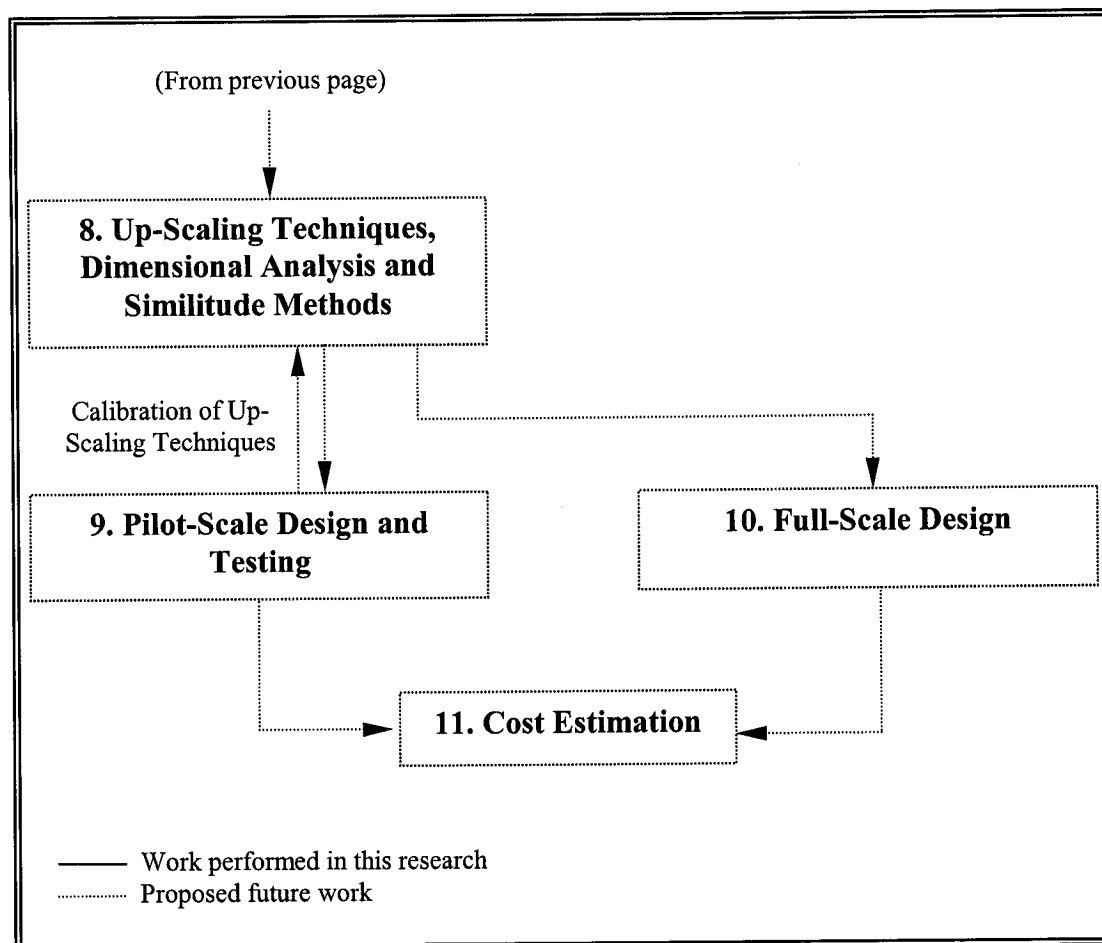


Figure 4.4 Protocol for modeling and design of FBAR process for biological denitrification (continued)

CHAPTER 5

MATERIALS AND METHODS

This chapter presents the experimental techniques employed throughout the research in three sections, namely materials used, experimental methods incorporated and analytical techniques employed to measure the contaminant concentrations.

5.1 Materials

5.1.1 Source of Brine Reject

The raw brine reject used throughout the experimental studies was originated from the RO membrane system at the Water Factory-21 of Orange County Water District, Fountain Valley, CA. The RO pressure vessels housed polyamide thin film composite (TFC) membrane filters. The system was operated at a constant feed flow of 13.8 gpm, and produced a permeate flowrate of 10.4 gpm and brine reject flowrate of 3.4 gpm. Precipitation onto the membrane surfaces was prevented by adjusting the pH to 7.4 with sulfuric acid and adding a scale inhibitor. The brine reject was collected in a 24-L holding tank, and used in the biological nitrification studies employing laboratory-scale fluidized bioreactors and pilot-scale rotating biological contactors. The average concentrations of constituents present in the brine reject were presented in Table 1.1, Chapter 1.

5.1.2 Characteristics of Support Media

The GAC employed in the aerobic fluidized bioreactor nitrification and anaerobic fluidized bioadsorber reactor denitrification studies was coconut-shell-based activated carbon (COCL60) provided by Carbon Activated Corp. (Los Angeles, CA). The effective particle size was 8-12 U.S. mesh, corresponding to a mean geometric diameter of 1.85 mm. The particle size was chosen in such a way that the bioreactor size to particle diameter ratio did not cross 50 in order to minimize the wall effects.

The PAC employed in rotating biological contactor tank was of WPL-Pulverized type PAC manufactured by Calgon Carbon Corp. (Pittsburgh, PA). The activated carbon used in biofiltration column was of 4-10 mesh size provided by the same company as PAC. The Ottawa sand used in fluidized bioadsorber denitrification studies was of 20-30 mesh size obtained from VWR Scientific Products (San Diego, CA).

5.1.3 Sources of Microbial Cultures

The mixed microbial culture used in nitrification studies was obtained from the activated sludge tank of two different municipal wastewater treatment plants, Terminal Island Treatment Plant, Long Island, CA and Orange County Sanitation District Treatment Plant, Fountain Valley, CA. The nitrifying bacteria were acclimated from these cultures using raw brine reject.

The mixed microbial culture used in denitrification studies was obtained from one of the sequencing batch reactors of a municipal wastewater treatment plant (Rancho California Water District, Temecula, CA) during its anoxic stage, acclimated with respect to denitrifying bacteria using nitrified brine reject. The sulfate-reducing bacterial culture was acclimated from the same microbial culture used in denitrification studies.

The biofilter microorganisms were isolated from another culture of activated sludge obtained from Terminal Island Treatment Plant, Long Island, CA. The nutrient solution used for the biofilter microorganisms during the acclimation periods and later during the experimental stage was prepared using the following composition (g/l): Glucose - 0.2; KH_2PO_4 - 2; K_2HPO_4 - 2; NH_4Cl - 0.4; $\text{MgCl}_2 \cdot 6\text{H}_2\text{O}$ - 0.2; $\text{FeSO}_4 \cdot 7\text{H}_2\text{O}$ - 0.01.

5.1.4 Chemicals

The chemicals employed in this research were sulfuric acid and hydrochloric acid (Aldrich Chemical Co., Milwaukee, WI), sodium hydroxide (Aldrich Chemical Co., Milwaukee, WI), sodium thiosulfate (Mallinckrodt Chemicals, Phillipsburg, NJ), monobasic and dibasic sodium phosphate (Mallinckrodt Chemicals, Inc., Phillipsburg, NJ), and high purity ethanol (Aldrich Chemical Co., Milwaukee, WI). All other chemicals used in the preparation of synthetic brine reject were obtained from Mallinckrodt Chemicals (Phillipsburg, NJ).

All solutions used throughout the studies including acids (0.1 N of H_2SO_4 and 2 N of HCl), base (0.1 N and 2 N of NaOH), sodium thiosulfate solution (3.5 g $\text{Na}_2\text{S}_2\text{O}_3 \cdot 5\text{H}_2\text{O}/\text{l}$) as dechlorinating agent, phosphate solution (15 mg/l KH_2PO_4 and 25 mg/l K_2HPO_4) as supplemental nutrient, buffer solution (1.2 g/l Na_2CO_3 and 1.8 g/l NaHCO_3) for pH control and ethanol dilutions as organic carbon source were prepared using deionized-distilled water with conductivity readings less than 5 $\mu\text{mhos}/\text{cm}$, and stored in the refrigerator at 4°C when not used. Acids and base solutions were preserved in borosilicate glass bottles. Sodium thiosulfate solution was prepared fresh on a weekly basis, according to Standard Methods (1998).

5.2 Experimental Methods

5.2.1 Nitrification Studies

Two different nitrification processes, fluidized bioreactor and RBC enhanced with PAC, were used to nitrify the brine reject under optimized conditions. The nitrified brine reject obtained from the fluidized bioreactor was used in the batch and continuous flow chemostat studies, while that obtained from RBC was used in mini-pilot scale FBAR experiments. The main reason for employing RBC was to generate sufficient nitrified brine reject for the FBAR denitrification and sulfate reduction studies, as laboratory-scale fluidized bioreactor was not capable of producing large quantities of nitrified brine reject due to its limited size.

5.2.1.1 Fluidized Bioreactor for Nitrification Process

A laboratory-scale fluidized bioreactor made of glass, having 4.8-L capacity, was employed for the nitrification. The bioreactor consisted of two sections; the upper wide portion housed the recycle line and effluent port, the bottom portion was used to charge the GAC medium into the bioreactor. The top of the bioreactor was covered with a perforated plastic cap. Figure 5.1 shows the schematic of the fluidized bioreactor, and Figure 5.2 shows the photograph of the same bioreactor.

Before charging the bioreactor, the GAC was washed with deionized-distilled water to remove carbon fines, dried at 105°C overnight, and stored in sealed containers. A 2-inch layer of glass beads was placed in the bottom of the bioreactor to provide a uniform flow distribution. The bioreactor was subsequently charged with 300 g of GAC. The bioreactor was initially run for a few hours with brine reject to wash out the powder portion of the GAC, and to equilibrate the system. Then, it was inoculated with mixed bacterial culture, and placed in recycle mode for about 3 weeks. During this time, the content of the bioreactor was replenished several times when the ammonia concentration decreased to 5 mg N/l. Finally, when the decrease in the ammonia concentration occurred in a reasonably short period of time, the bioreactor was placed on continuous flow mode. The initial flowrate was adjusted to 16 ml/min, which corresponded to a hydraulic retention time of 300 minutes.

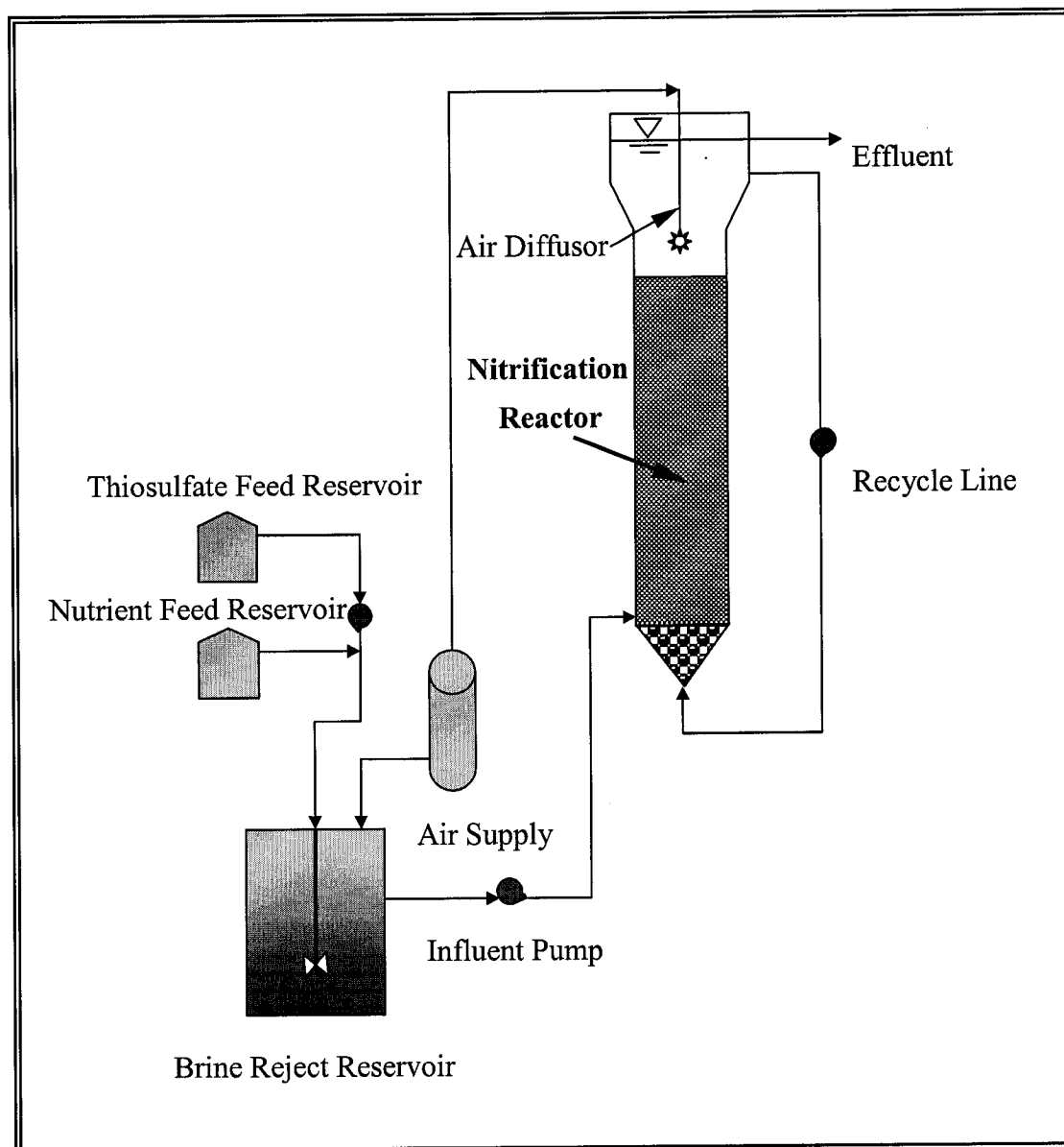


Figure 5.1. Schematic representation of laboratory-scale fluidized bioreactor used for nitrification process

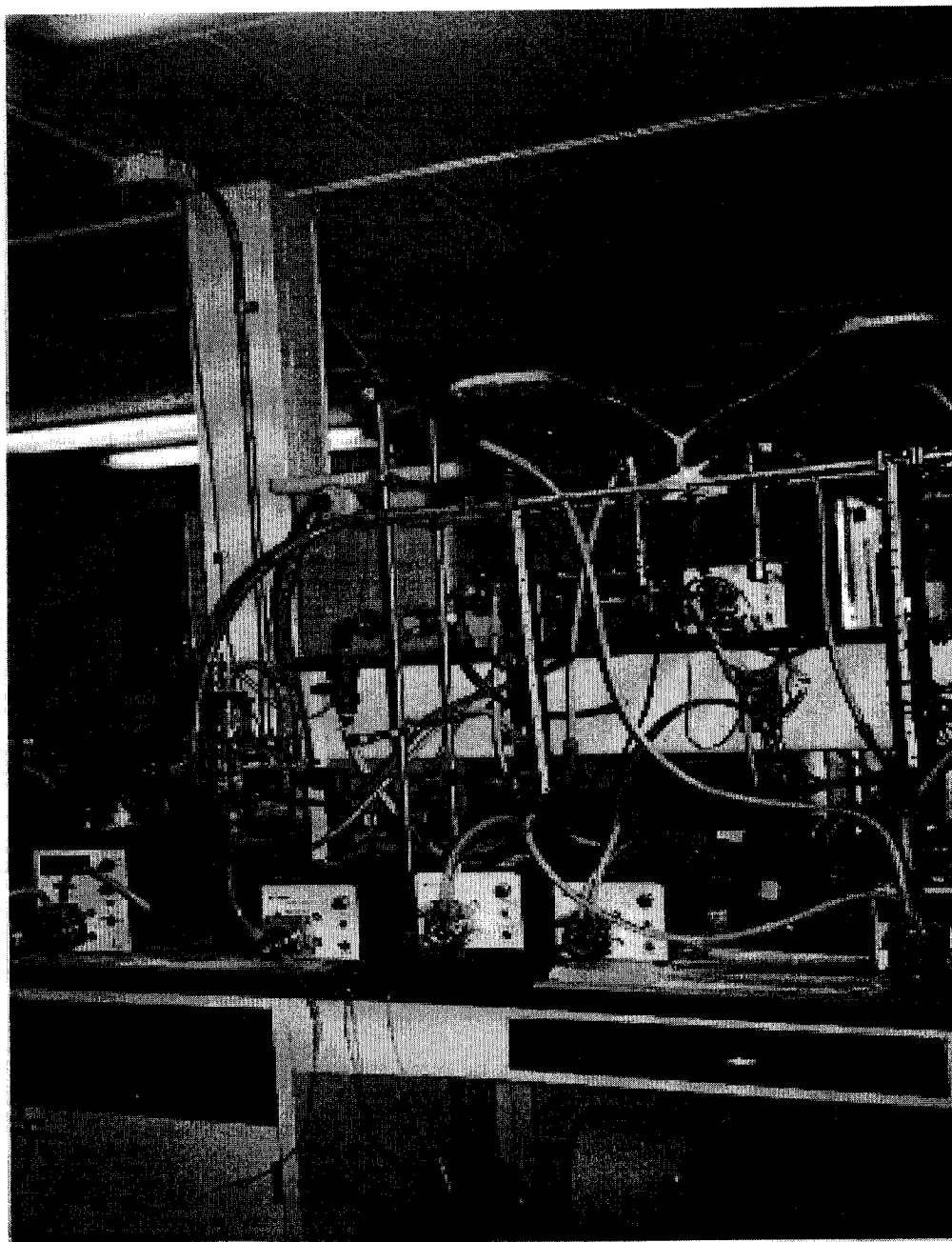


Figure 5.2. Photograph of the fluidized bioreactor used in nitrification studies

The brine reject feed to the bioreactor was collected in a glass reservoir. Sodium thiosulfate as dechlorinating agent and phosphate solution as nutrient supplement were introduced into the reservoir. The pH was maintained at 7.5 with the addition of 0.1 N HCl and/or 0.1 N NaOH. The content of the reservoir was aerated through air diffusers to maintain aerobic conditions. The fluidized bioreactor was also aerated with diffusers from the top where the recirculation line was connected to enhance the fluidization and aerobic conditions. The feed was pumped to the bioreactor using a Masterflex peristaltic pump (Cole Parmer Instrument Co., IL). A recycle ratio of 50:1 was maintained in order to ensure good fluidization using another Masterflex peristaltic pump of the same kind as the feed pump.

The bacterial growth was kept under control by regularly cleaning the walls of the reactors. The stability of the system was checked regularly by measuring the influent and effluent ammonia concentrations. The nitrified brine reject was collected in a 30-gallon black polyethylene storage container, and used in batch and continuous chemostat experiments for the experimental parameter optimization and biokinetic studies, respectively.

5.2.1.2 Rotating Biological Contactors for Nitrification Process

A pilot-scale aerobic RBC unit was used for the nitrification process. The RBC tank had 125-L capacity with three compartments, each holding one rotating disk made of polypropylene with a surface area of approximately $150 \text{ m}^2/\text{m}^3$ as shown in Figure 5.3. Figure 5.4 demonstrates the photograph of the unit.

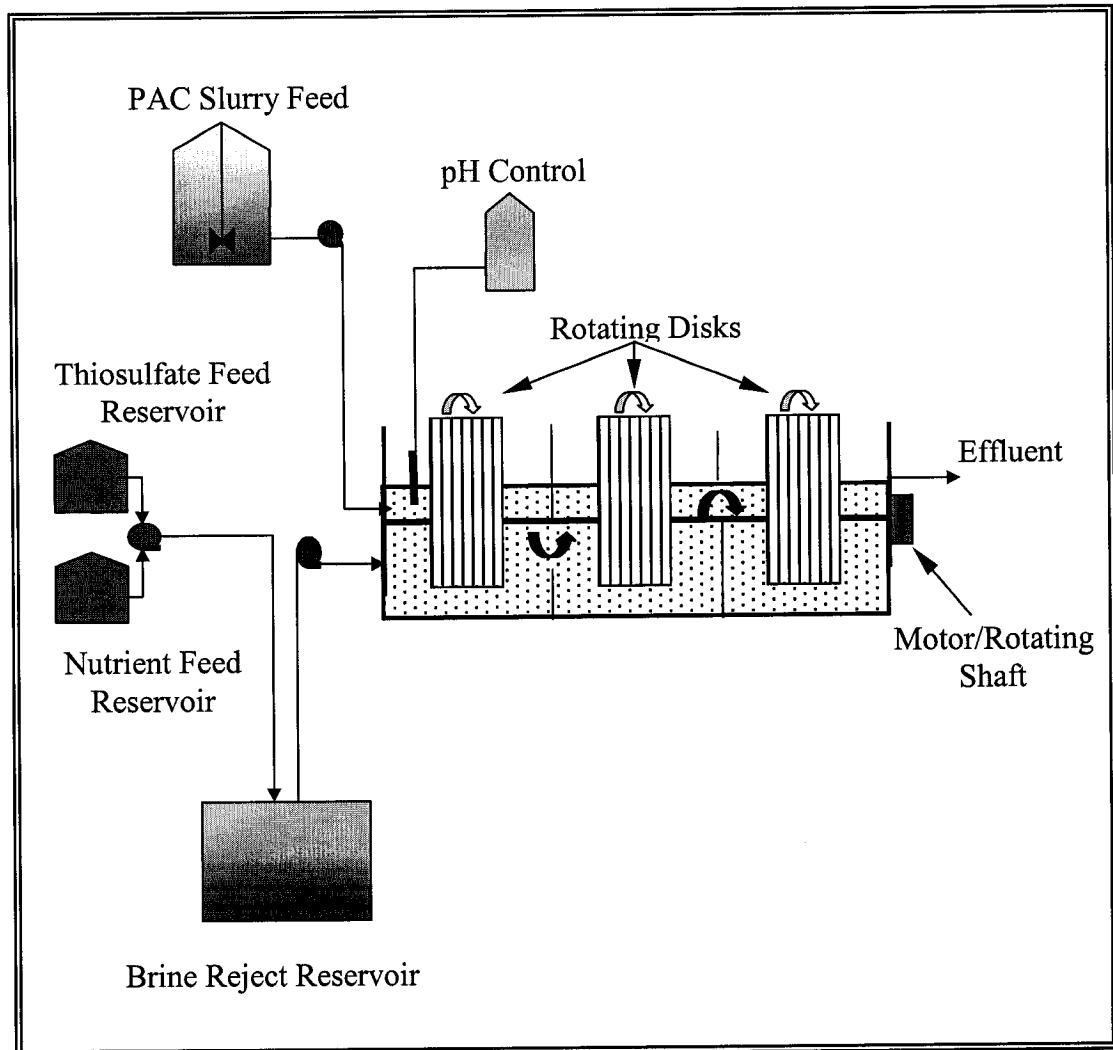
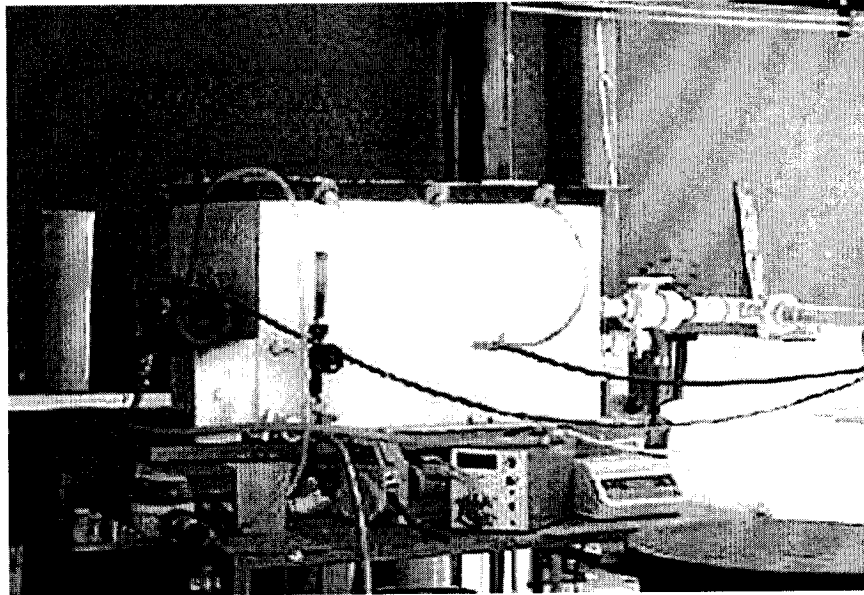
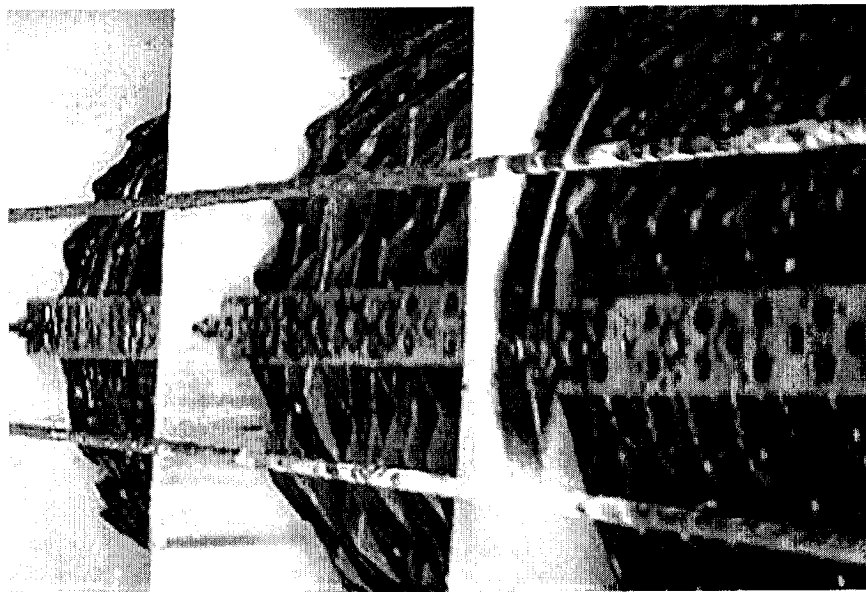


Figure 5.3. Pilot-scale rotating biological contactor unit used for nitrification process



(a) Side view of the RBC unit



(b) Top view of the rotating disks

Figure 5.4. Photographs of the RBC unit and the rotating disks used in nitrification studies

At the start-up of the RBC process, the tank was filled with raw brine reject, and dechlorinated using sodium thiosulfate solution. Phosphate solution was added into the tank as the supplemental nutrient solution for the nitrifying bacteria. Buffering capacity, when low, was provided by the buffer solution. Since the unit was kept open to atmosphere, additional aeration was not provided. The microbial culture was added, and the pH was carefully maintained at around 7.8 through the addition of 2 N HCl and/or 2 N NaOH *via* an automatic pH controller (Cole Parmer Instrument Co., IL). All the feed and dosing pumps employed were of Masterflex peristaltic pumps (Cole Parmer Instrument Co., IL). The RBC tank was then placed in recycle mode for about 1.5 months to ensure bacteria acclimation, growth and attachment on to the contactor disks. The content of the tank was replenished when the ammonia concentration dropped below 5 mg N/l. Finally, when the decrease in the ammonia concentration occurred in a reasonably short period of time, the tank was placed on continuous flow mode. Initially, the influent flowrate was maintained at 125 ml/min. The nitrified brine was collected in a 30-gallon black polyethylene storage container.

PAC slurry was added to the system continuously to enhance the nitrification process, and also to produce similar quality of nitrified brine used in batch and continuous flow chemostat experiments. The PAC was dosed to the RBC tank with varying rates (0.5 to 3.9 g/l) depending on the influent flowrate. The amount of PAC that had washed out of the tank with the nitrified brine reject effluent and accumulated on the bottom of the collection container was recycled to the RBC tank

on a weekly basis. The stability of the system was checked regularly by measuring the influent and effluent ammonia concentrations and pH. The effluent from this tank was used for mini pilot-scale FBAR denitrification and sulfate reduction studies.

5.2.2 Batch Denitrification Studies for Environmental Parameter Optimization

Completely mixed batch experiments were conducted in a BioFlu IIC batch/continuous fermentor (Boston, MD) to determine the effects of temperature, pH, and total dissolved solids on the denitrification activity, and to determine the optimum carbon-to-nitrogen ratio. The fermentor chemostat was constructed of glass with a capacity of 1.5-L (1.35-L working volume), and tightly sealed with a stainless steel cover. The apparatus was equipped with a built-in pH control electrode, a dissolved oxygen electrode and an agitator with dissolved oxygen control. The apparatus was also equipped with a pump delivery system for acid, base, nutrients and feed water. The temperature was maintained at a pre-determined level *via* a built-in circulating water bath. The schematic and the photograph of the fermentor are presented in Figures 5.5 and 5.6, respectively.

At the start of each experiment, the solution in the fermentor chemostat was deoxygenated with nitrogen gas to maintain anaerobic conditions. The pH was maintained at the required level by using 0.1 N H₂SO₄ and 0.1 N NaOH. The main carbon source was high purity ethanol, and supplementary phosphate solution was

added to ensure that it was not the growth-limiting nutrient for the denitrifying bacteria. Mixing was provided at 400 rpm by a paddle blade rotator.

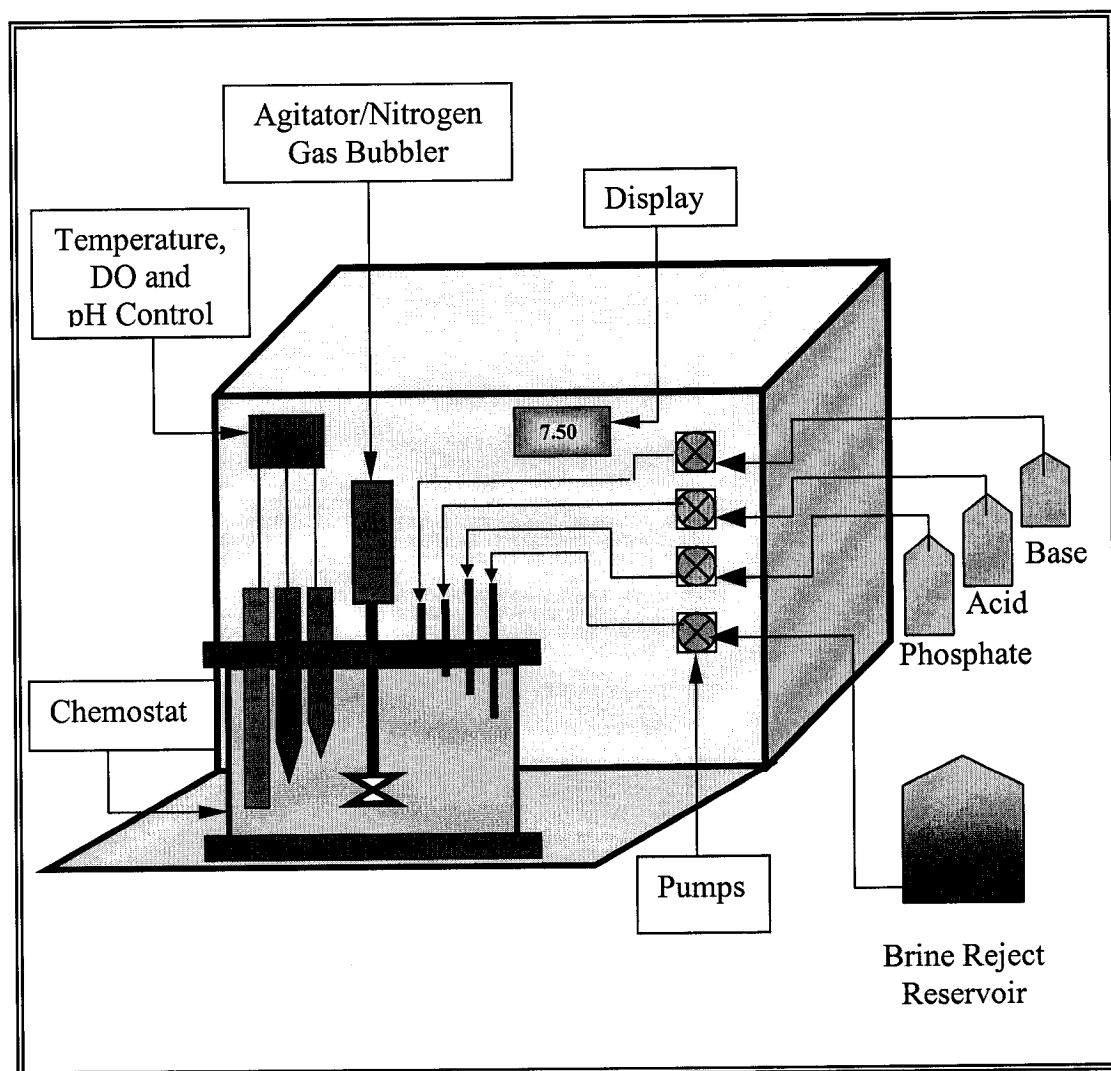


Figure 5.5. Schematic of the fermentor used for batch and continuous flow chemostat studies

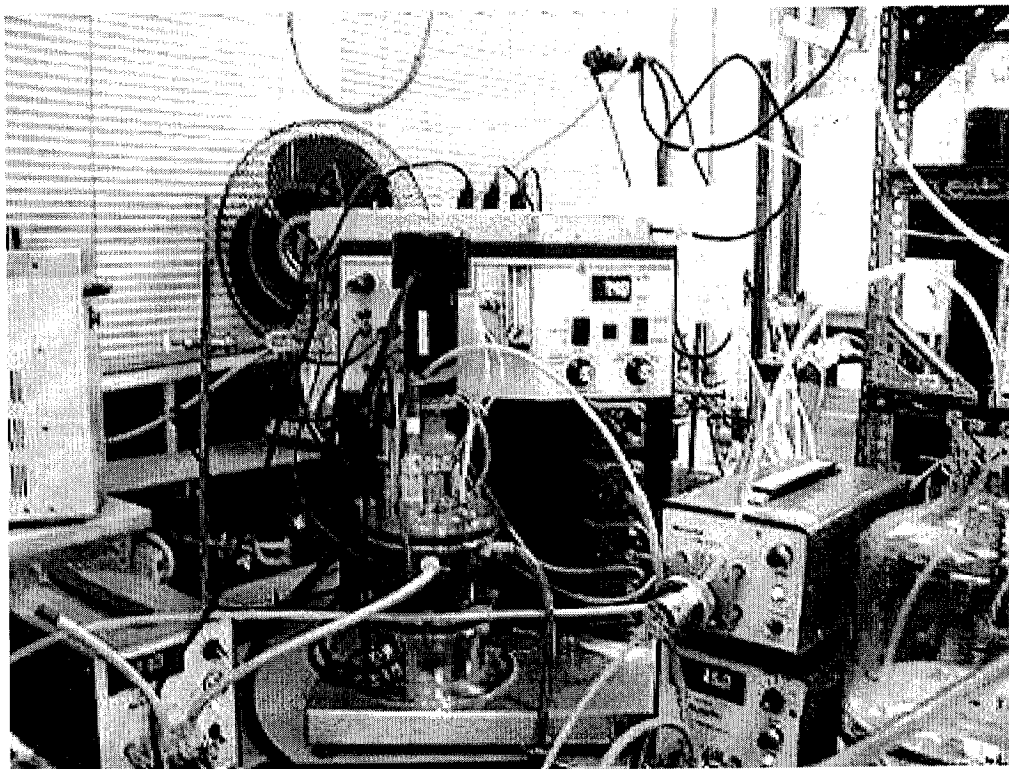


Figure 5.6. Photograph of the fermentor employed in batch and continuous flow chemostat studies

For each set of environmental parameter experiments, only the tested parameter was varied within a pre-determined range, and the other environmental conditions were maintained constant. The acclimated denitrifying culture was added to the chemostat at time zero, and samples and replicates were taken at regular time intervals until nitrate concentration dropped to zero or stabilized. All samples were analyzed for nitrate, nitrite, ethanol and biomass concentrations.

Sodium chloride was added to the nitrified brine reject solution to provide the desired concentration of total dissolved solids.

5.2.3 Continuous Flow Chemostat Studies for Biokinetic Parameter Determination

Biokinetic parameters including maximum specific growth rate (μ_m), Monod half saturation constant (K_s), growth yield coefficient (Y) and decay coefficient (k_d) were determined from the results of a series of completely mixed anaerobic continuous flow chemostat experiments using the fermentor described in Section 5.2.2.

At the start of each experimental cycle, the nitrified brine feed, which was initially deoxygenated with nitrogen gas in order to maintain a dissolved oxygen level of less than 1 percent, was introduced into the chemostat, and mixed. After adjusting the solution pH to 7.5, temperature to 30°C and ethanol to 1.8:1 (the optimum values were selected based on the results obtained from the batch denitrification experiments), acclimated denitrifying culture was added at time zero. As soon as the nitrate was consumed in the batch cycle, the brine feed pump was turned on to provide nitrified brine reject to the chemostat at a specific dilution rate. After reaching steady state at a particular dilution rate, that is, after nitrate concentration in the chemostat reached a steady value, the next dilution rate was applied. This procedure was continued until all the biomass was washed out from the chemostat with the effluent. All samples and replicates were collected at steady state when the effluent nitrate concentration remained constant with time, and analyzed for nitrate, nitrite, ethanol and biomass concentrations.

For the chemostat experiments that did not contain nitrate, a synthetic brine reject whose constituents were presented in Table 5.1, was prepared by maintaining all the constituents same as raw brine reject with the exception of nitrate.

Table 5.1. Constituents and their approximate concentrations of synthetically prepared nitrified brine

Constituent	Represented By	Unit	Concentration
Total Organic Carbon	Humic Acid	mg/l	20
Total Dissolved Solids	NaCl	mg/l	4,000
Organic Nitrogen	Urea	mg/l	5
Ammonia-Nitrogen	$(\text{NH}_3)_2\text{SO}_4$	mg/l	2
Nitrite-Nitrogen	NaNO_2	mg/l	120
Sulfate	CaSO_4	mg/l	1,150
Chloride	NaCl	mg/l	1,000
Fluoride	NaF	mg/l	1.5
Phosphate	$\text{Ca}(\text{H}_2\text{PO}_4)_2$	mg/l	20
Alkalinity	KHCO_3	mg/l	600
Cyanide	KCN	$\mu\text{g/l}$	40
Calcium	CaCl_2	mg/l	500
Magnesium	MgSO_4	mg/l	50
Silver	Ag_2SO_4	$\mu\text{g/l}$	1.5
Arsenic	As_2O_3	$\mu\text{g/l}$	14
Barium	BaCl_2	$\mu\text{g/l}$	100
Cadmium	CdSO_4	$\mu\text{g/l}$	1
Cobalt	CoCl_2	$\mu\text{g/l}$	2
Copper	CuCl_2	$\mu\text{g/l}$	30
Iron	$\text{Fe}_2(\text{SO}_4)_3$	$\mu\text{g/l}$	500
Mercury	--	$\mu\text{g/l}$	--
Manganese	MnSO_4	$\mu\text{g/l}$	100
Lead	$\text{Pb}(\text{NO}_3)_2$	$\mu\text{g/l}$	2.5
Zinc	ZnO	$\mu\text{g/l}$	60

5.2.4 FBAR Denitrification Studies with GAC or Sand

A series of mini pilot-scale up-flow anaerobic FBAR experiments were conducted to investigate the impact of the GAC quantity, nitrate concentration, and hydraulic retention time on the denitrification process efficiency. The 1.75 L fluidized bioadsorber reactor (2-inch I.D., 40-inch Length) was constructed of plexiglass, and equipped with a water jacket in order to maintain a constant temperature. The schematic diagram of the experimental setup is presented in Figure 5.7. Figure 5.8 demonstrates the photograph of the same column.

The GAC was washed with deionized-distilled water for the removal of fine carbon particles, and dried for several days at 105°C. It was stored in tightly sealed containers until the time of use. In the beginning of each experiment, a 3-inch layer of glass beads were placed on a perforated tray at the entrance port of the reactor to provide a uniform flow distribution. Pre-cleaned and weighed GAC was charged into the column, and the initial height was recorded. The GAC bed was then seeded with acclimated denitrifying culture and placed in recycle mode for about an hour. After adjusting the pH, the feeding of nitrified brine reject and ethanol was initiated at time zero. Samples were taken at regular time intervals and analyzed for nitrate, nitrite, ethanol and attached biomass. Excess bacterial growth was removed from the reactor by stirring the bioadsorber bed vigorously, and by scraping the reactor walls. The connecting tubes were cleaned periodically, and the excess pressure built in the tubing caused by the nitrogen gas generated by the bacterial reduction of nitrate was relieved when needed.

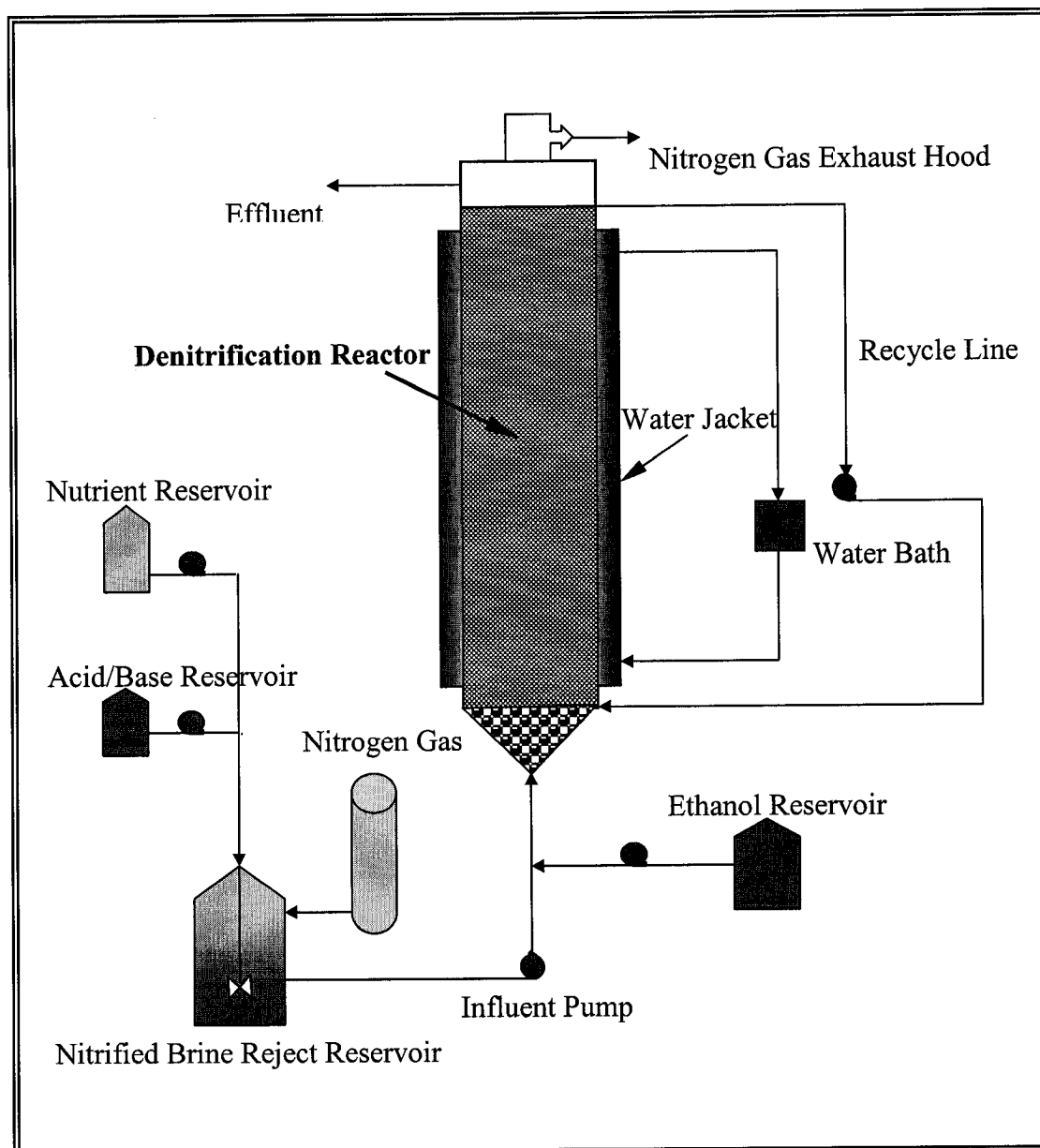


Figure 5.7. Experimental schematic of the mini pilot-scale FBAR denitrification system

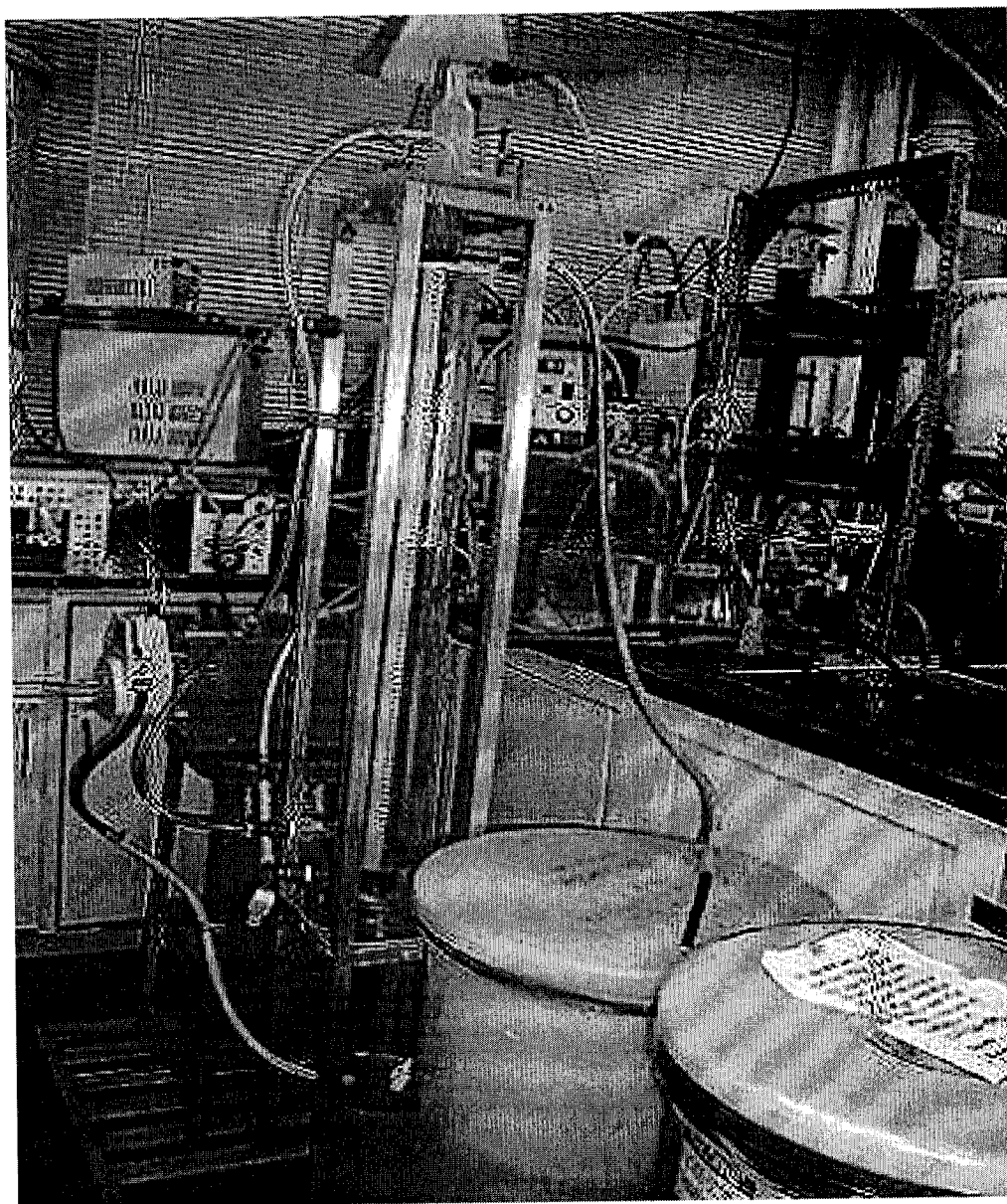


Figure 5.8. Photograph of the mini pilot-scale FBAR

The optimum temperature, pH and carbon-to-nitrogen ratio employed in these studies were determined previously from batch experiments. In all experimental runs, the following conditions were maintained constant; temperature at 30°C by means of a temperature-controlled water bath, pH at 7.5 by adding acid and/or base solution, and carbon-to-nitrogen ratio at 1.8:1 by adding ethanol. The feed nitrified brine reject was de-oxygenated with nitrogen gas to maintain the dissolved oxygen level below 1 percent. All feed, recirculation and dosing lines were connected to Masterflex peristaltic pumps (Cole Parmer Instrument Co., IL). The recycle flowrate was maintained within the range of 55:1-175:1, depending on the influent flowrate, to maintain the bioadsorber bed fluidized. Backflows in the feed lines were prevented using check valves. The nitrogen gas generated exited the bioadsorber through an exhaust hood.

In the first phase of the experimental period, a synthetic brine reject whose constituent characteristics were given in Table 5.1, was used instead of real brine reject due to the fact that the research RO unit at the OCWD experienced operational problems, and could not provide adequate amounts of brine reject. When the RBC unit was able to operate with full efficiency with the addition of PAC, the effluent from this reactor was used in the second phase of the experimental period under the same environmental conditions as those experiments that employed synthetic brine reject.

The FBAR experiments employing sand were conducted under the same conditions as the FBAR experiments with GAC.

5.2.5 Simultaneous Nitrate and Sulfate Reduction Studies

Mini pilot-scale FBAR experiments were conducted to investigate simultaneous nitrate and sulfate reduction. A similar FBAR as in the FBAR denitrification studies was employed for the investigation of simultaneous denitrification and sulfate reduction, and a second FBAR was connected to the first FBAR in series to investigate sulfate removal. The same environmental parameters mentioned in Section 5.2.4 were maintained for both bioadsorbers.

In the beginning of the first experiment, 300 g of pre-cleaned and weighed GAC was charged into the column, followed by seeding the bioadsorber bed with the acclimated denitrifying culture. The reactor was placed in recycle mode for about an hour. The continuous cycle commenced at time zero at the influent brine flowrate of 10 ml/min, which corresponded to a hydraulic retention time of 180 minutes. Samples and replicates were taken at regular intervals, and analyzed for nitrate, nitrite, sulfate and biomass concentrations. This cycle was repeated for the second experiment that used 150 g of GAC.

Excess bacterial growth was removed from the reactor by stirring the bioadsorber bed vigorously and by scraping the column walls. The reactor walls and tubes needed occasional cleaning due to excess microbial growth and blackening. The excess pressure built in the tubes due to the generation of nitrogen and hydrogen sulfide gas was relieved when needed. The gas stream containing hydrogen sulfide gas generated as a result of sulfate reduction was directed to a biofiltration column.

5.2.6 Biofiltration Column Studies

Hydrogen sulfide gas evolved as a result of sulfate reduction in both FBAR systems was removed by a laboratory-scale, tightly sealed biofilter column made of plexiglass (4-inch I.D., 2-foot Length). Figure 5.9 shows a photograph of the biofiltration system. After washing and drying, the GAC was blended with limestone, charged into the column, and then seeded with the acclimated microbial culture. A perforated tray placed 3-inch above the bottom of the column was used as the base for the bed medium. The contaminated gas stream was directly fed into the biofilter. The up-flow feeding commenced immediately after the first sign of hydrogen sulfide odor.

The biofilter column was fed once a week with a nutrient solution whose specifications were given in Section 5.1.4. The sulfate-containing solution accumulated in the bottom of the column was discarded regularly.

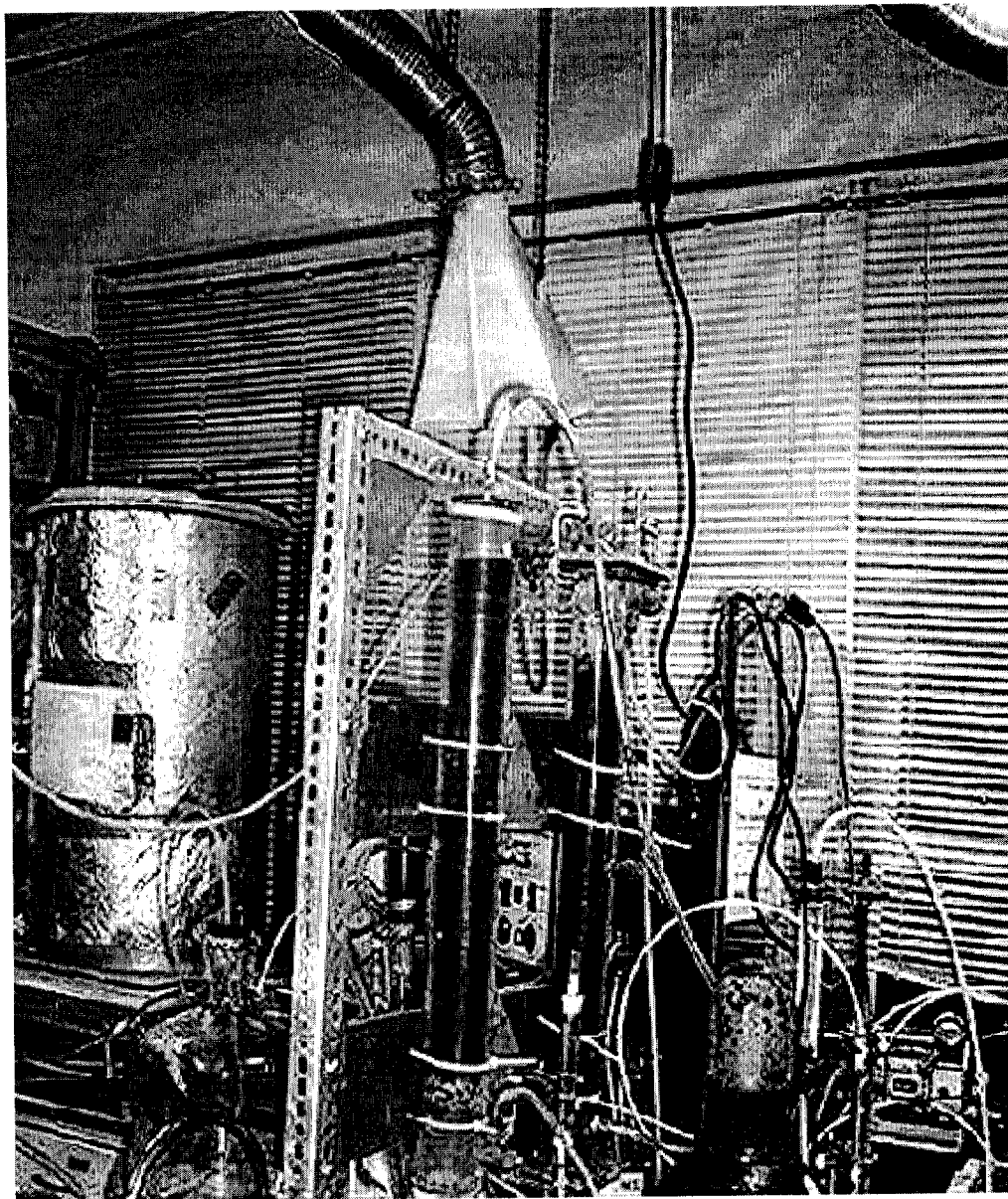


Figure 5.9 Photograph of the biofiltration unit

5.3 Analytical Methods

Chemical and microbiological analyses were performed during all stages of the experimental period. All chemical analyses on raw brine reject including ammonia, anions, TDS, organic nitrogen, TOC, alkalinity and metals were conducted in accordance with Standard Methods and/or relevant U.S. EPA methods. In the field, additional analyses including pH, temperature, ammonia, nitrate, nitrite, ethanol, hydrogen sulfide, biomass assay were carried out and scanning electron micrographs were conducted. Replicates were taken on regular intervals for quality assurance and control purposes. The methods and descriptions are presented in the following sections.

5.3.1 Analysis of Ammonia

Two different methods were used for the analysis of ammonia in the brine reject. For the analysis of ammonia concentration in the influent brine reject, a LACHAT QuikChem 8000 Flow Injection Analyzer (Milwaukee, WI) equipped with an automatic sampling unit was used (EPA Method No. 350.1). Reagent quality distilled-deionized water was used as the carrier solution, while a mixture of disodium ethylene diamine tetraacetate (Na_2EDTA) and sodium hydroxide (NaOH) served as the buffer solution. High purity helium gas was employed to degas the solutions.

For monitoring the effluent ammonia concentration throughout the nitrification studies, a commercial colorimetric test kit with Nessler's Reagent (HACH Company, Loveland, CO), similar to Glass et al. (1997), was used. The influent brine reject was diluted up to 100 times to fall within the concentration range of the method. All samples collected during the experimental cycles were filtered through 0.22 μ cellulose acetate syringe filters (VWR Scientific, West Chester, PA) to eliminate any microbial growth.

5.3.2 Analysis of Anions

For the analysis of anions including nitrate, nitrite, sulfate and chloride in the samples, a DIONEX DX-100 Ion Chromatograph (DIONEX Corporation, Sunnyvale, CA) equipped with a conductivity detector was used (Standard Methods, 1998; EPA Method No. 353.2). The instrument was equipped with an automatic sampler, integrator and a computer based data processor. The eluent was composed of a mixture of sodium carbonate and bicarbonate. Several duplicate samples were prepared in every batch of samples to check the analysis accuracy. The accuracy of the instrument was also monitored on a regular basis by calibration and regular maintenance service.

All samples collected during the experiments were filtered through 0.22 μ cellulose acetate syringe filters (VWR Scientific, West Chester, PA) to eliminate any microbial growth, and stored in the refrigerator at 4°C until the time of analysis.

5.3.3 Analysis of Total Organic Carbon

A TOC analyzer (Model 1010) manufactured by O.I. Corporation (College Station, TX) equipped with an automatic sampler was used to analyze samples for total organic carbon (Standard Methods, 1998; EPA Method No. 415.1). The reagent water contained less than 20 $\mu\text{g/l}$ total organic carbon, and was constantly purged with nitrogen gas. The sample loop configuration consisted of two 1 ml loops for total carbon and total inorganic carbon. All samples were filtered through 0.2 μ nylon filters (Corning Inc., Garden Grove, CA) to remove dissolved organic carbon. Standard solutions with known amounts of total organic carbon were used for calibration and preparation of standard curves. The total organic carbon content in the samples was calculated as the difference in the total carbon and total inorganic carbon concentrations.

5.3.4 Analysis of Ethanol

A Perkin Elmer Sigma 2B Gas Chromatograph (Norwalk, CT) equipped with a single flame ionization detector (GC-FID) was used to analyze for ethanol concentration in the samples (Standard Methods, 1998). The chromatograph was interfaced with an integrator and computer based data processor. The GC column employed was Restek RTX-1 capillary type (0.53-mm I.D., 60-m Length). Helium was used as carrier gas at a flowrate of 30 ml/min, and compressed air and hydrogen mixture as combustion gas. The column oven, GC injection and detector

temperatures were maintained at 80, 200 and 80°C, respectively. Duplicate samples were prepared, and the results were averaged.

5.3.5 Analysis of Organic Nitrogen

The same LACHAT QuikChem 8000 Flow Injection Analyzer (Milwaukee, WI) whose specifications are given in Section 5.3.1 was used to analyze the influent brine reject for organic nitrogen content. The only difference was in the reagents used for analysis and sample preparation (Standard Methods, 1998; EPA Method No. 351.1). A number of different reagents were required, and the samples were digested in a block digester unit. All samples were vortexed, and then centrifuged for 10 minutes at 3,000 rpm. The decant supernatant was used for the analysis.

5.3.6 Analysis of Total Dissolved Solids

The total dissolved solids content of the influent brine reject was determined using the gravimetric method (Standard Methods, 1998; EPA Method No. 310.1). Well-mixed samples were filtered through Whatman glass fiber filters (VWR Scientific, West Chester, PA) before the analysis. Measured volume of filtrate was dried in a pre-weighed evaporating dish on water bath. It was then transferred to the oven, and dried to constant weight for at least 1 hour at 180°C. Subsequently, it was cooled in the desiccator and weighed. The cycle of drying, cooling and weighing was repeated until the weight change was less than 4 percent of the previous weight or

0.5 mg, whichever was less. The total dissolved solid concentration was recorded as the weight of the residue divided by the volume of the sample.

For the batch experiments with varying total dissolved solids concentrations of up to 25,000 mg/l, the salinity adjustment was made using a conductivitymeter equipped with a probe (VWR, San Diego, CA). The conductivitymeter was calibrated using calibration standards of different ranges (100 to 100,000 mg/l TDS) prior to each adjustment. Samples with high total dissolved solids content were filtered through silver impregnated filters (No. 39637, DIONEX, Sunnyvale, CA) to reduce the chloride ion interference with nitrite analysis.

5.3.7 Analysis of Total Alkalinity

A Brinkmann model 716 DMS Titrino Autotitrator (Westbury, NY) was used to analyze the samples for total alkalinity (Standard Methods, 1998; EPA Method No. 350.1). The instrument was equipped with a sample changer equipped with a combination pH reference electrode. The analyzer employed 0.02 N sulfuric acid as titrant, and distilled water. Buffer solutions with pHs 4, 7 and 10 were used for calibration of the pH electrode. The required sample volume was 50 ml, and the samples were unfiltered and undiluted.

5.3.8 Analysis of Hydrogen Sulfide

Total sulfide analysis in the samples was conducted using the methylene blue method (Standard Methods, 1998). Sample preservation was achieved using zinc

acetate. Photometric analysis of samples for color was performed using a Perkin Elmer Lambda 4A UV/VIS Spectrophotometer (Norwalk, CT) at 664 nm.

5.3.9 Analysis of Metals

Two different instruments were used to analyze the metal content of the brine reject. Iron analysis was conducted using a Perkin Elmer Inductively Coupled Plasma-Optical Emission Spectrometer (ICP-OES) (Norwalk, CT) (Standard Methods, 1992; EPA Methods No. 200.7 and No. 200.15). The ICP-OES was equipped with an ultrasonic nebulizer (CETAC U-5000RT) with an operating temperature of 140°C, and an automatic sampling unit. High purity argon gas was employed as the cryogenic liquid. Filtered samples were injected into the plasma *via* the automatic sampler tube, subjecting the constituent atoms to 6,000-8,000°K of temperature in the quartz torch of the plasma. The ionized atoms produced atomic emission spectra that were corrected for the background noise automatically by the computerized interface.

The analyses of the rest of the metals including arsenic, barium, cadmium, cobalt, copper, lead, manganese, mercury, selenium, silver and zinc were conducted using a Perkin Elmer Sciex 6000 Inductively Coupled Plasma-Mass Spectrometer - ICP-MS (Norwalk, CT) as described by Standard Methods (1998) and EPA Method No. 200.8. The ICP-MS was equipped with an automatic sampling unit. High purity argon gas was employed as the cryogenic liquid at 70-120 psi. All standards and

spikes were prepared fresh daily. Samples were diluted as total dissolved solids content of the samples exceeded the 40 ppm limit.

5.3.10 Biomass Assay

The biomass obtained during the batch and continuous flow chemostat experiments were assayed gravimetrically according to Standard Methods (1998). Samples were filtered through 0.45 μ Whatman glass fiber filters (VWR Scientific, West Chester, PA). The filters were then dried at 103-105°C, and the difference in weight before and after drying was recorded. Subsequently, the filters were placed in 550°C oven to remove the volatile organic content. After desiccation, the filters were weighed again, and the difference between the weight after drying and combusting was recorded.

The biomass for the FBAR experiments was measured in terms of attached volatile solids (AVS) per gram of dry GAC, in conformance with the procedure described by Hancher et al. (1978). Bioparticles were removed from the FBAR by carefully lowering a sampling vial into the reactor and allowing it to fill with bioparticles. The bioparticles obtained from the reactor were carefully washed with water in order to remove any non-attached biomass, and dried at 105°C for 24 hours, cooled in the air and weighed. The bioparticles were then combusted at 550°C for 30 minutes, cooled and re-weighed. After washing the biomass-free particles with weak acid (0.1 N HCl) to remove its ash content, it was dried at 105°C for another 24 hours, cooled and weighed. The difference in the weights was used to estimate the

amount of attached biomass. The remaining GAC amount after final drying was weighed, and used in the calculation of biomass in terms of attached biomass per gram of dried GAC.

5.3.11 Scanning Electron Microscopy

Scanning electron microscope (SEM) was used to observe the physical and structural characteristics of coverage of biological growth on the GAC particles. For this purpose, when the biological growth was abundant, several GAC particles (bioparticles) were removed from the FBAR, and fixed for SEM observation. The bioparticles were subjected to the standard sequence of fixation, post-fixation, dehydration, mounting and coating described by Weber et al. (1978) and Pirbazari et al. (1990). In this method, the bioparticles were immersed in a 25 percent electron microscopy-grade glutaraldehyde (Ted Pella Co., Tustin, CA) in 0.1 M sodium cacodylate buffer for fixation at pH 7.2 for 2 hours at room temperature. The bioparticles were then gently washed with 0.1 M cacodylate buffer solution, and post-fixed in 1 percent osmium oxide for an hour followed by rinsing in two consecutive changes of deionized distilled water. After dehydration in a graded series of ethyl alcohol (50, 70, 80, 90 and 100 percent), the bioparticles were prepared for critical-point drying in a 1:1 100 percent ethanol-amylacetate solution, and stored overnight in amylacetate. Finally, the bioparticles were mounted on aluminum stubs, and coated with 100°A gold in a glow-discharge coater to minimize charging and increase the conductivity.

The samples were then analyzed using a Cambridge 3600 Scanning Electron Microscope (Cambridge Instruments, Woburn, MA) equipped with an energy-dispersive spectrometer and a lanthanum hexaboride filament.

CHAPTER 6

NITRIFICATION OPTIMIZATION STUDIES WITH FLUIDIZED BIOREACTOR AND ROTATING BIOLOGICAL CONTACTORS

This chapter focuses on the optimization of the biological nitrification process using two different technologies, namely a laboratory-scale fluidized bioreactor with GAC and a pilot-scale RBC unit with and without PAC. The objectives are: (i) to evaluate and compare ammonia removal efficiencies obtained from the two systems, and (ii) to optimize the two systems with respect to the nitrification process in order to effectively nitrify the RO brine reject.

6.1 Results and Discussions

6.1.1 Nitrification Optimization Studies with Fluidized Bioreactor

The laboratory-scale fluidized bioreactor described in Section 5.2.1.1, Chapter 5 was used to oxidize the ammonia present in the RO brine reject into nitrate. Initially, the bioreactor was charged with 300 g of pre-cleaned GAC. It was then inoculated with the activated sludge sample, and placed in batch recycle mode for about three weeks in order to acclimate nitrifying bacteria and provide attachment and growth on the GAC particles. During this period, the brine reject in the bioreactor was replenished several times when the ammonia concentration

dropped below 5 mg N/l and the nitrite accumulated in the system was completely oxidized to nitrate. Following the batch recycle period, the bioreactor was placed in continuous feed mode.

The fluidized bioreactor effectively reduced an ammonia concentration range of 90-110 mg N/l of by more than 95 percent at a flowrate of up to 25 ml/min. At this flowrate, hydraulic retention time was 180 minutes. Nitrite accumulation occurred only during the batch cycle mode and in the beginning of the continuous feed; but once the steady state was reached, no nitrite was detected in the effluent.

The acclimation and growth of nitrifying bacteria in the initial batch cycle took much longer time than anticipated. This observation confirmed the historically well-known fact that nitrifying bacteria possess a lower specific growth rate and low cellular yield per mass of ammonia oxidized compared to other heterotrophic bacteria, and that this could be the major limiting factor for complete ammonia removal unless every effort is made to provide the optimal environmental conditions, as reported by Shammas (1986). During the operational period of the bioreactor, the pH of the influent brine reject, one of the environmental parameters affecting the nitrification process, was carefully monitored and maintained at optimal levels (around 7.5) in order to establish active nitrifying population and, thereby, obtain maximum nitrifying activity.

The other factor influencing the efficiency of the nitrification process was the hydraulic retention time provided. The minimum hydraulic retention time to obtain good ammonia removal efficiencies of 95 percent and above was 180 minutes.

Below this value, the bioreactor achieved only partial ammonia removal ranging between 20 to 85 percent, and completely failed at hydraulic retention times below 90 minutes. Furthermore, nitrite began to accumulate, and its concentration continued to increase in the effluent below 180 minutes of hydraulic retention times. Apparently, lower hydraulic retention times did not allow sufficient time for nitrite reduction. In addition to this, the biomass concentration in the bioreactor decreased drastically as the hydraulic retention time was lowered, indicating that low hydraulic retention times caused severe loss of biomass as a result of slough-off. The biomass yield was not high enough to compensate for this loss.

The feed brine reject normally contained about 4,500 mg/l of TDS. However, fluctuations in the TDS concentrations of up to 6,000 mg/l were experienced during the experimental period. These fluctuations did not seem to adversely affect the nitrification process performance. This result seemed to contradict with the result reported by Yanguba (1998). In his fluidized bioreactor nitrification system fed by RO brine reject, the elevated TDS concentrations from 4,000 mg/l to 12,000 mg/l at 3 hours of mean cell residence time resulted in a decrease of the nitrification efficiency from 75 percent to 26 percent.

On the contrary to the TDS concentration, the fluidized bioreactor was not capable of effectively handling high or sudden spikes of ammonia at 180 minutes of hydraulic retention time. The sudden increase in the feed ammonia concentration from about 100 mg N/l to 125 mg N/l caused a sudden increase in the effluent ammonia concentration. However, when longer hydraulic retention times of at least

240 minutes were provided during the high ammonia spikes, the ammonia removal efficiency was restored and the nitrification process reached completeness.

Soluble microbial products were observed to accumulate in the bioreactor after a 3-month continuous run period without media replacement. The GAC particles were fully covered by a thick and sticky slime layer that caused the particles to adhere to each other. As the slime layer grew further, the nitrification efficiency declined substantially to the point where there was no nitrification at all. The slime layer surrounding the particles most probably prevented the diffusion of ammonia into the biofilm layer. Mattiasson and Hahn-Hagerdal (1982) stated that high concentration of polymers in gels and biofilms might alter the activity of metabolic pathways by depressing the water activity. At this point, half of the biofilm-covered media was replaced with fresh GAC, and mixed vigorously in order to provide contact between the new GAC particles and the biofilm-covered particles. After a few days of batch mode cycle, the nitrification activity was restored and full nitrification was achieved.

6.1.2 Nitrification Optimization Studies with Rotating Biological Contactors

A pilot-scale aerobic RBC tank was used to nitrify the RO brine reject to be used in the FBAR denitrification and sulfate reduction studies. Upon filling with brine reject and inoculating the tank contents with the activated sludge sample, the RBC tank was initially placed in batch recycle mode. The batch acclimation period took almost 1.5 months, longer than that experienced in the laboratory-scale

fluidized bioreactor. During this cycle, the mixed liquor content of the tank was replenished with fresh brine reject several times to supply ammonia. The batch acclimation cycle continued until ammonia removal rate reached approximately 95 percent and the accumulated nitrite was completely oxidized to nitrate. At this point, it was decided that the microbial slime layer on the contactor disks and the balance between the growth and the washout rate of the nitrifiers were well established. Following the initial start-up problems, the continuous flow feeding was commenced at 125 ml/min, and gradually increased to 350 ml/min within two weeks. However, the ammonia concentration in the effluent also gradually increased. Furthermore, the nitrifying biomass in the mixed liquor content of the RBC tank slowly washed out with the effluent as well. To increase the nitrification efficiency and maintain the biomass concentration at a level necessary to obtain high nitrification activity, a portion of the effluent was recycled back into the tank and the feed flowrate decreased to 200 ml/min (hydraulic retention time = 10.5 hours). The system pH and dissolved oxygen concentration were carefully maintained at 7.8 and well above 3 mg/l, respectively. Even at this flowrate, the efficiency of nitrification process was below 75 percent.

It was then determined to enhance and accelerate the nitrification process by introducing PAC into the mixed liquor content of the tank. PAC slurry was dosed into the tank at a rate of 0.5-3.9 g/l, depending on the influent flowrate. Following the PAC addition, it was observed that the surfaces of the RBC disks were covered with a thin layer of PAC enmeshed within the bacterial biopolymeric secretion. The

recycling of PAC that left the tank with the nitrified effluent and settled on the bottom of the collection container not only increased the active biomass concentration in the tank but also lowered the fresh PAC demand and wastage rate. Nitrification efficiencies of well above 95 percent were achieved in the RBC-PAC system throughout the study. The unit was able to produce up to 450 ml/min of nitrified brine reject at a hydraulic retention time of 275 minutes. The average effluent characteristics of the nitrified brine reject from RBC-PAC unit are summarized in Table 6.1. PAC apparently assisted in maintaining a larger population of active biomass within the tank and improved the overall nitrification efficiency.

The system occasionally encountered problems. The pH of the feed brine reject showed a day-to-day variation because of the addition of sulfuric acid to the secondary wastewater to be treated by the RO unit. Membrane cleaning cycles also contributed acid that caused low pH in the system brine reject. Since nitrifiers are known to be highly sensitive to pH changes, this occasionally resulted in very poor nitrification performances, and even brought the nitrification process almost to a halt, or The RBC-PAC unit, therefore, required constant attention and careful monitoring of the pH to maintain steady state conditions throughout the operational period.

Table 6.1. Average characteristics of nitrified brine reject effluent from RBC-PAC system

Constituent	Unit	Concentration
Total Dissolved Solids	mg/l	4,440
Iron	μg/l	492
Arsenic	μg/l	14
Barium	μg/l	105
Cadmium	μg/l	1.1
Cobalt	μg/l	2.5
Copper	μg/l	33
Lead	μg/l	1.5
Manganese	μg/l	170
Mercury	μg/l	<0.1
Selenium	μg/l	34.7
Silver	μg/l	1.5
Zinc	μg/l	110
Ammonia-Nitrogen	mg/l	1.2
Organic Nitrogen	mg/l	3.8
Total Alkalinity (as CaCO ₃)	mg/l	450
Nitrite-Nitrogen	mg/l	<0.1
Nitrate-Nitrogen	mg/l	82.1
Sulfate	mg/l	1,190
Total Organic Carbon (TOC, Unfiltered)	mg/l	8.4

6.2 Summary and Conclusions

- Following a long microbial acclimation period and during the course of the experiments, the efficiency of the nitrification process using fluidized bioreactor exceeded 95 percent at a hydraulic retention time of minimum 180 minutes. Only partial nitrification was achieved below this retention time. However, no ammonia removal took place at a hydraulic retention time of 90 minutes and shorter.

- The fluidized bioreactor remained unaffected by the fluctuations of TDS concentration, but was incapable of handling high spikes of ammonia without an increase in the applied hydraulic retention time. Longer hydraulic retention times of at least 240 minutes were needed to effectively handle high ammonia concentrations.

- RBC alone was incapable of handling high flowrates due to biomass washout. Even at relatively lower flowrates of 200 ml/min (hydraulic retention time = 10.5 hours), carefully monitored pH and sufficient dissolved oxygen concentration, the efficiency of nitrification process was below 75 percent.

- Introduction of PAC into the RBC tank enhanced the nitrification efficiency well above 95 percent by assisting to maintain higher biomass concentrations in the tank. The system was capable of producing nitrified brine reject at a flowrate of up to 450 ml/min corresponding to a retention time of 275 minutes.

CHAPTER 7

BATCH BIOKINETIC STUDIES: ENVIRONMENTAL PARAMETER OPTIMIZATION FOR DENITRIFICATION PROCESS

This chapter focuses on evaluating the effects of various environmental parameters such as temperature, pH, C:N ratio and the concentration of TDS on the denitrification of RO brine rejects through a series of batch experiments. The main objectives are: (i) to evaluate the effect of these environmental parameters on specific denitrification rate and nitrite accumulation, and (ii) to select the optimum conditions for the subsequent denitrification studies that result in the highest denitrification efficiency in a cost-effective manner.

7.1 Results and Discussions

7.1.1 Batch Studies for Environmental Optimization of Denitrification Process

The experimental matrix used in the batch studies is presented in Table 7.1. Four different sets of experiments were conducted to optimize the denitrification process for various environmental parameters including temperature, pH, C:N ratio and TDS. As observed from the table, for each experimental set, only the main parameter tested was varied within a pre-determined range of the experimental matrix, while the other parameters were maintained constant.

Table 7.1. Experimental matrix used in batch studies

Varying Parameter	Experimental Matrix	Constant Parameters
Temperature (°C)	10; 15; 20; 25; 30; 35; 40; 45	pH: 7.5 Ethanol: Excess TDS: 4,000 mg/l
pH	6; 6.5; 7; 7.5; 8; 8.5; 9	Temperature: 30°C Ethanol: Excess TDS: 4,000 mg/l
C:N Ratio (mg C/mg N)	1.2:1; 1.5:1; 1.8:1; 2.2:1	Temperature: 30°C pH: 7.5 TDS: 4,000 mg/l
TDS (mg/l)	4,000; 8,000; 15,000; 25,000	Temperature: 30°C pH: 7.5 Ethanol: Excess

7.1.1.1 Effect of Temperature

A series of batch experiments covering a temperature range of 10 to 45°C with 5°C increments were conducted to investigate the effect of temperature on the specific denitrification rate and the dynamics of the denitrification process. Figure 7.1 demonstrates the variations in nitrate, nitrite and biomass concentrations in 30°C batch experiment that employed 61 mg N/l of nitrate and 307 mg/l of biomass concentration. As seen from the figure, nitrate was completely consumed in about 95 minutes. Significant amount of nitrite accumulated as the intermediate product, and the accumulated nitrite concentration reached its peak at 88 percent of the initial nitrate concentration. It then began to decrease and was completely reduced to nitrogen gas in approximately 240 minutes. The biomass concentration increased until all nitrate was exhausted, followed by a gradual decline and again a slight rise

as nitrite concentration approached zero. After the completion of nitrite reduction and hence denitrification, the biomass concentration began to decrease as well.

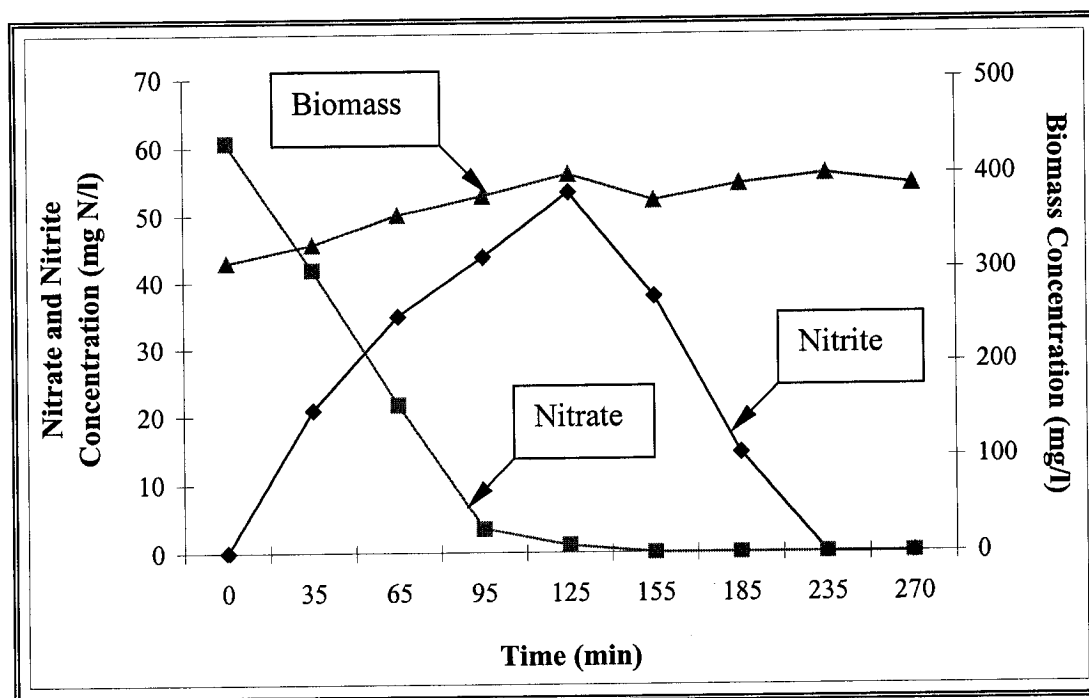


Figure 7.1. Variations of nitrate-nitrogen, nitrite-nitrogen and biomass concentration in the batch experiment at 30°C temperature

The specific denitrification rates (SDR) were plotted against temperature as shown in Figure 7.2 to determine the temperature range in which the denitrification process proceeded efficiently. As can be observed from the figure, the SDR increased with temperature increase up to 35°C, underwent a slight decline at 40°C, followed by a sudden decline thereafter. Delanghe et al. (1994) observed similar results in their denitrification system. At low temperatures of 10 and 15°C, even though the net amount of biomass produced over the course of the experiments was

higher, the specific denitrification rates were lower because the completion of nitrate removal took longer at these low temperatures as compared to the time required for completion at higher temperatures. At 45°C, the specific denitrification activity declined sharply possibly due to the denaturation of bacterial enzymes, as suggested by Rittmann and McCarty (2001).

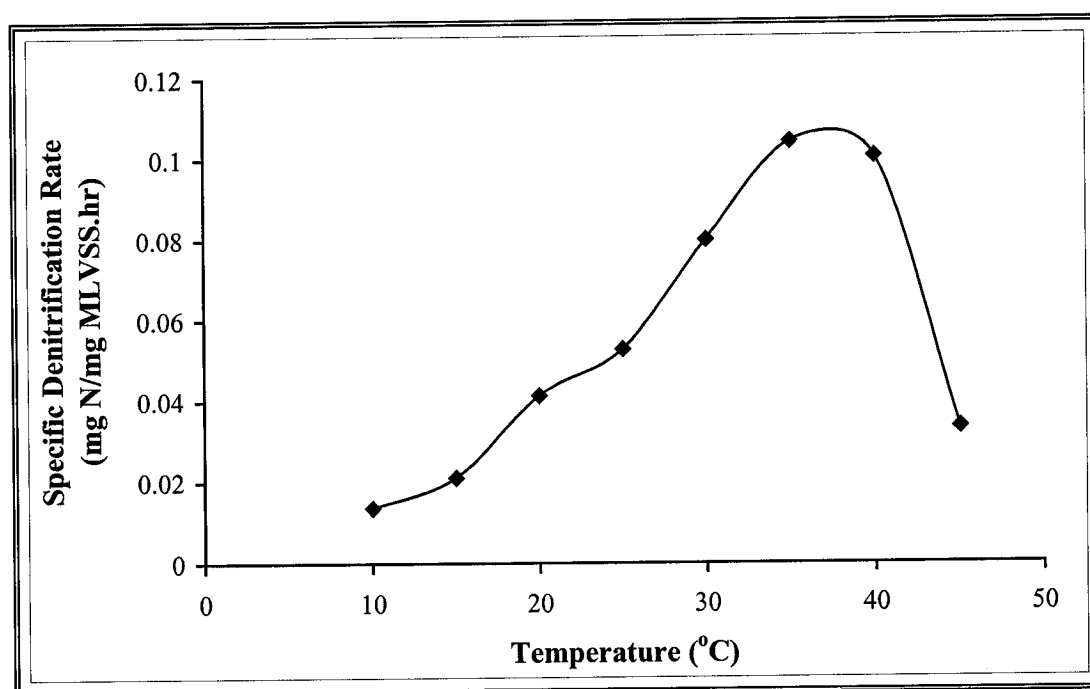


Figure 7.2. Specific denitrification rates at different temperatures

At all temperatures, nitrite accumulation was inevitable, and the removal of nitrite did not begin to take place until almost all nitrates were removed. This phenomenon has been reported in the literature, and four possible reasons have been advanced. One reason is that nitrate is used preferentially over nitrite resulting in

accumulation of nitrite due to some unfavorable environmental conditions despite the presence of both nitrate and nitrite reductases (Engberg & Schroeder, 1975; Glass & Silverstein, 1998; Timmermans & Van Haute, 1983). The second reason suggested that natural selection in mixed microbial cultures might favor those microorganisms referred to as nitrate respiring bacteria that are capable of reducing nitrate only to nitrite (Wilderer et al., 1987). The third reason emphasized that certain strains of denitrifiers can use nitrate and nitrite sequentially with nitrate being consumed first, suggesting that nitrate exerts a high degree of inhibition on the uptake of nitrite (Wang et al., 1995). The last reason suggested that nitrite accumulation could result either from nitrate inhibition on nitrite reduction, or from a difference in the rates of nitrate and nitrite reduction (Betlach & Tiedje, 1981).

At temperatures from 20°C to 45°C, the removal of nitrite was very rapid only after the conversion of all nitrates into nitrite. This might indicate that nitrite reductase could either be produced very efficiently at higher temperatures, or it could perform better than the nitrate reductase at higher temperatures in the absence of nitrate. In fact, Gayle et al. (1989) reported an increase in nitrite reductase activity after having substantial nitrite accumulation, which gave way to the conversion of nitrite into nitrogen gas, thereby, completing the denitrification process. However, at 45°C, although nitrate removal was unexpectedly faster, significant nitrite accumulation was observed, and it took a relatively long time for the denitrifiers to reduce the accumulated nitrite. From this observation, it could be postulated that nitrate reductase could withstand high temperatures beyond the optimum range

despite the fact that some denaturation could still occur, while nitrite reductase could be highly susceptible to denaturation at higher temperatures beyond the optimum range.

Specific denitrification kinetics response to temperature can be expressed by a modified Arrhenius formula as follows (Lewandowski, 1982):

$$SDR_T = SDR_{20} 10^{k(T-293)} \quad (7.1)$$

where

SDR_T = Specific denitrification rate at any temperature (mg N/mg MLVSS.hr)

SDR_{20} = Specific denitrification rate at 20°C (mg N/mg MLVSS.hr)

k = Temperature constant ($^{\circ}\text{K}^{-1}$)

T = Temperature ($^{\circ}\text{K}$)

Figure 7.3 demonstrates a plot of natural logarithm of the specific denitrification rates as a function of temperature, indicating a linear relationship between 10°C and 35°C. This linearity showed that denitrification was achieved in the temperature ranges of 10°C to 35°C. This result is consistent with that reported by Delanghe et al. (1994) who found a linear relationship between the specific denitrification activity and temperature in the range 10°C to 40°C for their groundwater denitrification process, and by Lewandowski (1982) who reported 5°C to 35°C as the optimum range for his two-stage nitrification-denitrification process. The slope of the line in Figure 7.3 yields a temperature constant (k) value of

$0.0357^{\circ}\text{K}^{-1}$. This value is slightly higher than the value found by Lewandowski (1982) and Delanghe et al. (1994), which were 0.029 and $0.028^{\circ}\text{K}^{-1}$, respectively.

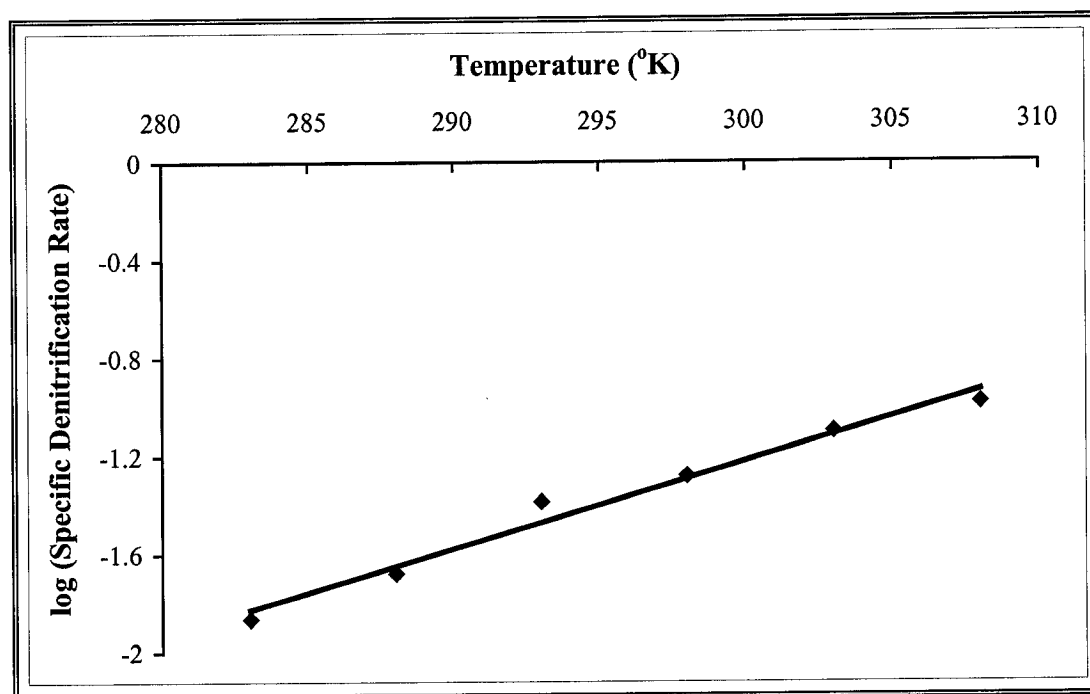


Figure 7.3. Natural logarithms of specific denitrification rates with respect to temperatures between 10°C and 35°C at which the linearity could be established (correlation coefficient = 0.979)

In order to evaluate the sensitivity of the denitrification process to changing temperatures, it is necessary to calculate the activation energy of the system using the Arrhenius equation:

$$SDR = A \cdot \exp \left(\frac{-E_a}{RT} \right) \quad (7.2)$$

where

SDR = Specific denitrification rate (mg N/mg MLVSS.hr)

A = Arrhenius constant (dimensionless)

E_a = Activation energy (cal/mol)

R = Universal gas constant (cal.gr/mol. $^{\circ}$ K)

By taking the natural logarithm of each side of the equation, it is possible to plot $\ln(\text{SDR})$ vs. $(1/T)$ and obtain a linear relationship with the slope equal to $(-E_a/R)$. From Figure 7.4, the activation energy was calculated to be 14.25 Kcal/mol. This was slightly higher than the values reported by Lewandowski (1982), Delanghe et al. (1994) and Wang et al. (1995) possibly due to the characteristics of the RO brine reject. The concentrated contaminant levels in the brine reject may place additional strain on the activity of denitrifying bacteria, especially on the nitrite reducing bacteria present in the system. As a result, denitrifiers must overcome a slightly larger energy barrier to achieve nitrate reduction.

Computation of a temperature quotient is another way to evaluate the response of the system to the changes in temperatures. Temperature quotient shows the approximate degree of increase or decrease in the denitrification reaction rate for a temperature change by 10°C according to the following formula (Delanghe et al., 1994):

$$Q_a = \frac{SDR_{T+10}}{SDR_T} \quad (7.3)$$

where

Q_a = Temperature quotient (dimensionless)

SDR_{T+10} = Specific denitrification rate at temperature $T+10$ (mg N/mg MLVSS.hr)

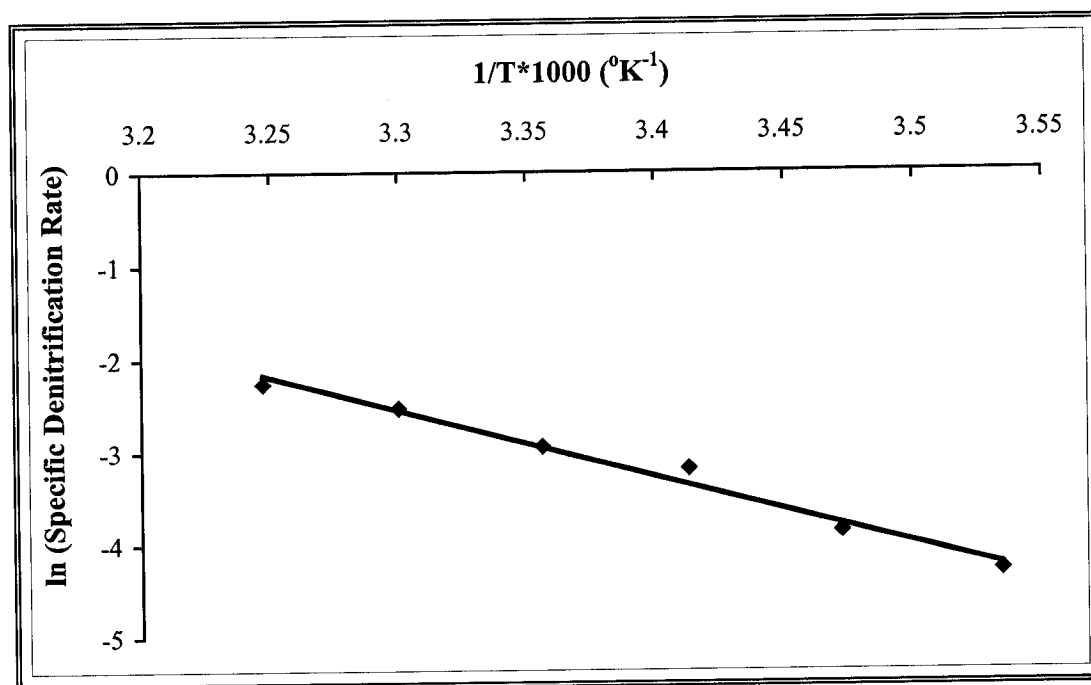


Figure 7.4. Arrhenius plot at the temperatures at which linearity with respect to specific denitrification rates were established (correlation coefficient = 0.984)

In this study, Q_a was determined to be between 1.96 and 2.93 between 10°C and 35°C . At lower temperatures, the coefficient appeared to be high (2.93) implying that a 10°C increase in temperature from 10°C to 20°C could cause a substantial increase (almost tripling) in the specific denitrification rate. As the temperature increased from 25°C to 35°C , the value approached 1.96, which implied that at higher temperatures, the reaction rate would only double. When the temperature

increased from 30°C to 40°C, the quotient was only 1.26, which implies that increasing the temperature beyond a certain optimum level would not necessarily cause any further increase in the specific denitrification rate. From this, it is possible to conclude that the rate of slow-down of the process was more severe at low temperatures than the rate of increase of the process at high temperatures. It was also because of this result that an optimal temperature of 30°C was selected for the future experimental work instead of 35°C or 40°C.

7.1.1.2 *Effect of pH*

A series of batch tests were conducted between the pH values of 6 and 9 with increasing increments of 0.5 to evaluate the effect of pH fluctuation on the specific denitrification rate and nitrite accumulation. The plot of SDR vs. pH constituted a bell-shaped curve with a peak around pH of 8, as demonstrated in Figure 7.5. Similar curves were obtained by several other researchers (Delanghe et al., 1994; Timmermans & Van Haute, 1983).

According to Timmermans and Van Haute (1983), denitrification activity in a system is reduced by pH deviations due to non-competitive inhibition, and the following mathematical expression can be used:

$$SDR = SDR_{\max} \frac{1}{1 + k_i I} \quad (7.4)$$

where

k_i = Constant (dimensionless)

I = Concentration of inhibitor (mg/l), which is equal to

$$I = 10^{|pH_{\max} - pH|} - 1$$

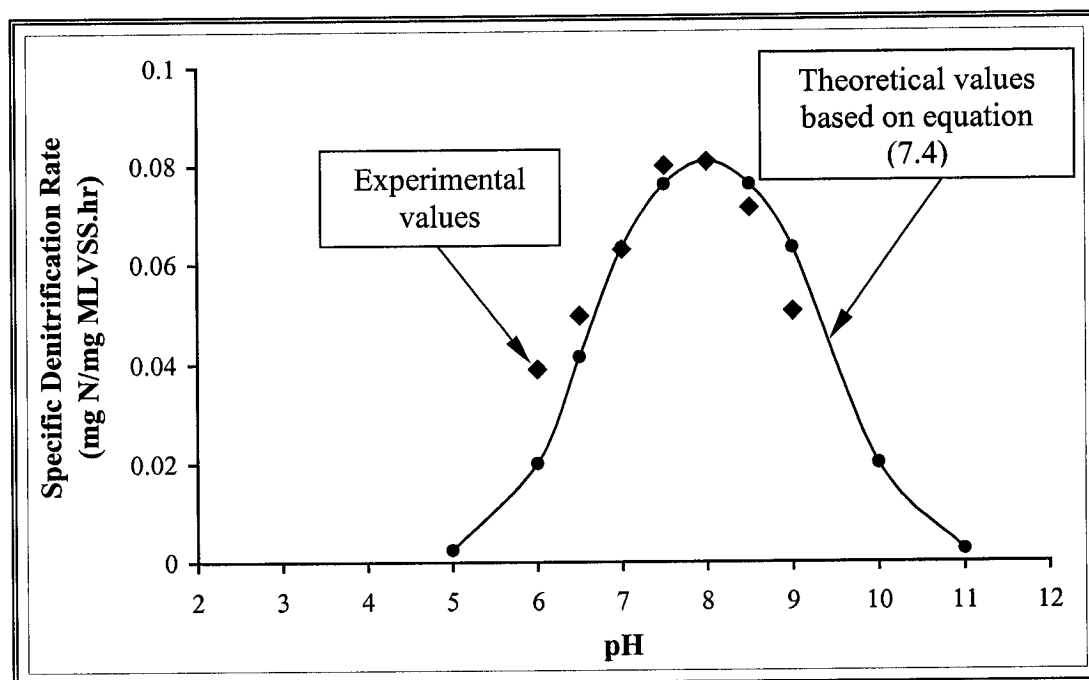


Figure 7.5. Experimental and theoretical specific denitrification rates at different pH values

The inhibitor concentration was determined using the value of 8 for the pH_{\max} term. The theoretical curve that best-fit the experimental data, as shown in Figure 7.5, was obtained using equation (7.4) with the maximum value of SDR (SDR_{\max}) at the maximum pH and the values for inhibitor concentration at the respective pH values. The curve that best-fit the experimental data yielded a k_i value of 0.0357.

This value is in good agreement with the results obtained by Timmermans and Van Haute (1983) and Delanghe et al. (1994).

From these results, the combined effect of temperature and pH on the specific denitrification rate could be determined by combining equations (7.1) and (7.4), and expressed in a single mathematical relationship as (Delanghe et al., 1994; Timmermans & Van Haute, 1983):

$$SDR = SDR_{\max, 293} \frac{10^{0.0357 (T-293)}}{1 + 0.0357 (10^{|8-pH|} - 1)} \quad (7.5)$$

After determining the variation of the specific denitrification rate as a function of pH and temperature, it is important to also evaluate nitrite accumulation with respect to pH. At lower pH values, especially at pH 6, denitrification activity still occurred with a substantial increase in the accumulated amount of nitrite. Accumulation continued to take place until almost all nitrate was consumed, at which time nitrite reduction took over at a slower rate, causing a delay in the completion of the process. This result was in accordance with the result obtained by Glass and Silverstein (1997) who hypothesized that nitrite reduction rate was low at the lower pH probably because of nitrous acid accumulation in the system.

Higher pH values, especially above 7.5, favored faster nitrate or nitrite conversion into nitrogen gas with less accumulation of nitrite. This was very apparent at pH 9. This result seemed to be consistent with Glass and Silverstein's (1998) report. However, it was observed that nitrite accumulation was minimal at pH 9 in spite of the presence of nitrate, indicating that nitrite reduction or nitrite

reductase activity peaked at reasonably higher pH values around 9. This observation was not in accord with the result obtained by Glass and Silverstein (1998). They stated that at pH values from 8.5 to 9, the suppression in nitrite reduction increased from 33 to 60 percent in the presence of nitrate.

At pH 9, the color of the brine reject in the vessel became cloudy white, and formation of white flocs was observed possibly due to the precipitation of metals. The batch run was continued to evaluate the effect of high pH as well as the effect of precipitation on the denitrification activity. The specific denitrification rate appeared to decline although nitrate reduction was completed in a reasonably short period of time with less nitrite accumulation.

The optimal pH for the future experimental work was selected as 7.5 despite the fact that the highest denitrification rate was achieved at pH 8. Since the pH of the nitrified brine reject was closer to 7.5, no substantial addition of acid or base was required for pH adjustment.

7.1.1.3 Optimum Carbon-to-Nitrogen Ratio

Based on the literature studies, a series of batch experiments were conducted on several C:N ratios of 1.2:1, 1.5:1, 1.8:1 and 2.2:1 mg C/mg N at 30°C and pH of 7.5 in order to determine the optimal C:N ratio required by the denitrifying bacteria. Carbon source serves as the principal electron donor in denitrification process, and the determination of the carbon quantity is of utmost significance from the economical point of view.

Figure 7.6 shows the variations of nitrate, nitrite and biomass for the batch experiment that employed the C:N ratio of 1.8:1 mg C/mg N, initial nitrate concentration of 70 mg N/l and biomass concentration of 608 mg/l. As can be observed from the figure, nitrate consumption was completed in 70 minutes at which time the nitrite accumulation reached a maximum at 68 percent of the initial nitrate concentration, and immediately thereafter began to decline and was completely depleted at 125 minutes. The biomass concentration initially increased and reached a plateau around 30 minutes. It started to decline at about 90 minutes at which time insignificant amount of nitrate and nitrite were present in the system.

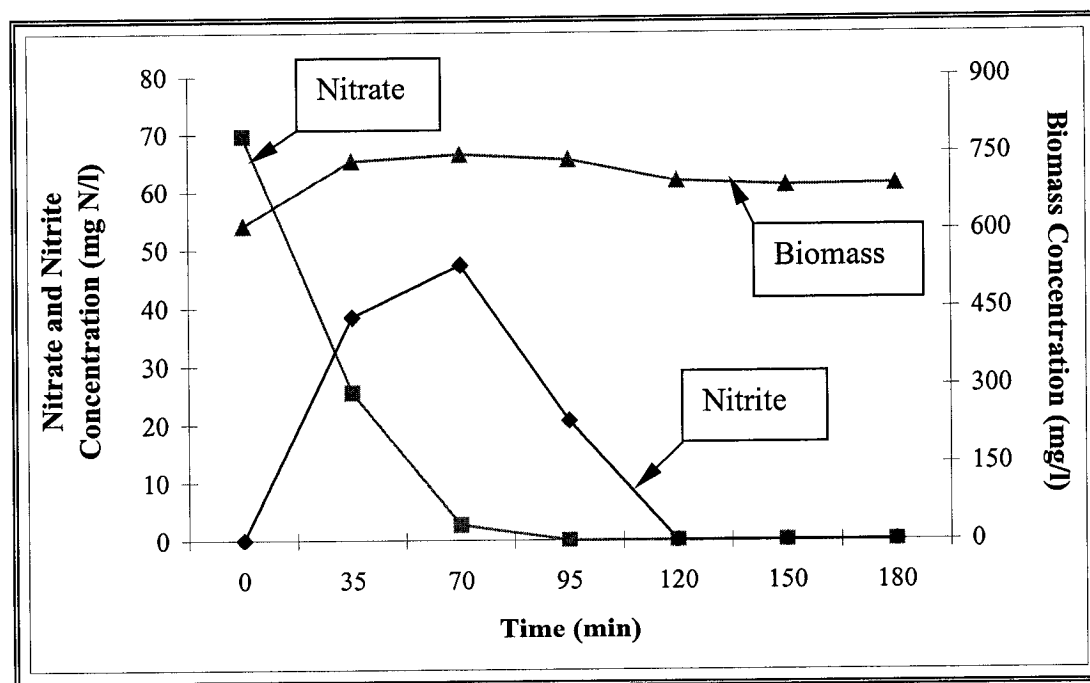


Figure 7.6. Variations of nitrate-nitrogen, nitrite-nitrogen and biomass concentrations in batch experiment with C:N ratio of 1.8:1

Figure 7.7 illustrates the change in specific denitrification rates with respect to the range of C:N ratios employed. As evident from the figure, the optimal C:N ratio appears to be between 1.5:1 and 1.8:1 mg C/mg N, 1.5:1 mg C/mg N being the critical ratio. Delanghe et al. (1994) reported a critical value of 1.4:1-1.5:1 for their system using ethanol. As can be observed from Figure 7.7, there is a significant decline in specific denitrification rate value below the C:N ratio of 1.5:1 mg C/mg N. Also, no marked change is observed between ratios of 1.5:1 and 2.2:1 mg C/mg N.

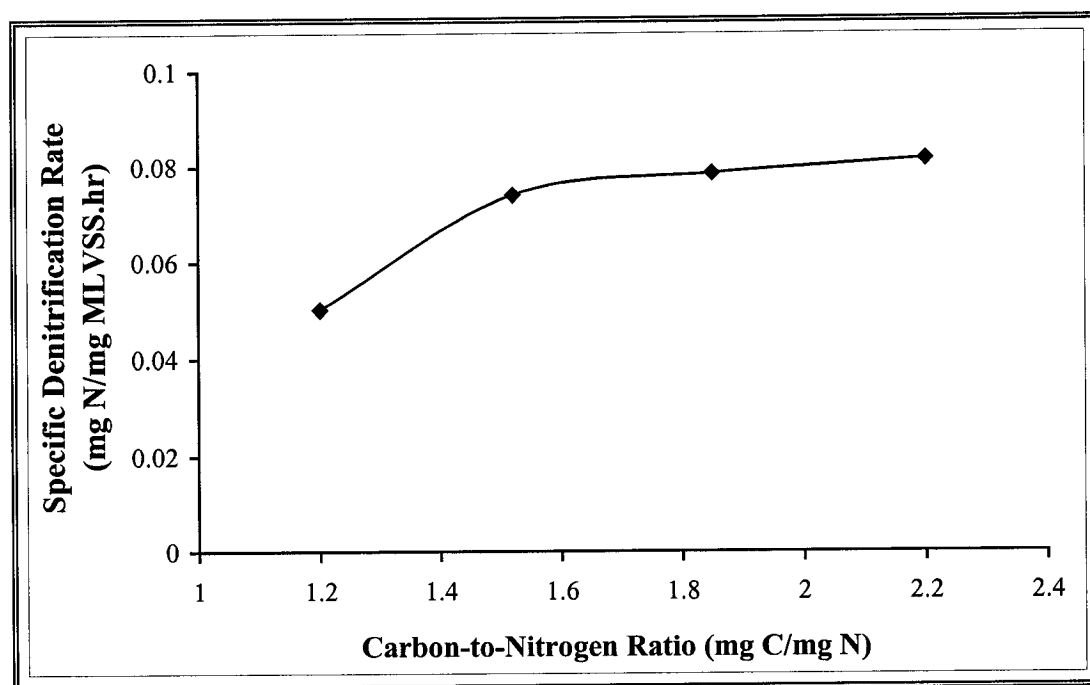


Figure 7.7. Change in specific denitrification rates with respect to different C:N ratios

It is important to note that at lower C:N ratios, such as 1.2:1 mg C/mg N, although nitrate was completely consumed, nitrite accumulated in significant

amounts, and its reduction remained incomplete, even though the experiment took longer than anticipated. Oh and Silverstein (1999) reported that complete denitrification occurred within a reasonable amount of time without any significant nitrite accumulation when carbon source was provided in sufficient quantities, while carbon source limitation resulted in partial denitrification with significant nitrite accumulation.

Although, as mentioned earlier, the optimal C:N ratio lied between 1.5:1 and 1.8:1 mg C/mg N, the ratio 1.8:1 mg C/mg N was chosen to avoid the ethanol from becoming a limiting substrate, should the influent nitrate concentration fluctuate. At this ratio, the carbon demand for new biomass formation can also be accommodated without leaving significant organic carbon residual in the effluent stream.

7.1.1.4 Effect of Total Dissolved Solids

To assess the effect of TDS concentration of the denitrification dynamics, a series of batch tests were carried out with TDS concentrations of 8,000 mg/l (0.75%), 15,000 mg/l (1.45%) and 25,000 mg/l (2.4%) at 30°C and pH of 7.5. Figure 7.8 illustrates the variations in nitrate, nitrite and biomass concentration for TDS concentration of 8,000 mg/l. As evident from the figure, nitrate was removed within 90 minutes, whereas nitrite reduction was complete in approximately 120 minutes. Nitrite accumulation was about 70 percent of the initial nitrate concentration. Biomass concentration, however, fluctuated depending on the relative

concentrations of nitrate and nitrite in the system. When both nitrate and nitrite were exhausted, the biomass concentration began to decline.

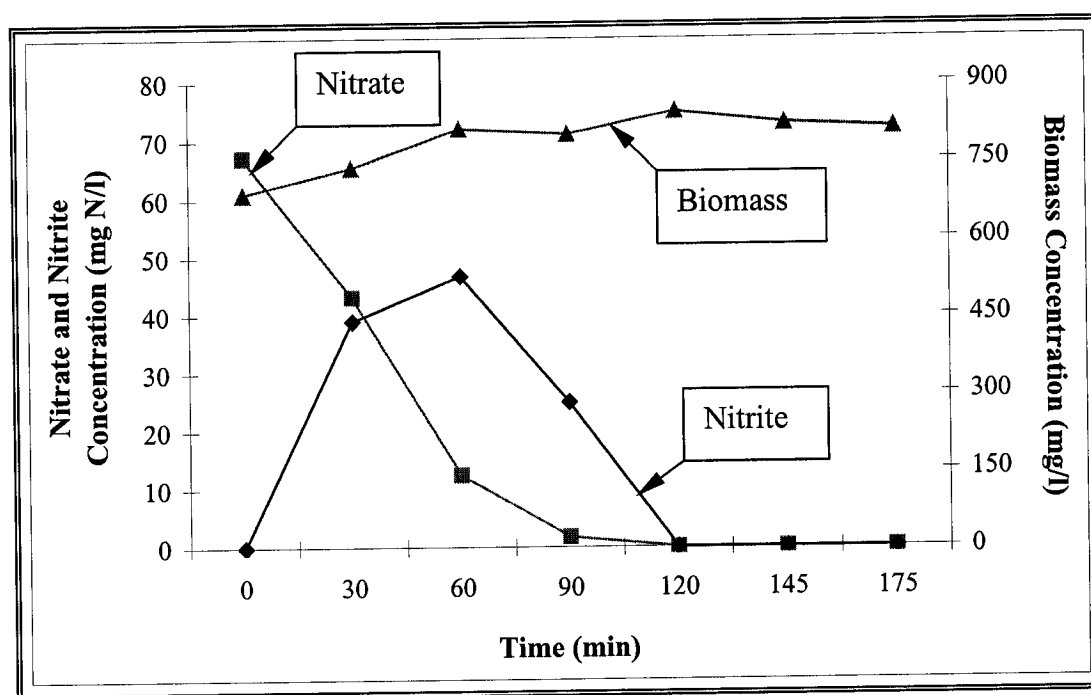


Figure 7.8. Variations of nitrate-nitrogen, nitrite-nitrogen and biomass concentrations in batch experiment with 8,000 mg/l TDS concentration

Figure 7.9 shows the variations in specific denitrification rate as a function of different TDS concentrations. As evident from the figure, the specific denitrification rate dropped sharply by about 30 percent as the TDS concentration was increased from 4,000 to 8,000 mg/l. This sudden decline could be due to the fact that, even though the same denitrifying culture was used in both batch tests, the culture had not been acclimated sufficiently to increased salt concentration. As the TDS increased

further from 15,000 mg/l to 25,000 mg/l, the denitrification activity declined only slightly, as the microorganisms had already been acclimatized. Glass and Silverstein (1999) reported the importance of microbial acclimation to high TDS concentrations at optimum pH values. In fact, their effort to denitrify the wastewater with unacclimated activated sludge culture was unsuccessful even at relatively high pH values. In their later investigation, they developed a “stepwise-increase” acclimation strategy to increase the nitrate concentration causing denitrification of high-nitrate and high-salinity wastewater.

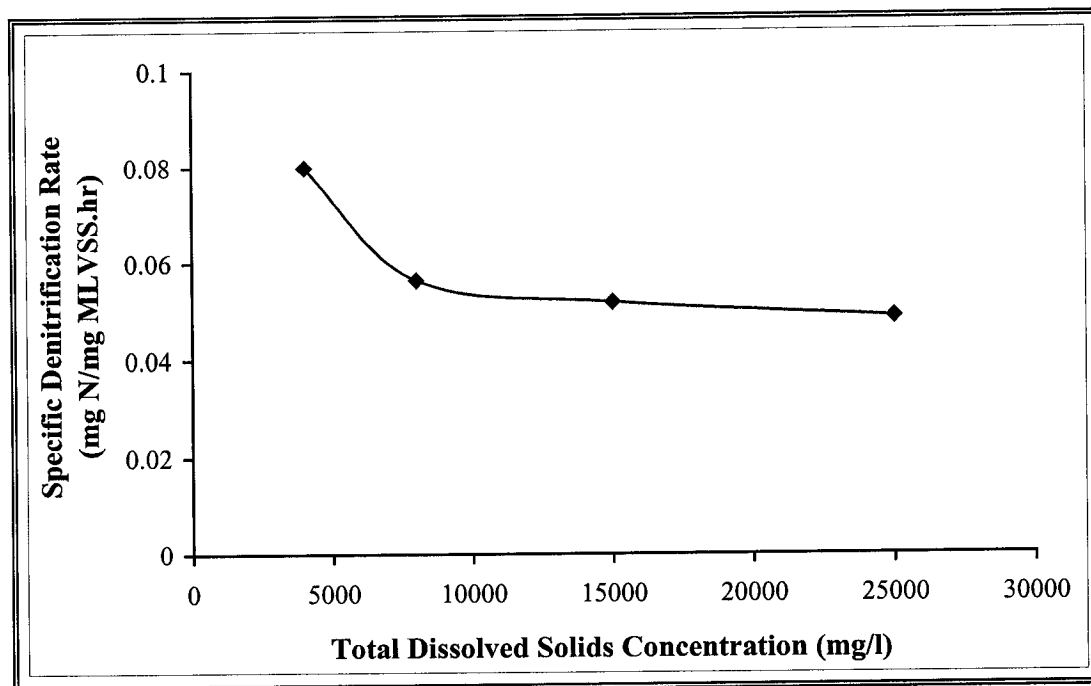


Figure 7.9. Change in specific denitrification rates as a function of TDS concentrations

In all cases, there was some nitrite accumulation that, interestingly, was consumed in a relatively short period of time. This might be due to the fact that nitrite reductase is less susceptible to high TDS concentrations than nitrate reductase or that the gradual acclimation of the denitrifiers to the elevated salt concentration during the process could result in reduction of nitrite production or reduction of accumulation over an extended period (Yang et al., 1995).

In conclusion, the effect of high TDS concentration on the denitrification rate was not as severe as anticipated. In fact, it is reported that pH, temperature and carbon to nitrogen ratio could have more significant impacts on the denitrification activity than the TDS concentration (Clifford & Liu, 1993). It is, therefore, anticipated that the fluctuations in the influent TDS concentration of brine reject would not significantly alter the denitrification efficiency of the system.

7.2 Summary and Conclusions

- It was demonstrated that the specific denitrification rate reached maximum at around 35°C. Denitrification rate declined at temperatures below and above 35°. In all batch tests, nitrite accumulation occurred until almost all nitrate was consumed. After the consumption of nitrate, nitrite depletion took place at a much shorter time as compared to that of nitrate.
- The highest denitrification activity was observed around pH 8. Nitrite accumulated in all experiment. However, at pH values above 7.5, substantial decline

in nitrite accumulation was experienced. At pH 9, the cloudiness and floc formation in the brine reject test solutions suggested the possibility of metal precipitation, indicating that pH control is necessary during the denitrification process.

- The critical C:N ratio was determined to be 1.5:1. However, a somewhat higher value of 1.8:1 was selected as optimum ratio to provide sufficient carbon source. Above this ratio, the specific denitrification activity did not differ significantly. At lower C:N ratios such as 1.2:1, although nitrate was totally consumed, substantial amount of nitrite accumulated in the system with no further reduction due to insufficient carbon source.

- Although the denitrification rate declined when the TDS concentration doubled from 4,000 to 8,000 mg/l, due to lack of sufficient microbial acclimation period, it was concluded that any possible fluctuation in the TDS concentration up to 25,000 mg/l would not adversely affect the denitrification process.

CHAPTER 8

CONTINUOUS FLOW CHEMOSTAT STUDIES: BIOKINETIC PARAMETERS DETERMINATION

This chapter discusses the determination of Monod biokinetic constants including maximum specific growth rate (μ_m), Monod half saturation constant (K_s), growth yield coefficient (Y), and decay rate (k_d) through a series of continuous flow chemostat studies under growth-limiting conditions with respect to nitrate, nitrite and ethanol. The main objectives are: (i) to apply a biokinetic model that adequately describes the rates and extend of biodegradation and mechanistic limitations of the reactions involved, (ii) to determine the Monod biokinetic constants under nutrient-limiting (nitrogen and carbon source) conditions, and (iii) to provide the Monod biokinetic inputs for the FBAR denitrification model used to predict and simulate process performance under various conditions.

8.1 Results and Discussions

As mentioned earlier, the information on biodegradability obtained as a result of biokinetic studies conducted on denitrification process using the RO brine reject: (i) provides a basis for the performance and feasibility assessment of the denitrification process for this specific waste stream, (ii) offers opportunity to compare the biokinetic values obtained from these studies with the literature values,

and (iii) provides the necessary parameters for the mathematical model to predict the FBAR process dynamics under a variety of operating conditions. As emphasized by Kornaros et al. (1996), since these parameters all greatly affect the performance and economy of any treatment system, they can be utilized to determine the optimal design criteria and operational strategies for the denitrification systems.

The biokinetic parameters for the denitrification process are usually determined through a series of nitrogen source-limiting and carbon source-limiting batch biokinetic or continuous flow chemostat studies (Kornaros et al., 1996; Shimizu et al., 1978;). In such studies, a pre-determined dilution rate, represented by D or μ , which is equal to the feed flowrate divided by the volume of the chemostat, is applied into the chemostat of known volume until the system reaches steady state conditions with respect to substrate removal and/or biomass growth rate. When the steady state is reached, the next dilution rate is applied, and this process is continued with increasing increments until the substrate of concern accumulates in the chemostat in quantities that indicate no reaction is taking place or until biomass is washed out of the chemostat, whichever occurs first. Representative samples and replicates are taken at each dilution rate, and analyzed for substrate, intermediate products and biomass concentrations.

In light of these explanations, two sets of continuous flow chemostat experiments operated at various different dilution rates were conducted to determine the biokinetic parameters describing the biological activity in the denitrification process:

1. Nitrogen-Limiting Chemostats:

- Nitrite-limiting chemostat with excess ethanol
- Nitrate-limiting chemostat with excess ethanol

2. Ethanol-Limiting Chemostats:

- Ethanol-limiting chemostat with excess nitrite
- Ethanol-limiting chemostat with excess nitrate

The results obtained from each of these experiments are discussed in the following sections.

8.1.1 Nitrogen-Limiting Chemostat Studies

Nitrogen-limiting chemostats were conducted with limited quantities of nitrite and nitrate in the abundance of ethanol as the carbon source. The results of these studies are used to determine the Monod biokinetic constants.

8.1.1.1 Nitrite-Limiting Chemostat

The nitrite-limiting chemostat experiment employed a synthetic brine reject solution whose constituents are given in Table 5.1, Chapter 5. The reactor contained 119.3 mg N/l of nitrite and 550 mg/l of ethanol, but no nitrate. Figure 8.1 presents the variations in nitrite, ethanol and biomass concentrations over the course of the chemostat run. The initial feed flowrate was 3 ml/min corresponding to a dilution rate (μ) of 0.133 hr⁻¹. Only trace amounts of nitrite were detected up to 1,500 minutes of operation. Nitrite began to accumulate at the flowrate of 8 ml/min ($\mu = 0.356$ hr⁻¹),

and its concentration progressively increased until total washout occurred at a flowrate of 15 ml/min ($\mu = 0.667 \text{ hr}^{-1}$). The ethanol concentration fluctuated depending on the applied dilution rate. However, its effluent concentration increased with the increase in the effluent nitrite concentration. The biomass began to wash out of the system after 1,300 minutes of operation, and no biomass remained in the reactor around 2,500 minutes at the flowrate of 15 ml/min ($\mu = 0.667 \text{ hr}^{-1}$).

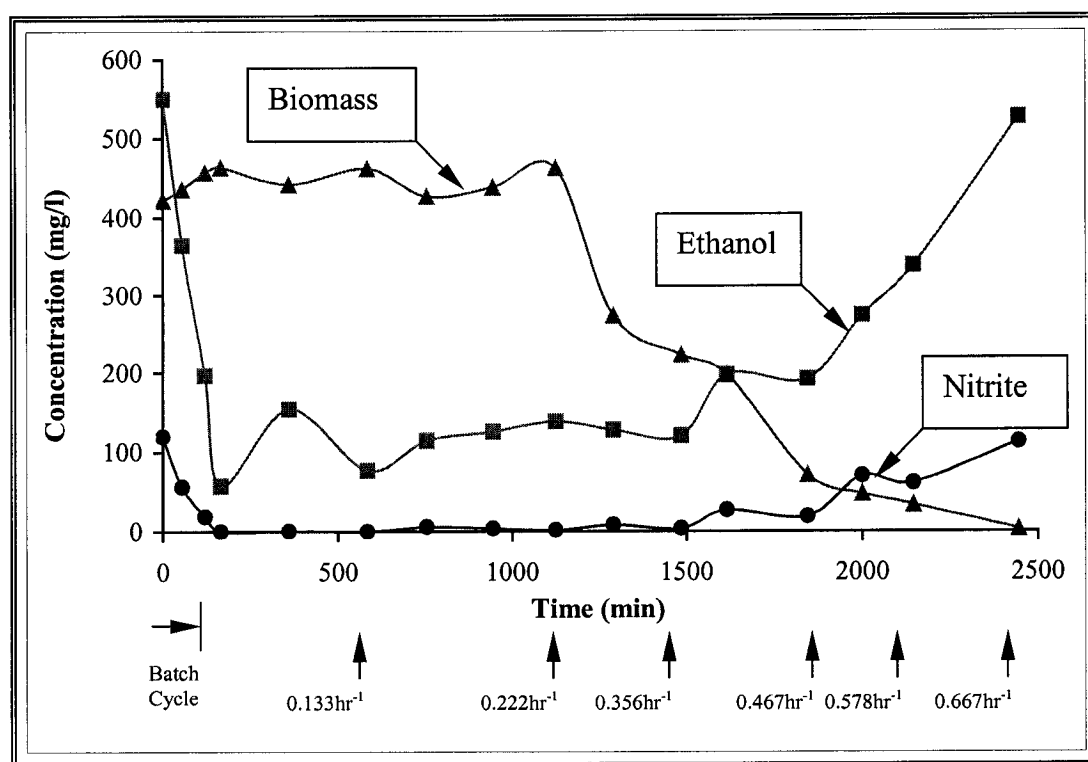


Figure 8.1. Variations in nitrite, ethanol and biomass concentration profiles with respect to time in nitrite-limiting chemostat (Initial concentrations: Nitrite = 119.3 mg N/l, Nitrate = 0 mg N/l, Ethanol = 550 mg/l); Arrowheads indicate the applied dilution rates

The plot of specific denitrification rates as a function of applied dilution rates according to the equation (3.12) is presented in Figure 8.2. The reciprocal of slope of the line provided the growth yield coefficients of 0.32 and 0.29 with respect to nitrite utilization ($Y_{b,N}$) and ethanol utilization ($Y_{b,E}$), respectively. Further, according to

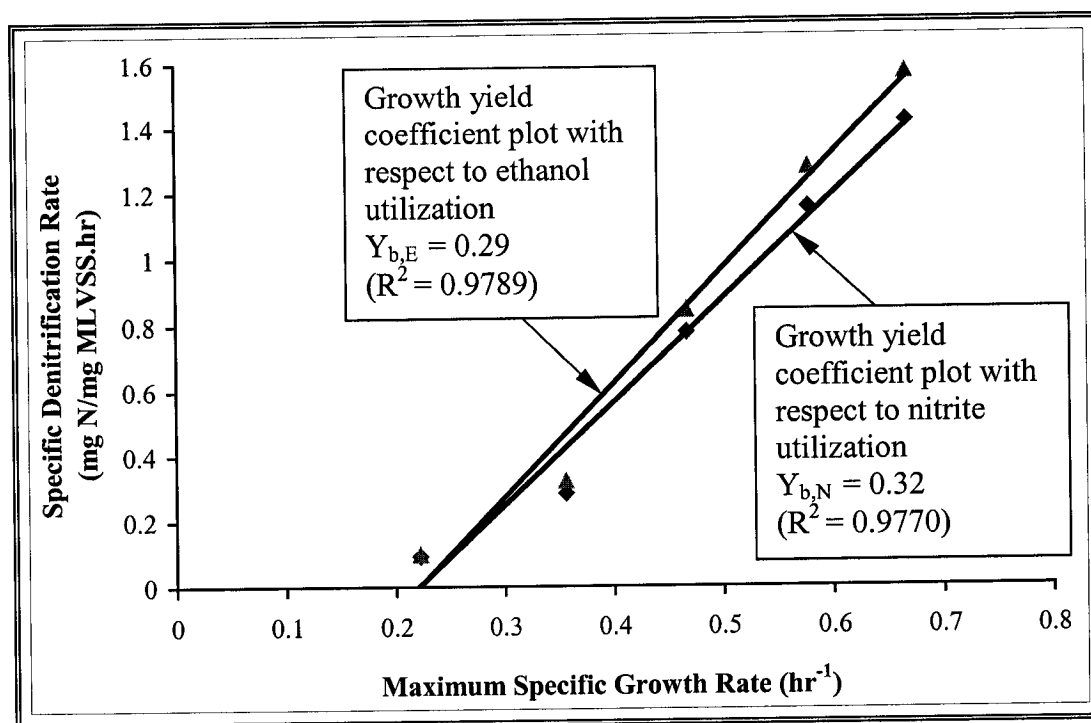


Figure 8.2. Relationship between specific denitrification rate and maximum specific growth rate with respect to nitrite and ethanol utilization in nitrite-limiting chemostat

equation (3.14), the reciprocal of the intercept of the Lineweaver-Burke plot presented in Figure 8.3 provided an estimate of the maximum specific growth rate ($\mu_{m,b}$), while the Monod half saturation constant ($K_{s,b}$) was found by multiplying the

value of $\mu_{m,b}$ by the slope. As determined from the plot, $\mu_{m,b}$ is equal to 0.60 hr^{-1} , and $K_{s,b}$ is equal to 8.8 mg/l .

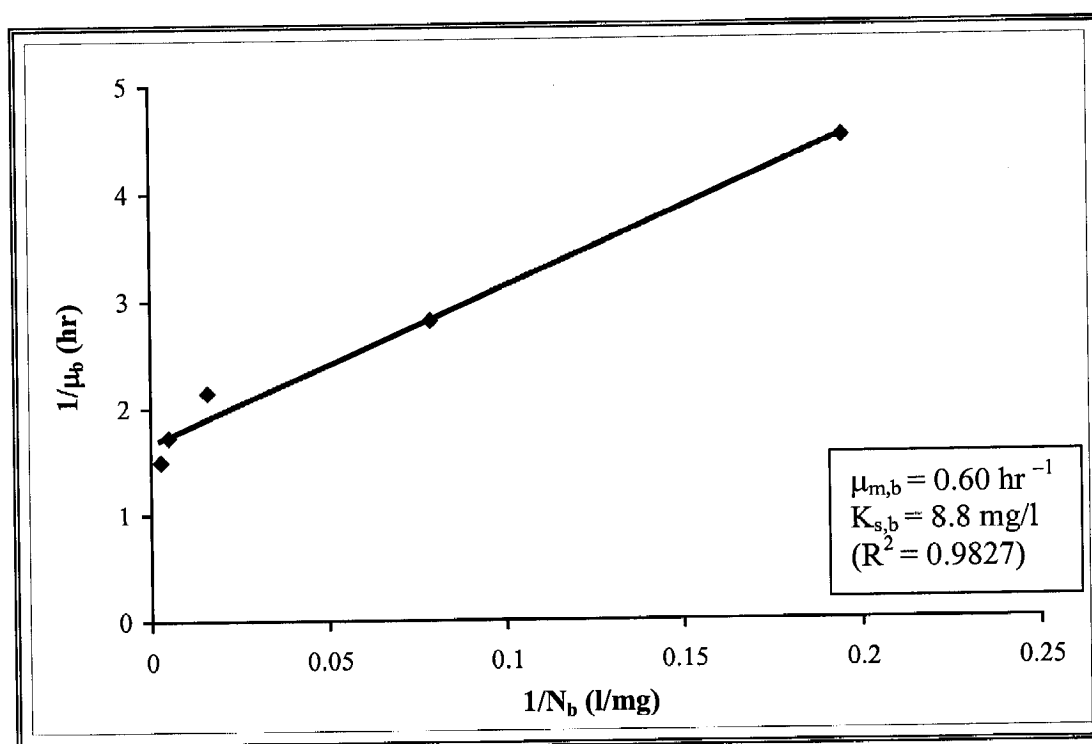


Figure 8.3. Lineweaver-Burke plot to determine the Monod biokinetic constants for nitrite-limiting chemostat according to equation (3.14)

8.1.1.2 Nitrate-Limiting Chemostat

Nitrate-limiting chemostat initially contained 75.2 mg N/l of nitrate, 650 mg/l of ethanol, and no nitrite. Figure 8.4 represents the variations in nitrate, nitrite, ethanol and biomass concentrations as a function of time over the course of the chemostat run. At completion of the “batch mode” operation of the chemostat that took approximately 255 minutes, the feeding of brine reject was commenced at an

initial flowrate of 2 ml/min ($\mu = 0.089 \text{ hr}^{-1}$). Only small quantities of nitrate were detected in the chemostat until 2,350 minutes of operation at a dilution rate below 7 ml/min ($\mu = 0.311 \text{ hr}^{-1}$), and its concentration progressively increased until washout occurred at 3,075 minutes. At a flowrate of 10.5 ml/min ($\mu = 0.467 \text{ hr}^{-1}$), most of the biomass and ethanol were already washed out, and neither nitrate nor nitrite reduction was observed. As seen from the figure, nitrite accumulation occurred only in the initial batch stage, and close to the washout stage, but not in significant amounts in the interim period.

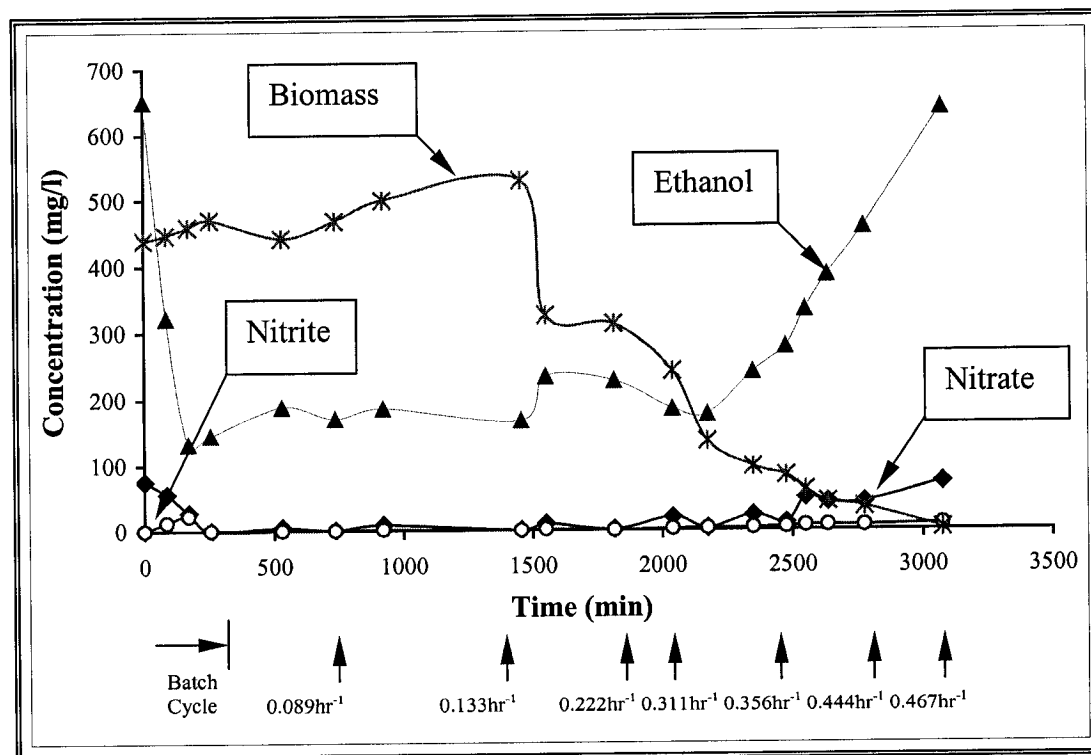


Figure 8.4. Variations in nitrate, nitrite, ethanol and biomass concentration profiles in nitrate-limiting chemostat (Initial concentrations: Nitrate = 75.3 mg N/l, Nitrite = 0 mg N/l, Ethanol = 650 mg/l); Arrowheads indicate the applied dilution rates

From equation (3.12), the estimates of the growth yield coefficients with respect to nitrate utilization ($Y_{a,N}$) was 0.38, and with respect to ethanol utilization ($Y_{a,E}$) 0.29, as presented in Figure 8.5. A Lineweaver-Burke plot shown in Figure 8.6

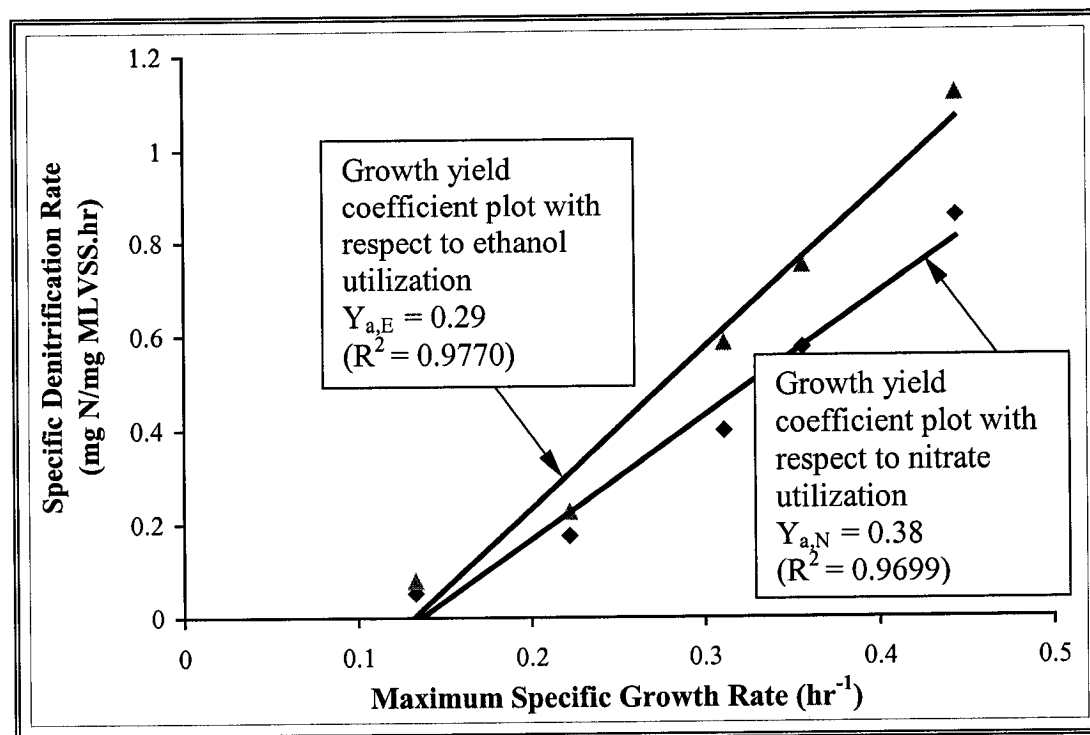


Figure 8.5. Relationship between specific denitrification rate and maximum specific growth rate with respect to nitrate and ethanol utilization in nitrate-limiting chemostat

using equation (3.17) yielded the maximum specific growth rate ($\mu_{m,a}$) and Monod half saturation constant ($K_{s,a}$) as 0.75 hr⁻¹ and 1.9 mg/l, respectively. However, at higher dilution rates, it can be postulated that since $N_a \gg K_{s,a}$ and $N_b \gg K_{s,b}$, the

overall maximum specific growth rate for nitrate-limiting step can be represented as the combination of $\mu_{m,a}$ and $\mu_{m,b}$ (Shimizu et al., 1978):

$$\mu_m = \mu_{m,a} + \mu_{m,b} = 0.60 + 0.75 = 1.35 \text{ hr}^{-1}$$

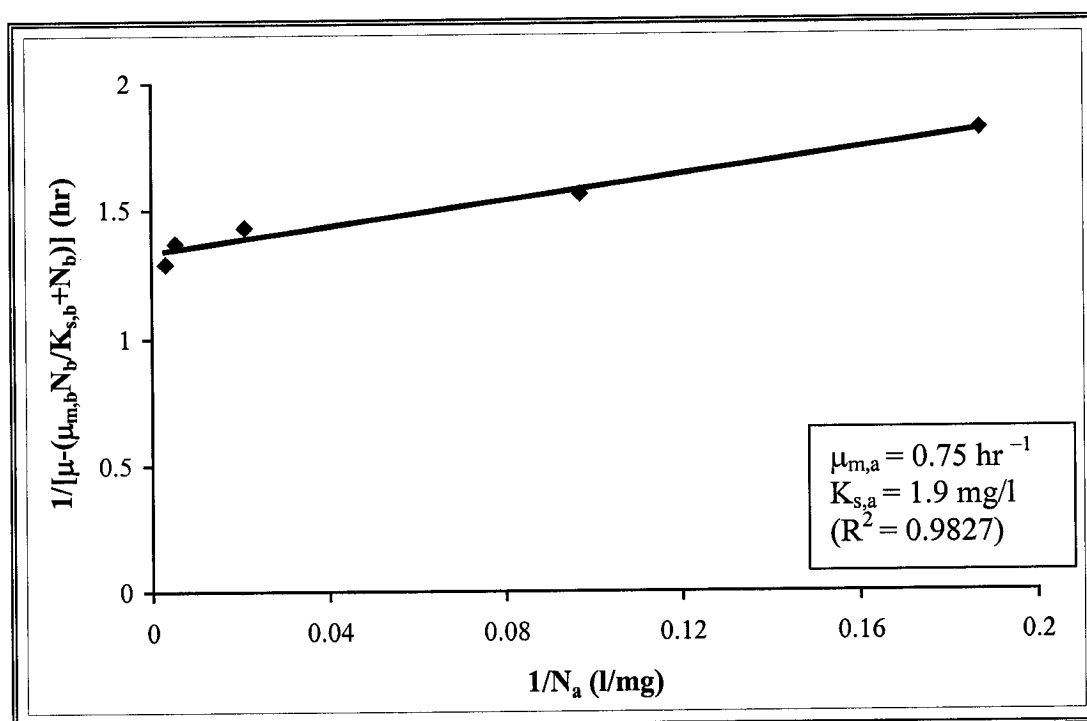


Figure 8.6. Lineweaver-Burke plot of the data obtained from nitrate-limiting chemostat to determine the Monod biokinetic constants according to equation (3.17); Overall, the maximum specific growth rate for this chemostat ($\mu_{m,a}$) is equal to the sum of maximum specific growth rates for nitrite- and nitrate-limiting chemostats, which is 1.35 hr^{-1}

8.1.1.3 Comparison of Nitrite- and Nitrate-Limiting Chemostats

As discussed earlier, the growth yield coefficient for nitrate-limiting chemostat ($Y_{a,N} = 0.38$) was determined to be slightly higher than that for nitrite-

limiting chemostat ($Y_{b,N} = 0.32$). This was due to the fact that the net amount of biomass production rate for the nitrate-limiting chemostat was 0.062 mg/l.min, while that of nitrite-limiting chemostat was 0.036 mg/l.min. However, the growth yield coefficients corresponding to ethanol utilization in both chemostats were lower ($Y_{b,E} = 0.29$ and $Y_{a,E} = 0.29$) than those for nitrate and nitrite utilizations. This may imply that nitrogen compounds (nitrate and nitrite) are associated with cell growth, as also suggested by Shimizu et al. (1978).

The maximum specific growth rate for the nitrate-limiting chemostat was slightly higher ($\mu_{m,a} = 0.75 \text{ hr}^{-1}$) than that of the nitrite-limiting chemostat ($\mu_{m,b} = 0.60 \text{ hr}^{-1}$), which differed slightly from the results of Shimizu et al. (1978) who found identical specific growth rates for both chemostats. In this study, however, nitrate reduction appeared to be more favorable than nitrite reduction by the denitrifying culture used. Another reason for this difference could be that the concentrated constituents of the brine reject may have exerted an inhibitory effect on the activity of the nitrite reducing bacteria or the activity of the nitrite reductase itself or its production. This was also apparent from the Monod half saturation constants, which were 1.9 mg/l and 8.8 mg/l for nitrate- and nitrite-limiting chemostats, respectively. Half saturation constant of a system signifies the affinity of the system biomass for the substrate, i.e., lower values indicate lower affinity of the biomass for that particular substrate. The denitrifying biomass used in the biokinetic studies apparently had more affinity for nitrate than nitrite.

In the nitrate-limiting chemostat, nitrite did not accumulate in substantial amounts, not even at higher dilution rates. The denitrification model suggested by Shimizu et al. (1978) predicted that nitrite concentration in continuous chemostats would be very low even at high dilution rates. They hypothesized the possible reasons as: (i) nitrite could be washed out of the reactor, and/or (ii) the saturation constant for nitrite reduction could be much lower than that for nitrate reduction. In this study, since the Monod half saturation constant for nitrite-limiting chemostat was much higher than that of nitrate-limiting chemostat, the reason for not having significant amount of nitrite accumulation in nitrate-limiting chemostat could be its fast washout rate.

8.1.2 Ethanol-Limiting Chemostat Studies

Ethanol-limiting chemostats were conducted in a similar manner as the nitrite- and nitrate-limiting chemostats, only with limited quantity of ethanol in the abundance of nitrite or nitrate. These studies are important in order to evaluate the dynamics of the denitrification system under limited carbon source.

8.1.2.1 Ethanol-Limiting Chemostat with Nitrite in Excess

Ethanol-limiting chemostat in which nitrite was in excess had 121.7 mg N/l nitrite, no nitrate and only 325 mg/l ethanol. The variations in nitrite, ethanol and biomass concentrations with time are presented in Figure 8.7. The initial feed flowrate after the completion of batch cycle was 2.5 ml/min ($\mu = 0.111 \text{ hr}^{-1}$), and the

ethanol and biomass washout occurred at 7 ml/min ($\mu = 0.311 \text{ hr}^{-1}$) approximately after 2,915 minutes of chemostat operation. Nitrite began to accumulate at 4 ml/min ($\mu = 0.178 \text{ hr}^{-1}$) around 1,720 minutes of operation, and almost no nitrite reduction occurred at the washout flowrate ($\mu = 0.311 \text{ hr}^{-1}$).

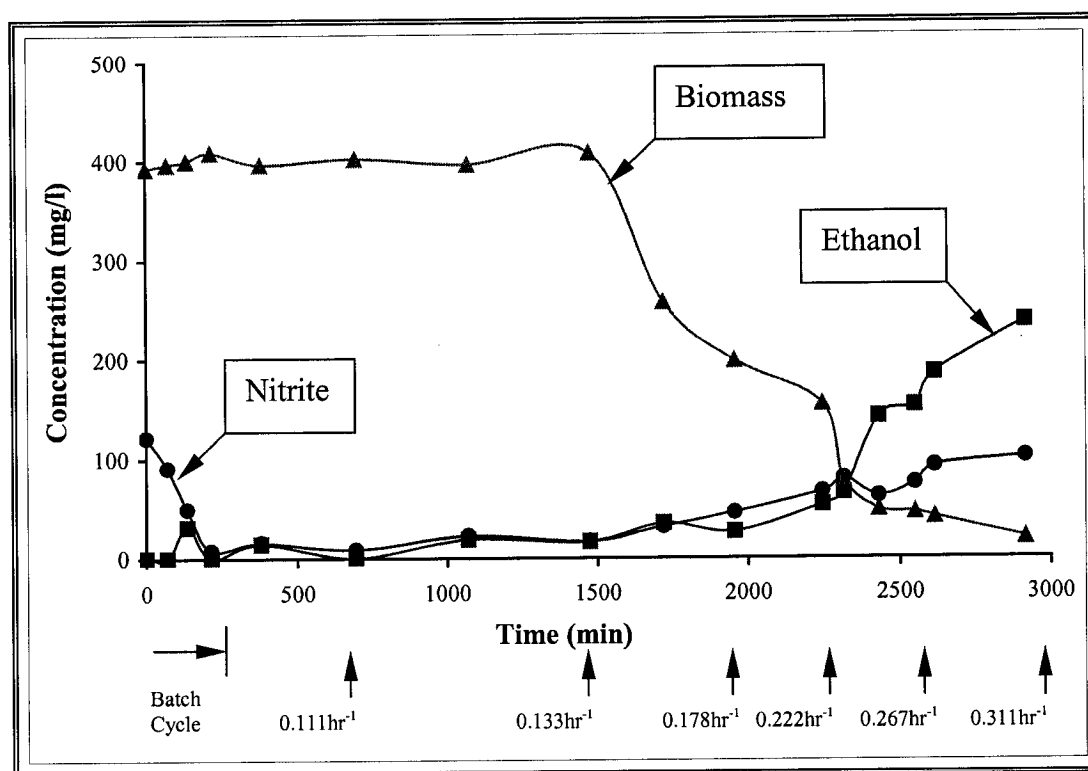


Figure 8.7. Variations in nitrite, ethanol and biomass concentration profiles in ethanol-limiting (nitrite in excess) chemostat (Initial concentrations: Nitrite = 121.7 mg N/l, Nitrate = 0 mg N/l, Ethanol = 325 mg/l); Arrowheads indicate the applied dilution rates

Equations 3.12, 3.14 and 3.17 discussed earlier for the nitrite-limiting chemostat (ethanol in excess), were applied here to the ethanol-limiting step (Kornaros et al. 1996; Shimizu et al., 1978). The growth yield coefficient with

respect to nitrite ($Y_{b,N'}$) was determined to be 0.29, and that of ethanol ($Y_{b,E'}$) was determined as 0.23, as demonstrated in Figure 8.8. The Lineweaver-Burke plot as presented in Figure 8.9 determined the maximum specific growth rate ($\mu_{m,b'}$) as 0.32 hr^{-1} , and Monod half saturation constant ($K_{s,b'}$) as 79.5 mg/l .

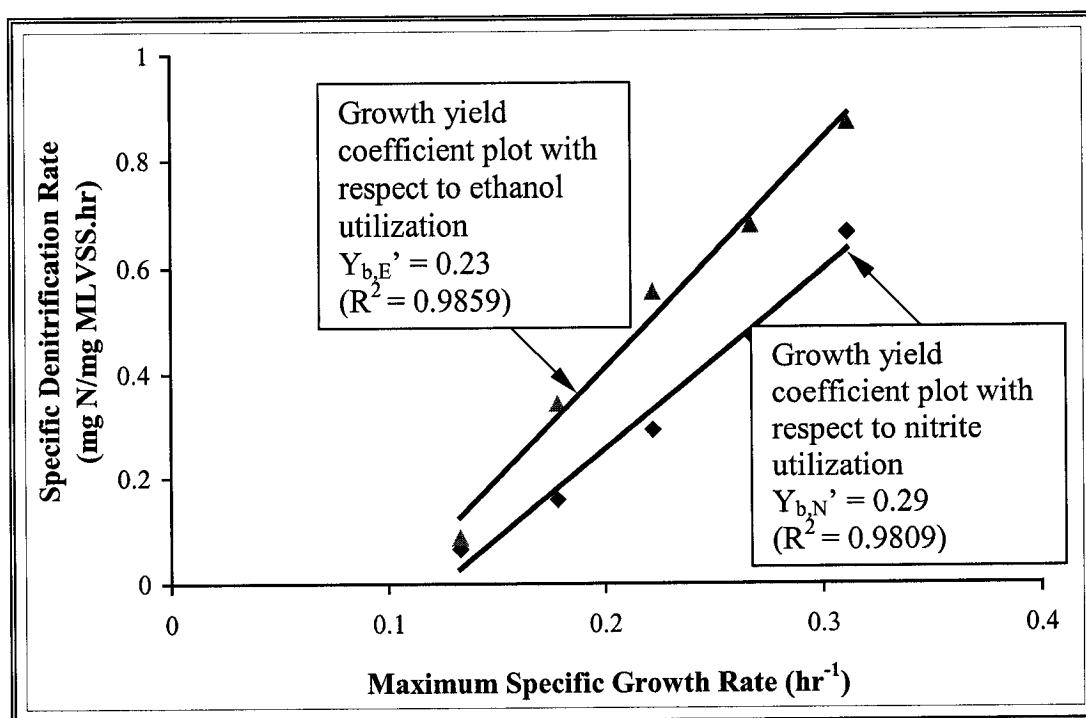


Figure 8.8. Relationship between specific denitrification rate and maximum specific growth rate with respect to nitrite and ethanol utilization in ethanol-limiting (nitrite excess) chemostat

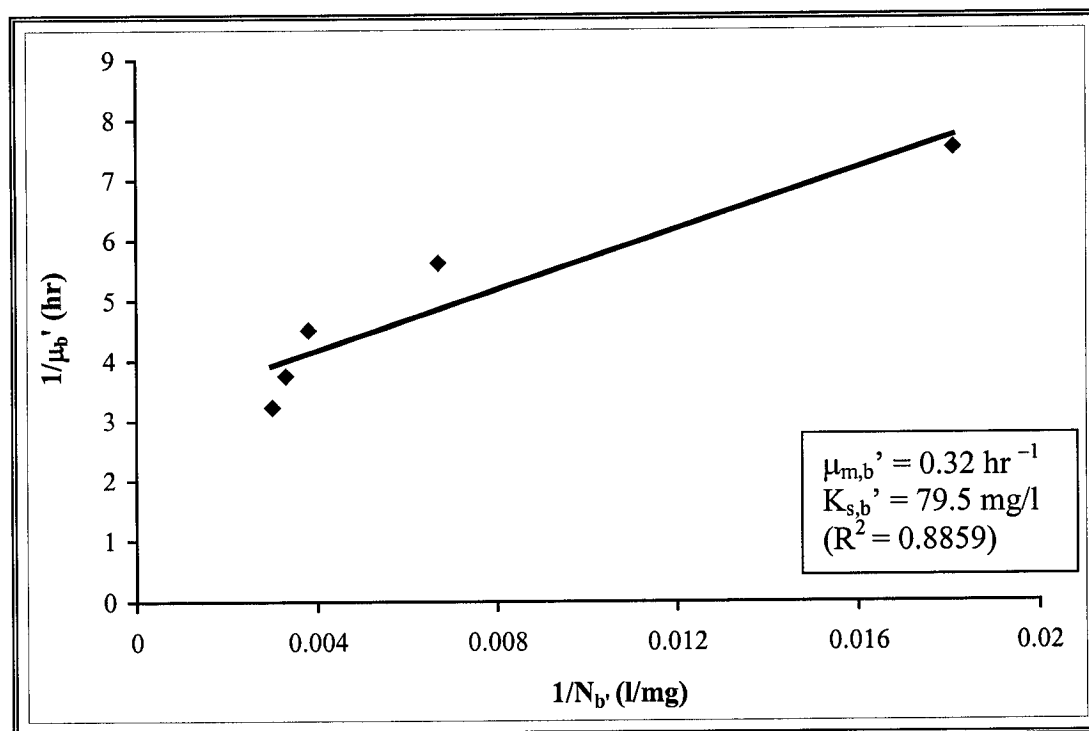


Figure 8.9. Lineweaver-Burke plot to determine the Monod biokinetic constants for ethanol-limiting (nitrite excess) chemostat

8.1.2.2 Ethanol-Limiting Chemostat with Nitrate in Excess

The second ethanol-limiting chemostat (nitrate in excess) contained 79 mg/l nitrate-nitrogen, no nitrite and only 280 mg/l ethanol concentration. The variations in nitrate, nitrite, ethanol and biomass concentrations over the course of the chemostat run are illustrated in Figure 8.10. The initial feed flowrate was 1.5 ml/min, which corresponded to a dilution rate of $\mu = 0.067 \text{ hr}^{-1}$, and the washout occurred at the flowrate of 5 ml/min ($\mu = 0.222 \text{ hr}^{-1}$). Neither nitrate nor nitrite reduction was completely reduced during the experimental run. The concentration of both species continued to increase until most of the ethanol and biomass were washed out of the

chemostat. The chemostat was discontinued after about 2,500 minutes of operation because no reaction occurred beyond.

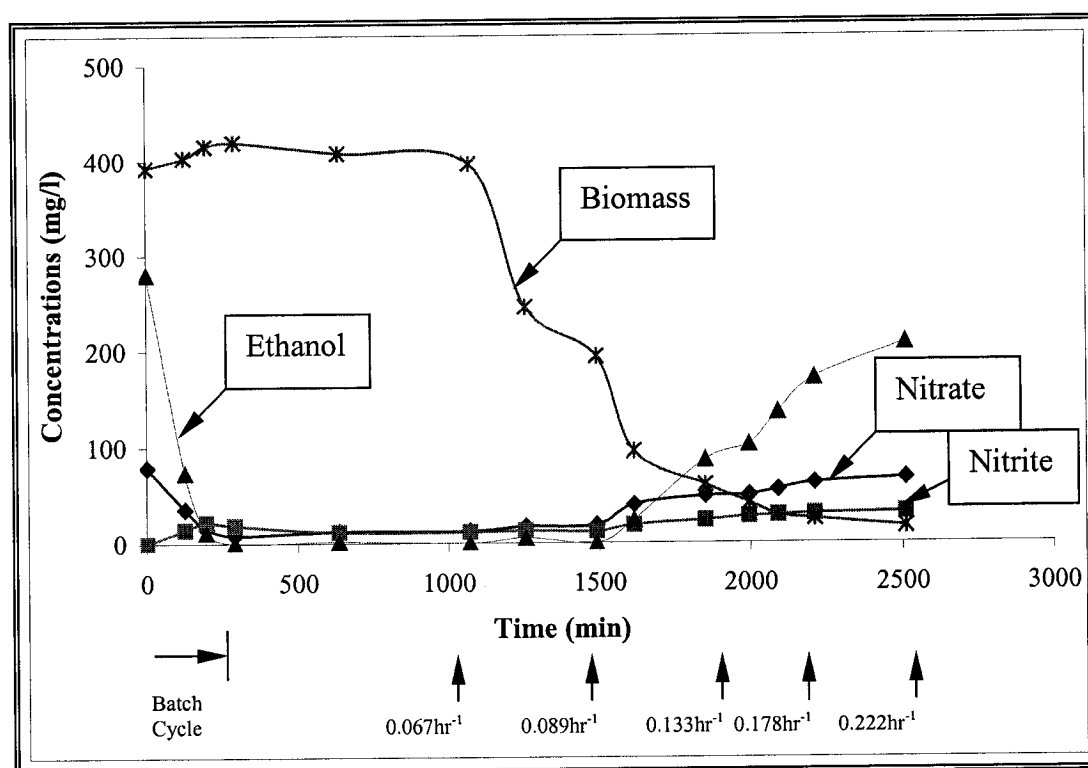


Figure 8.10. Variations in nitrate, nitrite, ethanol and biomass concentration profiles in ethanol-limiting (nitrate excess) chemostat (Initial concentrations: Nitrate = 79 mg N/l, Nitrite = 0 mg N/l, Ethanol = 280 mg/l); Arrowheads indicate the applied dilution rates

A plot of specific denitrification rates vs maximum specific growth rates is presented in Figure 8.11. The growth yield coefficient with respect to nitrate ($Y_{a,N'}$) and ethanol ($Y_{a,E'}$) were determined as 0.29 and 0.23, respectively. Furthermore, the maximum specific growth rate ($\mu_{m,a'}$) and Monod half saturation constant ($K_{s,a'}$) from the Lineweaver-Burke plot were determined to be 0.34 hr^{-1} and 37.5 mg/l ,

respectively (Figure 8.12). The overall maximum specific growth rate for ethanol-limiting step can be represented as follows:

$$\mu_{m'} = \mu_{m,a'} + \mu_{m,b'} = 0.32 + 0.34 = 0.66 \text{ hr}^{-1}$$

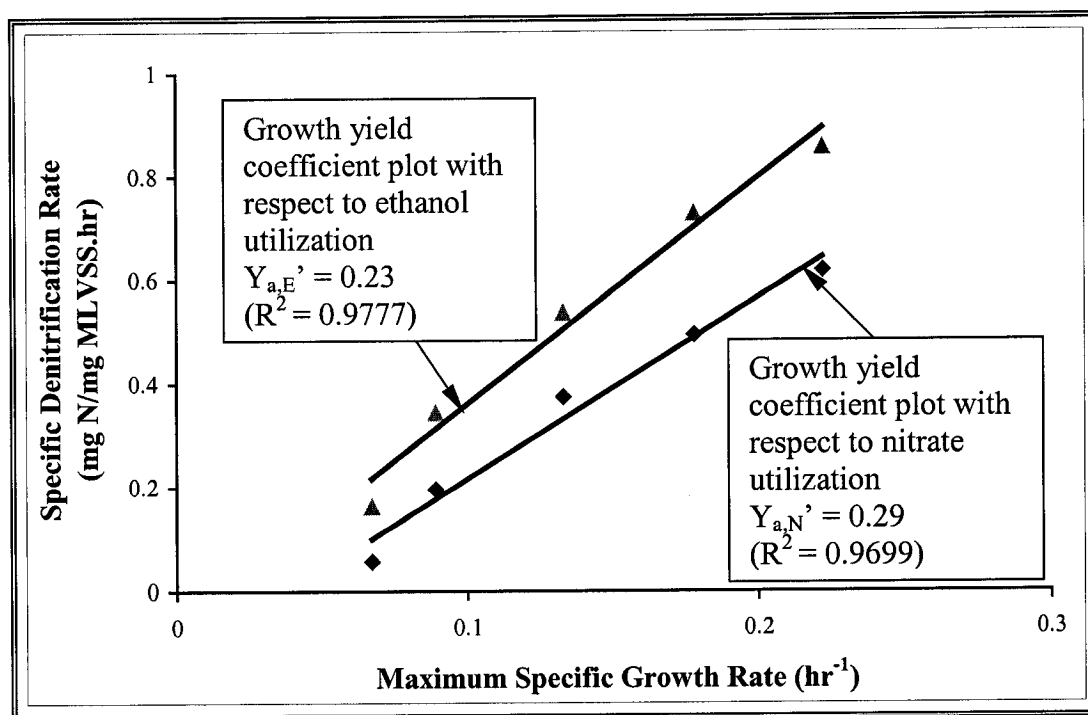


Figure 8.11. Relationship between specific denitrification rate and maximum specific growth rate with respect to nitrate and ethanol utilization in ethanol-limiting (nitrate excess) chemostat

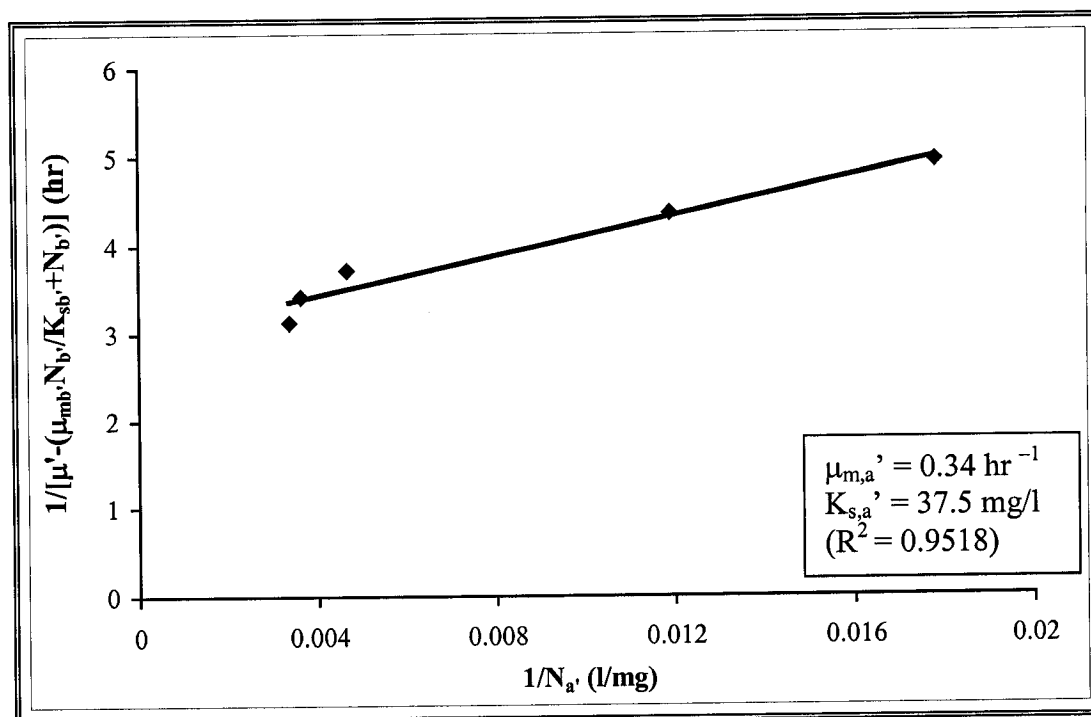


Figure 8.12. Lineweaver-Burke plot of the data to determine the Monod biokinetic constants obtained from ethanol-limiting (nitrate excess) chemostat

8.1.2.3 Comparison of Ethanol- and Nitrogen-Limiting Chemostats

The washout dilution rate in both ethanol-limiting chemostats was approximately half that under nitrogen-limiting chemostats. This phenomenon, also observed by Shimizu et al. (1978), suggested that insufficient carbon source caused system instability due to inhibitory effect of nitrate and/or nitrite accumulation. Moreover, in both chemostats, nitrate and nitrite reductions were never complete, not even in the initial batch cycle where no feed was provided to the chemostat. According to Engberg and Schroeder (1975), in order to be able to produce effluents with low nitrate concentrations, sufficient quantity of organic carbon source must be

added to the influent. These investigators also stated that economic considerations would be a deciding factor in establishing a balance between the influent organic carbon concentrations and effluent nitrogen concentrations.

The net biomass production rate in both ethanol-limiting chemostats was much lower than that for the nitrogen-limiting chemostats, 0.011 mg/l.min for nitrite excess chemostat and 0.024 mg/l.min nitrate excess chemostat (Table 8.1). The growth yield coefficients for the ethanol-limiting chemostats with respect to nitrate and ethanol utilization were 0.29 and 0.23, respectively. These coefficients are significantly lower than those for the nitrogen-limiting chemostats. The maximum specific growth rates for both chemostats were also close to each other (0.32 hr^{-1} and 0.34 hr^{-1} for nitrite excess and nitrate excess chemostats, respectively). However, the Monod half saturation constants in both chemostats were significantly higher than those estimated for the nitrogen-limiting chemostats, which could be the result of the instability of the systems due to the absence of sufficient carbon source. Also, the specific denitrification rates determined for both ethanol-limiting reactors were much lower than the rates for nitrite- and nitrate-limiting chemostats in which ethanol was not limited (Table 8.1).

In conclusion, the biokinetic model (Equations 3.9 through 3.11 in Chapter 3) for a two-step denitrification process employed in this study was capable of accurately predicting the nitrate and nitrite reduction rates as well as the nitrite accumulation as the intermediate product in continuous flow chemostats. The model

rate equations also adequately described the extent of biodegradation and biomass production in all nitrogen- and ethanol-limiting chemostats.

Table 8.1. Summary of biokinetic parameters and net biomass production rates obtained from nitrogen- and ethanol-limiting chemostat studies

Parameter		Nitrogen-Limiting Chemostat		Ethanol-Limiting Chemostat	
		Nitrite-Limiting	Nitrate-Limiting	Nitrite Excess	Nitrate Excess
Growth Yield Coefficient (mg Substrate /mg Biomass)	With Respect to Nitrogen Utilization	$Y_{b,N} = 0.32$	$Y_{a,N} = 0.38$	$Y_{b,N'} = 0.29$	$Y_{a,N'} = 0.29$
	With Respect to Ethanol Utilization	$Y_{b,E} = 0.29$	$Y_{a,E} = 0.29$	$Y_{b,E'} = 0.23$	$Y_{b,N'} = 0.23$
Maximum Specific Growth Rate (hr^{-1})		$\mu_{m,b} = 0.60$	$\mu_{m,a} = 1.35$	$\mu_{m,b'} = 0.32$	$\mu_{m,a'} = 0.66$
Monod Half Saturation Constant (mg/l)		$K_{s,b} = 8.80$	$K_{s,a} = 1.90$	$K_{s,b'} = 79.5$	$K_{s,a'} = 37.5$
Decay Coefficient (hr^{-1})		$k_{d,b} = 0.221$	$k_{d,a} = 0.137$	--	--
Net Biomass Production Rate (mg/l.min)		0.036	0.064	0.011	0.024

The biokinetic parameters obtained from the nitrogen-limiting chemostat experiments, presented in Table 8.2, will be used: (i) to evaluate optimal operational strategies for effective denitrification process, and (ii) in FBAR model to simulate/predict denitrification performance under various operating conditions. The results obtained from ethanol-limiting chemostats will be used to evaluate the

performance of denitrification process when the carbon source (ethanol) is insufficient.

Table 8.2. Biokinetic parameters to be used in FBAR studies

Biokinetic Parameter	Value
Growth Yield Coefficient (mg Substrate/mg Biomass)	0.70
Maximum Specific Growth Rate (hr^{-1})	1.35
Monod Half Saturation Constant (mg/l)	1.90
Decay Coefficient (hr^{-1})	0.137

8.2 Summary and Conclusions

- The growth yield coefficients for nitrate- and nitrite-limiting chemostats were not significantly different from each other, which implied that both nitrate and nitrite reductions were closely associated with cell growth. The growth yield coefficients corresponding to nitrogen utilization, however, were higher than that for ethanol utilization, which implied that nitrogen compounds were associated with cell growth.
- The maximum specific growth rate for the nitrate-limiting chemostat was higher than that of the nitrite-limiting chemostat. Also, the Monod half saturation constant for the nitrate-limiting chemostat was significantly lower than that of the nitrite-limiting chemostat. This may suggest that nitrate reduction was more favorable than nitrite reduction by the denitrifying culture used in the study.

- The washout dilution rate in both ethanol-limiting chemostats was approximately half that under nitrite- and nitrate-limiting chemostats, which suggested that insufficient carbon source might cause instability of the system due to inhibitory effect of nitrate and/or nitrite accumulation.
- The growth yield coefficients and the maximum specific growth rates for both ethanol-limiting chemostats were nearly identical, but were significantly lower than that of the nitrite- and nitrate-limiting chemostats. As a result, net biomass production in both ethanol-limiting chemostats was much lower than the nitrogen-limiting chemostats.
- The modified Monod kinetics model was capable of accurately predicting the following: (i) nitrate and nitrite reduction rates, (ii) extend of biodegradation, and (iii) nitrite accumulation as the intermediate product.

CHAPTER 9

FLUIDIZED BIOADSORBER REACTOR DENITRIFICATION STUDIES: MODEL PREDICTION, SIMULATION AND VERIFICATION

This chapter presents the results of anaerobic FBAR denitrification studies conducted using RO brine reject, and discusses the efficiency of the FBAR process. It includes model prediction/simulation as well as sensitivity analyses performed using the model. The main objectives are: (i) to evaluate the feasibility of the FBAR denitrification process in treating RO brine rejects, (ii) to simulate, calibrate and verify the FBAR model using different operational scenarios, (iii) to compare the performance of the FBAR process employing GAC to that employing sand as the support medium, (iv) to evaluate the sensitivity of each biokinetic parameter using the model, and (v) to evaluate the performance of the model for up-scaling of the FBAR process.

9.1 Results and Discussions

9.1.1 Experimental Results of FBAR Denitrification Studies with GAC

9.1.1.1 Evaluation and Comparison of Experimental Results

A series of mini pilot-scale anaerobic FBAR experiments were conducted using various GAC quantities, nitrate concentrations, and hydraulic retention times

to assess the system efficiency and to predict, simulate and verify the FBAR-GAC denitrification model. The basic rationale for these studies was to maximize the nitrate removal efficiency without nitrite accumulation. The overall experimental matrix is presented in Table 9.1. As seen from the table, the first six FBAR experiments (1 through 6) were conducted using synthetic (nitrified) brine reject whose constituents were presented in Table 5.1, Chapter 5. Following the successful optimization of the RBC-PAC nitrification process, more FBAR experiments (7 through 13) were carried out using actual nitrified brine reject with constituents presented in Table 6.1, Chapter 6.

Initially, the influent brine reject was deoxygenated with nitrogen gas to maintain the dissolved oxygen level at less than 1 percent (0.1 mg/l), and stored in the tightly sealed feed container throughout the study. The temperature and pH of the feed was maintained at 30°C and 7.5, respectively. Ethanol was fed to the bioadsorber to maintain a C:N ratio of 1.8:1 mg C/mg N.

In each experiment, the initial height of the bed was recorded after charging the bioadsorber with GAC and after the start of the experimental run. The superficial fluid velocity was chosen in such a way to have the final bed expansion reach approximately twice the size of the initial bed height. For instance, if the amount of GAC medium used was 300 g, the initial and final bed heights were 33 cm and 55 to 60 cm, respectively. The corresponding initial and fluidized bed heights in the FBAR with 150 g GAC were 18 cm and 30 to 33 cm, respectively.

Table 9.1. Experimental matrix for the mini pilot-scale FBAR studies with GAC (T = 30°C and pH = 7.5 for all experiments)

Run No.	Source of Brine Reject	GAC (g)	Operational Conditions	
			Nitrate (mg N/l)	Hydraulic Retention Time (hr)
1	Synthetic	300	87.2	180
2	Synthetic	300	64.7	120
3	Synthetic	300	81.8	60
4	Synthetic	150	89.4	180
5	Synthetic	150	89.4	120
6	Synthetic	150	93.8	60
7	Actual	150	309.0	90
8	Actual	300	316.1	90
9	Actual	300	190.6	56
10	Actual	150	190.4	56
11	Actual	150	151.9	82
12	Actual	150	78.8	40
13	Actual	300	78.8	40

The results of FBAR experiments conducted to investigate the effect of support medium quantities on the denitrification efficiency using 150 g and 300 g of GAC with initial nitrate concentration of approximately 79 mg N/l and hydraulic retention time of 40 minutes (Experiment Nos. 12 and 13) are presented in Figure 9.1. It was observed that, at steady state, the reactor containing 150 g of GAC achieved 96 percent removal efficiency with respect to nitrate, with 2 mg N/l of nitrite remaining, whereas the reactor containing 300 g of GAC achieved complete denitrification with no nitrite in the effluent under similar conditions. It is evident from Figure 9.1 that both reactors reached steady state around the same time. Substantial nitrite accumulation was inevitable in both reactors before steady state

was achieved. Nitrite concentration reached a peak as nitrate was reduced to about 45 mg N/l. At steady state, no nitrite accumulated in either reactor.

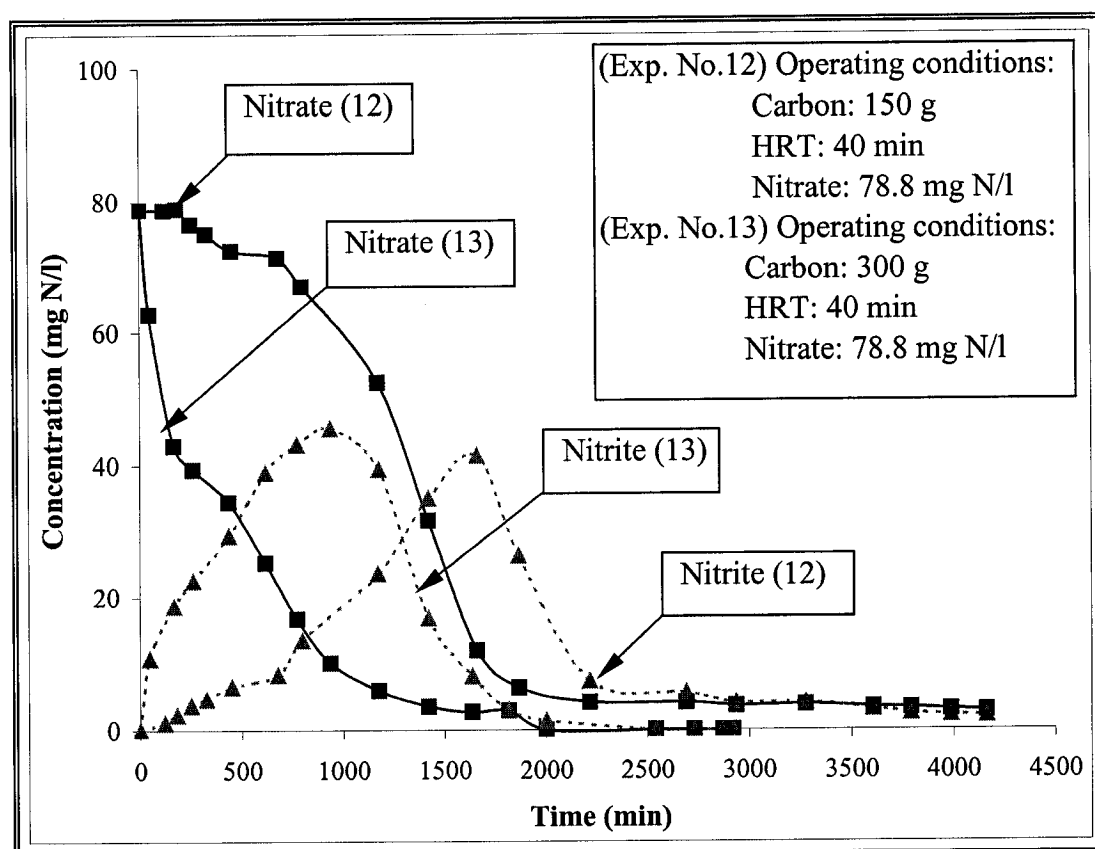


Figure 9.1. Effect of GAC quantities on the FBAR denitrification efficiency (Temperature = 30°C, pH = 7.5 and C:N = 1.8:1)

Similar FBAR studies were conducted to evaluate the effect of hydraulic retention time on the denitrification efficiency. Figure 9.2 compares the FBAR process efficiency with respect to 40 and 60 minutes using 300 g of GAC and approximately 80 mg N/l of initial nitrate concentration (Experiment Nos. 3 and 13).

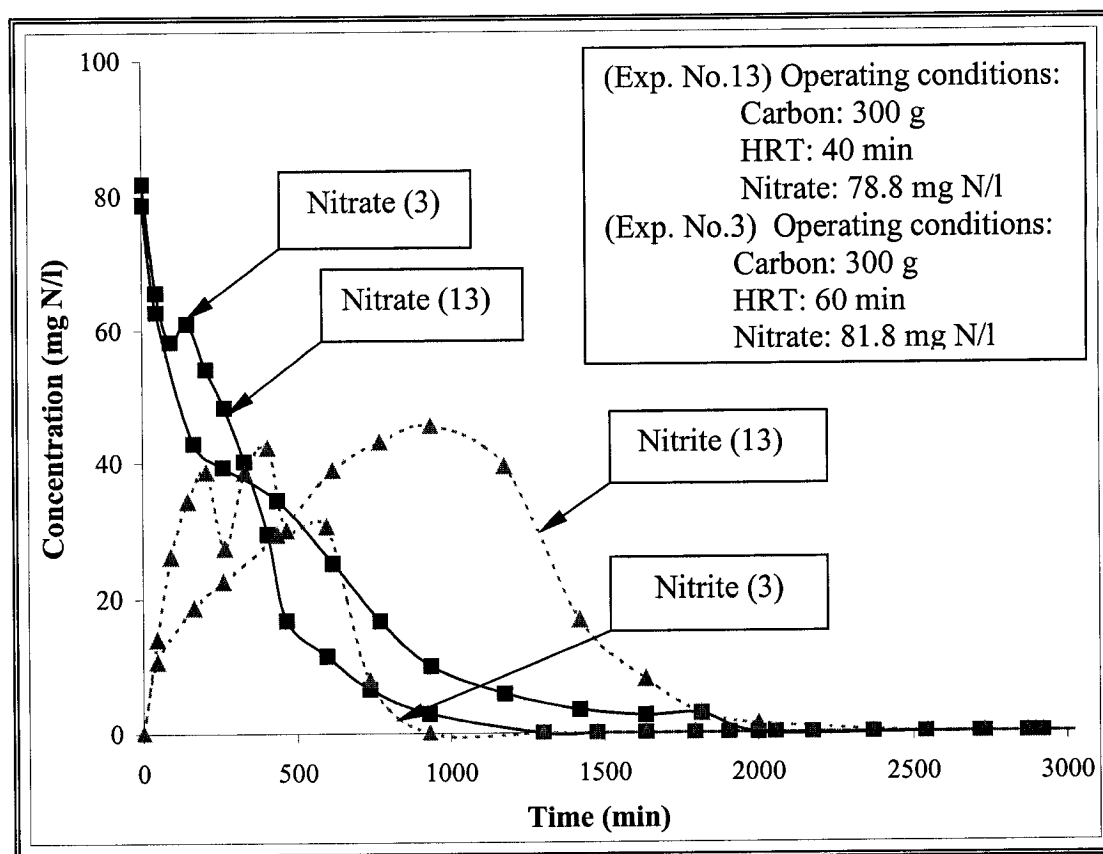


Figure 9.2. Effect of hydraulic retention time on the FBAR denitrification efficiency (Temperature = 30°C, pH = 7.5 and C:N = 1.8:1)

Complete denitrification was achieved in both columns at steady state. As evident from the figure, steady state was reached around 1,300 minutes in the reactor with the longer hydraulic retention time of 60 minutes, whereas it took 2,000 minutes for the reactor having 40 minutes hydraulic retention time. Although nitrite accumulated in significant quantities in both reactors in the earlier stages of operation, it was completely consumed when nitrate concentration approached steady state. Also,

nitrite reduction took significantly longer time in the reactor with shorter hydraulic retention time.

The experimental results on evaluating the effect of influent nitrate concentration on the FBAR denitrification efficiency are presented in Figure 9.3 for Experiments Nos. 6 and 10. Both reactors employed identical amounts of GAC (150 g) and used similar hydraulic retention times (56 minutes), but different influent nitrate concentrations (94 mg N/l and 190 mg N/l). The reactor with the influent nitrate concentration of 94 mg N/l reached steady state in about 1,400 minutes with no detectable nitrate in the effluent. Also, nitrite accumulation was not detected in the system. However, after reaching the steady state conditions, the reactor with influent nitrate concentration of 190 mg N/l was able to achieve only 97 percent denitrification efficiency with 5 mg N/l of nitrate concentration remaining in the effluent. No nitrite was detected in the effluent of this reactor.

The results obtained from these studies demonstrated that the FBAR denitrification technology is highly efficient in removing nitrate and nitrite under a broad spectrum of operating conditions. Moreover, since nitrite is considered more of a health hazard than nitrate, its complete removal from any system is essential (Langley et al., 2001). The average effluent characteristics of denitrified brine reject generated from the FBAR denitrification experiments are presented in Table 9.2.

Heijnen et al. (1989) report in their review of application of fluidized bioreactors in wastewater treatment that some investigators have encountered problems with the initial start-up of their anaerobic fluidized bed systems. They

further state that these problems mostly lie in the development of microbial biofilm on the particles of the support media employed. In the study reported herein, the start-up of the FBAR denitrification process was easy and virtually trouble-free. Even during the bacterial acclimation period, excellent microbial attachment and biofilm formation on the GAC particles was experienced.

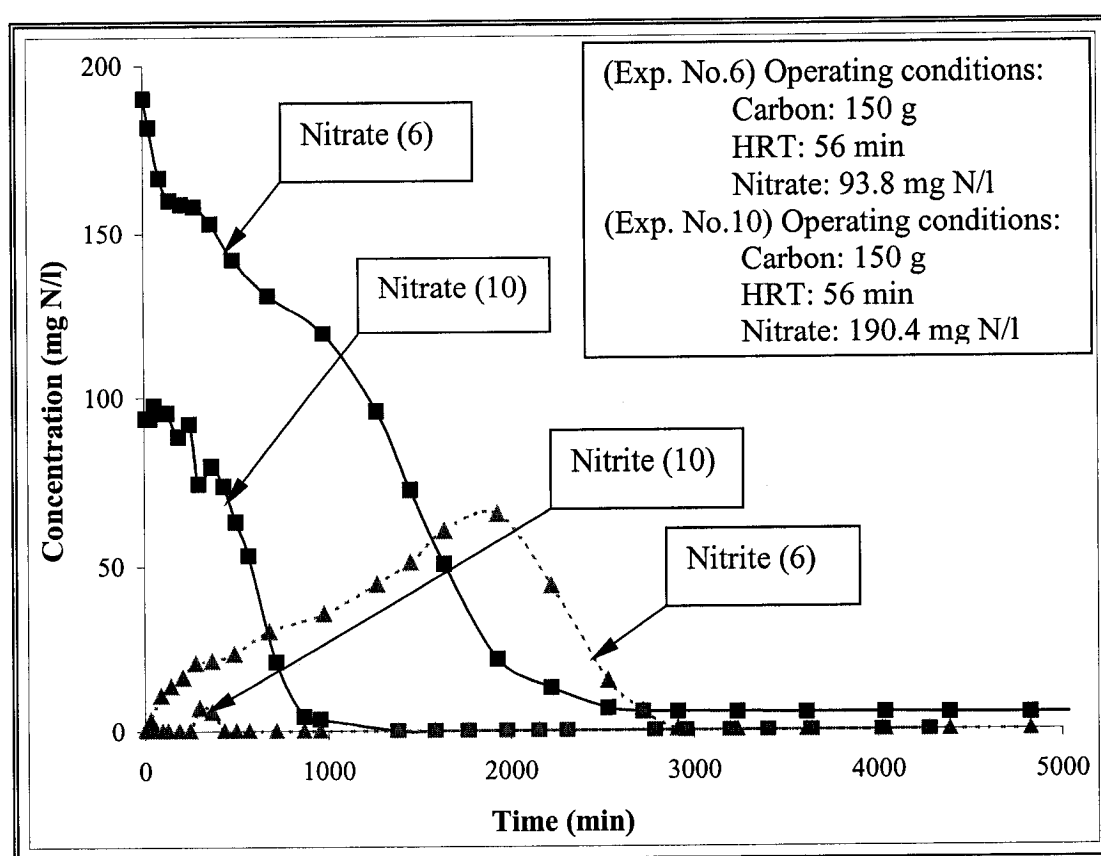


Figure 9.3. Effect of influent nitrate concentration on the FBAR denitrification efficiency (Temperature = 30°C, pH = 7.5 and C:N = 1.8:1)

Table 9.2. Average characteristics of denitrified brine reject effluent from FBAR experiments with GAC

Constituent	Unit	Concentration	
		Influent	Effluent
Total Dissolved Solids	mg/l	4,550	4,440
Iron	µg/l	495	448
Arsenic	µg/l	14	9.9
Barium	µg/l	105	53.2
Cadmium	µg/l	1.1	<1.0
Cobalt	µg/l	2.5	1.2
Copper	µg/l	33	18.4
Lead	µg/l	1.5	<1.0
Manganese	µg/l	170	68.6
Mercury	µg/l	<0.1	<0.1
Selenium	µg/l	38	21.7
Silver	µg/l	8.5	6.6
Zinc	µg/l	116	32.2
Ammonia-Nitrogen	mg/l	1.0	<1.0
Organic Nitrogen	mg/l	4.0	0.5
Total Alkalinity (as CaCO ₃)	mg/l	450	489
Nitrite-Nitrogen	mg/l	<0.1	0.55
Nitrate-Nitrogen	mg/l	82	<1.0
Sulfate	mg/l	1,200	1,190
Total Organic Carbon (TOC, Unfiltered)	mg/l	10	138

9.1.1.2 Evaluation of FBAR Operational Parameters

In the FBAR experiments, hydraulic retention time, influent nitrate concentrations and quantity of GAC were the most significant factors influencing the process performance. At high hydraulic retention times, for instance at 40 minutes (Figure 9.1), nitrate removal efficiency was well above 96 percent with insignificant

amount of nitrite in the reactor effluent. The quantity of GAC and the initial nitrate concentration were related to the biomass concentration in the system.

It is important to evaluate the FBAR denitrification process performance in terms of attached biomass concentration, which is considered another most significant variable in FBAR operations, in relation to the above mentioned parameters. As mentioned earlier, GAC provides a favorable environment for biological growth (Kim & Pirbazari, 1989; Pirbazari et al., 1993). The rough surfaces of GAC particles provide shelter for the microorganisms from high fluid shear due to high recycle ratios. Furthermore, bioadsorbers with GAC are resistant to shock loads and fluctuating substrate concentrations and can remove a broad spectrum of toxic chemical compounds.

Following the initial start-up period, the bioadsorber bed began to expand slowly as the biofilms developed on the surfaces of the GAC particles. The expansion was especially considerable at steady state operation. The prolific growth of biofilms in the bioadsorber bed led to the migration of overgrown bioparticles to the top of the bed due to their density reduction. This caused additional bed expansion beyond that attributed to incipient fluidization. At this point, the recycle flowrate was reduced in order to prevent bioparticle washout. The top portion of the GAC bed was frequently mixed to detach the biomass, and provided even biofilm distribution throughout the reactor depth. Without any mixing of the media particles, the top layer of the reactor appeared to host thicker biofilms whereas the lower layers hosted much thinner biofilms due to relatively high levels of biofilm shearing. In

addition to recycle flowrate, nitrogen gas bubbles produced during denitrification moved upward, contributing to additional bed expansion.

In these experiments, the amount of attached biomass at steady state increased slightly as the hydraulic retention time decreased. For instance, the attached biomass concentration increased only about 30 percent as the hydraulic retention time was lowered three orders of magnitude from 180 minutes to 60 minutes in both FBARs with 150 and 300 g of GAC. As discussed by Shieh et al. (1996), once the microbial community along the bioadsorber bed became established, the degree of fluidization conditions or media bed expansion did not have any significant mechanical attrition effect on the biomass concentration along the reactor. In fact, Lazarova and Manem (1995) demonstrated that strong shear stresses could lead to more rigid and homogeneous biofilms along the reactor. In this study, the sloughed off and lost biomass did not seem to adversely affect the denitrification process possibly due to the rigid biofilm layers. On the other hand, Sison et al. (1995) reported for their system that adsorption rate of ethanol as the carbon source by the GAC particles may not be sufficient at low hydraulic retention times. However, even if this phenomenon occurred in the bioadsorber, it did not seem to have an adverse impact on the denitrification efficiencies obtained even at lower hydraulic retention times.

The highest concentration of attached biomass expressed as attached volatile solids (AVS) was generally obtained when the nitrate concentration was high, and the corresponding hydraulic retention time was relatively lower. For example, the

attached biomass concentration reached a maximum value of 428 mg AVS/g GAC in the FBAR containing 150 g GAC operated with 310 mg N/l influent nitrate concentration and 90 minutes of hydraulic retention time. Similarly, the biomass concentration reached at its maximum value of 625 mg AVS/g GAC in the FBAR containing 300 g GAC that was operated with 316 mg N/l initial nitrate concentration. This proved the fact that biomass growth was a factor of substrate concentration, i.e., the higher the nitrate concentration, the higher the attached biomass concentration. This phenomenon was also observed by Hancher et al. (1978). The biomass densities for each FBAR experiment are summarized in Table 9.3 along with the experimental matrix.

Table 9.3. Experimental matrix and biomass density for the mini pilot-scale FBAR studies with GAC (T = 30°C and pH = 7.5 for all experiments)

Run No	Quantity of GAC (g)	Nitrate (mg N/l)	Hydraulic Retention Time (hr)	Biomass Density (mg AVS/g GAC)
1	300	87.2	180	288
2	300	64.7	120	227
3	300	81.8	60	205
4	150	89.4	180	234
5	150	89.4	120	206
6	150	93.8	60	163
7	150	309.0	90	428
8	300	316.1	90	625
9	300	190.6	56	389
10	150	190.4	56	217
11	150	151.9	82	252
12	150	78.8	40	148
13	300	78.8	40	195

Another parameter was the accumulation of nitrite during the FBAR operation and the steady state effluent nitrite concentration. Nitrite accumulation was observed in the initial stages of the process, the degree of which depended on the initial influent nitrate concentration. After reaching a peak concentration, it was reduced along with nitrate and no further nitrite accumulation was detected at steady state operation. Based on this observation, it is appropriate to assume a single-step denitrification process at steady state conditions, in which nitrate is directly converted into nitrogen gas even at higher hydraulic retention times and high influent nitrate concentrations (provided that sufficient ethanol is present in the system). This kind of an assumption assists in up-scaling and design of an effective FBAR system for the denitrification process.

In the final part of the study, GAC particles were removed from different locations along the FBAR, and prepared for scanning electron microscope in a manner described in Section 5.3.11, Chapter 5, to study the nature and extent of the biogrowth on the carbon particles. Figure 9.4 presents a typical micrograph of bacterial growth on a GAC particle. The SEM images revealed that the carbon particles were covered with a uniform layer of microbial population.

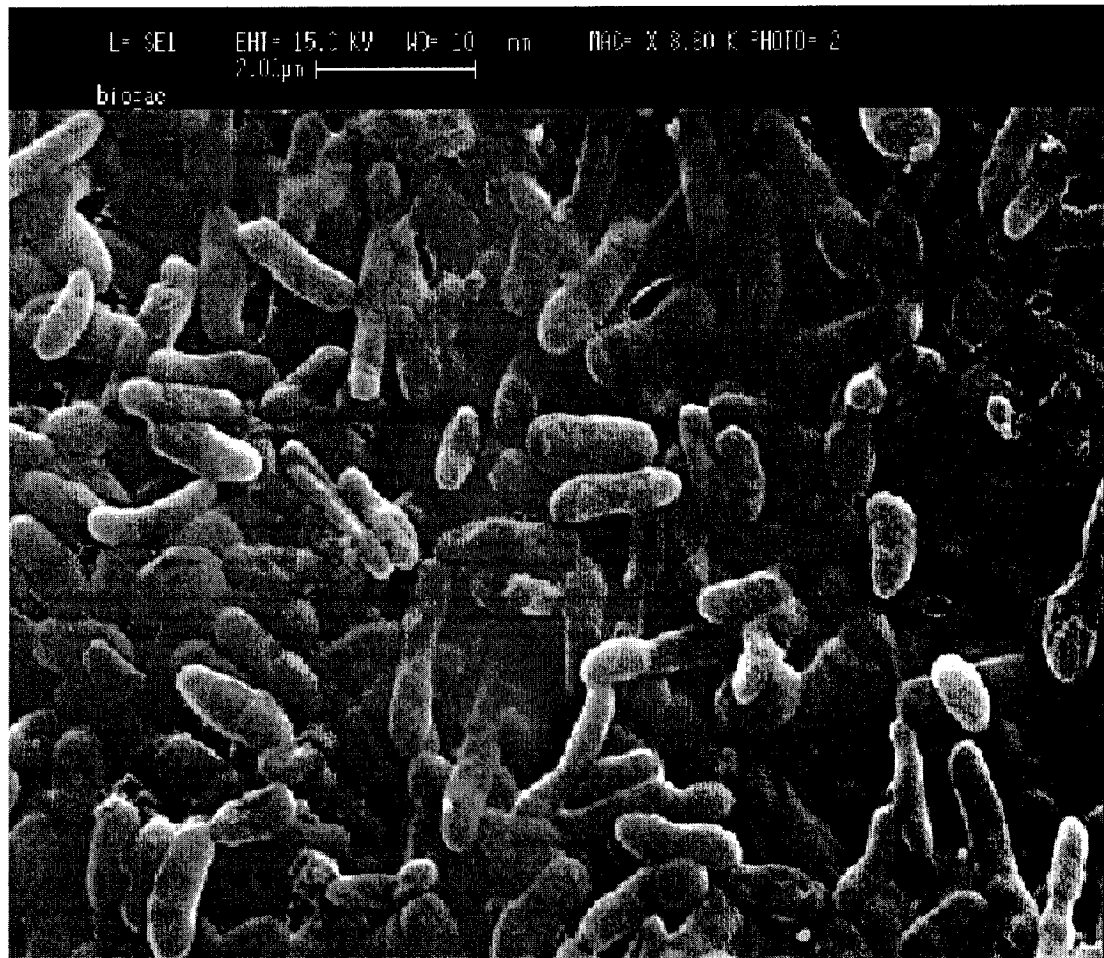


Figure 9.4. Micrograph of a biofilm at the final stages of growth

9.1.2 Experimental Results of FBAR Denitrification Studies with Sand

Two sets of experiments were conducted to compare the denitrification performance and efficiency of the FBAR employing sand as the support medium versus GAC. The experimental matrix is presented in Table 9.4. Both sets used a hydraulic retention time of 180 minutes. The first set of the experiments employed 150 g of sand, while the second set employed 300 g of sand. The experimental profiles obtained from sand experiments were compared with those obtained from the FBAR experiments with GAC conducted previously.

Table 9.4. Experimental matrix for the mini pilot-scale FBAR studies with sand (T = 30°C and pH = 7.5 for all experiments)

Experiment No.	Media		Nitrate Concentration (mg N/l)	Hydraulic Retention Time (hr)
	Type	Quantity (g)		
1	Sand	150	85.4	180
	GAC	150	89.4	180
2	Sand	300	84.7	180
	GAC	300	87.2	180

The first experiment employed 150 g of sand and approximately 85 mg N/l of influent nitrate concentration. As can be observed from Figure 9.5, denitrification process was complete in about 2,350 minutes as opposed to 500 minutes in the FBAR with GAC. Significant amount of nitrite accumulated in the reactor with sand, and the complete removal took almost 2,200 minutes, whereas no significant nitrite accumulation was observed in the FBAR with GAC.

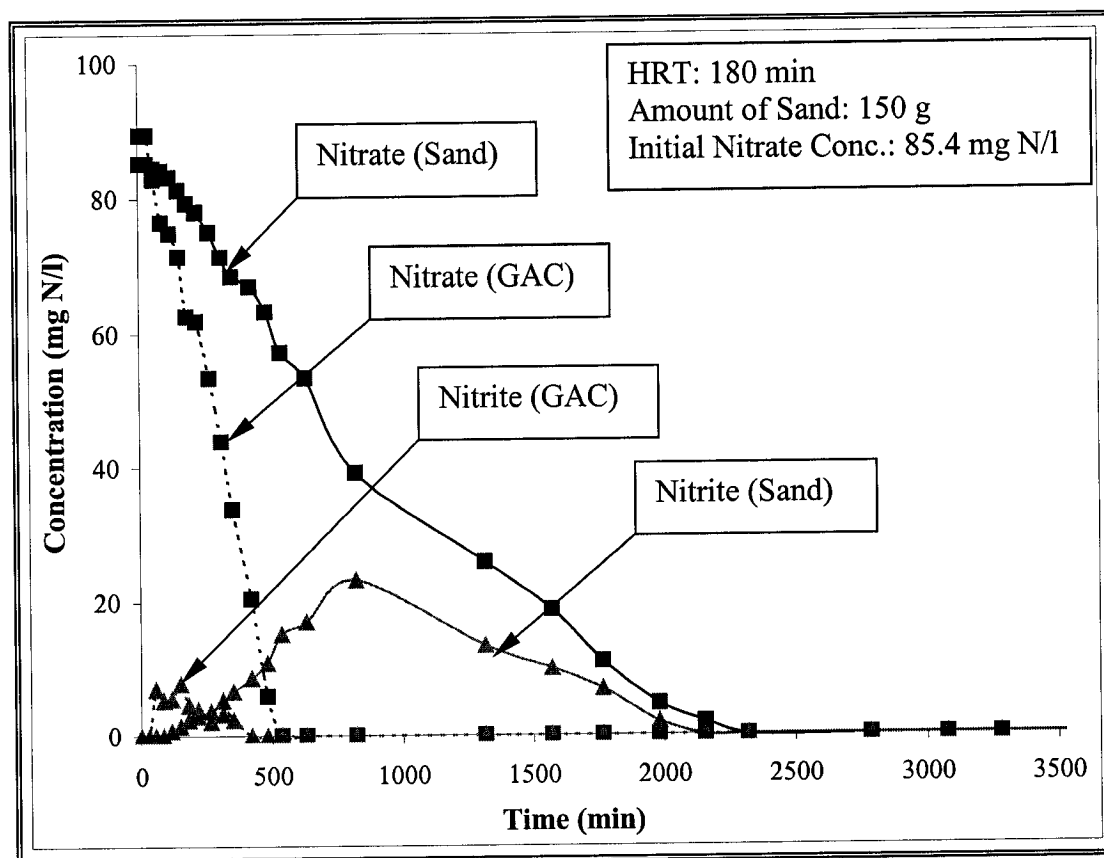


Figure 9.5. Comparison of FBAR denitrification profile with 150 g of sand and GAC (Temperature = 30°C, pH = 7.5 and C:N = 1.8:1)

The second experiment was conducted using 300 g of sand and about 85 mg N/l of initial nitrate concentration. Steady state was reached after 1,400 minutes of experimental run (Figure 9.6). The nitrite concentration that accumulated in substantial amount as the nitrate was reduced, approached zero around 850 minutes of operation. However, the experimental results of an identical FBAR with GAC (Experiment Nos. 1 and 4) showed that the reactor reached the steady state around 500 minutes of operation with no substantial nitrite accumulation. Both Figures 9.5

and 9.6 indicate that GAC was significantly more effective than sand during the transitional period of operation.

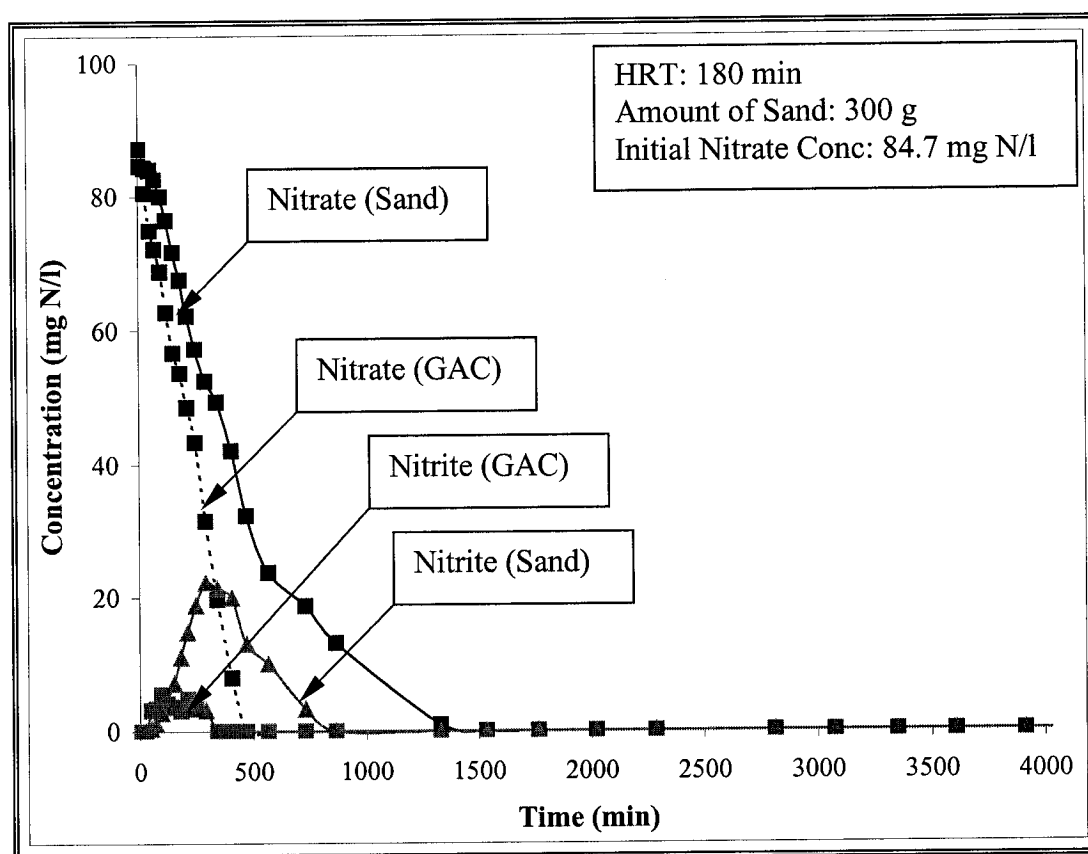


Figure 9.6. Comparison of FBAR denitrification profile with 300 g of sand and GAC (Temperature = 30°C, pH = 7.5 and C:N = 1.8:1)

In the studies reported herein, the amount of attached biomass at steady state in the FBAR column with 150 g of sand was measured to be 93 mg AVS/g sand, and that of FBAR with 300 g of sand was assayed to be 166 mg AVS/g sand. These estimates are about 40 percent and 58 percent of the amount of biomass

concentration for the corresponding FBARs containing 150 g and 300 g GAC, respectively. These relative biomass values are in accord with the observations of Coelho et al. (1992) who reported that the biomass yield in their fluidized bioreactor with activated carbon was three times greater than that with sand.

An important result yielded in these studies was the relative efficiency of sand and GAC in removing metals from the brine reject. Average characteristics of denitrified brine reject effluent from sand experiments are presented in Table 9.5. As seen from the table, sand does not appear to be as effective as GAC in that the metal removal with GAC ranged between 10 and 73 percent (Table 9.2), while sand did not achieve any remarkable metal removal except selenium (72 percent). This could be considered one of the major benefits of using GAC as the support media in the FBAR process as opposed to the sand.

In conclusion, a number of issues must be considered and evaluated in order to make a selection between GAC and sand as the support medium. First of all, although the cost of GAC is relatively higher, the expense for the energy consumed will be considerably lower as the FBAR system reaches equilibrium in a much shorter time than sand, as observed in this study. On the other hand, even though sand is much cheaper than GAC, relatively longer retention times would be needed, another observation of this study, in order for the system to reach steady state. Secondly, due to the heavier density of sand, much higher recycle flowrates as compared to GAC may be required to keep the sand bed fluidized. This may be considered another disadvantage of using sand with respect to energy consumption.

Table 9.5. Average characteristics of influent and effluent denitrified brine reject from FBAR experiments with sand

Constituent	Unit	Concentration	
		Influent	Effluent
Total Dissolved Solids	mg/l	4,285	4,240
Iron	µg/l	548	523
Arsenic	µg/l	16.7	16.7
Barium	µg/l	115	115
Cadmium	µg/l	3.1	3.1
Cobalt	µg/l	4.2	4.1
Copper	µg/l	39.6	39
Lead	µg/l	<1.0	<1.0
Manganese	µg/l	215	210
Mercury	µg/l	<0.1	<0.1
Selenium	µg/l	6.5	1.8
Silver	µg/l	4.8	4.8
Zinc	µg/l	150	142
Ammonia-Nitrogen	mg/l	1.8	<0.1
Organic Nitrogen	mg/l	12.6	5.4
Total Alkalinity (as CaCO ₃)	mg/l	925	1186
Nitrite-Nitrogen	mg/l	<0.1	<0.1
Nitrate-Nitrogen	mg/l	75.4	<1.0
Sulfate	mg/l	1,100	1,058
Total Organic Carbon (TOC, Unfiltered)	mg/l	11.5	16.5

Thirdly, FBAR with GAC appear to handle high influent nitrate concentrations without compromising the efficiency and reliability of the system, as it can support very high biomass density. For the FBAR system with sand, on the other hand, significant reduction in the effluent quality in terms of nitrates and nitrites may be expected because sand supports relatively less amount of biomass. Lastly, GAC removed a number of metals present in the brine reject, whereas sand showed no

tendency for such removals. It can be said that GAC should be used for waste streams that include toxic materials such as metals and adsorbable organics, whereas sand should be employed for waste streams for which such toxicity is of no concern.

9.1.3 Prediction/Simulation of the FBAR Denitrification Model

9.1.3.1 Results of Model Parameter Estimation Studies

The parameters employed in the proposed model are presented in Table 9.6 together with the references used in the estimations of these parameters. The results of adsorption isotherm studies indicated that nitrate had no adsorption affinity for the carbon tested, and hence adsorption phenomenon was disregarded in this research. Two reasons speculated in this research would be that: (i) nitrate is hydrophilic and well soluble in water and other liquid, and (ii) nitrate ions form hydrogen bonding with the water molecules instead of bonding to the functional groups on the surface of GAC particles.

The Monod biokinetic parameters were obtained through continuous flow chemostat studies as explained in Chapter 8. The maximum biofilm thickness ($L_{f,max}$) and the biofilm density (X_f) were estimated using the correlation techniques presented in Chapter 4. The free liquid diffusivity (D_l) and the substrate mass transfer coefficient (k_{fc}) related to the hydrodynamic characteristics of a fluid particle systems were estimated via trial and error method as explained in Chapter 4. The biofilm diffusion coefficient (D_f) was estimated from the free liquid diffusivity (D_l)

Table 9.6. Operational parameters used in the proposed FBAR denitrification model

Input Parameters	Unit	Value	Reference
Bioadsorber diameter, d	cm	5.08	--
Bioadsorber length, L	cm	100	--
Carbon particle radius, r	cm	0.09	--
GAC amount, W	g	Variable	--
Initial nitrate concentration, N_0	mg/l	Variable	--
Influent flowrate, Q	ml/min	Variable	--
Recycle flowrate, Q_r	l/sec	0.0291	--
Maximum specific growth rate, $\mu_{m,a}$	hr ⁻¹	1.35	--
Monod half saturation constant, $K_{s,a}$	mg/l	1.90	--
Growth yield coefficient, Y_a	mg/mg	0.70	--
Decay coefficient, $k_{d,a}$	hr ⁻¹	0.137	--
Biomass density, X_f	mg/l	60,000	Kim, 1987
Initial biofilm thickness, $L_{f,0}$	cm	0.00005	--
Maximum biofilm thickness, $L_{f,max}$	cm	0.01	Law et al., 1976
Biofilm substrate diffusion coefficient, D_f	cm ² /s	0.00000587	Williamson & McCarty, 1976
Substrate mass transfer coefficient, k_{fc}	cm/s	0.00505	Wakao & Funazkri, 1978
Axial substrate dispersion coefficient, D_x	cm ² /s	0	Chung & Wen, 1968

using the ratio proposed by Williamson and McCarty (1976) presented in the same chapter. The axial substrate dispersion coefficient (D_x) was neglected due to higher degree of mixing, which is typical for FBARs.

9.1.3.2 Model Prediction, Verification and Sensitivity Analyses

9.1.3.2.1 Predictive Capability of the FBAR Model

FBAR mini-pilot studies were conducted to estimate the nitrate removal efficiencies as well as to verify the predictive capability of the proposed FBAR denitrification model. The model parameters employed are presented in Table 9.6 and include mass transfer coefficient, diffusion coefficients, bioadsorber characteristics such as particle size and density, initial and maximum biofilm thickness, hydraulic retention time, influent nitrate concentration, influent and recycle flow characteristics. Data for effluent nitrate concentration were obtained for each set of the FBAR denitrification study employing varying operating conditions including influent concentration of nitrate, hydraulic retention time and quantity of GAC as presented in Table 9.1. These data were compared with the FBAR model simulation and prediction profiles. The prediction/simulation results are shown in Figures 9.7 through 9.15. As evident from the figures, good agreement is observed between the experimental data and model predictions. These results indicate a reasonably good predictive capability of the FBAR denitrification model.

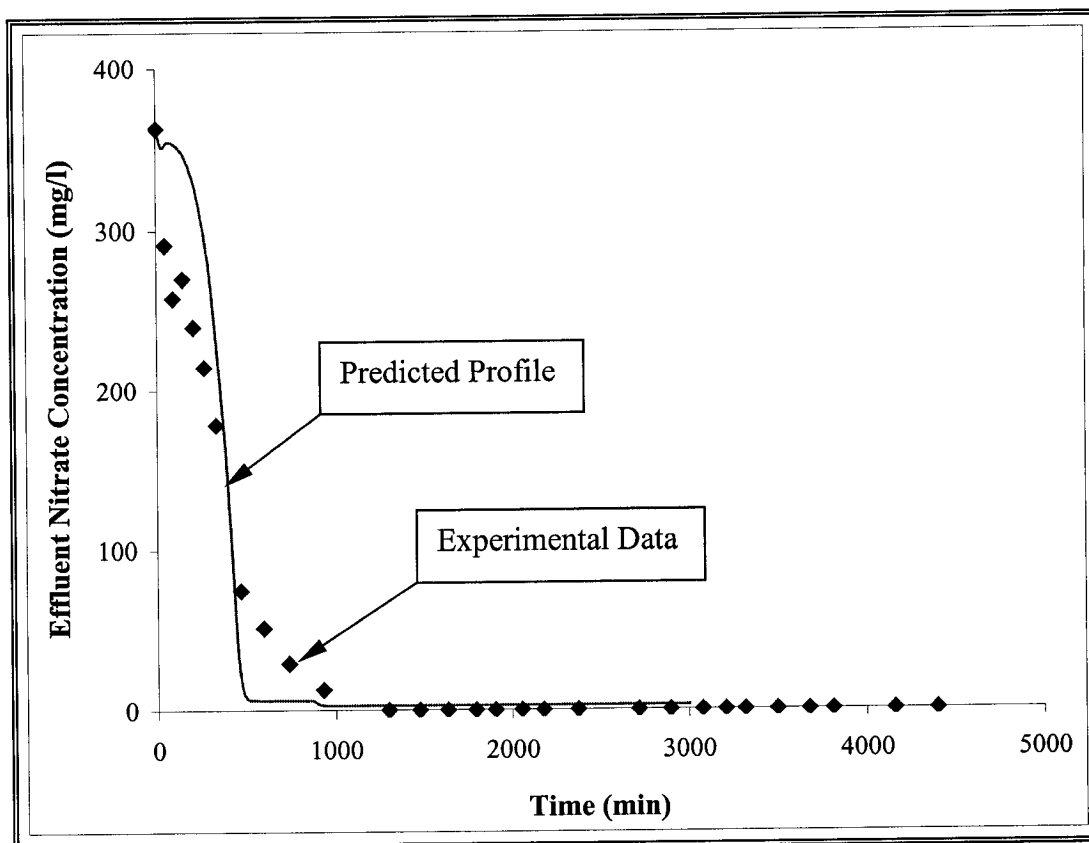


Figure 9.7. Experimental data and predicted profile for the FBAR with GAC = 300 g, HRT = 60 min and Nitrate = 362 mg/l

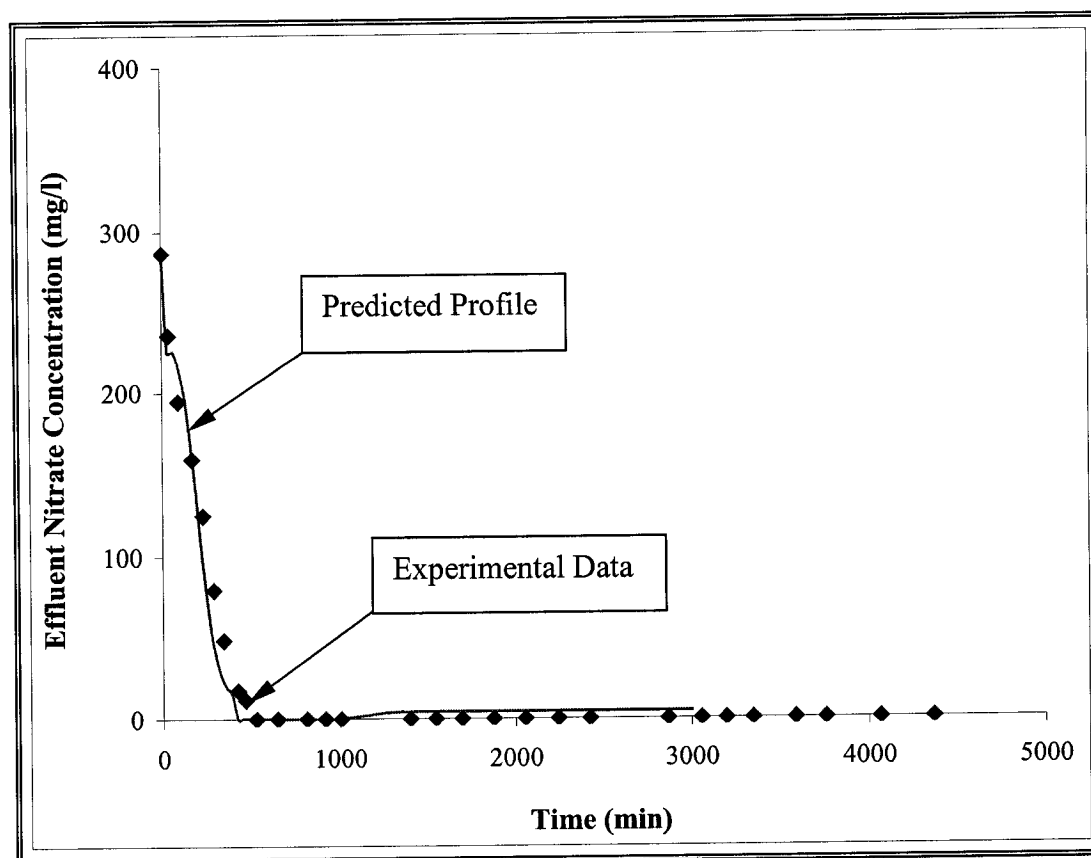


Figure 9.8. Experimental data and predicted profile for the FBAR with GAC = 300 g, HRT = 120 min and Nitrate = 287 mg/l

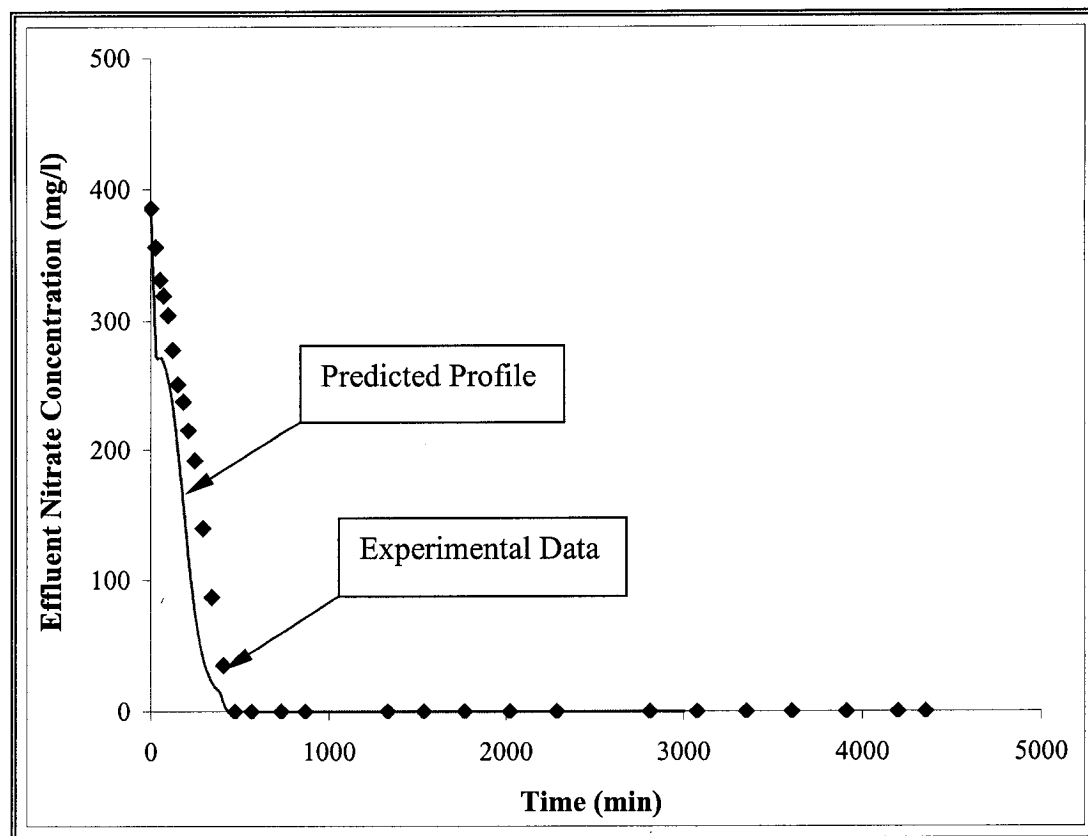


Figure 9.9. Experimental data and predicted profile for the FBAR with GAC = 300 g, HRT = 180 min and Nitrate = 386 mg/l

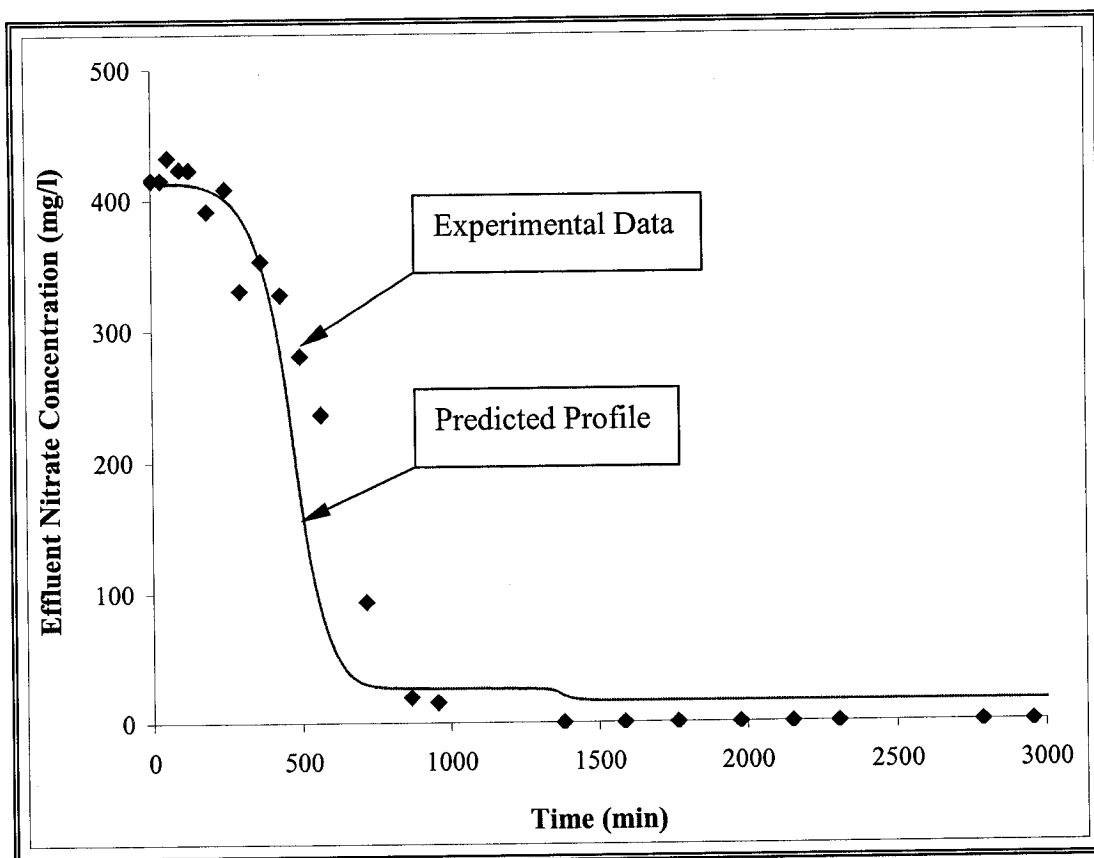


Figure 9.10. Experimental data and predicted profile for the FBAR with GAC = 150 g, HRT = 60 min and Nitrate = 416 mg/l

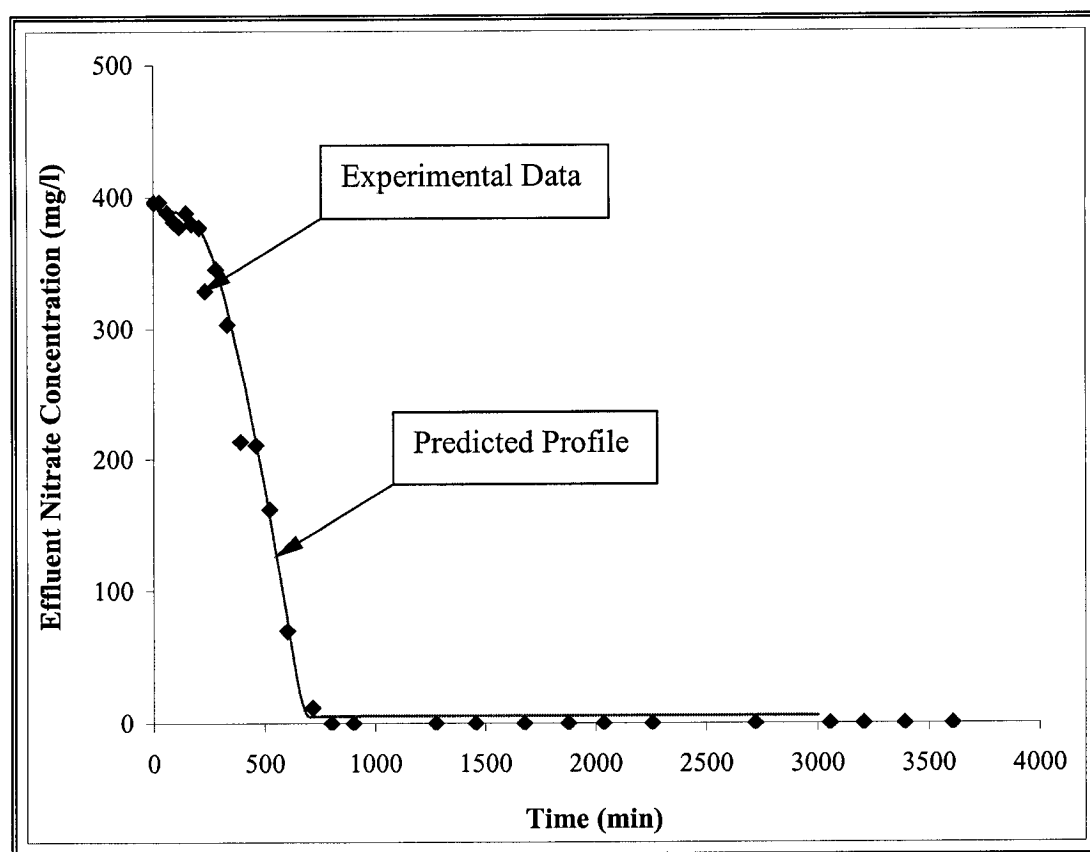


Figure 9.11. Experimental data and predicted profile for the FBAR with GAC = 150 g, HRT = 120 min and Nitrate = 396 mg/l

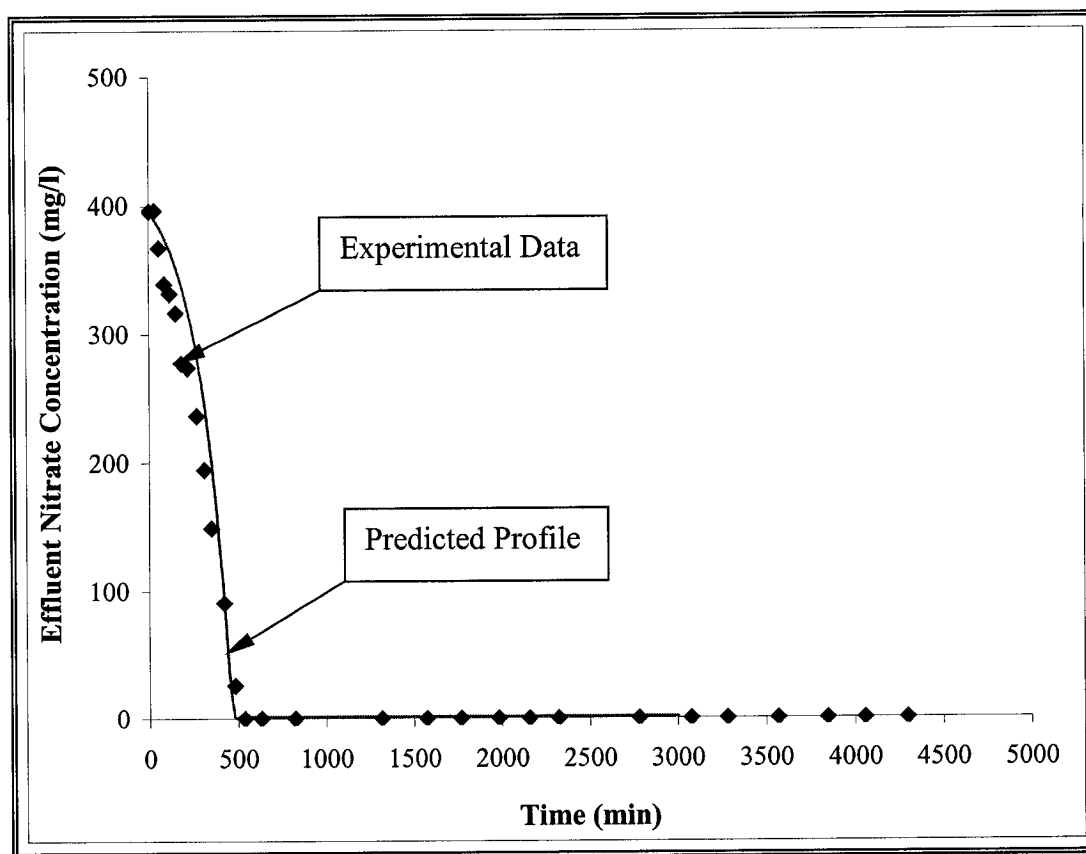


Figure 9.12. Experimental data and predicted profile for the FBAR with GAC = 150 g, HRT = 180 min and Nitrate = 396 mg/l

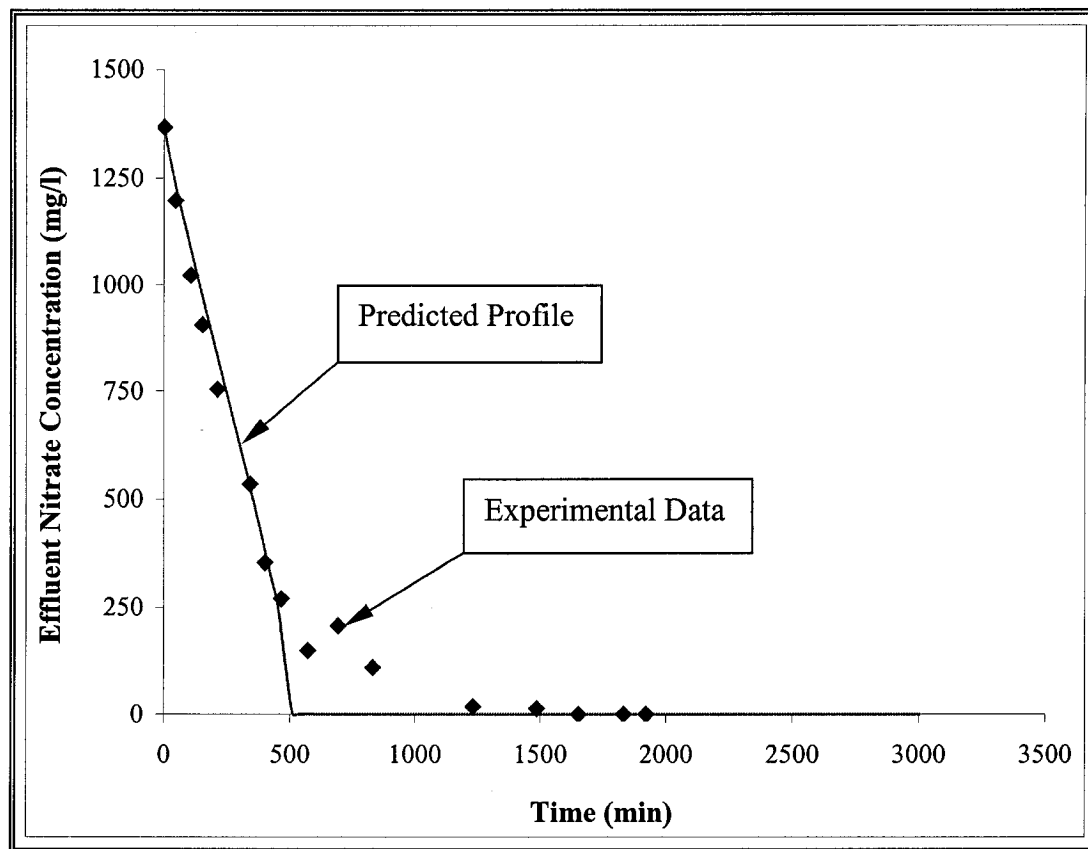


Figure 9.13. Experimental data and predicted profile for the FBAR with GAC = 150 g, HRT = 90 min and Nitrate = 1,368 mg/l

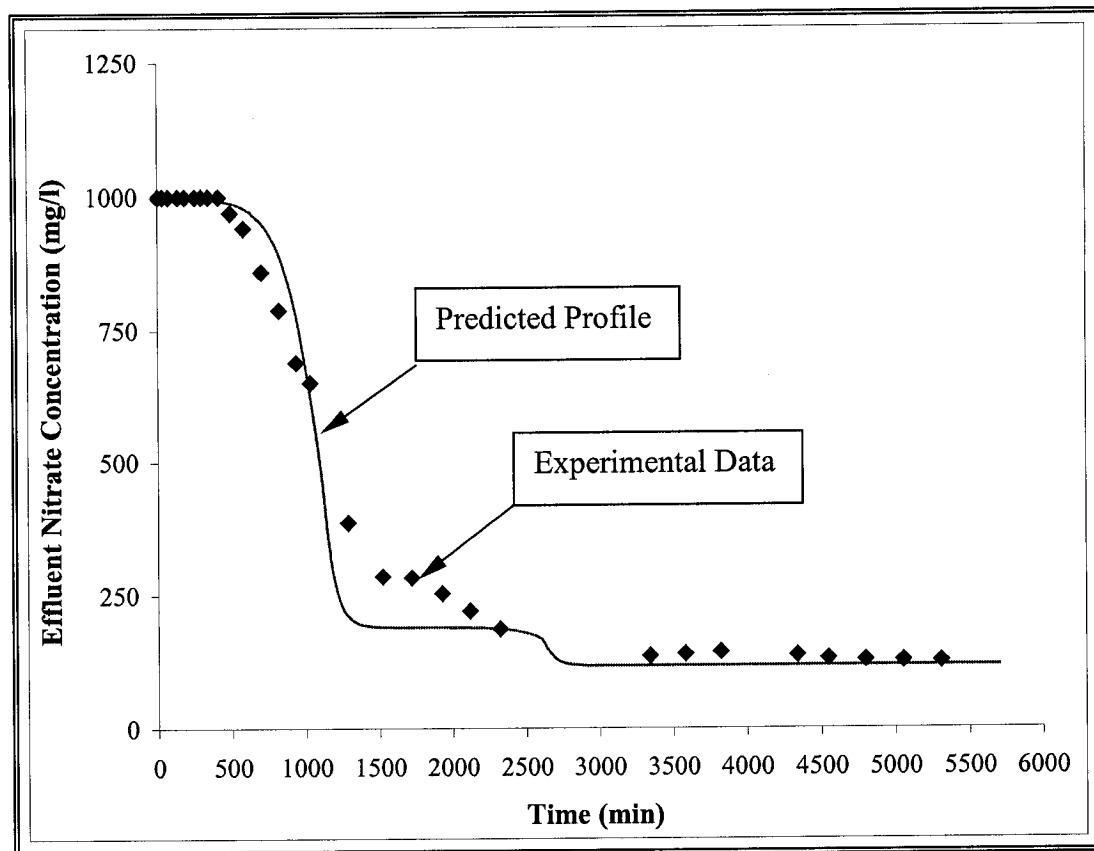


Figure 9.14. Experimental data and predicted profile for the FBAR with GAC = 150 g, HRT = 60 min and Nitrate = 1,000 mg/l

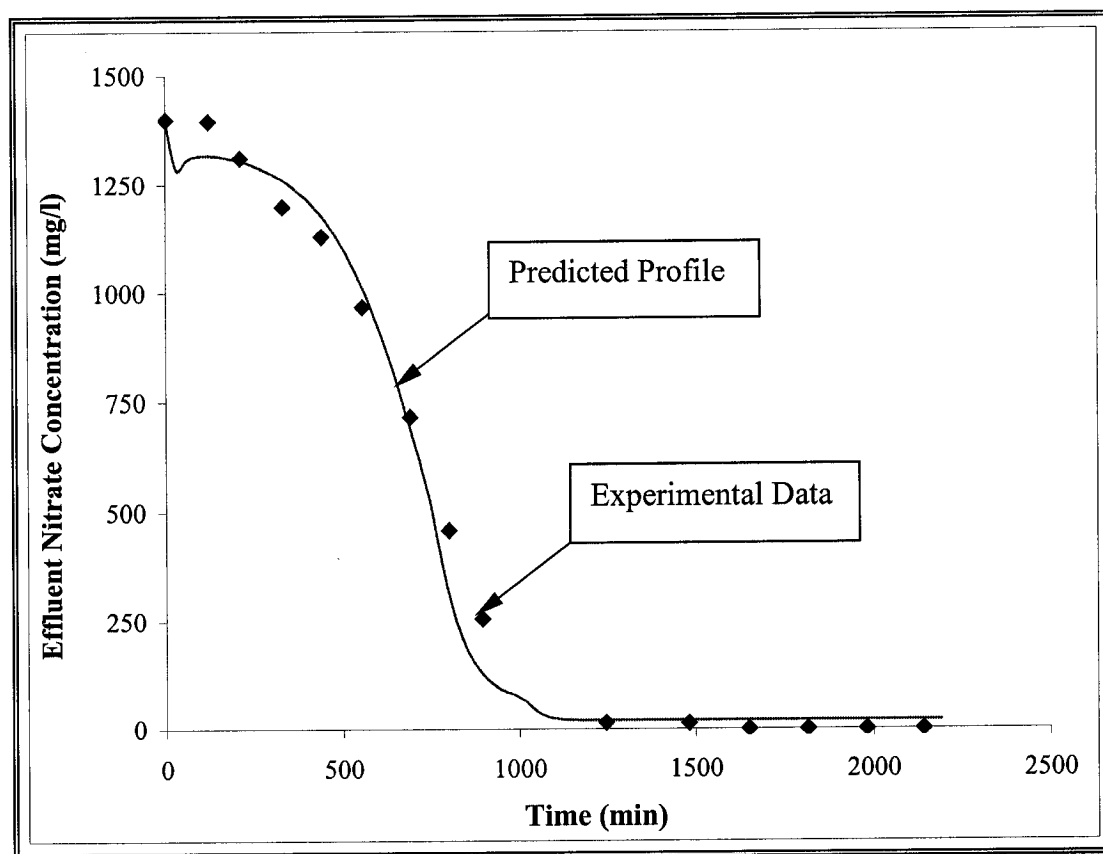


Figure 9.15. Experimental data and predicted profile for the FBAR with GAC = 300 g, HRT = 90 min and Nitrate = 1,400 mg/l

9.1.3.2.2 *Model Sensitivity Analyses*

Sensitivity analyses were carried out to evaluate the qualitative influence of various parameters on the overall performance of the FBAR denitrification process and the model proposed for FBAR denitrification, and to examine the level of accuracy required for the estimation of each parameter for the model. These parameters included the influent nitrate concentration (N_o), the biofilm density in the biofilm (X_f), the growth yield coefficient (Y_a), the maximum specific growth rate ($\mu_{m,a}$) and the Monod half saturation constant ($K_{s,a}$). A 50 percent increase or decrease in each of these parameters was used to demonstrate the changes in the FBAR effluent concentration profiles.

The results of model sensitivity analyses are presented in Figures 9.16 through 9.20. The investigations revealed that the effluent profile concentrations were sensitive to the influent nitrate concentrations and the biofilm density, as shown in Figures 9.16 and 9.17. Typical results of sensitivity analysis for the growth yield coefficient are presented in Figure 9.18. As evident from the figure, growth yield coefficient significantly influenced the FBAR efficiency in that a 50 percent decrease in this parameter reduced the time to reach steady state by nearly 50 percent. On the other hand, a 50 percent increase in this parameter reduced increased the steady state removal efficiency by 75 percent. Similar results were obtained for the maximum specific growth rate, as illustrated in Figure 9.19. The effluent nitrate concentration profiles were insensitive to Monod half saturation constant, as seen from Figure 9.20.

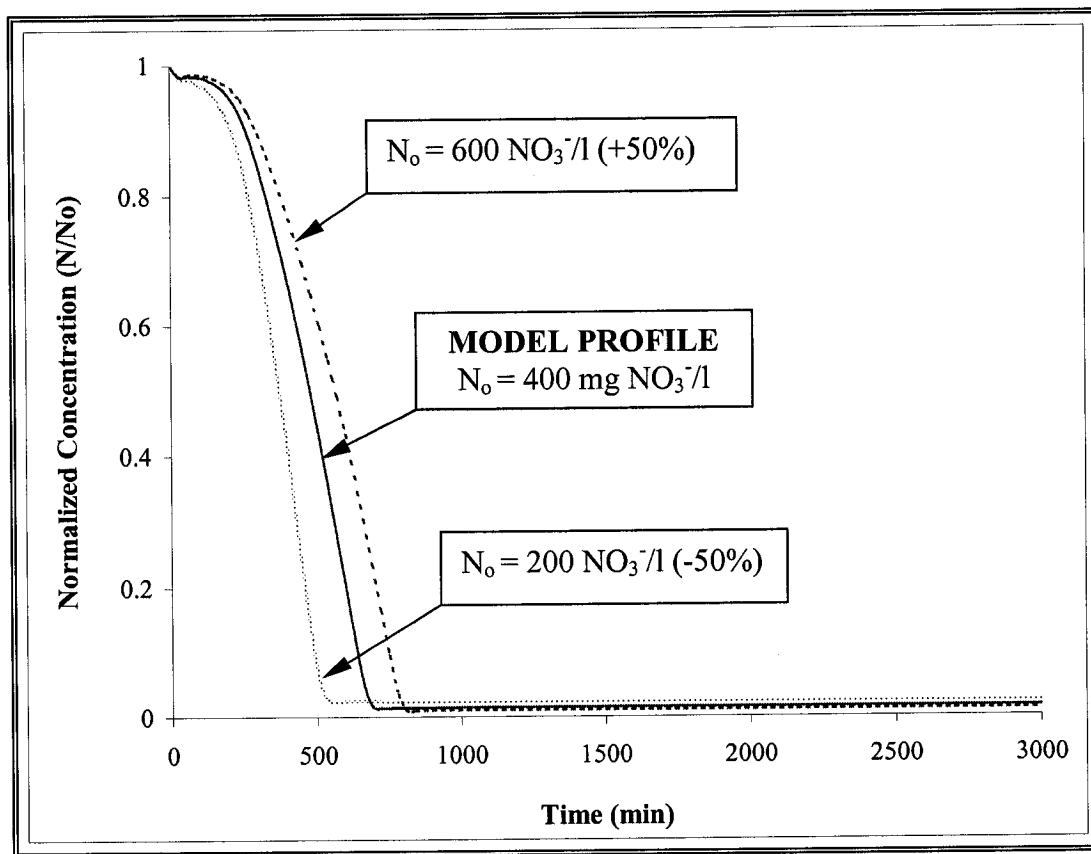


Figure 9.16. Sensitivity analysis for changes in influent nitrate concentration

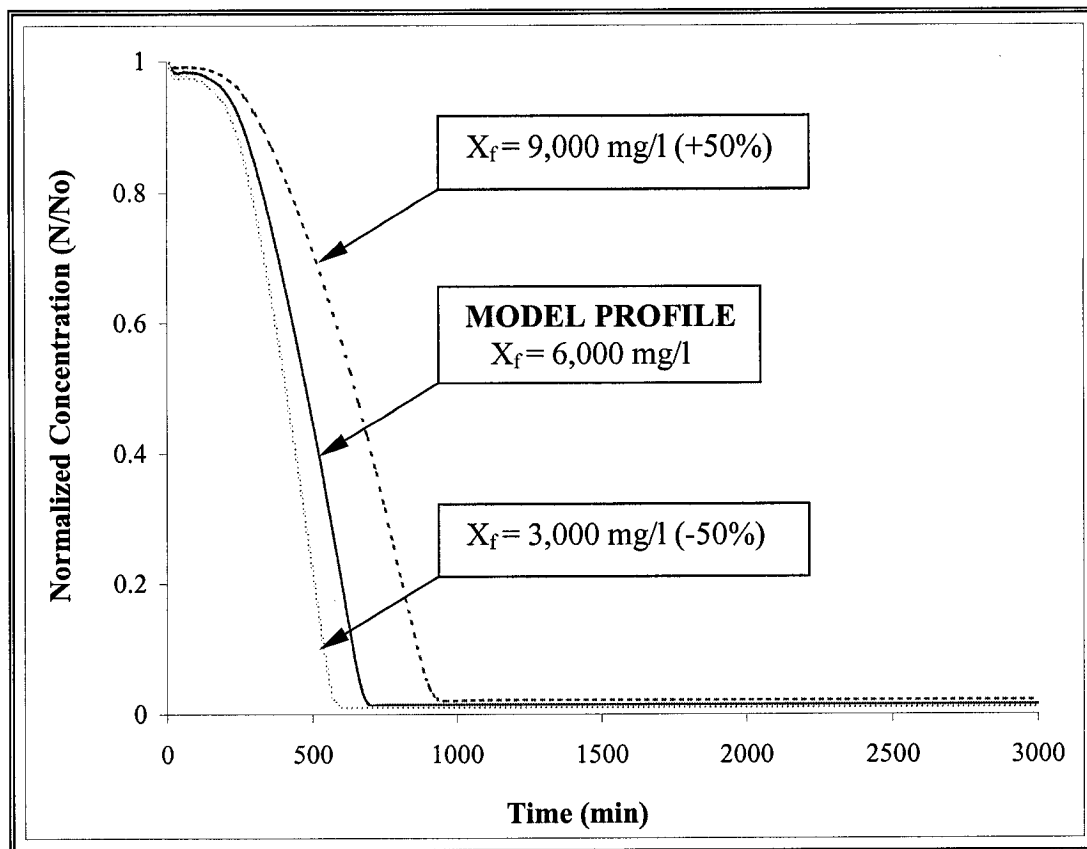


Figure 9.17. Sensitivity analysis for changes in biofilm density

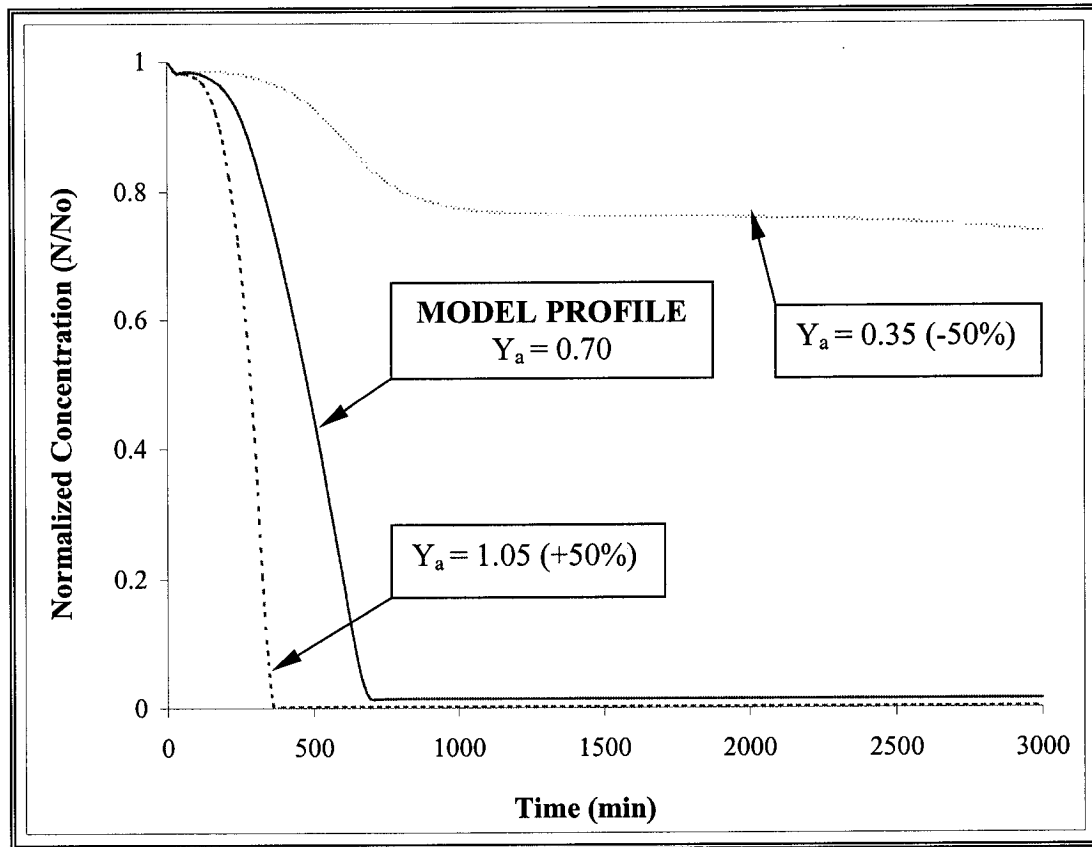


Figure 9.18. Sensitivity analysis for changes in growth yield coefficient

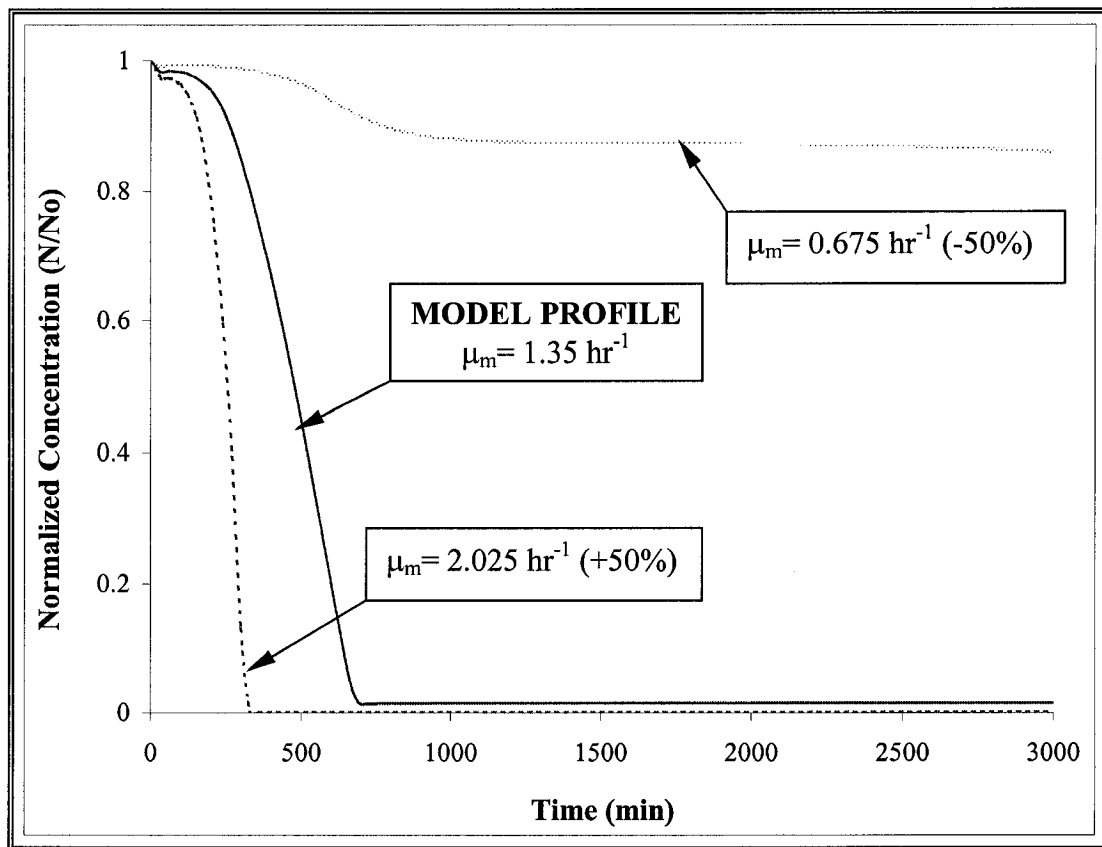


Figure 9.19. Sensitivity analysis for changes in maximum specific growth rate

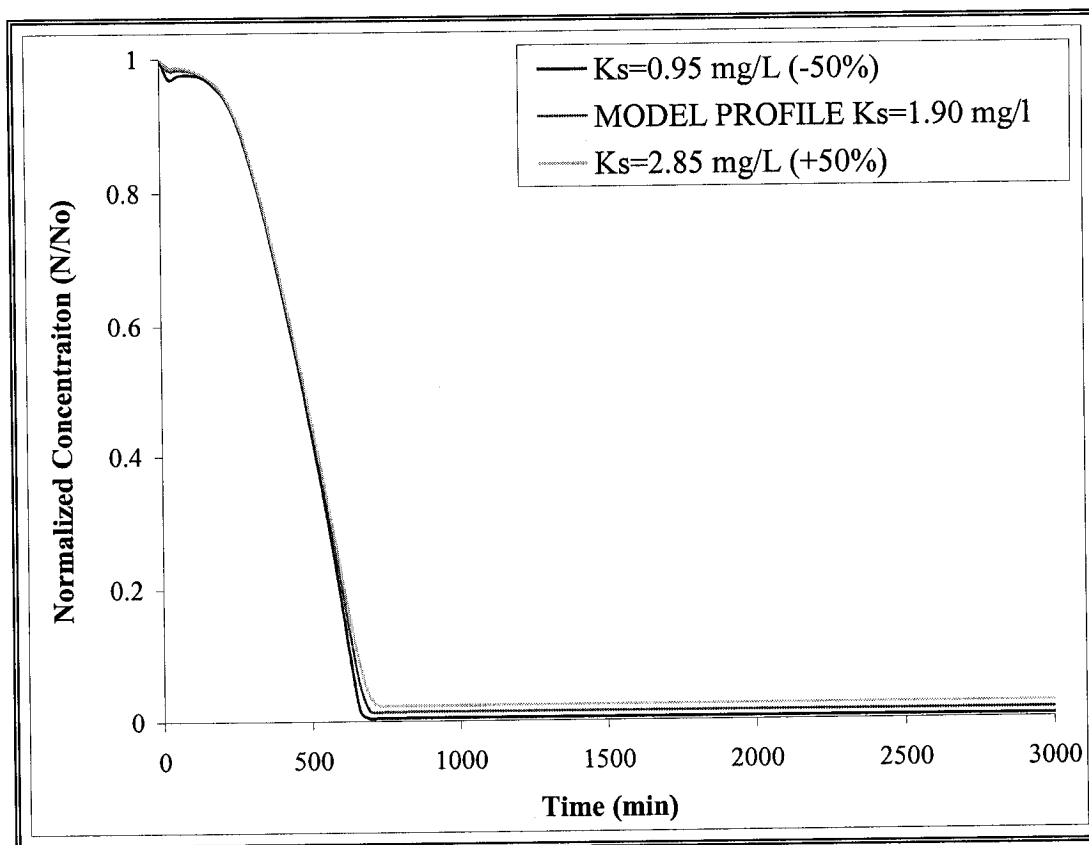


Figure 9.20. Sensitivity analysis for changes in Monod half saturation constant

9.2 Summary and Conclusions

- The results of the FBAR denitrification studies demonstrated that the process was significantly affected by the quantity of carbon, the influent nitrate concentration and the hydraulic retention time. FBAR virtually exhibited over 96 percent denitrification efficiencies at hydraulic retention times ranging from 40 to 180 minutes. Higher nitrate concentration and GAC quantity promoted higher biomass growth and bioparticle densities.

- Because nitrite build-up was insignificant at steady state operation, the FBAR denitrification system could be considered as a single-step treatment process in design considerations.
- SEM images revealed that the GAC particles supported a uniform and homogeneous biofilm layer.
- The FBAR model was found to adequately describe the experimental data. The model was tested to predict the performance of the FBAR process for various operating conditions including carbon quantity, influent nitrate concentration and hydraulic retention time. The effluent nitrate concentration data obtained in these studies were in good agreement with the predicted model profile.
- Sensitivity studies for the FBAR model indicated that the growth yield coefficient (Y_a) and the maximum specific growth rate ($\mu_{m,a}$) significantly influenced the process performance. However, the effect of the Monod half saturation constant ($K_{s,a}$) on the process performance was insignificant.
- It was concluded that sand could be an effective support medium in the FBAR denitrification process, especially in cases where no toxic chemicals are present in the waste stream.

CHAPTER 10

FBAR PROCESS FOR SULFATE REDUCTION FOLLOWED BY BIOFILTRATION

In this chapter, denitrification coupled with sulfate reduction, sulfate reduction alone and biofiltration processes were investigated. The main objectives are: (i) to evaluate the FBAR process efficiency for the simultaneous removal of sulfate and nitrate, (ii) to investigate the FBAR process efficiency for sulfate reduction in the absence of nitrate, and (iii) to study the efficiency of biofiltration process in removing hydrogen sulfide gas.

10.1 Results and Discussions

10.1.1 FBAR Process for Simultaneous Denitrification and Sulfate Reduction

In accord with the work of Postgate (1979), it was decided that the brine rejects with high salinity (TDS) and sulfate concentration should be amenable to biological sulfate reduction due to high tolerance of sulfate reducing bacteria to high salt concentrations. This part of the research investigated the simultaneous denitrification and sulfate reduction for the brine rejects employing the FBAR process. This process was preferred over others because FBARs have the advantage of enhancing the mass transfer rates for both sulfate and product gas (hydrogen

sulfide), and the process could be used to achieve high rates of sulfate reduction at high liquid throughputs depending on the feed sulfate concentration, hydraulic retention time and efficiency of the reduction capacity (Nagpal et al., 2000).

In this part of the study, a similar FBAR process used for the denitrification studies as discussed in Chapter 9 was employed. The hydraulic retention time was set at 180 minutes, corresponding to an influent flowrate of 10 ml/min. The carbon to sulfur ratio was maintained near approximately 41:1 complete sulfate removal and to minimize the residual pollution in the effluent stream caused by ethanol. The temperature and pH were maintained at 30°C and 7.5, similar to all the other FBAR denitrification experiments.

As shown in Figure 10.1, nitrate removal was complete within the first 400 minutes of FBAR operation, and neither nitrate nor nitrite was detected in the effluent stream at steady state conditions. During this 400 minutes, no sulfate reduction took place, as nitrate was preferentially used over sulfate as the primary substrate, a phenomenon also observed by Payne (1981).

The experiment was continued for approximately 585 hours to investigate the extent of sulfate removal. Gradual decrease in the effluent sulfate concentration was achieved over the length of 133 hours of experimental run, and a sulfate reduction of nearly 45 percent, corresponding to an effluent sulfate concentration of 720 mg/l at a reduction rate of 8.5 g S/l.day, was achieved at the end of 585 hours. Such long time periods required for the growth and activity of the sulfate-reducing bacteria are also reported by Postgate (1979) who explained this phenomenon as the exhibition of

non-exponential trend for the growth of sulfate-reducing bacteria cultures. Finally, after 585 hours of reactor operation, the experiment was stopped due to prolific bacterial growth and consequential clogging of the reactor inlet and recycle and effluent tube.

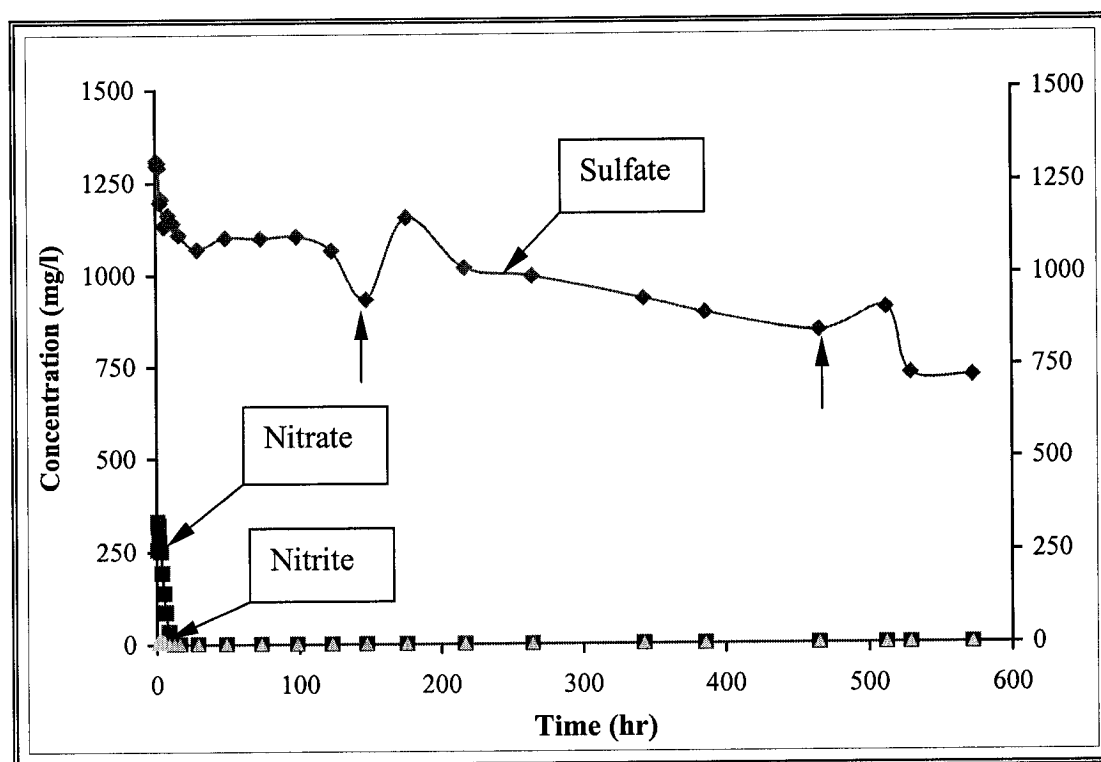


Figure 10.1. Simultaneous nitrate and sulfate reduction in the first FBAR (Single arrows indicate the time when the bioadsorber bed was vigorously agitated to remove excess biomass growth)

A discussion on the performance of the FBAR process in the removal of sulfate and nitrate follows (Figure 10.1). Initially, nitrate reduction occurred along the bioadsorber bed with no sulfate removal. However, once the population of the

sulfate-reducing bacteria began to establish, sulfate reduction was observed along with nitrate reduction, as there was neither nitrate nor nitrite detected in the bioadsorber effluent and sulfate concentration was reduced by about 45 percent. The fact that nitrate and nitrite were completely reduced, while sulfate was only partially reduced, could be attributed to the slow growth of sulfate-reducing bacteria in an environment where a more favorable substrate (nitrate) is available to the microbial community in the system (Payne, 1981). This phenomenon could systematically be explained using the oxidation-reduction potential order of several chemicals from the most preferred by the microorganisms to the least preferred. From an evolutionary point of view, the biologically mediated reactions that yield more energy for the microorganisms take precedence over those that are less energy-yielding. In other words, since microorganisms would like to obtain as much energy from a reaction as possible, the biological reaction sequence is paralleled by an ecological succession of microorganisms, i.e., aerobic heterotrophs, denitrifiers, fermentors, sulfate reducers and methane bacteria. The sequence of redox reactions observed in a system with ethanol is summarized in Table 10.1. In a closed aqueous system containing an organic substrate (in this case, ethanol), the oxidation of the organic substrate is observed to occur first by reduction of oxygen ($pe^0 = +13.75$). This will be followed by the reduction of nitrate into nitrogen gas ($pe^0 = +12.65$). When sufficiently negative potentials levels have been reached, fermentation reactions, sulfate reduction and carbon dioxide reduction may occur almost simultaneously. As

observed from the table, the succession of these reactions follows the decreasing $p\epsilon^\circ$ level (Stumm & Morgan, 1996).

Table 10.1. Biological oxidation-reduction reactions, their standard potentials and Gibbs free energies* (pH = 7 and Temperature = 25°C)

Reduction		$p\epsilon^\circ(w)$
$\frac{1}{4} \text{O}_2(g) + \text{H}^+(w) + e^- = \frac{1}{2} \text{H}_2\text{O}$ (Aerobic heterotrophs)	A	+ 13.75
$\frac{1}{5} \text{NO}_3^- + \frac{6}{5} \text{H}^+(w) + e^- = \frac{1}{10} \text{N}_2(g) + \frac{3}{5} \text{H}_2\text{O}$ (Denitrifiers)	B	+ 12.65
$\frac{1}{2} \text{CH}_2\text{O} + \text{H}^+(w) + e^- = \frac{1}{2} \text{CH}_3\text{OH}$ (Fermentors)	C	- 3.01
$\frac{1}{8} \text{SO}_4^{2-} + \frac{9}{8} \text{H}^+(w) + e^- = \frac{1}{8} \text{HS}^- + \frac{1}{2} \text{H}_2\text{O}$ (Sulfate reducers)	D	- 3.75
$\frac{1}{8} \text{CO}_2(g) + \text{H}^+(w) + e^- = \frac{1}{8} \text{CH}_4(g) + \frac{1}{4} \text{H}_2\text{O}$ (Methane bacteria)	E	- 4.13
Oxidation		$p\epsilon^\circ(w)$
$\frac{1}{12} \text{C}_2\text{H}_5\text{OH} + \frac{1}{4} \text{H}_2\text{O} = \frac{1}{6} \text{CO}_2 + \text{H}^+(w) + e^-$ (Ethanol oxidation)	F	- 1.66
Combinations		$\Delta G^\circ(w)$ (Kcal/mol)
Denitrification with Ethanol	B + F	-26.5
Sulfate Reduction with Ethanol	D + F	-3.6

* Adapted from Stumm & Morgan (1996)

As mentioned above, the reduction of nitrate precedes the reduction of sulfate. In other words, the free energy for nitrate reduction is much lower than that required for sulfate reduction (-26.5 Kcal/mol vs. to -3.6 Kcal/mol), which suggests that, when there is nitrate in the system, bacteria will prefer to utilize nitrate first. However, as time progresses, some bacteria will become acclimated to the sulfate,

and begin to utilize sulfate in the upper portions of the reactor bed where nitrate is virtually absent. This so-called “zoning” phenomenon that occurs in packed- or fluidized-bed systems could be attributed to this phenomenon. Providing longer hydraulic retention times also assists the acclimation of the sulfate-reducing bacteria and the establishment of zoning regions. Sison et al. (1995) reported similar observations in their study using packed bed reactors. They showed that denitrification process took place within the first few inches of the packed bed entrance, whereas sulfate reduction took place in the region near the exit of the reactor.

In this study, as time progressed, the GAC particles in the upper regions of the bioadsorber appeared to be covered with a thick layer of biofilm, whereas lower regions appeared to support relatively thinner biofilms. The reason speculated for the formation of such layers specifically on the upper layers of the bioadsorber bed is that the relative concentrations of nitrate and sulfate in the influent brine reject. Influent sulfate concentration in the RO brine reject was much higher than the nitrate concentration (1,300 mg /l sulfate as opposed to 330 mg/l nitrate). As mentioned earlier, influent substrate concentration is one of the primary factors that affect the amount of biomass in FBAR systems. In light of this phenomenon, the limited nitrate concentration that was available to the denitrifying bacteria in the lower layers of the bioadsorber bed, coupled with long hydraulic retention time did not allow the denitrifying bacteria to grow in substantial amounts. On the other hand, the high concentration of sulfate in the influent, coupled with the lower oxidation-reduction

potential, led to prolific biomass growth in the upper portions of the bioadsorber bed. As the bioparticles became thicker in the upper regions, they tended to leave the bioadsorber with the effluent due to the reduction in the density. The bioparticle wash-out is usually prevented by periodic mixing to detach the excess biofilm layer from the media surface. The arrows in Figure 10.1 indicate the time when the upper layers of the bioadsorber bed were vigorously agitated.

Plugging of the outlet and recycle tube was unavoidable after 585 hours of system operation. The biomass growth in the recycle tubing that maintained the bioadsorber bed in fluidized condition was the main cause of clogging. Biomass that was carried along with the recycle line also clogged the perforated tray that supported the bed media, which in turn resulted in pressure built-up in the influent tube. Other researchers also reported similar problems for their systems (Chen et al., 1994; Raiders et al., 1986).

10.1.2 FBAR Process for Sulfate Reduction Alone

In order to investigate the extent of sulfate removal by the FBAR process, the denitrified effluent from the above mentioned FBAR unit was pumped through an identical second unit, which operated in a similar manner as the first one. The hydraulic retention time was maintained at 180 minutes corresponding to a flowrate of 10 ml/min. The feed sulfate concentration was 720 mg/l. The unit was seeded with acclimated sulfate-reducing bacteria obtained from the first FBAR unit. Since

ethanol was fed into the first FBAR unit in excess to allow complete sulfate removal, no ethanol was fed into this second unit.

Figure 10.2 demonstrates the system efficiency in achieving complete sulfate reduction. As evident from the figure, a gradual decrease in the sulfate concentration started immediately after the reactor start-up. After 412 hours of operation, the effluent sulfate concentration dropped from 720 mg/l to zero, which corresponded to a sulfate reduction rate of 10.3 g S/l.day.

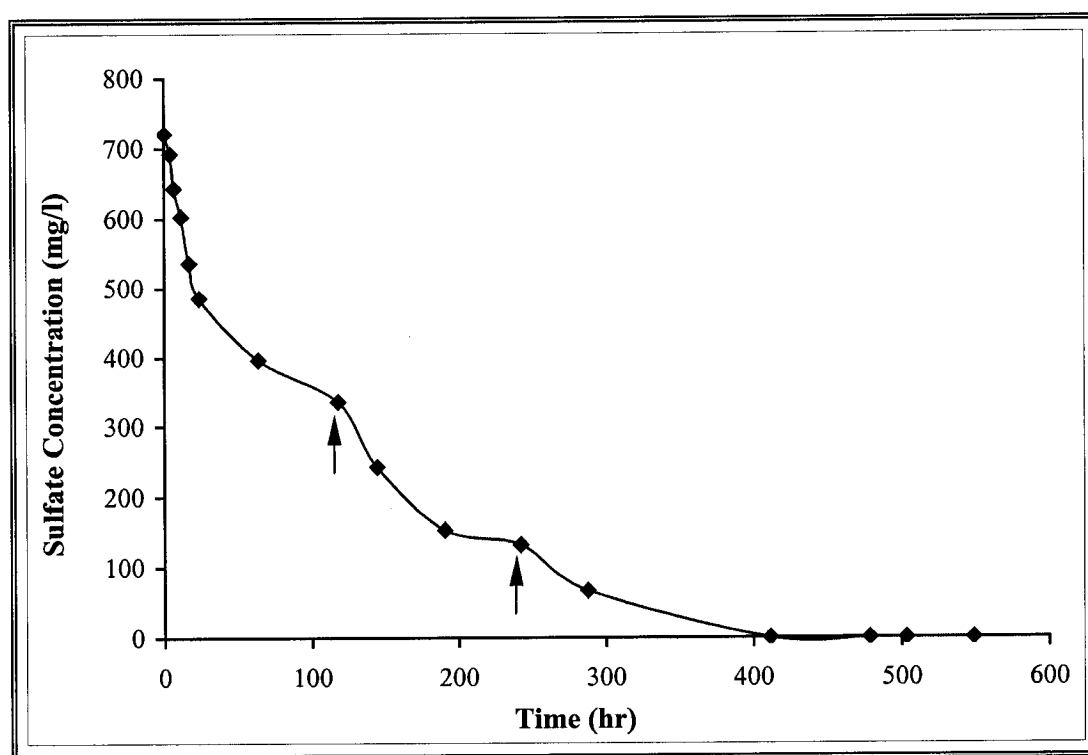


Figure 10.2. Sulfate reduction profile in the second FBAR unit (Arrows indicate the time when the bioadsorber bed was vigorously agitated to remove excess biomass growth)

The bioadsorber bed was mixed vigorously twice over a period of 412 hours to break the excess biofilm layer formed on the GAC particles, as indicated in Figure 10.2.

10.1.3 Sulfate Reduction and Metal Removal in FBAR

A major finding from the two FBAR sulfate reduction studies was the substantial decrease in the metal concentration. As mentioned earlier, metal removal in biological sulfate reduction process has been described by a number of investigators (Chen et al., 1994; Dovark et al., 1992; Middleton, 1975; Postgate, 1979).

In this study, the reactor walls were gradually covered with well-separated dark spots, a possible indication of microbial sulfate reduction and a process called “souring” due to the generation of hydrogen sulfide gas (Chen et al., 1994). The formation of these dark spots was most likely due to the presence of iron in the feed brine reject, which reacted with the hydrogen sulfide to form ferric sulfide precipitate. Table 10.2 presents the steady state characteristics of the brine reject solution after the denitrification and (partial) sulfate reduction in the first FBAR unit and after complete sulfate reduction in the second FBAR unit. As seen from this table, the iron concentration in the nitrified brine reject declined from 448 $\mu\text{g/l}$ to less than 1 $\mu\text{g/l}$ at steady state, corresponding to a 100 percent removal. In fact, Dovark et al. (1992) reported a similar finding, and observed that very little iron ever leached from their sulfate removal system due to the retention of iron within the system.

Similarly, Chen et al. (1994) noted that part of the hydrogen sulfide gas could accumulate in the system leading to the scavenging of hydrogen sulfide as ferric sulfide.

Table 10.2. Characteristics of brine reject effluent at steady state after denitrification in the first FBAR and after complete sulfate reduction in the second FBAR

Constituent	Unit	Steady State Concentration	
		After Denitrification	After Sulfate Reduction
Total Dissolved Solids	mg/l	4,440	3,960
Iron	µg/l	448	<1.0
Arsenic	µg/l	9.9	6.7
Barium	µg/l	53.2	49
Cadmium	µg/l	<1.0	<1.0
Cobalt	µg/l	1.2	1.1
Copper	µg/l	18.4	9.4
Lead	µg/l	<1.0	<1.0
Manganese	µg/l	68.6	52
Mercury	µg/l	<0.1	<0.1
Selenium	µg/l	21.7	9.8
Silver	µg/l	6.6	<1.0
Zinc	µg/l	32.2	12.3
Ammonia-Nitrogen	mg/l	1.3	<0.1
Organic Nitrogen	mg/l	0.5	0.5
Total Alkalinity	mg/l	489	452
Nitrite-Nitrogen	mg/l	0.55	<0.1
Nitrate-Nitrogen	mg/l	<1.0	<0.1
Sulfate	mg/l	720	9.0
Total Organic Carbon (Unfiltered)	mg/l	138*	12.3

* Ethanol was fed only to the first FBAR at a ratio of 41:1 to accomplish complete sulfate removal in both FBARs

Another observation and the proof of metal removal by precipitation was that pH within the FBAR dropped significantly instead of increasing most possibly due to the volatilization of hydrogen sulfide gas generated as a result of sulfate reduction. This could be interpreted as the indication of entrapment of sulfide as insoluble derivatives of metals, that is, metal precipitation on the surfaces of GAC particles. As mentioned in Section 3.3.5, Chapter 3, Postgate (1979) stated that the environment tends to become acidic when there are compensating metabolic reactions leading to acid formation or when the sulfite generated from sulfate reduction is trapped as insoluble derivatives of heavy metals.

The results presented in Table 10.2 also demonstrated that the FBAR was not only efficient in the removal of iron, but also achieved arsenic, copper, manganese, selenium, silver and zinc removal in the range from 24 percent to 100 percent. Apart from iron, the highest efficiency was obtained with silver (100 percent), followed by zinc (62 percent), selenium (55 percent), copper (49 percent) and manganese (24 percent) as steady state FBAR operation. This is in good agreement with the findings of Lappan (1987), who reported the sequence as copper being removed first, then zinc second, followed by other heavy metals in their up-flow anaerobic fixed-film reactor. In another study, Chuichulcherm et al. (2001) reported a complete sulfide conversion into metal sulfide when zinc concentration in their waste circulation tank decreased rapidly without leaving any hydrogen sulfide gas in the medium wastewater. Other studies carried out by different researchers (Dovark et al., 1991;

Wang, 1993; Wijaya, 1993) revealed similar metal removals in their sulfate reducing systems.

10.1.4 Biofiltration for the Removal of Hydrogen Sulfide Gas

Bio-oxidation of mineral compounds, such as sulfide, supplies energy to the microbial cells, and produces odorless compounds, such as elemental sulfur or sulfate, in addition to carbon dioxide, water and new biomass. In this research, a biofilter column packed with GAC employed for the biomass attachment was used to remove the hydrogen sulfide gas evolved from the FBAR sulfate reduction processes. GAC was chosen as the support media due to its excellent stability (no self-degradation by column microorganisms), large surface areas, high buffering and adsorptive capacity, effective handling of shock loads and adaptation to higher influent contaminant concentrations in a very short period of time without any offset in the process efficiency (Den et al., 1998).

After the attachment of microbial cells onto the GAC particles, the column began its operation as soon as the sulfate reduction took place in the FBARs and the characteristic hydrogen sulfide odor was sensed, and operated during the entire course of the denitrification-sulfate reduction experiments. The contaminated gas stream was fed into the column from the bottom and the clean air stream was vented off at the top. The column effectively removed the hydrogen sulfide (well over 99 percent), as no hydrogen sulfide gas was detected in the column effluent and in the ambient air during the entire experimental period.

The pH control within the column was accomplished through limestones mixed with the GAC medium (Webster, 1996). The pH change throughout the column was gradual due to the aerobic metabolic reactions of the microorganisms. Over a week's period, the pH in the column fluctuated between 6 and 7 ± 0.2 . The nutrient solution whose constituents were given in Section 5.1.3, Chapter 5, not only provided the biofilter microorganisms with necessary substrates and moisture content, but also restored the column pH back to about 7.

Since the biofilms on the GAC particles appeared to be rather thin, which is another parameter related to the efficiency and pressure drop across the filter bed, there was neither channeling occurrence throughout the bed, nor bed plugging. Therefore, the GAC bed was never replaced during the entire course of the study. The only by-product that accumulated on the bottom of the biofilter was sulfuric acid, and it was collected and discarded on a weekly basis.

Biofiltration technology is usually preferred in cleaning the contaminated air streams because of its high cleaning efficiency with respect to hydrogen sulfide and organic sulfur compounds of dilute to moderate concentration ranges (Hansen et al., 1999). The biofilter column used in this research operated well and trouble-free during the entire experimental course of the sulfate reduction. The column not only removed hydrogen sulfide but also may have been effective in the removal of other sulfurous compounds, such as methyl mercaptan, dimethyl sulfide and dimethyl disulfide, collectively known as reduced sulfur compounds. These compounds do not necessarily pose a health hazard as hydrogen sulfide gas, but are considered to

produce pungent odor. A number of studies indicated that good results could be obtained with mixtures of mercaptans and that biofiltration was shown to be a viable technology (Wani et al., 1999). However, the removal of these contaminants may require different environmental parameters and process configurations, as shown by Pinjing et al. (2001). These researchers suggested, for example, a two-stage biofilter operated in series under different pH values to remove hydrogen sulfide gas and methyl mercaptan. In this research, however, no attempt was made to investigate the biofiltration efficiency with respect these compounds. Therefore, further research efforts are needed in this area.

10.2 Summary and Conclusions

- The first FBAR operated at 180 minutes hydraulic retention time with 330 mg/l initial nitrate and 1,300 mg/l initial sulfate concentration was capable of achieving complete denitrification and partial sulfate reduction. Nitrate was reduced from 330 mg/l to zero in about 400 minutes, while sulfate reduction from 1,300 mg/l to 720 mg/l was achieved at the end of 585 hours of column operation.
- The denitrification process appeared to take place in the lower portion of the bioadsorber bed and the biofilm appeared to be thin, while sulfate reduction occurred on the top portions where biofilms appeared to be much thicker.

- The second FBAR fed by the effluent from the first FBAR reduced the sulfate concentration from 720 mg/l to 9 mg/l in about 412 hours in the absence of nitrate.
- Sulfate reduction process was found to be very effective in the removal of heavy metals. Iron was removed 100 percent by precipitation as ferric sulfide. Removal percentages for other metals at steady state FBAR operation were: Silver (100 percent), zinc (62 percent), selenium (55 percent), copper (49 percent) and manganese (24 percent).
- Biofiltration column was able to achieve complete removal of hydrogen sulfide generated from the FBAR sulfate reduction processes.

CHAPTER 11

GRAND SUMMARY, CONCLUSIONS AND RECOMMENDATIONS FOR FUTURE RESEARCH

Experiments and modeling studies on a number of biotechnologies, including biological nitrification, denitrification, sulfate reduction and hydrogen sulfide removal, were conducted in this research. Among the treatment technologies employed were fluidized bioreactor with GAC and RBC-PAC systems for the nitrification process, FBAR with GAC and sand for the denitrification process, FBAR with GAC for sulfate reduction, and finally biofilter for hydrogen sulfide gas removal. Conclusions were presented at the end of each chapter. In this last chapter, the general experimental conclusions and a preliminary economic evaluation of the FBAR technology will be discussed to provide guideline for application of the FBAR technology for RO brine rejects in full-scale. Finally, recommendations and future work will be presented.

11.1 Grand Summary and Conclusions

11.1.1 Optimization of Biological Nitrification Process

The first stage of this research investigated the nitrification process in which the toxic ammonia present in the RO brine reject was oxidized first into nitrite and then nitrate. For this purpose, a laboratory-scale fluidized bioreactor with GAC and a

pilot-scale rotating biological contactor (RBC) with PAC unit were employed, and their process efficiencies were optimized. The fluidized bioreactor with GAC achieved nitrification efficiencies about 95 percent at a minimum hydraulic retention time of 180 minutes. Lower retention times achieved lower ammonia removal rates even though the system pH was carefully monitored. Media replacement was necessary after 3 months of operation due to the formation of a thick and sticky microbial slime layer around the GAC particles. The nitrification efficiency was fully restored after approximately half of the bioreactor media was replenished. However, due to the length of the retention time maintained to achieve high nitrification efficiencies, the bioreactor had restricted capacity to produce higher quantities of nitrified brine reject and, therefore, a second technology; i.e., RBC-PAC, was selected and optimized.

The RBC tank containing three contactors was employed in order to produce sufficient quantity of nitrified brine reject for further experimental studies. Initially, the unit was incapable of operating at a flowrate beyond 125 ml/min due to gradual washout of biomass concentration from the tank. At higher flowrates, the biomass in the suspension washed out of the tank very quickly. However, after being supplemented with PAC, it was able to produce high quantity of nitrified brine reject at a flowrate of 450 ml/min even at considerably shorter retention times. Continuous recycling of PAC provided higher and steady state nitrification efficiencies well above 95 percent during the entire operational period.

11.1.2 Batch Denitrification Studies

A series of laboratory-scale batch studies were conducted to determine the effects of various environmental parameters on the denitrification process, including temperature, pH, TDS and C:N ratio. The optimum temperature range for the denitrification process was demonstrated to fall between 20 and 40°C. The highest specific denitrification activity occurred at 35°C, and declined thereafter. The optimum pH for the denitrification process was determined to be 8.0. At this pH, the specific denitrification rate was at its maximum. Another set of batch experiments determined the optimal range of carbon-to-nitrogen ratios to be between 1.5:1 and 1.8:1. The ratio of 1.8:1 was chosen as the optimal C:N ratio to prevent the ethanol from becoming a limiting substrate in the case of fluctuating nitrate concentrations. In addition, the carbon demand for new biomass formation could also be accommodated at this ratio without leaving any significant organic carbon residual in the effluent stream. The batch experiments demonstrated that TDS concentration did not have significant impact on the specific denitrification rate. Although the rate declined marginally when the TDS concentration was doubled from 4,000 mg/l to 8,000 mg/l, further studies suggested the cause to be the insufficient acclimation of denitrifying bacteria to higher TDS concentrations. Further increase in the TDS concentration up to 25,000 mg/l did not cause significant rate reductions unless sufficient bacterial acclimation was provided.

11.1.3 Continuous Flow Chemostat Studies

The Monod kinetic parameters, including the maximum specific growth rate, Monod half saturation constant, growth yield coefficient and decay coefficient were determined through a series of continuous flow chemostat experiments. These constants were determined under nitrate (ethanol excess), nitrite (ethanol excess) and ethanol limited (nitrate and nitrite excess) conditions to better simulate the two-stage denitrification process. They were used to assess the feasibility of the denitrification process for the RO brine rejects, to provide basis for comparison with the literature values, and to obtain the biokinetic inputs for the mathematical model developed for the denitrification process.

The nitrate and nitrite-limited (ethanol in excess) experiments indicated that nitrate was far more favorable as the main substrate for the denitrifying culture used in the study than nitrite, as the maximum specific growth rate for the nitrate-limiting chemostat was higher than that of nitrite-limiting chemostat. Moreover, nitrite accumulated in the chemostat as the dilution rates increased, and finally washed out without being reduced to nitrogen gas. Similarly, the Monod half saturation constant for the nitrate-limited chemostat was substantially lower than that of nitrite-limited chemostat, which also indicated nitrate as the favorable substrate.

The major outcome of the ethanol-limited experiments was that denitrification process did not reach completion when the carbon source (ethanol) was insufficient. The washout dilution rate in both ethanol-limiting chemostats was approximately 50 percent of that under nitrite- and nitrate-limiting chemostats, which

suggested that insufficient carbon source might cause instability of the system due to inhibitory effect of nitrate and/or nitrite accumulation.

11.1.4 FBAR Denitrification Studies

The mini pilot-scale FBAR denitrification experiments were carried out with GAC at different GAC quantities, retention times and nitrate concentrations. Six experimental runs were performed using a synthetic brine reject and seven runs with real brine reject. The FBAR demonstrated nitrate removal efficiencies as high as 96 to 100 percent at hydraulic retention times ranging from 40 to 180 minutes. The quantity of GAC played an important role in removing considerable amounts of metals and adsorbing the carbon source (ethanol). Similarly, high nitrate concentrations resulted in increased biomass growth.

Two FBAR experiments were also conducted with sand using 150 g of sand at 180 minutes of hydraulic retention time and 300 g of sand and 90 minutes of hydraulic retention time in order to compare the denitrification efficiency to that of GAC. Completion of denitrification process with 150 g of sand took much longer time than with 150 g of GAC (2,350 minutes as opposed to 500 minutes). Nitrite accumulated in significant amounts in both experiments, and then depleted as nitrate concentration declined.

It was concluded that a compromise has to be made between the cost of media, process efficiency and the cost of energy, as GAC is more expensive than sand but at the same time promotes more effective and reliable operation.

11.1.5 FBAR Modeling

The results of the FBAR experiments with GAC were used to verify and refine a mathematical model developed for the FBAR denitrification process. The model incorporated all the important features of biodegradation and assumed that biodegradation occurred not only in the biofilm immobilized onto GAC particles, but also in the liquid phase suspension. The results clearly demonstrated the predictive capability of the model, as good agreement was observed between the experimental data and model predictions.

Sensitivity analyses of the model provided excellent qualitative appreciation of the parameters influencing the denitrification process dynamics under a variety of operating conditions such as Monod biokinetic constants, varying feed nitrate concentration and biofilm density. The sensitivity analyses results indicated that the FBAR model was highly sensitive to growth yield coefficient and maximum specific growth rate, whereas changes in the magnitude of Monod half saturation constant, nitrate concentrations and biofilm density did not have any significant impact.

11.1.6 FBAR Sulfate Reduction Studies

Simultaneous denitrification and sulfate removal process was investigated using the FBAR process with GAC at a hydraulic retention time of 180 minutes. Denitrification process was complete after 400 minutes of operation, while sulfate reduction from 1,300 mg/l to 720 mg/l took 585 hrs. The “zoning” phenomenon occurred in the FBAR in such a way that denitrification occurred on the lower layers

of the bioadsorber bed where thinner biofilms were supported, whereas sulfate reduction occurred in the upper layers of the reactor where low-density bioparticles were obtained as a result of prolific bacteria growth. This phenomenon was explained *via* the oxidation-reduction potential of nitrate and sulfate. The reduction of nitrate to nitrogen gas preceded the reduction of sulfate to hydrogen sulfide gas. In the presence of nitrate, bacteria preferred to use nitrate first. As the time progressed, sulfate-reducing bacteria became acclimated and began to utilize sulfate in the upper portions of the bioadsorber bed where nitrate was virtually absent. Another criterion contributing to the establishment of the zoning was the longer hydraulic retention time (at least 180 minutes) provided for the acclimation of sulfate-reducing bacteria.

A second FBAR was employed to completely remove the sulfate from the effluent of the first FBAR. After 412 hours of operation, the sulfate concentration in the second reactor reached zero.

11.1.7 FBAR Metal Removal

The walls of the FBAR in which sulfate reduction process occurred were gradually covered with well-separated dark spots, a possible indication of microbial sulfate reduction and a process called “souring” due to the generation of hydrogen sulfide gas. The formation of these dark spots was due to the presence of iron in the feed brine reject, which reacted with the hydrogen sulfide to form ferric sulfide precipitate. At steady state, the iron concentration in the nitrified brine reject declined from 448 $\mu\text{g/l}$ to less than 1 $\mu\text{g/l}$, corresponding to a 100 percent removal.

The FBAR not only demonstrated effective iron removal, but also achieved arsenic, copper, manganese, selenium, silver and zinc removal in the range from 24 to 100 percent at steady state. The highest efficiency was obtained with silver (100 percent), followed by zinc (62 percent), selenium (55 percent), copper (49 percent) and manganese (24 percent). During this process, the pH dropped significantly most probably due to the volatilization of hydrogen sulfide gas generated as a result of sulfate reduction. This was an indication of entrapment of sulfite as insoluble metal precipitates on the surfaces of GAC particles.

11.1.8 Biofiltration Study

A biofilter column was employed to remove the hydrogen sulfide gas generated by the FBAR sulfate reduction process. The column effectively removed the hydrogen sulfide (well over 99 percent), as no hydrogen sulfide gas was detected in the column effluent during the entire experimental period.

The column exhibited a trouble-free operation during the entire experimental period. The column may have been effective in the removal of other sulfurous compounds, such as methyl mercaptan, dimethyl sulfide and dimethyl disulfide, collectively known as reduced sulfur compounds. These compounds do not necessarily pose a health hazard as hydrogen sulfide gas, but are considered to cause pungent odor. In this research, however, no attempt was made to investigate the biofiltration efficiency with respect to these compounds.

11.2 Cost-Benefit Analysis

The applicability of a technology greatly depends on its capital, operation and maintenance costs. Once the technology has been proven effective and feasible through a series of laboratory-scale experiments, the decision whether or not the full-scale implementation is possible is made after a thorough evaluation of the associated cost of the technology. The capital cost of any full-scale FBAR technology is associated with the influent and recycle pumps and reactor body. The operation and maintenance cost, on the other hand, is significantly affected by the support media replacement and energy consumed.

FBARs are considered to have low capital costs as compared to other conventional treatment technologies due to their relatively small space requirements and simpler operational features. FBAR technology employs smaller diameter but taller reactors and, therefore, is ideal for those treatment plants located in residential areas where the space is scarce and plant expansion is impossible. The FBAR process itself is not complex in that less costly equipment and associated parts are required for initial installation.

The major material cost for the FBARs arises from the support media and its replacement. However, significant benefits are realized through: (i) high process performance, (ii) efficiencies over a long period of time with trouble-free operation, (iii) good effluent quality with respect to a broad range of undesirable contaminants, and (iv) possibility of on-site regeneration of the spent GAC.

Energy consumption of the FBARs can be high due to high recirculation ratios necessary to maintain the reactor support media in fluidized condition. Nonetheless, it is recommended to compare all the advantages of using the FBAR technology as opposed to other conventional technologies in the long run through a life cycle cost and then make the final decision.

Aside from the capital and operation costs, FBAR denitrification technology is proven to be effective in removing nitrates from the RO brine rejects even at shorter hydraulic retention times. When provided with longer retention times, FBARs are also capable of reducing high concentrations of sulfate. A major side benefit of this technology lies in its capability to remove heavy metals as well. The sulfate-reducing bacteria acclimated to the RO brine rejects can remove not only sulfate but also a number of metals including but not limited to iron, copper, manganese, silver, cadmium, lead, selenium, zinc as precipitates of metal sulfides. These sulfides are insoluble and can easily be separated. This method is far cheaper than other techniques, such as ion exchange, absorption or chemical precipitation, and adds another side benefit as to the application of FBAR technology.

11.3 Future Research Recommendations

The followings are the recommendations for future research:

- More in-depth research should be conducted to evaluate the nitrification process performance under different operating conditions including temperature, pH, heavy metals, etc., for the brine rejects.

- Fluidized bioreactor and RBC-PAC technologies for the biological nitrification of RO brine rejects should be evaluated in terms of process performance and cost-effectiveness. The optimum PAC dosing should be determined and comparative economics should be determined.

- Depth specific analyses for the simultaneous FBAR denitrification and sulfate reduction process should be made and the “zoning” phenomenon should be addressed in detail. The future research should also investigate the interactions between the denitrifying and sulfate-reducing bacteria.

- Up-scaling and similitude analyses should be performed for the FBAR denitrification process.

- Other organic carbon sources should be investigated for the FBAR denitrification process, and the process efficiencies and economics should be compared.

- More research should be performed on biofiltration process for the removal of not only hydrogen sulfide but also several mercaptans, such as methyl mercaptan, dimethyl sulfide and dimethyl disulfide, also known as organo-sulfur compounds, as their threshold odor is lower than hydrogen sulfide.

REFERENCES

- Acquaviva, P.G., Westrick, J.D., Dohme, C.I., & Derowitsch, R.W. (1997). *Reverse Osmosis Concentrate Disposal Alternatives for Small and Medium Sized Systems in Southwest Florida*. Membrane Technology Conference Proceedings, AWWA, pp. 961-977, New Orleans, LA.
- Aesoy, A., Odegaard, H., Bach, K., Pujal, R., & Hamon, M. (1998). Denitrification in a Packed Bed Biofilm Reactor (BIOFOR) - Experiments with Different C-Sources. *Wat. Res.*, 32(5): 1463-1470.
- Akunna, J.C., Bizeau, C., & Moletta, R. (1993). Nitrate and Nitrite Reductions with Anaerobic Sludge Using Various Carbon Sources: Glucose, Glycerol, Acetic Acid, Lactic Acid and Methanol. *Wat. Res.*, 27(8): 1303-1312.
- American Desalting Association (1995). *Concentrate from Membrane Desalting: A Logical Approach to its Disposal*. A White Paper, Sacramento, CA.
- Andrews, G.F., & Tien, C. (1981). Bacterial Film Growth in Adsorbent Surface. *AIChE Jour.*, 27(3): 396-403.
- Annachhatre, A.P., & Suktrakoolvait, S. (2001). Biological Sulfate Reduction Using Molasses as a Carbon Source. *Wat. Env. Res.*, 73(1): 118-126.
- Arbuckle, T.E., Sheman, G.J., & Corey, P.N. (1988). Water Nitrates and CNS Birth Defects: A Population Based Case-Control Study. *Arch. Env. Health*, 43: 162-167.
- Badriyha, B.N. (1997). *Advanced Oxidation Processes, Carbon Adsorption and Biofilm Degradation of Synthetic Organic Chemicals in Drinking Water*. Ph.D. Thesis, Civil and Environmental Engineering Dept., University of Southern California, CA.
- Bansal, R.C., Donnet, J.B., & Stoeckli, F. (1988). *Activated Carbon*. Marcel Decker, Inc., New York.
- Barnes, L.J., Sherren, J., Janssen, F.J., Scheeren, P.J.M., Versteegh, J.H., & Koch, R.D. (1991a). *Simultaneous Microbial Removal of Sulfate and Heavy Metals from Wastewater*. European Metlas Conference, Non-ferrous Metallurgy: Present and Future, pp. 391-401.

- Beer, C. (1970). Evaluation of Anaerobic Denitrification Process. *Jour. San. Engr. Div., A.S.C.E.*, 96: 1452-1459.
- Beltrame, P., Beltrame, P.L., & Carniti, P. (1984). Influence of Feed Concentration on the Kinetics of Biodegradation of Phenol in a Continuous Stirred Reactor. *Wat. Res.*, 18(4): 403-407.
- Betlach, M.R. & Tiedje, J.M. (1981). Kinetic Explanation for Accumulation of Nitrite, Nitric Oxide and Nitrous Oxide During Bacterial Denitrification. *App. and Env. Microbiol.*, 42(6): 1074-1084.
- Bettens, L. (1979). Powdered Activated Carbon in an Activated Sludge Unit. *Effl. and Water Treat. Jour.*, 9: 129-135.
- Blanco, V.D., Garcia Encina, P.A., & Fdz-Polanco, F. (1995). Effects of Biofilm Growth, Gas and Liquid Velocities on the Expansion of an Anaerobic Fluidized Bed Reactor (AFBR). *Wat. Res.*, 29(7): 1649-1654.
- Boaventura, R.A., & Rodrigues, A.E. (1988). Consecutive Reactions in Fluidized Bed Biological Reactors: and Experimental Study of Wastewater Denitrification. *Chem. Engr. Sci.*, 43(11): 2715-2728.
- Bohn, H.L. & Bohn, R.K. (1988). Soil Beds Weed Out Air Pollutants. *Chem. Engr.*, 95(4): 73-76.
- Braam, F. & Klapwijk, J.P. (1981). Effect of Copper on Nitrification in Activated Sludge. *Wat. Res.*, 15: 1093-1098.
- Buswell, A.M., Shiota, T., Lawrence, N., & Van Meter, I. (1954). Laboratory Studies on the Kinetics of the Growth of *Nitrosomonas* with Relation to the Nitrification Phase of the BOD Test. *App. Microbiol.*, 2: 21-25.
- Caetano et. al. (Ed.). (1995). *Membrane Technology: Applications to Industrial Wastewater Treatment*. Kluwer Academic Publishers, Netherlands.
- California State Water Resources Control Board (1990). *California Municipal Wastewater Reclamation in 1987*, Sacramento, CA.
- Cappor, S. (1995). Membranes Minimize Liquid Discharge. *Chem. Engr.*, 102: 102-104.

- Chang, H.T. & Rittman, B.E. (1987). Mathematical Modeling of Biofilm on Activated Carbon. *Env. Sci. Tech.*, 21(3): 273-288.
- Chen, C.I., Mueller, R.F., & Griebel, T. (1994). Kinetic Analysis of Microbial Sulfate Reduction by *Desulfovibrio desulfuricans* in an Anaerobic Upflow Porous Media Biofilter Reactor. *Biotech. Bioeng.*, 43(4): 267-274.
- Chiu, W.A., Erickson, L.E., Fan, L.T., & Kao, I.C. (1972). Kinetic Model Identification in Mixed Populations Using Continuous Culture Data. *Biotech. Bioeng.*, 14(2): 207-231.
- Chuichulcherm, S., Nagpal, S. Peeva, L., & Livingston, A. (2001). Treatment of Metal-Containing Wastewaters with a Novel Extractive Membrane Reactor Using Sulfate Reducing Bacteria. *Jour. Chem. Techn. Biotechn.*, 74(1): 61-68.
- Chung, S.F. & Wen, C.F. (1968). Longitudinal Dispersion of Liquid Flow Through Fixed and Fluidized Beds. *AIChE. Jour.*, 14(6): 857-866.
- Chung, Y.C., Huang, C., & Tseng, C.P. (1996). Microbial Oxidation of Hydrogen Sulfide with Biofilter. *Jour. Env. Sci. Health*, A31(6): 1264-1278.
- Clifford, D. & Liu, X. (1993). Biological Denitrification of Spent Regenerant Brine Using a Sequencing Batch Reactor. *Wat. Res.*, 27(9): 1477-1484.
- Coelhoso, I., Boaventura, R., & Rodrigues, A. (1992). Biofilm Reactors: An Experimental and Modeling Study of Wastewater Denitrification in Fluidized Bed Reactors of Activated Carbon Particles. *Biotech. Bioeng.*, 40: 625-633.
- Comb, L.F. (1994). Going Forward with Reverse Osmosis. *Chem. Engr.*, 101: 90-92.
- Constantin, H. & Fick, M. (1997). Influence of C-Sources on the Denitrification Rate of a High-Nitrate Concentrated Industrial Wastewater. *Wat. Res.*, 31(3): 583-589.
- Cooney, M.J., Roschi, E., Marison, I.W., Comninellis, C., & Von Stockar, U. (1996). Physiologic Studies with the Sulfate Reducing Bacterium *Desulfovibrio desulfuricans*: Evaluation for Use in a Biofuel Cell. *Enzyme Microbiol. Tech.*, 18: 358.

- Cork, D.J., & Cusanovich, M.A. (1978). *Sulfate Decomposition: A Microbiological Process. In Metallurgical Applications of Bacterial Leaching and Related Microbiological Phenomena*, L.E. Murr and A.E. Thorma (Eds.), pp. 207-221, Academic Press, New York.
- Croen, L.A., Todoroff, K., & Sha, G.M. (2001). Maternal Exposure to Nitrate from Drinking Water and Diet and Risk for Neural Tube Defects. *American Jour. of Epidemiol.*, 153(4): 325-331.
- Curi, K., & Eckenfelder, W.W. (1980). *Theory and Practice of Biological Waste Treatment*. Sijthoff and Noordhoff, (Eds.), pp. 49-118, Alphen and den Rjn, Netherlands.
- Dawson, R.N., & Murphy, K.L. (1972). The Temperature Dependency of Biological Denitrification. *Wat. Res.*, 6: 71-83.
- Delanghe, B., Nakamura, F., Myoga, H., & Magara, Y. (1994). Biological Denitrification with Ethanol in a Membrane Bioreactor. *Env. Tech.*, 15: 61-70.
- Delwiche, C.C., & Finstein, M.S. (1965). Carbon and Energy Sources for the Nitrifying Autotroph Nitrobacter. *Jour. Bacteriol.*, 9(1): 102-107.
- Den, W., Pirbazari, M., Huang, C.C., & Shen, K.P. (1998). Technology Review for Vapor Phase Biofiltration, Part I: Technological Development and Applications. *Jour. of the Chinese Inst. of Env. Engr.*, 8(3): 159-179.
- Den, W., Pirbazari, M., Huang, C.C., & Shen, K.P. (1998). Technology Review for Vapor Phase Biofiltration, Part II: Biofilter Design and Operation. *Jour. of the Chinese Inst. of Env. Engr.*, 8(3): 181-196.
- Denton, L. (1996). *Microbiological Diversity of Denitrifying Bacteria in High Nitrate Brines of Varying Salinity*. M.S. Thesis, University of Colorado, Boulder, CO.
- Devinny, J.S. (1998a). Cleaning the Air Biologically. *Civil Engr.*, 68(9): 46-49.
- Devinny, J.S. (1998b). Monitoring Biofilters Used for Air Pollution Control. *Practice Periodical of Hazard. Toxic and Radioact. Waste Manag.*, 2(2): 78-85.

- Dietrich, J.A. (1995). Membrane Technology Comes to Age. *Polln. Engr.*, pp. 20-25.
- Dombroski, E.C., Gaudet, I.D., & Coleman, R.N. (1995). *Reduction of Odorous and Toxic Emissions from Kraft Pulp Mills Using Biofilters*. Proceeding of the 1995 Conference on Biofiltration, Los Angeles, CA.
- Dovark, D.H., Hedin, R.S., Edenborn, H.M., & McIntire, P.E. (1992). Treatment of Metal Contaminated Water Using Bacterial Sulfate Reduction: Results from Pilot-Scale Reactors. *Biotech. Bioeng.*, 40(5): 609-616.
- Downing, A.L., Tomlinson, C.G., & Truesdale, G.A. (1964). Effect of Inhibitors on Nitrification in the Activated Sludge Process. *Jour. Inst. Sewage Purif.*, 6: 537-554.
- Duncan, B. (1995). *Effect of Ionic Strength on Denitrification of a High Salt, High Nitrate Brine Simulating Rocky Flats Evaporation Pond Water Using Activated Sludge*. M.S. Thesis, University of Colorado, Boulder, CO.
- Duranceau, S.J. (Ed.). (2001). *Membrane Practices for Water Treatment*. AWWA Trends in Water Series.
- Engberg, D.J. & Schroeder, E.D. (1975). Kinetics and Stoichiometry of Bacterial Denitrification as a Function of Cell Residence Time. *Wat. Res.*, 9: 1051-1054.
- Filteau, G. (1995). Water Reuse Fuels Economic Growth. *Jour. AWWA.*, 87: 116.
- Finlayson, B.A. (1972). *The Method of Weighed Residuals and Variational Principles*. Academic Press, New York.
- Focht, D.D. & Chang, A.C. (1975). Nitrification and Denitrification Process Related to Wastewater Treatment. *Adv. Appl. Microbiol.*, 19: 153-186.
- Freeman, S., Leither, G.F., Crook, J., & Vernon, W. (2002). *Issues in the Application of Membranes for Water Reclamation*. AWWA, Water Sources Conference Proceedings, pp. 1-11.
- Gayle, B.P., Boardman, G.D. Sherrard, J.H., & Benoit, R.E. (1989). Biological Denitrification of Water. *Jour. Env. Engr.*, 115: 930-942.
- Gear, C.W. (1971). The Automatic Integration of Ordinary Differential Equations. *Comm. Assoc. Comp. Mach.*, 14: 176-179.

- Gear, C.W. (1971). The Automatic Integration of Ordinary Differential Equations. *Comm. Assoc. Comp. Mach.*, 14: 185-190.
- Gear, C.W. (1976). *Numerical Solutions to Initial Value Problems in Ordinary Differential Equations*. Prentice Hall, Engelwood Cliffs, NJ.
- Gee, C.S., Pfeiffer, J.T., & Suidan, M.T. (1990). Nitrosomonas and Nitrobacter Interactions in Biological Nitrification. *Jour. Env. Engr.*, 116: 4-17.
- Gee, C.S., Suidan, M.T., & Pfeiffer, J.T. (1990). Modeling of Nitrification Under Substrate-Inhibiting Conditions. *Jour. Env. Engr.*, 116: 18-31.
- Ghosh, S. & Pohland, F.G. (1971). Population Dynamics in Continuous Culture of Heterogeneous Microbial Populations. *Devel. Ind. Microbiol.*, 12(3): 295-311.
- Glass, C. & Silverstein, J. (1998). Denitrification Kinetics of High Nitrate Concentration Water: pH Effect on the Inhibition and Nitrate Accumulation. *Wat. Res.*, 32(3): 831-839.
- Glass, C. & Silverstein, J. (1999). Denitrification of High-Nitrate, High-Salinity Wastewater. *Wat. Res.*, 33(1): 223-229.
- Glass, C., Silverstein, J., & Oh, J. (1997). Inhibition of Denitrification in Activated Sludge by Nitrite. *Wat. Env. Res.*, 69(6): 1086-1093.
- Godia, F. & Sola, C. (1995). Review: Fluidized Bed Bioreactors. *Biotech. Prog.*, 11: 479-497.
- Grabinska-Loniewska, A., Slomczynski, T., & Kanska, Z. (1985). Denitrification with Glycerol as a C Source. *Wat. Res.*, 19(12): 1471-1477.
- Hallin, S. & Pell, M. (1998). Metabolic Properties of Denitrifying Bacteria Adapting to Methanol and Ethanol in Activated Sludge. *Wat. Res.*, 32(1): 13-18.
- Hancher, C.W. & Perona, J.J. (1982). Kinetic Model for a Fluidized Bed Bioreactor for Denitrification of Wastewaters. *Biotech. Bioeng. Symp.*, 12: 317-326.
- Hancher, C.W., Taylor, P.A., & Napier, J.M. (1978). Operation of Fluidized Bed Bioreactor for Denitrification. *Biotech. Bioeng. Symp.*, 8: 361-378.

- Hansen, N.G. & Rindel, K. (1999). Bioscrubbing, an Effective and Economic Solution to Odour Control at Wastewater Treatment Plants. *Wat. Sci. Techn.*, 41(6): 155-164.
- Haug, R.T. & McCarty, P.L. (1972). Nitrification with Submerged Filters. *JWPCF*, 44: 2086-2102.
- Heijnen, J.J., Mulder, A., Enger, W., & Hoeks, F. (1989). Review on the Application of Anaerobic Fluidized Bed Reactors in Wastewater Treatment. *The Chem. Engr. Jour.*, 41: B37-B49.
- Ida, S. & Alexander, M. (1965). Permeability of *Nitrobacter agilis* to Organic Compounds. *Jour. Bacteriol.*, 90(1): 151-156.
- Jain, M.K. (1985). *Numerical Solutions of Differential Equations*. John Wiley, New York.
- Jeris, J.S. (1982). *Industrial Waste-water Treatment Using Anaerobic Fluidized Bed Reactors*. I.A.W.P.R.C. Special Seminar, Anaerobic Treatment of Wastewater in Fixed Film Reactors, Technical University of Denmark, Lyngby, Denmark.
- Jeris, J.S., Beer, C., & Mueller, J.A. (1974). High Rate Biological Denitrification Using A Granular Fluidized Bed. *JWPCF*, 46: 2118- 2124.
- Kang, S.W. (1978). *Kinetics of Simultaneous Diffusion and Reaction for the Nitrification Process in Suspended Growth Systems*. Ph.D. Thesis, University of Massachusetts, MA.
- Kenna, E. & Zander, A.K. (2001). *Survey of Membrane Concentrate Reuse and Disposal*. AWWA, S.J. Duranceau (Ed.), pp. 513-540.
- Kim, B.R. (1992). Research Note: Approximate Solution for a Fluidized Bed Biofilm Model. *Wat. Res.*, 26(9): 1271-1275.
- Kim, S.H. (1987). *Mathematical Modeling of Integrated Biological and Physico-Chemical Treatment Process for Industrial Wastewater*. Ph.D. Thesis, Environmental Engineering Department, University of Southern California, Los Angeles, CA.
- Kim, S.H. & Pirbazari, M. (1989). Bioactive Adsorber Model for Industrial Wastewater Treatment. *Jour. Env. Engr.*, 115(6): 1235-1256.

- Knopp, P.V. & Burant, W. Jr. (1981). *Wastewater Treatment*. U.S. Patent No. 4,289,626.
- Knopp, P.V. & Gitchel, W.B. (1976). *Waste-water Treatment*. U.S. Patent No. 3,957,632.
- Knowles, R. (1982). Denitrification. *Microbiol. Rev.*, 46(1): 43-70.
- Kornaros, M. & Lyberatos, G. (1998). Kinetic Modeling of *Pseudomonas denitrificans* Growth and Denitrification Under Aerobic, Anoxic and Transient Operating Conditions. *Wat. Res.*, 32(6): 1912-1922.
- Kornaros, M., Zafiri, C., & Lyberatos, G. (1996). Kinetics of Denitrification by *Pseudomonas denitrificans* Under Conditions Limited by Carbon and/or Nitrate and Nitrite. *Wat. Env. Res.*, 68(5): 934-945.
- LaMotta, E.J. & Cascante, P. (1996). Substrate Consumption Kinetics in Anaerobic Biofilm Fluidized Bed Reactor. *Jour. Env. Engr.*, 122: 198-204.
- Langley, W.G., Wu, J.S., & Chao, A.C. (2001). Reaction Kinetics of Immobilized-Cell Denitrification. I: Background and Model Development. *Jour. Env. Engr.*, 127(8): 682-688.
- Lappan, R.E. (1987). *Anaerobic Treatment of Metal Plating Wastewater*. MASc Thesis, University of Windsor, Windsor, Ontario, Canada.
- Law, A.T. et. al. (1976). On Describing Microbial Growth Kinetics from Continuous Culture Data: Some General Considerations, Observations, and Concepts. *Microbiol. Ecol.*, 2(3): 261-283.
- Lazarova, V., Capdeville, B., & Nikolov, L. (1994). Influence of Seeding Conditions on Nitrite Accumulation in a Denitrifying Fluidized Bed Reactor. *Wat. Res.*, 28(5): 1189-1197.
- Lazarova, V. & Manem, J. (1995). Biofilm Characteristics and Activity Analysis in Water and Wastewater Treatment. *Wat. Res.*, 29(1): 2227-2245.
- Leipzig, N.A. (1980). *Effectiveness of Powdered Activated Carbon/Activated Sludge System in Removing Ammonia from an Organic Chemical Production Wastewater*. Proceedings of the 35th Annual Industrial Wastewater Conference, Purdue University, pp. 889-897, Ann Arbor, MI.

- Leson, G. & Winer, A.M. (1991). Biofiltration: An Innovative Air Pollution Control Technology for VOC Emissions. *Jour. of the Air and Waste Manag. Assoc.*, 41: 1045-1054.
- Lewandoswki, Z. (1982). Temperature Dependency of Biological Denitrification with Organic Materials Addition. *Wat. Res.*, 16: 19-22.
- Mandrup-Poulsen, J. (1995). *Dealing with Membrane Concentrate Disposal in Florida*. Protocols for Determining Major - Seawater - Ion Toxicity in Membrane-Technology. Water-Treatment Concentrate, Florida Department of Environmental Protection (FDEP), pp. 917-921, Tallahassee, FL.
- Maree, J.P. & Hill, E. (1989). Biological Removal of Sulfate from Industrial Effluents and Contaminant Production of Sulphur. *Wat. Sci. Tech.*, 21: 265-276.
- Martienssen, M. & Schops, R. (1999). Population Dynamics of Denitrifying Bacteria in a Model Biocommunity. *Wat. Res.*, 33(3): 639-646.
- Matsui, S., Yamamoto, R.I., Tsuchiya, Y., & Inanc, B. (1993). The Kinetics of Glucose Decomposition with Sulfate Reduction in the Anaerobic Fluidized Bed Reactor. *Wat. Sci. Tech.*, 28(2): 135-144.
- Mattiasson, B. & Hahn-Hazerdal, B. (1982). Microenvironmental Effects on Metabolic Behavior of Immobilized Cells: A Hypothesis. *Eur. Jour. Appl. Microbiol. Biotech.*, 16: 52-55.
- McCleaf, P.R. & Schroeder, E.D. (1995). Denitrification Using a Membrane-Immobilized Biofilm. *Jour. AWWA*, 87: 77-86.
- Mechalas, B.J., Allen III, P.M., & Matyskiela, W.W. (1970). *A Study of Nitrification and Denitrification*. Water Pollution Control Research Series, Federal Water Quality Administration, Dept. of the Interior, Cincinnati, OH.
- Mickly, M., Briceno, G., & Case, J. (1997). *AWWARF Project: Common Ion Toxicity in Membrane Concentrate*. Membrane Technology Conference Proceedings, AWWA, pp. 893-915, New Orleans, LA.
- Middleton, A.C. (1975). *Microbially Mediated Dissimilatory Sulfate Reduction: Kinetics and Environmental Significance*. Ph.D. Thesis, Cornell University, Ithaca, NY.

- Moore, S.F. & Schroeder, E.D. (1970). An Investigation of the Effects of Residence Time on Anaerobic Bacterial Denitrification. *Wat. Res.*, 4: 685-694.
- Mulcahy, L.T. (1978). *Mathematical Model of the Fluidized Bed Biofilm Reactor*. Ph.D. Thesis, Civil Engineering Department, University of Massachusetts, MA.
- Mulcahy, L.T. & Shieh, W.K. (1987). Fluidization and Reactor Biomass Characteristics of the Denitrification Fluidized Bed Biofilm Reactor. *Wat. Res.*, 21(4): 451-458.
- Mulcahy, L.T., Shieh, W.K., & LaMotta, E.J. (1980). Simplified Mathematical Models for a Fluidized Bed Biofilm Reactor. *Am. Inst. of Chem. Engrs. Symp. Series*, Water, 77(209): 273-285.
- Muthumbi, W., Boon, N., Boterdaele, R., De Vreese, I., Top, E.M., & Verstraete, W. (2001). Microbial Sulfate Reduction with Acetate: Process Performance and Composition of the Bacterial Communities in the Reactor at Different Salinity Levels. *Appl. Microbiol. Biotech.*, 55: 787-793.
- Myers, C. (1996). *Water Recycling in California*. World Water and Env. Engr.
- Nagpal, S., Chuichulcherm, S., Peeva, L., & Livingston, A. (2000). Microbial Sulfate Reduction in a Liquid-Solid Fluidized Bed Reactor. *Biotech. Bioeng.*, 70(4): 370-380.
- Namkung, E. (1985). *Kinetics and Mechanism of Low Concentration Multi-Substrate Utilization by Biofilm*. Ph.D. Thesis, University of Illinois, Urbana Champaign, IL.
- Narjari, N.K., Khilar, K.C., & Mahajan, S.P. (1984). Biological Denitrification in a Fluidized Bed. *Biotech. Bioeng.*, 26: 1445-1448.
- Narkis, N., Rebhun, M., & Sheindorf, C.H. (1979). Denitrification at Various Carbon to Nitrogen Ratios. *Wat. Res.*, 13: 93-98.
- Ng, A.S. (1985). *Nitrification Enhancement by Powdered Activated Carbon Addition in Activated Sludge*. Ph.D. Thesis, University of California, Los Angeles, CA.
- Ngian, K. & Martin, W.R.B. (1980). Bed Expansion Characteristics of Liquid Fluidized Particles with Attached Microbial Growth. *Biotech. Bioeng.*, 22: 1843-1856.

- Oh, J. & Silverstein, J. (1999). Acetate Limitation and Nitrite Accumulation During Denitrification. *Jour. Env. Engr.*, 125(3): 234-242.
- Okabe, S., Nielsen, P.H., & Characklis, W.G. (1992). Factors Effecting Microbial Sulfate Reduction by *Desulfovibrio desulfuricans* in Continuous Culture: Limiting Nutrients and Sulfate Concentration. *Biotech. Bioeng.*, 340(6): 725-734.
- Okun, D.A. (1991). *Realizing the Benefits of Water Reuse in Developing Countries*. Municipal Wastewater Reuse: Selected Readings on Water Reuse, Reprinted Articles from WPCF's Water Env. & Tech. Jour., EPA 430/09-9-022, pp. 13-17.
- Orange County Water District and County Sanitation District of Orange County, (1995). *Final Feasibility Study Report*. OCWD Reclamation Project.
- Painter, H.A. (1977). Microbial Transformation of Inorganic Nitrogen. *Prog. Wat. Technol.*, 8(4/5): 3-29.
- Painter, H.A. & Loveless, J.E. (1968). Effect of Temperature and pH Values on the Growth Rate Constants of Nitrifying Bacteria in Activated Sludge Process. *Wat. Res.*, 17(3): 237-248.
- Patel, M.V., Leslie, G., Yanguba, J., Pirbazari, M., & Ersever, I. (2001). Options for Treatment of Disposal of Residuals Produced by Membrane Processes in the Reclamation of Municipal Wastewater. *AWWA*, S.J. Duranceau, (Ed.), pp. 541-557.
- Payne, W.J. (1973). Reduction of Nitrogenous Oxides by Microorganisms. *Bacteriol. Rev.*, 37: 409.
- Payne, W.J. (1981). *Denitrification*. John Wiley & Sons, Inc., USA.
- Pinjing, H., Liming, S, Zhiwen, Y., & Uojian, L. (2001). Removal of Hydrogen Sulfide and Methyl Mercaptan by a Packed Tower with Immobilized Microorganism Beads. *Wat. Sci. Techn.*, 44(9): 327-333.
- Pirbazari, M., Badriyha, B.N., Ravindran, V., & Kim, S.H. (1989). *Treatment of Landfill Leachate by Biologically Active Carbon Adsorbers*. 44th Purdue Industrial Waste Conference Proceedings, MI.

- Pirbazari, M., Ravindran, R., & Badriyha, B.N. (1996). Hybrid Membrane Filtration Process for Leachate Treatment. *Wat. Res.*, 27: 2691-2706.
- Pirbazari, M., Ravindran, R., Badriyha, B.N., Craig, S., & McGuire, M. J. (1993). GAC Adsorber Design Protocol for the Removal of Off-Flavors. *Wat. Res.*, 27(7): 1153.
- Pirbazari, M., Voice, T.C., & Weber Jr., W.J. (1990). Evaluation of Biofilm Development on Various Natural and Synthetic Media. *Hazard. Waste Hazard. Mtrls.*, 7(3): 239-250.
- Postgate, J.R. (1979). *The Sulphate-Reducing Bacteria*, Cambridge University Press, New York.
- Postgate, J.R. (1984). *The Sulphate-Reducing Bacteria*, 2nd Ed., Cambridge University Press, New York.
- Raiders, R.A., McNery, M.J., Revus, D.E., Torbati, H.M., Knapp, R.M., & Jenneman, G.E. (1986). Selectivity and Depth of Microbial Plugging in Berea Sandstone Cores. *Jour. Ind. Microbiol.*, 1: 195-203.
- Ravindran, V., Badriyha, B.N., Pirbazari, M., & Kim, S.H. (1996). Modeling of Bioactive Carbon Adsorbers: A Hybrid Weighed Residual Finite Difference Numerical Technique. *App. Math. Comp.*, 76: 99-131.
- Ravindran, V., Kim, S.H., Badriyha, B.N., & Pirbazari, M. (1997). Predictive Modeling for Bioactive Fluidized Bed and Stationary Bed Reactors: Application to Dairy Wastewater. *Env. Tech.*, 18: 861-881.
- Requa, D.A. & Schroeder, E.D. (1973). Kinetics of Packed-bed Denitrification. *Journal WPCF*, 45(8): 1696-1707.
- Richardson, J.F. & Zaki, W.W. (1954). Sedimentation and Fluidization: Part I *Trans. Inst. Chem. Engrs.*, 32: 35-53.
- Rittmann, B. E. & McCarthy, P. L. (2001). *Environmental Biotechnology*, McGraw-Hill, Inc, New York.
- Ro, K.S. & Neethling, J.B. (1991). Biofilm Density for Biological Fluidized Beds. *JWPCF*, 68: 815-818.

- Rorech, G.J. & Bond, S.G. (1993). Reverse Osmosis: A Cost Effective, Versatile Water Purification Tool. *Instrum. Control Syst.*, 66: 35-37.
- Rowley, M.V., Warkentin, D.D., & Sicotte, V. (1997). *Site Demonstration of the Biosulfide Process at the Former Britannia Mine*. In Proceedings of the 4th International Conference on Acid Rock Drainage, pp. 1533-1548.
- Sadick, T., Semon, J., Palumbo, D., Keenan, P., & Daigger, G. (1996). Fluidized Bed Denitrification. *Wat. Env. Tech.*, 8: 81-84.
- Safferman, S. I. & Bishop, P. L. (1997). Operating Strategies for Aerobic Fluidized Bed Reactor. *Jour. Haz. Mat.*, 54: 241-253.
- Shammas, N.K. (1971). *Optimization of Biological Nitrification*. Ph.D. Thesis, University of Michigan, MI.
- Shammas, N.K. (1986). Interactions of Temperature, pH and Biomass on the Nitrification Process. *JWPCF*, 58(1): 52-59.
- Sharma, B. & Ahlert, R.C. (1977). Nitrification and Nitrogen Removal. *Wat. Res.*, 11: 897-925.
- Shieh, W.K. (1980). Suggested Kinetic Model for the Fluidized Bed Biofilm Reactors. *Biotech. Bioeng.*, 22: 667-676.
- Shieh, W.K. & Hsu, Y. (1996). Biomass Loss from an Anaerobic Fluidized Bed Reactor. *Wat. Res.*, 30(5): 1253-1257.
- Shimizu, T., Sakamoto, Y., Waki, T., Suga, K., & Ichikawa, K. (1978). Kinetic Study on Denitrification by *Paracoccus denitrificans*. *Jour. Ferment. Tech.*, 56(3): 214-223.
- Sich, H. & Van Rijn, J. (1997). Scanning Electron Microscopy of Biofilm Formation in Denitrifying Fluidized Bed Reactors. *Wat. Res.*, 31(4): 733-742.
- Simpkin, T.J. & Boyle, W.C. (1988). The Lack of Repression by Oxygen of the Enzymes in Activated Sludge. *Wat. Res.*, 22(2): 201-206.
- Sison, N.F., Hanaki, K., & Matsuo, T. (1995). High Loading Denitrification by Biological Activated Carbon Process. *Wat. Res.*, 29(12): 2776-2779.

- Sison, N.F., Hanaki, K., & Matsuo, T. (1996). Denitrification with External Carbon Source Utilizing Adsorption and Desorption Capability of Activated Carbon. *Wat. Res.*, 30(1): 217-227.
- Skinner, F.A. & Walker, N. (1961). Growth of *Nitrosomonas europaea* in Water and Continuous Culture. *Archs. Microbiol.*, 38: 339-349.
- Skowland, C.T. (1990). Effect of Biofilm Growth on Steady State Biofilm Models. *Biotech. Bioeng.*, 35: 502-510.
- Somlev, V.P. & Tishkov, S. (1994). Anaerobic Corrosion and Bacterial Sulfate Reduction: Application for the Purification of Industrial Wastewater. *Geomicrobiol. Jour.*, 12(1): 53-60.
- Sorial, G.A., Smith, F.L., Suidan, M.T., Biswas, P., & Brenner, R.C. (1995). Evaluation of Trickling Bed Biofilter Media for Toluene Removal. *Jour. of the Air and Waste Manag. Assoc.*, 45: 801-810.
- Specchia, V. & Gianetto, A. (1984). Powdered Activated Carbon in an Activated Sludge Treatment Plant. *Wat. Res.*, 18(2): 133-137.
- Speitel Jr., G.E., Dovantzis, K., & DiGiano, F.A. (1987). Mathematical Modeling of Bioregeneration in GAC Columns. *Jour. Env. Engr, ASCE*, 113(1): 32-48.
- Squire, D., Muffer, P., & Fitzpatrick, C. (1996). Disposal of RO Membrane Concentrate. *Disalination*, 108: 143-147.
- Standard Methods for the Examination of Water and Wastewater. (1993). *APPA, AWWA and WPCF*, 18th Ed., Washington DC.
- Standard Methods for the Examination of Water and Wastewater. (1998). *APPA, AWWA and WPCF*, 20th Ed., Washington DC.
- Stensel, D., Loehr, R.C., & Lawrence, A.W. (1973). Biological Kinetics of Suspended-growth Denitrification. *Jour. WPCF*, 45(2): 249-261.
- Stenstrom, M. K. & Grieves, C.G. (1977). *Enhancement of Oil Refinery Activated Sludge by Addition of Powdered Activated Carbon*. Proceedings of the 32nd Purdue Industrial Waste Conference, Ann Arbor, MI.
- Stucki, G., Hanselman, K.W., & Hurzeler, R.A. (1993). Biological Sulfuric Acid Transformation. *Biotech. Bioeng.*, 41: 303-315.

- Stumm, W. & Morgan, J.J. (1996). *Aquatic Chemistry*, 3rd Ed., John Wiley and Sons, New York.
- Survey of Future Water Reclamation Potential (1993). *Final Report*, WaterReuse, Sacramento, CA.
- Sutton, P.M. & Mishra, P.N. (1991). Biological Fluidized Beds for Water and Wastewater Treatment. *Wat. Env. Tech.*, 3: 53-56.
- Tabazadeh, A., Santee, M.L., Danilin, M.Y., Pumprey, H.C., Newman, P.A., Hamill, P.J., & Mergenthaler, J.L. (2000). Quantifying Denitrification and its Effect on Ozone Recovery. *Science*, 288(5470): 1407-1411.
- Taylor, S. W., Milly, P.C.D., & Jaffe, P.R. (1990). Biofilm Growth and the Related Changes in the Physical Properties of a Porous Medium, 2: Permeability. *Wat. Res.*, 26: 2161-2169.
- Tchobanoglous, G. & Burton, F.L. (1991). *Wastewater Engineering: Treatment, Disposal and Reuse*, McGraw-Hill, Inc., New York.
- Templeton, L.L. & Grady, C.P.L. (1988). Effect of Culture History on the Determination of Biodegradation Kinetics by Batch and Fed-Batch Techniques. *JWPCF*, 60: 651-658.
- Teske, A., Alm, A., Regan, J. M., Toze, S., Rittmann, B. E., & Sthal, D. A. (1994). Evolutionary Relationships Among Ammonia- and Nitrite-oxidizing Bacteria. *Jour. Bacteriol.*, 176: 6623-6630.
- Timmermans, P. & VanHaute, A. (1983). Denitrification with Methanol: Fundamental Study of the Growth and Denitrification Capacity of *Hypomicrobium*. *Sp. Wat. Res.*, 17(10): 1249-1255.
- Torres, E.M., Basrai, S.S., & Kogan, V. (1996). *Evaluation of Two Biotechnologies Controlling POTW Air Emissions*. Proceedings of 1996 Conference on Biofiltration, Los Angeles, CA.
- Tucker, M.D., Barton, L., & Thomson, B.M. (1998). Removal of Uranium and Molibdenum from Water by Immobilized *Desulfovibrio desulfuricans* in Column Reactors. *Biotech. Bioeng.*, 60: 88-96.

- Turner, C.D., Moncada, J., & Walton, J. (1997). *Designing for Brine Reject Utilization*. Membrane Technology Conference Proceedings, AWWA, pp. 883-891, New Orleans, LA.
- U.S. Environmental Protection Agency (1992). *Guidelines for Water Reuse*, EPA/625/R-92/004, EPA, September 1992.
- Van der Hoek, P., Latour, J., & Klapwijk, A. (1987). Denitrification with Methanol in the Presence of High Nitrate Waste Solutions. *Appl. Microbiol. Biotech.*, 27: 199-205.
- Van Houten, R.T., Pol, L.W.H., & Lettinga, G. (1994). Biological Sulfate Reduction Using Gas Lift Reactors Fed with H₂ and CO₂ as Energy and C-Source. *Biotech. Bioeng.*, 44: 586, 594.
- Van Langenhove, H. & Smet, E. (1996). *Biofiltration of Organic Sulfur Compounds*. Proceeding of the 1996 Conference on Biofiltration, Los Angeles, CA.
- Villadsen, J.V. & Stewart, W.E. (1967). Solution of Boundary Value Problems by Orthogonal Collocation. *Chem. Engr. Sci.*, 22: 1483-1501.
- Wakao, N. & Funazkri, T. (1978). Effects of Fluid Dispersion Effect on Particle to Fluid Mass Transfer Coefficients in Packed Beds: Correlation of Sherwood Numbers. *Chem. Engr. Sci.*, 33: 1375-1384.
- Wang, J.H., Baltzis, B.C., & Lewandowski, G.A. (1995). Fundamental Denitrification Kinetic Studies with *Pseudomonas denitrificans*. *Biotech. Bioeng.*, 47: 26-41.
- Wang, L.K., Poon, C.P.C., Wong, M.H., & Bergenthal, J. (1978). Chemistry of Nitrification-Denitrification Process. *Jour. Env. Sci.*, 20(6): 23-28.
- Wang, P. (1993). Study on Removing Hexavalent Chromium by Sulfate Reducing Bacteria. *Jour. Env. Sci., Beijing*, 14(6): 1-4.
- Wani, A.H., Lau, A.K. & Branion, R.M.R. (1999). Biofiltration Control of Pulp Odors - Hydrogen Sulfide: Performance, Macrokinetics and Coexistence Effects of Organo-Sulfur Species. *Jour. Chem. Techn. Biotechn.*, 74: 9-16.
- WaterReuse Association of California (1993). *Enhancing California's Future through Recycling Wastewater*.

- Weber Jr., W.J., Pirbazari, M., & Melson, G.L. (1978). Biological Growth on Activated Carbon: An Investigation by Scanning Electron Microscopy. *Env. Sci. Tech.*, 12(7): 817-819.
- Webster, T.S. (1996). *Control of Air Emissions from Publicly Owned Treatment Works Using Biological Filtration*. Ph.D. Thesis, Civil and Environmental Engineering Department, University of Southern California, Los Angeles, CA.
- Weyer, P.J., Cerhan, J.R., Kross, B.C., Hallberg, G.R., Kantamneni, J., Breuer, G., Jones, M.P., Zheng, W., & Lynch, C.F. (2001). Municipal Drinking Water Nitrate Level and Cancer Risk in Older Women: The Iowa Women's Health Study. *Epidemiology*, 11(3): 327-338.
- Wiesner, M.R. & Chellam, S. (1999). The Promise of Membrane Technology. *Env. Sci. Tech.*, 33(11): 360A-366A.
- Wijaya, S. (1993). *Optimization of Dissolved Heavy Metals Removal Using Sulfate Reducing Bacteria*. MASc Thesis, University of Windsor, Windsor, Ontario, Canada.
- Wilderer, P.A., Jones, W.L., & Du, U. (1987). Competition in Denitrification Systems Affecting Reduction Rate and Accumulation of Nitrite. *Wat. Res.*, 21(2): 239-245.
- Williamson, K. (1973). *The Kinetics of Substrate Utilization by Bacterial Films*. Ph.D. Dissertation, Department of Civil Engineering, Stanford University, Stanford, CA.
- Williamson, K. & McCarty, P.L. (1976). A Model of Substrate Utilization by Bacterial Biofilm. *JWPCF*, 48: 9-24.
- Woolard, C.R. & Irvine, R.L. (1994). Biological Treatment of Hypersaline Wastewater by a Biofilm of *Halophilic* Bacteria. *Wat. Env. Res.*, 66(3): 230-235.
- Yamamoto, R.I., Matsui, S., & Komori, T. (1994). Ecological Interactions Among Denitrification, Poly-P Accumulation, Sulfate Reduction and Filamentous Sulfur Bacteria in Activated Sludge. *Wat. Sci. Tech.*, 30(11): 201-210.

- Yang, P.Y., Nitorisavut, S., & Wu, J.Y.S. (1995). Nitrate Removal Using a Mixed-Culture Entrapped Microbial Cell Immobilization Process Under High Salt Conditions. *Wat. Res.*, 29(6): 1525-1532.
- Yanguba, J.B. (1998). *Inhibitory Effect of Total Dissolved Solids on Biological Nitrification of Brine*. M.S.C.E. Thesis, University of California, Long Beach, CA.
- Ying, W. & Weber, W.J., Jr. (1979). Bio-Physicochemical Adsorption Systems for Wastewater Treatment. *WPCF*, 51(11): 2661-2667.
- Yoder, M.W. et al. (1995). Denitrification Trio. *Water. Env. Tech.*, 7: 50-54.

APPENDICES

A – Experimental Data for Batch Studies

Table A.1. Data obtained from batch experiments at various temperatures
(pH = 7.5, Ethanol = Excess, TDS = 4,000 mg/l)

	Temperatures (°C)							
	10	15	20	25	30	35	40	45
Time Required for NO ₃ -N Reduction (min)	535	360	275	275	125	95	85	190
Amount of Nitrate Removed (mg N/l)	72.0	62.1	72.4	65.7	59.6	52.5	53.1	58.1
Biomass Concentration* (mg MLVSS/l)	591.8	492.9	383.0	272.1	357.9	317.9	372.4	551.4
Specific Denitrification Rate (mg N/mg MLVSS.hr)	0.014	0.021	0.041	0.053	0.080	0.104	0.101	0.033

* Biomass concentrations were taken at half the duration of the experiment

Table A.2. Data obtained from batch experiments at various pH values
(Temperature = 30°C, Ethanol = Excess, TDS = 4,000 mg/l)

	pH						
	6	6.5	7	7.5	8	8.5	9
Time Required for NO ₃ -N Reduction (min)	230	175	165	125	100	125	165
Amount of Nitrate Removed (mg N/l)	58.6	57.8	64.3	59.6	58.1	64.1	59.2
Biomass Concentration* (mg ML VSS/l)	393.5	400.0	371.9	357.9	432.2	432.4	427.3
Specific Denitrification Rate (mg N/mg ML VSS.hr)	0.039	0.050	0.063	0.080	0.081	0.071	0.050

* Biomass concentrations were taken at half the duration of the experiment

Table A.3. Data obtained from batch experiments at various C:N ratios
(Temperature = 30°C, pH = 7.5, TDS = 4,000 mg/l)

	C:N Ratios (mg/mg)			
	1.2:1	1.5:1	1.85:1	2.2:1
Time Required for NO ₃ -N Reduction (min)	120	70	70	80
Amount of Nitrate Removed (mg N/l)	62.4	67.4	66.9	69.1
Biomass Concentration* (mg MLVSS/l)	690.9	779.0	729.8	636.1
Specific Denitrification Rate (mg N/mg MLVSS.hr)	0.050	0.074	0.079	0.082

* Biomass concentrations were taken at half the duration of the experiment

Table A.4. Data obtained from batch experiments at various TDS concentrations
(Temperature = 30°C, pH = 7.5, C:N = Excess)

	TDS (mg/l)			
	4,000	8,000	15,000	25,000
Time Required for NO ₃ -N Reduction (min)	125	90	90	100
Amount of Nitrate Removed (mg N/l)	59.6	65.4	57.0	57.7
Biomass Concentration* (mg MLVSS/l)	757.9	773.6	734.1	711.0
Specific Denitrification Rate (mg N/mg MLVSS.hr)	0.080	0.056	0.052	0.049

* Biomass concentrations were taken at half the duration of the experiment

B – Experimental Data for Continuous Flow Chemostat Studies

Table B.1. Data obtained from the nitrite-limited chemostat at 30°C and pH 7.5
(Initial concentrations: Nitrite = 119.3 mg N/l, Nitrate = 0 mg N/l, Ethanol = 550 mg/l)

Time (min)	Flowrate (ml/min)	Dilution (hr ⁻¹)	Nitrate Conc. (mg N/l)	Nitrite Conc. (mg N/l)	Ethanol Conc. (mg/l)	Biomass Conc. (mg/l)
0	0	0	0	119.3	550.0	421.6
55	0	0	0	56.1	364.2	435.5
120	0	0	0	19.0	196.7	456.8
165	0	0	0	0	57.3	463.4
360	3	0.133	0	0.5	154.3	441.6
585	3	0.133	0	0	76.5	462.1
755	5	0.222	0	6.0	114.3	426.4
945	5	0.222	0	3.9	125.4	438.3
1125	5	0.222	0	1.6	138.2	462.2
1290	8	0.356	0	8.3	127.3	273.9
1485	8	0.356	0	3.9	119.9	222.6
1615	10.5	0.467	0	26.6	197.6	197.5
1845	10.5	0.467	0	19.0	192.5	70.7
2000	13	0.578	0	69.5	274.2	47.3
2145	13	0.578	0	60.9	337.7	33.3
2445	15	0.667	0	112.7	526.0	3.0

Table B.2. Data of nitrate-limited chemostat at 30°C and pH 7.5
(Initial concentrations: Nitrate = 75.2 mg N/l, Ethanol = 650 mg/l)

Time (min)	Flowrate (ml/min)	Dilution (hr ⁻¹)	Nitrate Conc. (mg N/l)	Nitrite Conc. (mg N/l)	Ethanol Conc. (mg/l)	Biomass Conc. (mg/l)
0	0	0	75.2	0	650.0	438.5
85	0	0	55.9	12.4	321.6	446.7
170	0	0	28.0	6.9	132.9	458.2
255	0	0	0	0	145.6	469.6
530	2	0.089	4.8	0	188.5	441.6
735	2	0.089	0.3	0	170.2	467.8
920	3	0.133	8.7	1.4	185.8	498.7
1455	3	0.133	0.7	0	167.6	528.6
1550	5	0.222	10.3	1.7	233.8	325.2
1815	5	0.222	1.2	0	226.9	312.1
2040	7	0.311	19.5	2.0	184.5	241.2
2175	7	0.311	2.3	2.3	176.1	135.5
2350	8	0.356	22.3	3.4	239.5	96.6
2475	8	0.356	10.8	4.2	277.5	83.0
2550	10	0.444	49.4	6.5	332.3	61.2
2635	10	0.444	42.6	6.8	384.6	42.8
2775	10	0.444	41.8	6.5	456.9	34.5
3075	10.5	0.467	72.4	8.6	638.2	2.1

Table B.3. Data of ethanol-limited (nitrite in excess) chemostat at 30°C and pH 7.5
(Initial concentrations: Nitrite = 121.7 mg N/l, Nitrate = 0 mg N/l, Ethanol = 325 mg/l)

Time (min)	Flowrate (ml/min)	Dilution (hr ⁻¹)	Nitrate Conc. (mg N/l)	Nitrite Conc. (mg N/l)	Ethanol Conc. (mg/l)	Biomass Conc. (mg/l)
0	0	0	0	121.7	325.0	392.2
70	0	0	0	90.8	0	396.7
135	0	0	0	49.4	31.4	400.3
215	0	0	0	7.8	0	408.6
380	2.5	0.111	0	15.7	14.3	396.7
695	2.5	0.111	0	8.6	0	402.5
1070	3	0.133	0	22.3	18.8	396.4
1475	3	0.133	0	16.8	16.5	408.0
1720	4	0.178	0	31.6	34.7	257.5
1955	4	0.178	0	45.4	26.4	198.4
2245	5	0.222	0	66.6	53.3	155.3
2315	5	0.222	0	80.1	65.4	78.1
2430	6	0.267	0	65.2	142.1	48.7
2550	6	0.267	0	75.1	153.5	45.7
2615	6	0.267	0	92.2	186.0	41
2915	7	0.311	0	101.5	237.8	20.1

Table B.4. Data of ethanol-limited (nitrate in excess) chemostat at 30°C and pH 7.5
(Initial concentrations: Nitrate = 79 mg N/l, Ethanol = 280 mg/l)

Time (min)	Flowrate (ml/min)	Dilution (hr ⁻¹)	Nitrate Conc. (mg N/l)	Nitrite Conc. (mg N/l)	Ethanol Conc. (mg/l)	Biomass Conc. (mg/l)
0	0	0	79.0	0	280.0	392.4
125	0	0	35.9	14.5	73.5	403.2
195	0	0	15.4	22.4	11.5	415.7
290	0	0	8.5	19.1	0	419.8
635	1.5	0.067	12.5	11.7	1.7	407.9
1070	1.5	0.067	12.7	11.9	0	396.5
1255	2	0.089	17.7	13.7	5.5	245.4
1490	2	0.089	19.0	12.6	0	193.9
1615	3	0.133	39.8	19.0	23.9	95.3
1850	3	0.133	48.6	23.8	86.2	60.1
1995	4	0.178	50.0	27.4	102.2	41.3
2090	4	0.178	55.0	28.8	135.5	28.9
2210	4	0.178	62.4	30.0	171.3	24.8
2510	5	0.222	67.2	31.8	207.5	17.0

C – Experimental Data for Fluidized Bioadsorber Reactor Studies

Table C.1. Data for fluidized bioadsorber reactor denitrification experiment no 1 (Steady State Biofilm Density = 288 mg AVS/g GAC)

Time (min)	Nitrate Conc. (mg N/l)	Nitrite Conc. (mg N/l)
0	87.2	0
25	80.5	0
50	74.9	3.1
70	72.2	3.4
95	68.8	5.5
120	62.8	4.2
150	56.7	3.7
180	53.7	3.1
210	48.6	4.9
245	43.4	3.4
290	31.5	3.1
340	19.7	0
405	8	0
470	0	0
565	0	0
730	0	0
865	0	0
1330	0	0
1535	0	0
1765	0	0
2020	0	0
2285	0	0
2810	0	0
3075	0	0
3350	0	0
3605	0	0
3910	0	0
4195	0	0
4350	0	0

Table C.2. Data for fluidized bioadsorber reactor denitrification experiment no 2 (Steady State Biofilm Density = 227 mg AVS/g GAC)

Time (min)	Nitrate Conc. (mg N/l)	Nitrite Conc. (mg N/l)
0	64.7	0
35	53.2	8.3
90	43.9	12.1
165	36	12.7
225	28.2	8.2
285	18	3.7
340	11.1	0
420	4	0
465	2.7	0
525	0	0
645	0	0
810	0	0
915	0	0
1005	0	0
1400	0	0
1545	0	0
1695	0	0
1875	0	0
2055	0	0
2240	0	0
2420	0	0
2865	0	0
3055	0	0
3195	0	0
3345	0	0
3585	0	0
3756	0	0
4065	0	0
4365	0	0

Table C.3. Data for fluidized bioadsorber reactor denitrification experiment no 3 (Steady State Biofilm Density = 205 mg AVS/g GAC)

Time (min)	Nitrate Conc. (mg N/l)	Nitrite Conc. (mg N/l)
0	81.8	0
45	65.7	14
90	58.2	26.2
145	61	34.4
205	54.2	38.6
265	48.4	27.4
330	40.2	38.6
405	29.5	42.3
465	16.8	30
595	11.6	30.6
735	6.6	7.9
930	2.9	0
1300	0	0
1475	0	0
1635	0	0
1795	0	0
1905	0	0
2055	0	0
2175	0	0
2370	0	0
2715	0	0
2895	0	0
3075	0	0
3205	0	0
3315	0	0
3495	0	0
3675	0	0
3810	0	0
4155	0	0
4395	0	0

Table C.4. Data for fluidized bioadsorber reactor denitrification experiment no 4 (Steady State Biofilm Density = 234 mg AVS/g GAC)

Time (min)	Nitrate Conc. (mg N/l)	Nitrite Conc. (mg N/l)
0	89.4	0
30	89.4	0
55	82.9	6.9
85	76.6	5.3
115	74.9	5.5
150	71.6	7.7
180	62.7	4.6
215	61.9	3.9
265	53.4	2.1
310	43.9	3.2
350	33.8	2.4
420	20.5	0
480	5.9	0
535	0	0
630	0	0
820	0	0
1315	0	0
1570	0	0
1765	0	0
1980	0	0
2155	0	0
2320	0	0
2785	0	0
3075	0	0
3280	0	0
3565	0	0
3845	0	0
4055	0	0
4295	0	0

Table C.5. Data for fluidized bioadsorber reactor denitrification experiment no 5 (Steady State Biofilm Density = 206 mg AVS/g GAC)

Time (min)	Nitrate Conc. (mg N/l)	Nitrite Conc. (mg N/l)
0	89.4	0
25	89.5	2.3
60	87.6	4
90	86.1	5.1
115	85.3	6.6
145	87.6	7.2
170	85.7	7.8
205	85.2	6.9
230	74.3	4
280	78	5.5
330	68.6	4.7
390	48.2	2.5
460	47.6	0
520	36.5	0
600	15.8	0
715	2.7	0
800	0	0
900	0	0
1275	0	0
1455	0	0
1675	0	0
1875	0	0
2035	0	0
2255	0	0
2720	0	0
3055	0	0
3205	0	0
3390	0	0
3605	0	0
3875	0	0
4020	0	0
4305	0	0

Table C.6. Data for fluidized bioadsorber reactor denitrification experiment no 6 (Steady State Biofilm Density = 163 mg AVS/g GAC)

Time (min)	Nitrate Conc. (mg N/l)	Nitrite Conc. (mg N/l)
0	93.8	0
30	93.8	0
55	97.6	0
95	95.6	0
125	95.5	0
185	88.5	0
245	92.2	0
295	74.6	7.2
365	79.8	5.9
430	74	0
495	63.4	0
565	53.3	0
715	21.1	0
865	4.5	0
955	3.5	0
1380	0	0
1585	0	0
1765	0	0
1975	0	0
2150	0	0
2305	0	0
2785	0	0
2955	0	0
3195	0	0
3400	0	0
3635	0	0
4020	0	0
4275	0	0

Table C.7. Data for fluidized bioadsorber reactor denitrification experiment no 7 (Steady State Biofilm Density = 428 mg AVS/g GAC)

Time (min)	Nitrate Conc. (mg N/l)	Nitrite Conc. (mg N/l)
0	308.8	5.4
45	270.5	25.1
105	230.9	52.9
150	204.5	65
210	170.3	77.4
340	120.8	82.9
400	79.9	114.3
465	61	84.8
570	33.8	70
690	46.7	56
830	24.9	35.9
1230	4.1	7.2
1485	3	0
1650	0	0
1830	0	0
1920	0	0

Table C.8. Data for fluidized bioadsorber reactor denitrification experiment no 8 (Steady State Biofilm Density = 625 mg AVS/g GAC)

Time (min)	Nitrate Conc. (mg N/l)	Nitrite Conc. (mg N/l)
0	316.1	0
120	315.3	23.2
210	296.3	24.5
330	270.6	33.5
440	255.1	50
555	218.4	78.2
690	161.7	112.3
800	103.7	142.2
895	57.9	159.6
1245	3.3	10.5
1480	3	4.6
1650	0	0
1815	0	0
1980	0	0
2140	0	0

Table C.9. Data for fluidized bioadsorber reactor denitrification experiment no 9 (Steady State Biofilm Density = 389 mg AVS/g GAC)

Time (min)	Nitrate Conc. (mg N/l)	Nitrite Conc. (mg N/l)
0	190.6	0.1
75	187.8	0.9
180	183.7	1.2
300	186	1.4
440	182.6	3.4
615	182.1	3.9
720	178.5	8
1095	166.2	14.2
1225	164.2	19.7
1395	152.3	28.8
1545	136.2	37.8
1750	111.3	54.7
1920	83.5	79.7
2090	48.1	104.1
2655	5.7	28.6
2875	3.6	17.5
3170	3.4	12.8
3465	3.3	9.6
3705	3.2	7.3
3960	3.2	5.4
4260	3.2	3.4
4490	3.1	0.4
4770	3.1	0
5050	3.1	0
5285	3.1	0

Table C.10. Data for fluidized bioadsorber reactor denitrification experiment no 10 (Steady State Biofilm Density = 217 mg AVS/g GAC)

Time (min)	Nitrate Conc. (mg N/l)	Nitrite Conc. (mg N/l)
0	190.4	0
30	181.9	3.4
85	166.7	11
140	160.1	13.8
205	158.9	16.4
275	158.2	20.8
365	153.1	21.5
485	142	23.7
675	130.9	30.4
975	119.5	35.8
1265	95.9	44.7
1450	72.7	51.2
1635	50.7	60.6
1925	22	65.4
2220	13.1	44.1
2530	6.9	15.3
2720	5.9	6.1
2910	5.8	0.6
3235	5.6	0
3610	5.5	0
4035	5.4	0
4385	5.2	0
4825	5.2	0
5150	5.1	0

Table C.11. Data for fluidized bioadsorber reactor denitrification experiment no 11 (Steady State Biofilm Density = 252 mg AVS/g GAC)

Time (min)	Nitrate Conc. (mg N/l)	Nitrite Conc. (mg N/l)
0	151.9	2
25	126.1	6.4
70	113.3	15.6
125	97.9	22.7
205	85.7	26.8
260	77.2	26.5
315	65	21.9
400	58.9	20.9
520	50.7	19.7
670	39.2	14.2
805	27.1	13.8
980	10	4.3
1360	5.3	0
1635	4.7	0
1970	4.2	0
2270	3.8	0
2580	3.2	0
2985	2.4	0
3340	1.7	0
3685	0.7	0
4080	0.3	0
4430	0.2	0
4815	0.2	0
5130	0.2	0

Table C.12. Data for fluidized bioadsorber reactor denitrification experiment no 12 (Steady State Biofilm Density = 148 mg AVS/g GAC)

Time (min)	Nitrate Conc. (mg N/l)	Nitrite Conc. (mg N/l)
0	78.8	0
120	78.7	1.1
180	78.9	2.3
250	76.5	3.7
325	75	4.7
450	72.5	6.5
675	71.4	8.2
795	67	13.5
1170	52.5	23.6
1420	31.7	35
1660	11.9	41.4
1865	6.4	26.3
2215	4.2	7.3
2690	4.1	5.6
2935	3.6	4.1
3275	3.8	4.1
3605	3.4	3.1
3790	3.3	2.5
3985	3	2.2
4160	2.8	2.1

Table C.13. Data for fluidized bioadsorber reactor denitrification experiment no 13 (Steady State Biofilm Density = 195 mg AVS/g GAC)

Time (min)	Nitrate Conc. (mg N/l)	Nitrite Conc. (mg N/l)
0	78.8	0
45	62.8	10.7
165	43	18.7
260	39.4	22.5
435	34.5	29.4
615	25.2	38.9
770	16.8	43.1
935	10.1	45.5
1175	5.9	39.4
1420	3.5	16.8
1635	2.7	8.1
1815	2.9	2.9
2000	0	1.4
2540	0	0
2730	0	0
2870	0	0
2920	0	0

D - Experimental Data for FBAR Studies with Sand

Table D.1. Data for FBAR denitrification experiment with 300 g sand
(Steady State Biofilm Density = 166 mg AVS/g Sand)

Time (min)	Nitrate Conc. (mg N/l)	Nitrite Conc. (mg N/l)
0	84.7	0
25	84.4	0
50	84	0.4
70	82.6	1.2
95	80	2.7
120	76.5	5
150	71.7	7.2
180	67.6	11
210	62.2	14.8
245	57.3	18.8
290	52.5	22.2
340	49.4	21.4
405	42.1	19.9
470	32.3	13
565	23.8	10.1
730	18.7	3.3
865	13.2	0
1330	1	0
1535	0	0
1765	0	0
2020	0	0
2285	0	0
2810	0	0
3075	0	0
3350	0	0
3605	0	0
3910	0	0
4195	0	0
4350	0	0

Table D.2. Data for FBAR denitrification experiment with 150 g sand
(Steady State Biofilm Density = 93 mg AVS/g Sand)

Time (min)	Nitrate Conc. (mg N/l)	Nitrite Conc. (mg N/l)
0	85.2	0
30	85.2	0
55	84.5	0
85	84.2	0
115	83.2	0.7
150	81.3	1.5
180	79.4	2.3
215	78.1	2.9
265	75.1	3.7
310	71.5	5.3
350	68.6	6.6
420	67	8.6
480	63.3	10.8
535	57.2	15.2
630	53.4	17
820	39.2	23.2
1315	25.9	13.4
1570	18.8	9.9
1765	11	6.8
1980	4.6	1.9
2155	1.9	0
2320	0	0
2785	0	0
3075	0	0
3280	0	0
3565	0	0
3845	0	0
4055	0	0
4295	0	0

E - Experimental Data for Sulfate Reduction Studies

Table E.1. Data for FBAR simultaneous nitrate and sulfate reduction experiment

Time (hr)	Sulfate Conc. (mg/l)	Nitrate Conc. (mg N/l)	Nitrite Conc. (mg N/l)
0	1308.4	58	0
0.8	1296.3	74.9	3.1
1.3	1305.7	72.2	3.4
1.8	1290.7	62.8	4.2
2.9	1195.4	56.7	3.7
3.8	1206.1	43.4	3.4
5.3	1132.5	31.1	3.1
6.3	1132.1	19.7	0
8.5	1162.6	8	0
12.3	1140	0	0
16	1108.3	0	0
28.8	1069	0	0
48.6	1100	0	0
73.2	1098.3	0	0
98.3	1103.9	0	0
123	1065.4	0	0
147.3	932.5	0	0
175.7	1154.2	0	0
216.8	1017.8	0	0
264.1	995	0	0
342.8	933.1	0	0
385.8	894.9	0	0
465.3	845.3	0	0
512.3	906.2	0	0
529	728.1	0	0
572.3	721.1	0	0

Table E.2. Data for (second) FBAR sulfate reduction experiment

Time (hr)	Sulfate Conc. (mg/l)
0	720
4	692.1
6.6	642.9
11.3	602.9
16.8	536.1
23.5	485.8
63.5	396.2
117.5	335.1
144.3	242.6
190.3	153.2
242	132.6
287.8	67.3
411.5	0
478.5	0
503	0
548.5	0

F - FBAR Biofilm Model Simulation Data

Table F.1. Model prediction data for FBAR denitrification experiment no 1

Time (min)	Predicted Nitrate Conc. (mg/l)	Time (min)	Predicted Nitrate Conc. (mg/l)	Time (min)	Predicted Nitrate Conc. (mg/l)	Time (min)	Predicted Nitrate Conc. (mg/l)
0	362.4	780	6.397983	1560	3.028241	2340	3.028241
30	351.1792	810	6.360675	1590	3.028241	2370	3.028241
60	354.0564	840	6.305756	1620	3.028241	2400	3.028241
90	353.6015	870	6.225739	1650	3.028241	2430	3.028241
120	351.0201	900	4.013448	1680	3.028241	2460	3.028241
150	346.4571	930	3.222943	1710	3.028241	2490	3.028241
180	339.494	960	3.071909	1740	3.028241	2520	3.028241
210	329.3297	990	3.038325	1770	3.028241	2550	3.028241
240	314.8643	1020	3.030585	1800	3.028241	2580	3.028241
270	294.8213	1050	3.028787	1830	3.028241	2610	3.028241
300	268.0392	1080	3.028368	1860	3.028241	2640	3.028241
330	234.0563	1110	3.028271	1890	3.028241	2670	3.028241
360	193.9742	1140	3.028248	1920	3.028241	2700	3.028241
390	151.1652	1170	3.028243	1950	3.028241	2730	3.028241
420	95.34486	1200	3.028241	1980	3.028241	2760	3.028241
450	37.91385	1230	3.028241	2010	3.028241	2790	3.028241
480	11.34725	1260	3.028241	2040	3.028241	2820	3.028241
510	7.054801	1290	3.028241	2070	3.028241	2850	3.028241
540	6.579603	1320	3.028241	2100	3.028241	2880	3.028241
570	6.494153	1350	3.028241	2130	3.028241	2910	3.028241
600	6.474277	1380	3.028241	2160	3.028241	2940	3.028241
630	6.466822	1410	3.028241	2190	3.028241	2970	3.028241
660	6.460522	1440	3.028241	2220	3.028241	3000	3.028241
690	6.452312	1470	3.028241	2250	3.028241		
720	6.440526	1500	3.028241	2280	3.028241		
750	6.4233	1530	3.028241	2310	3.028241		

Table F.2. Model prediction data for FBAR denitrification experiment no 2

Time (min)	Predicted Nitrate Conc. (mg/l)	Time (min)	Predicted Nitrate Conc. (mg/l)	Time (min)	Predicted Nitrate Conc. (mg/l)	Time (min)	Predicted Nitrate Conc. (mg/l)
0	286.7	780	0.053234	1560	4.530876	2340	4.545476
30	225.2367	810	0.052599	1590	4.535415	2370	4.545518
60	225.4165	840	0.051642	1620	4.538348	2400	4.545556
90	217.3064	870	0.050049	1650	4.540249	2430	4.545591
120	201.0627	900	0.047555	1680	4.54149	2460	4.545623
150	177.0273	930	0.043895	1710	4.542314	2490	4.545652
180	146.6455	960	0.038836	1740	4.542876	2520	4.545678
210	113.2265	990	0.032275	1770	4.543274	2550	4.545702
240	81.61608	1020	0.339987	1800	4.543571	2580	4.545724
270	56.12593	1050	0.813159	1830	4.543803	2610	4.545743
300	38.20609	1080	1.273618	1860	4.543995	2640	4.545761
330	26.60884	1110	1.630818	1890	4.54416	2670	4.545776
360	19.42209	1140	1.886879	1920	4.544307	2700	4.545791
390	15.16238	1170	2.385592	1950	4.54444	2730	4.545803
420	0.09184	1200	2.959866	1980	4.544562	2760	4.545815
450	0.313618	1230	3.41074	2010	4.544675	2790	4.545825
480	0.357946	1260	3.750773	2040	4.544779	2820	4.545834
510	0.302323	1290	3.997942	2070	4.544877	2850	4.545842
540	0.241527	1320	4.172924	2100	4.544967	2880	4.545849
570	0.179965	1350	4.294453	2130	4.54505	2910	4.545855
600	0.125622	1380	4.377637	2160	4.545127	2940	4.54586
630	0.088313	1410	4.433906	2190	4.545198	2970	4.545865
660	0.069317	1440	4.471592	2220	4.545264	3000	4.545869
690	0.06003	1470	4.49661	2250	4.545324		
720	0.055802	1500	4.513089	2280	4.545379		
750	0.054026	1530	4.523868	2310	4.545429		

Table F.3. Model prediction data for FBAR denitrification experiment no 3

Time (min)	Predicted Nitrate Conc. (mg/l)	Time (min)	Predicted Nitrate Conc. (mg/l)	Time (min)	Predicted Nitrate Conc. (mg/l)	Time (min)	Predicted Nitrate Conc. (mg/l)
0	386	780	0.082716	1560	0	2340	0
30	272.6215	810	0.082719	1590	0	2370	0
60	271.8674	840	0.081925	1620	0	2400	0
90	259.5094	870	0.080167	1650	0	2430	0
120	235.7943	900	0.077287	1680	0	2460	0
150	201.9507	930	0.073119	1710	0	2490	0
180	161.277	960	0.06753	1740	0	2520	0
210	119.4712	990	0.1138	1770	0	2550	0
240	83.00106	1020	0	1800	0	2580	0
270	55.83215	1050	0	1830	0	2610	0
300	37.71459	1080	0	1860	0	2640	0
330	26.1162	1110	0	1890	0	2670	0
360	18.74163	1140	0	1920	0	2700	0
390	14.10498	1170	0	1950	0	2730	0
420	2.782604	1200	0	1980	0	2760	0
450	0.164763	1230	0	2010	0	2790	0
480	1.020021	1260	0	2040	0	2820	0
510	0.28322	1290	0	2070	0	2850	0
540	0.188065	1320	0	2100	0	2880	0
570	0.135432	1350	0	2130	0	2910	0
600	0.111252	1380	0	2160	0	2940	0
630	0.093818	1410	0	2190	0	2970	0
660	0.085006	1440	0	2220	0	3000	0
690	0.082016	1470	0	2250	0		
720	0.081623	1500	0	2280	0		
750	0.08218	1530	0	2310	0		

Table F.4. Model prediction data for FBAR denitrification experiment no 4

Time (min)	Predicted Nitrate Conc. (mg/l)	Time (min)	Predicted Nitrate Conc. (mg/l)	Time (min)	Predicted Nitrate Conc. (mg/l)	Time (min)	Predicted Nitrate Conc. (mg/l)
0	415.5	780	27.38651	1560	16.278	2340	16.25509
30	412.0934	810	27.06884	1590	16.26471	2370	16.25509
60	412.8467	840	26.91415	1620	16.25914	2400	16.25509
90	412.8395	870	26.83575	1650	16.2568	2430	16.25509
120	412.2505	900	26.79205	1680	16.25581	2460	16.25509
150	411.079	930	26.76307	1710	16.2554	2490	16.25509
180	409.1893	960	26.73895	1740	16.25522	2520	16.25509
210	406.316	990	26.71457	1770	16.25515	2550	16.25509
240	402.0434	1020	26.68688	1800	16.25512	2580	16.25509
270	395.7677	1050	26.65367	1830	16.2551	2610	16.25509
300	386.652	1080	26.61295	1860	16.2551	2640	16.25509
330	373.5971	1110	26.56261	1890	16.2551	2670	16.25509
360	355.2707	1140	26.50022	1920	16.2551	2700	16.25509
390	330.282	1170	26.42288	1950	16.25509	2730	16.25509
420	297.6198	1200	26.32708	1980	16.25509	2760	16.25509
450	252.5679	1230	26.20864	2010	16.25509	2790	16.25509
480	197.6028	1260	26.06255	2040	16.25509	2820	16.25509
510	148.872	1290	25.88293	2070	16.25509	2850	16.25509
540	110.1496	1320	25.66306	2100	16.25509	2880	16.25509
570	81.03288	1350	24.07775	2130	16.25509	2910	16.25509
600	60.14747	1380	20.44322	2160	16.25509	2940	16.25509
630	46.0196	1410	18.11445	2190	16.25509	2970	16.25509
660	37.17123	1440	17.0283	2220	16.25509	3000	16.25509
690	32.09273	1470	16.57296	2250	16.25509		
720	29.39815	1500	16.38648	2280	16.25509		
750	28.04534	1530	16.3098	2310	16.25509		

Table F.5. Model prediction data for FBAR denitrification experiment no 5

Time (min)	Predicted Nitrate Conc. (mg/l)	Time (min)	Predicted Nitrate Conc. (mg/l)	Time (min)	Predicted Nitrate Conc. (mg/l)	Time (min)	Predicted Nitrate Conc. (mg/l)
0	396	780	5.623064	1560	5.790905	2340	5.790906
30	389.1793	810	5.685604	1590	5.790906	2370	5.790906
60	389.6084	840	5.725139	1620	5.790906	2400	5.790906
90	389.2074	870	5.749946	1650	5.790906	2430	5.790906
120	387.8843	900	5.765441	1680	5.790906	2460	5.790906
150	385.4135	930	5.775092	1710	5.790906	2490	5.790906
180	381.4049	960	5.781093	1740	5.790906	2520	5.790906
210	375.2566	990	5.784819	1770	5.790906	2550	5.790906
240	365.9834	1020	5.787131	1800	5.790906	2580	5.790906
270	352.6022	1050	5.788566	1830	5.790906	2610	5.790906
300	335.9731	1080	5.789455	1860	5.790906	2640	5.790906
330	316.8534	1110	5.790007	1890	5.790906	2670	5.790906
360	295.741	1140	5.790349	1920	5.790906	2700	5.790906
390	272.961	1170	5.79056	1950	5.790906	2730	5.790906
420	248.7262	1200	5.790692	1980	5.790906	2760	5.790906
450	223.179	1230	5.790773	2010	5.790906	2790	5.790906
480	196.4239	1260	5.790824	2040	5.790906	2820	5.790906
510	168.5562	1290	5.790855	2070	5.790906	2850	5.790906
540	139.6955	1320	5.790875	2100	5.790906	2880	5.790906
570	110.0385	1350	5.790887	2130	5.790906	2910	5.790906
600	79.95666	1380	5.790894	2160	5.790906	2940	5.790906
630	49.50882	1410	5.790899	2190	5.790906	2970	5.790906
660	21.36242	1440	5.790902	2220	5.790906	3000	5.790906
690	6.511028	1470	5.790903	2250	5.790906		
720	5.407171	1500	5.790904	2280	5.790906		
750	5.525944	1530	5.790905	2310	5.790906		

Table F.6. Model prediction data for FBAR denitrification experiment no 6

Time (min)	Predicted Nitrate Conc. (mg/l)	Time (min)	Predicted Nitrate Conc. (mg/l)	Time (min)	Predicted Nitrate Conc. (mg/l)	Time (min)	Predicted Nitrate Conc. (mg/l)
0	396	780	1.434803	1560	1.440983	2340	1.440984
30	389.5951	810	1.436534	1590	1.440984	2370	1.440984
60	382.6762	840	1.437781	1620	1.440984	2400	1.440984
90	374.4833	870	1.438679	1650	1.440984	2430	1.440984
120	364.789	900	1.439326	1680	1.440984	2460	1.440984
150	353.3218	930	1.439791	1710	1.440984	2490	1.440984
180	339.7591	960	1.440126	1740	1.440984	2520	1.440984
210	323.7179	990	1.440367	1770	1.440984	2550	1.440984
240	304.7467	1020	1.44054	1800	1.440984	2580	1.440984
270	282.3183	1050	1.440665	1830	1.440984	2610	1.440984
300	255.8286	1080	1.440754	1860	1.440984	2640	1.440984
330	224.609	1110	1.440819	1890	1.440984	2670	1.440984
360	187.9692	1140	1.440865	1920	1.440984	2700	1.440984
390	145.3113	1170	1.440899	1950	1.440984	2730	1.440984
420	95.44321	1200	1.440923	1980	1.440984	2760	1.440984
450	36.48405	1230	1.44094	2010	1.440984	2790	1.440984
480	1.284011	1260	1.440953	2040	1.440984	2820	1.440984
510	1.327277	1290	1.440961	2070	1.440984	2850	1.440984
540	1.35793	1320	1.440968	2100	1.440984	2880	1.440984
570	1.38057	1350	1.440973	2130	1.440984	2910	1.440984
600	1.397172	1380	1.440976	2160	1.440984	2940	1.440984
630	1.409283	1410	1.440978	2190	1.440984	2970	1.440984
660	1.418083	1440	1.44098	2220	1.440984	3000	1.440984
690	1.42446	1470	1.440981	2250	1.440984		
720	1.429071	1500	1.440982	2280	1.440984		
750	1.432401	1530	1.440983	2310	1.440984		

Table F.7. Model prediction data for FBAR denitrification experiment no 7

Time (min)	Predicted Nitrate Conc. (mg/l)	Time (min)	Predicted Nitrate Conc. (mg/l)	Time (min)	Predicted Nitrate Conc. (mg/l)	Time (min)	Predicted Nitrate Conc. (mg/l)
0	1367.64	780	0	1560	0	2340	0
30	1275.835	810	0	1590	0	2370	0
60	1198.893	840	0	1620	0	2400	0
90	1123.116	870	0	1650	0	2430	0
120	1048.717	900	0	1680	0	2460	0
150	975.732	930	0	1710	0	2490	0
180	904.0636	960	0	1740	0	2520	0
210	833.494	990	0	1770	0	2550	0
240	763.6903	1020	0	1800	0	2580	0
270	694.2046	1050	0	1830	0	2610	0
300	624.4801	1080	0	1860	0	2640	0
330	553.8823	1110	0	1890	0	2670	0
360	481.7901	1140	0	1920	0	2700	0
390	407.8056	1170	0	1950	0	2730	0
420	332.1661	1200	0	1980	0	2760	0
450	256.4326	1230	0	2010	0	2790	0
480	128.2857	1260	0	2040	0	2820	0
510	2.1883	1290	0	2070	0	2850	0
540	1.045884	1320	0	2100	0	2880	0
570	0.532016	1350	0	2130	0	2910	0
600	0.180855	1380	0	2160	0	2940	0
630	0.048614	1410	0	2190	0	2970	0
660	0	1440	0	2220	0	3000	0
690	0	1470	0	2250	0		
720	0	1500	0	2280	0		
750	0	1530	0	2310	0		

Table F.8. Model prediction data for FBAR denitrification experiment no 8

Time (min)	Predicted Nitrate Conc. (mg/l)	Time (min)	Predicted Nitrate Conc. (mg/l)	Time (min)	Predicted Nitrate Conc. (mg/l)	Time (min)	Predicted Nitrate Conc. (mg/l)
0	1400	780	387.4596	1560	19.63843	2340	19.63842
30	1286.518	810	282.828	1590	19.63842	2370	19.63842
60	1308.366	840	207.8085	1620	19.63842	2400	19.63842
90	1317.024	870	156.7749	1650	19.63842	2430	19.63842
120	1318.645	900	122.9655	1680	19.63842	2460	19.63842
150	1316.35	930	100.9346	1710	19.63842	2490	19.63842
180	1311.636	960	86.65378	1740	19.63842	2520	19.63842
210	1305.127	990	77.24649	1770	19.63842	2550	19.63842
240	1296.973	1020	62.07152	1800	19.63842	2580	19.63842
270	1287.05	1050	40.43428	1830	19.63842	2610	19.63842
300	1275.074	1080	27.89276	1860	19.63842	2640	19.63842
330	1260.642	1110	22.73081	1890	19.63842	2670	19.63842
360	1243.263	1140	20.8346	1920	19.63842	2700	19.63842
390	1222.364	1170	20.11926	1950	19.63842	2730	19.63842
420	1197.306	1200	19.83597	1980	19.63842	2760	19.63842
450	1167.394	1230	19.72039	2010	19.63842	2790	19.63842
480	1131.905	1260	19.67258	2040	19.63842	2820	19.63842
510	1090.132	1290	19.65268	2070	19.63842	2850	19.63842
540	1041.45	1320	19.64438	2100	19.63842	2880	19.63842
570	985.4081	1350	19.64091	2130	19.63842	2910	19.63842
600	921.8546	1380	19.63946	2160	19.63842	2940	19.63842
630	851.0734	1410	19.63885	2190	19.63842	2970	19.63842
660	773.9224	1440	19.6386	2220	19.63842	3000	19.63842
690	691.9301	1470	19.6385	2250	19.63842		
720	607.3017	1500	19.63845	2280	19.63842		
750	512.8886	1530	19.63843	2310	19.63842		

G - FBAR Biofilm Model Sensitivity Analyses Data

Table G.1. Model sensitivity analysis data for influent nitrate concentration

Time (min)	Influent Nitrate Conc. = 198 mg/l (-50%)	Influent Nitrate Conc. = 396 mg/l	Influent Nitrate Conc. = 594 mg/l (+50%)	Biomass Conc. = 6,000 mg/l
0	1	1	1	1
30	0.979975	0.982776	0.983719	0.98088
60	0.977905	0.98386	0.985874	0.978384
90	0.973031	0.982847	0.986187	0.958925
120	0.964571	0.979506	0.984626	0.915385
150	0.951265	0.973266	0.980884	0.828117
180	0.931249	0.963144	0.974333	0.671652
210	0.901949	0.947618	0.96393	0.42843
240	0.85934	0.924201	0.947922	0.259217
270	0.79771	0.890409	0.924757	0.182891
300	0.721398	0.848417	0.895886	0.151748
330	0.63454	0.800135	0.862563	0.139327
360	0.539916	0.746821	0.825612	0.133625
390	0.439591	0.689296	0.785567	0.129261
420	0.335499	0.628096	0.742756	0.121766
450	0.23029	0.563583	0.697369	0.084954
480	0.129605	0.49602	0.6495	0.068314
510	0.050736	0.425647	0.599176	0.06393
540	0.02467	0.352766	0.546383	0.062885
570	0.023571	0.277875	0.491062	0.062639
600	0.024165	0.201911	0.432179	0.062582
630	0.024598	0.125022	0.369619	0.062568

Table G.1. Model sensitivity analysis data for influent nitrate concentration (continued)

Time (min)	Influent Nitrate Conc. = 198 mg/l (-50%)	Influent Nitrate Conc. = 396 mg/l	Influent Nitrate Conc. = 594 mg/l (+50%)	Biomass Conc. = 6,000 mg/l
660	0.024861	0.053946	0.303924	0.062565
690	0.025011	0.016442	0.235679	0.062564
720	0.024172	0.013654	0.165801	0.062564
750	0.023237	0.013954	0.096413	0.062564
780	0.022687	0.0142	0.035217	0.062564
810	0.02237	0.014358	0.010526	0.062564
840	0.022184	0.014457	0.010008	0.062564
870	0.022074	0.01452	0.01037	0.062564
900	0.022008	0.014559	0.010621	0.062564
930	0.021969	0.014584	0.010786	0.062564
960	0.021945	0.014599	0.010891	0.062564
990	0.021931	0.014608	0.010959	0.062564
1020	0.021922	0.014614	0.011001	0.062564
1050	0.021917	0.014618	0.011029	0.062564
1080	0.021914	0.01462	0.011046	0.062564
1110	0.021912	0.014621	0.011056	0.062564
1140	0.021911	0.014622	0.011063	0.062564
1170	0.02191	0.014623	0.011067	0.062564
1200	0.02191	0.014623	0.01107	0.062564
1230	0.02191	0.014623	0.011072	0.062564
1260	0.02191	0.014623	0.011073	0.062564
1290	0.021909	0.014623	0.011073	0.062564

Table G.1. Model sensitivity analysis data for influent nitrate concentration (continued)

Time (min)	Influent Nitrate Conc. = 198 mg/l (-50%)	Influent Nitrate Conc. = 396 mg/l	Influent Nitrate Conc. = 594 mg/l (+50%)	Biomass Conc. = 6,000 mg/l
1320	0.021909	0.014623	0.011074	0.062564
1350	0.021909	0.014623	0.011074	0.062564
1380	0.021909	0.014623	0.011074	0.062564
1410	0.021909	0.014623	0.011074	0.062564
1440	0.021909	0.014623	0.011074	0.062564
1470	0.021909	0.014623	0.011074	0.062564
1500	0.021909	0.014623	0.011074	0.062564
1530	0.021909	0.014623	0.011074	0.062564
1560	0.021909	0.014623	0.011074	0.062564
1590	0.021909	0.014624	0.011074	0.062564
1620	0.021909	0.014624	0.011074	0.062564
1650	0.021909	0.014624	0.011074	0.062564
1680	0.021909	0.014624	0.011074	0.062564
1710	0.021909	0.014624	0.011074	0.062564
1740	0.021909	0.014624	0.011074	0.062564
1770	0.021909	0.014624	0.011074	0.062564
1800	0.021909	0.014624	0.011074	0.062564
1830	0.021909	0.014624	0.011074	0.062564
1860	0.021909	0.014624	0.011074	0.062564
1890	0.021909	0.014624	0.011074	0.062564
1920	0.021909	0.014624	0.011074	0.062564

Table G.1. Model sensitivity analysis data for influent nitrate concentration (continued)

Time (min)	Influent Nitrate Conc. = 198 mg/l (-50%)	Influent Nitrate Conc. = 396 mg/L	Influent Nitrate Conc. = 594 mg/l (+50%)	Biomass Conc. = 6,000 mg/l
1950	0.021909	0.014624	0.011074	0.062564
1980	0.021909	0.014624	0.011074	0.062564
2010	0.021909	0.014624	0.011074	0.062564
2040	0.021909	0.014624	0.011074	0.062564
2070	0.021909	0.014624	0.011074	0.062564
2100	0.021909	0.014624	0.011074	0.062564
2130	0.021909	0.014624	0.011074	0.062564
2160	0.021909	0.014624	0.011074	0.062564
2190	0.021909	0.014624	0.011074	0.062564
2220	0.021909	0.014624	0.011074	0.062564
2250	0.021909	0.014624	0.011074	0.062564
2280	0.021909	0.014624	0.011074	0.062564
2310	0.021909	0.014624	0.011074	0.062564
2340	0.021909	0.014624	0.011074	0.062564
2370	0.021909	0.014624	0.011074	0.062564
2400	0.021909	0.014624	0.011074	0.062564
2430	0.021909	0.014624	0.011074	0.062564
2460	0.021909	0.014624	0.011074	0.062564
2490	0.021909	0.014624	0.011074	0.062564
2520	0.021909	0.014624	0.011074	0.062564
2550	0.021909	0.014624	0.011074	0.062564
2580	0.021909	0.014624	0.011074	0.062564

Table G.1. Model sensitivity analysis data for influent nitrate concentration (continued)

Time (min)	Influent Nitrate Conc. = 198 mg/l (-50%)	Influent Nitrate Conc. = 396 mg/l	Influent Nitrate Conc. = 594 mg/l (+50%)	Biomass Conc. = 6,000 mg/l
2610	0.021909	0.014624	0.011074	0.062564
2640	0.021909	0.014624	0.011074	0.062564
2670	0.021909	0.014624	0.011074	0.062564
2700	0.021909	0.014624	0.011074	0.062564
2730	0.021909	0.014624	0.011074	0.062564
2760	0.021909	0.014624	0.011074	0.062564
2790	0.021909	0.014624	0.011074	0.062564
2820	0.021909	0.014624	0.011074	0.062564
2850	0.021909	0.014624	0.011074	0.062564
2880	0.021909	0.014624	0.011074	0.062564
2910	0.021909	0.014624	0.011074	0.062564
2940	0.021909	0.014624	0.011074	0.062564
2970	0.021909	0.014624	0.011074	0.062564
3000	0.021909	0.014624	0.011074	0.062564

Table G.2. Model sensitivity analysis data for biofilm thickness

Time (min)	Biomass Conc. = 3,000 mg/l (-50%)	Biomass Conc. = 6,000 mg/l	Biomass Conc. = 9,000 mg/l (+50%)	Biomass Conc. = 60,000 mg/l
0	1	1	1	1
30	0.991164	0.982776	0.974618	0.977932
60	0.991757	0.98386	0.976156	0.967961
90	0.991278	0.982847	0.974599	0.935359
120	0.98961	0.979506	0.969608	0.8671
150	0.986458	0.973266	0.960366	0.740645
180	0.981299	0.963144	0.945482	0.547631
210	0.973304	0.947618	0.922875	0.334366
240	0.961118	0.924201	0.889118	0.176793
270	0.943571	0.890409	0.840272	0.093155
300	0.921728	0.848417	0.77966	0.000767
330	0.896523	0.800135	0.710217	0
360	0.868576	0.746821	0.633855	0
390	0.838293	0.689296	0.551845	0
420	0.805929	0.628096	0.465086	0
450	0.771635	0.563583	0.374337	0
480	0.735488	0.49602	0.28049	0
510	0.697509	0.425647	0.18513	0
540	0.657682	0.352766	0.092568	0
570	0.615958	0.277875	0.022796	0
600	0.572249	0.201911	0.011673	0
630	0.525849	0.125022	0.011357	0

Table G.2. Model sensitivity analysis data for biofilm thickness (continued)

Time (min)	Biomass Conc. = 3,000 mg/l (-50%)	Biomass Conc. = 6,000 mg/l	Biomass Conc. = 9,000 mg/l (+50%)	Biomass Conc. = 60,000 mg/l
660	0.476683	0.053946	0.01117	0
690	0.425065	0.016442	0.011058	0
720	0.37127	0.013654	0.01099	0
750	0.315593	0.013954	0.010949	0
780	0.258436	0.0142	0.010924	0
810	0.200463	0.014358	0.010908	0
840	0.142945	0.014457	0.010899	0
870	0.088716	0.01452	0.010893	0
900	0.044881	0.014559	0.01089	0
930	0.023715	0.014584	0.010888	0
960	0.020317	0.014599	0.010886	0
990	0.020524	0.014608	0.010886	0
1020	0.02095	0.014614	0.010885	0
1050	0.021264	0.014618	0.010885	0
1080	0.021471	0.01462	0.010885	0
1110	0.021604	0.014621	0.010884	0
1140	0.021689	0.014622	0.010884	0
1170	0.021742	0.014623	0.010884	0
1200	0.021776	0.014623	0.010884	0
1230	0.021797	0.014623	0.010884	0
1260	0.02181	0.014623	0.010884	0
1290	0.021818	0.014623	0.010884	0

Table G.2. Model sensitivity analysis data for biofilm thickness (continued)

Time (min)	Biomass Conc. = 3,000 mg/l (-50%)	Biomass Conc. = 6,000 mg/l	Biomass Conc. = 9,000 mg/l (+50%)	Biomass Conc. = 60,000 mg/l
1320	0.021824	0.014623	0.010884	0
1350	0.021827	0.014623	0.010884	0
1380	0.021829	0.014623	0.010884	0
1410	0.02183	0.014623	0.010884	0
1440	0.021831	0.014623	0.010884	0
1470	0.021831	0.014623	0.010884	0
1500	0.021832	0.014623	0.010884	0
1530	0.021832	0.014623	0.010884	0
1560	0.021832	0.014623	0.010884	0
1590	0.021832	0.014624	0.010884	0
1620	0.021832	0.014624	0.010884	0
1650	0.021832	0.014624	0.010884	0
1680	0.021832	0.014624	0.010884	0
1710	0.021832	0.014624	0.010884	0
1740	0.021832	0.014624	0.010884	0
1770	0.021832	0.014624	0.010884	0
1800	0.021832	0.014624	0.010884	0
1830	0.021832	0.014624	0.010884	0
1860	0.021832	0.014624	0.010884	0
1890	0.021832	0.014624	0.010884	0
1920	0.021832	0.014624	0.010884	0
1950	0.021832	0.014624	0.010884	0

Table G.2. Model sensitivity analysis data for biofilm thickness (continued)

Time (min)	Biomass Conc. = 3,000 mg/l (-50%)	Biomass Conc. = 6,000 mg/l	Biomass Conc. = 9,000 mg/l (+50%)	Biomass Conc. = 60,000 mg/l
1980	0.021832	0.014624	0.010884	0
2010	0.021832	0.014624	0.010884	0
2040	0.021832	0.014624	0.010884	0
2070	0.021832	0.014624	0.010884	0
2100	0.021832	0.014624	0.010884	0
2130	0.021832	0.014624	0.010884	0
2160	0.021832	0.014624	0.010884	0
2190	0.021832	0.014624	0.010884	0
2220	0.021832	0.014624	0.010884	0
2250	0.021832	0.014624	0.010884	0
2280	0.021832	0.014624	0.010884	0
2310	0.021832	0.014624	0.010884	0
2340	0.021832	0.014624	0.010884	0
2370	0.021832	0.014624	0.010884	0
2400	0.021832	0.014624	0.010884	0
2430	0.021832	0.014624	0.010884	0
2460	0.021832	0.014624	0.010884	0
2490	0.021832	0.014624	0.010884	0
2520	0.021832	0.014624	0.010884	0
2550	0.021832	0.014624	0.010884	0
2580	0.021832	0.014624	0.010884	0
2610	0.021832	0.014624	0.010884	0

Table G.2. Model sensitivity analysis data for biofilm thickness (continued)

Time (min)	Biomass Conc. = 3,000 mg/l (-50%)	Biomass Conc. = 6,000 mg/l	Biomass Conc. = 9,000 mg/l (+50%)	Biomass Conc. = 60,000 mg/l
2640	0.021832	0.014624	0.010884	0
2670	0.021832	0.014624	0.010884	0
2700	0.021832	0.014624	0.010884	0
2730	0.021832	0.014624	0.010884	0
2760	0.021832	0.014624	0.010884	0
2790	0.021832	0.014624	0.010884	0
2820	0.021832	0.014624	0.010884	0
2850	0.021832	0.014624	0.010884	0
2880	0.021832	0.014624	0.010884	0
2910	0.021832	0.014624	0.010884	0
2940	0.021832	0.014624	0.010884	0
2970	0.021832	0.014624	0.010884	0
3000	0.021832	0.014624	0.010884	0

Table G.3. Model sensitivity analysis data for growth yield coefficient

Time (min)	Y = 0.35 mg X/mg NO ₃ (-50%)	Y = 0.70 mg X/mg NO ₃	Y = 1.05 mg X/mg NO ₃ (+50%)	Biomass Conc. = 6,000 mg/l
0	1	1	1	1
30	0.983067	0.982776	0.982437	0.98088
60	0.985168	0.98386	0.982039	0.978384
90	0.986194	0.982847	0.977207	0.958925
120	0.986387	0.979506	0.965351	0.915385
150	0.9859	0.973266	0.941318	0.828117
180	0.984824	0.963144	0.895491	0.671652
210	0.983201	0.947618	0.823316	0.42843
240	0.981039	0.924201	0.720329	0.259217
270	0.978316	0.890409	0.579584	0.182891
300	0.974985	0.848417	0.391807	0.151748
330	0.970976	0.800135	0.148254	0.139327
360	0.966201	0.746821	0.001535	0.133625
390	0.960549	0.689296	0.001654	0.129261
420	0.953888	0.628096	0.001735	0.121766
450	0.946066	0.563583	0.001788	0.084954
480	0.936907	0.49602	0.001823	0.068314
510	0.926212	0.425647	0.001845	0.06393
540	0.913759	0.352766	0.00186	0.062885
570	0.899005	0.277875	0.001869	0.062639
600	0.882932	0.201911	0.001875	0.062582
630	0.86707	0.125022	0.001879	0.062568

Table G.3. Model sensitivity analysis data for growth yield coefficient (continued)

Time (min)	Y = 0.35 mg X/mg NO ₃ (-50%)	Y = 0.70 mg X/mg NO ₃	Y = 1.05 mg X/mg NO ₃ (+50%)	Biomass Conc. = 6,000 mg/l
660	0.852254	0.053946	0.001881	0.062565
690	0.83888	0.016442	0.001882	0.062564
720	0.827081	0.013654	0.001883	0.062564
750	0.816838	0.013954	0.001884	0.062564
780	0.80805	0.0142	0.001884	0.062564
810	0.800576	0.014358	0.001885	0.062564
840	0.79426	0.014457	0.001885	0.062564
870	0.788949	0.01452	0.001885	0.062564
900	0.7845	0.014559	0.001885	0.062564
930	0.780784	0.014584	0.001885	0.062564
960	0.777686	0.014599	0.001885	0.062564
990	0.775107	0.014608	0.001885	0.062564
1020	0.772961	0.014614	0.001885	0.062564
1050	0.771177	0.014618	0.001885	0.062564
1080	0.769693	0.01462	0.001885	0.062564
1110	0.768457	0.014621	0.001885	0.062564
1140	0.767427	0.014622	0.001885	0.062564
1170	0.766567	0.014623	0.001885	0.062564
1200	0.765846	0.014623	0.001885	0.062564
1230	0.76524	0.014623	0.001885	0.062564
1260	0.764728	0.014623	0.001885	0.062564
1290	0.764293	0.014623	0.001885	0.062564

Table G.3. Model sensitivity analysis data for growth yield coefficient (continued)

Time (min)	Y = 0.35 mg X/mg NO ₃ (-50%)	Y = 0.70 mg X/mg NO ₃	Y = 1.05 mg X/mg NO ₃ (+50%)	Biomass Conc. = 6,000 mg/l
1320	0.76392	0.014623	0.001885	0.062564
1350	0.763599	0.014623	0.001885	0.062564
1380	0.763318	0.014623	0.001885	0.062564
1410	0.763071	0.014623	0.001885	0.062564
1440	0.76285	0.014623	0.001885	0.062564
1470	0.762649	0.014623	0.001885	0.062564
1500	0.762464	0.014623	0.001885	0.062564
1530	0.762291	0.014623	0.001885	0.062564
1560	0.762127	0.014623	0.001885	0.062564
1590	0.761968	0.014624	0.001885	0.062564
1620	0.761813	0.014624	0.001885	0.062564
1650	0.76166	0.014624	0.001885	0.062564
1680	0.761506	0.014624	0.001885	0.062564
1710	0.76135	0.014624	0.001885	0.062564
1740	0.76119	0.014624	0.001885	0.062564
1770	0.761027	0.014624	0.001885	0.062564
1800	0.760857	0.014624	0.001885	0.062564
1830	0.760681	0.014624	0.001885	0.062564
1860	0.760498	0.014624	0.001885	0.062564
1890	0.760306	0.014624	0.001885	0.062564
1920	0.760104	0.014624	0.001885	0.062564
1950	0.759893	0.014624	0.001885	0.062564

Table G.3. Model sensitivity analysis data for growth yield coefficient (continued)

Time (min)	Y = 0.35 mg X/mg NO ₃ (-50%)	Y = 0.70 mg X/mg NO ₃	Y = 1.05 mg X/mg NO ₃ (+50%)	Biomass Conc. = 6,000 mg/l
1980	0.75967	0.014624	0.001885	0.062564
2010	0.759435	0.014624	0.001885	0.062564
2040	0.759188	0.014624	0.001885	0.062564
2070	0.758926	0.014624	0.001885	0.062564
2100	0.75865	0.014624	0.001885	0.062564
2130	0.758359	0.014624	0.001885	0.062564
2160	0.75805	0.014624	0.001885	0.062564
2190	0.757724	0.014624	0.001885	0.062564
2220	0.75738	0.014624	0.001885	0.062564
2250	0.757015	0.014624	0.001885	0.062564
2280	0.75663	0.014624	0.001885	0.062564
2310	0.756222	0.014624	0.001885	0.062564
2340	0.75579	0.014624	0.001885	0.062564
2370	0.755334	0.014624	0.001885	0.062564
2400	0.754851	0.014624	0.001885	0.062564
2430	0.75434	0.014624	0.001885	0.062564
2460	0.753799	0.014624	0.001885	0.062564
2490	0.753227	0.014624	0.001885	0.062564
2520	0.752622	0.014624	0.001885	0.062564
2550	0.751982	0.014624	0.001885	0.062564
2580	0.751305	0.014624	0.001885	0.062564
2610	0.750588	0.014624	0.001885	0.062564

Table G.3. Model sensitivity analysis data for growth yield coefficient (continued)

Time (min)	Y = 0.35 mg X/mg NO ₃ (-50%)	Y = 0.70 mg X/mg NO ₃	Y = 1.05 mg X/mg NO ₃ (+50%)	Biomass Conc. = 6,000 mg/l
2640	0.74983	0.014624	0.001885	0.062564
2670	0.749028	0.014624	0.001885	0.062564
2700	0.748179	0.014624	0.001885	0.062564
2730	0.747281	0.014624	0.001885	0.062564
2760	0.746331	0.014624	0.001885	0.062564
2790	0.745327	0.014624	0.001885	0.062564
2820	0.744264	0.014624	0.001885	0.062564
2850	0.743061	0.014624	0.001885	0.062564
2880	0.741725	0.014624	0.001885	0.062564
2910	0.740391	0.014624	0.001885	0.062564
2940	0.739131	0.014624	0.001885	0.062564
2970	0.737982	0.014624	0.001885	0.062564
3000	0.73696	0.014624	0.001885	0.062564

Table G.4. Model sensitivity analysis data for maximum specific growth rate

Time (min)	$\mu\text{m} = 0.0112 \text{ mg NO}_3/\text{mg X.min} (-50\%)$	$\mu\text{m} = 0.0225 \text{ mg NO}_3/\text{mg X.min}$	$\mu\text{m} = 0.0337 \text{ mg NO}_3/\text{mg X.min} (+50\%)$	Biomass Conc. = 6,000 mg/l
0	1	1	1	1
30	0.991349	0.982776	0.974154	0.98088
60	0.992452	0.98386	0.973505	0.978384
90	0.993004	0.982847	0.966337	0.958925
120	0.993131	0.979506	0.948939	0.915385
150	0.99291	0.973266	0.914126	0.828117
180	0.99239	0.963144	0.847732	0.671652
210	0.991594	0.947618	0.743269	0.42843
240	0.990525	0.924201	0.594834	0.259217
270	0.989172	0.890409	0.39341	0.182891
300	0.987512	0.848417	0.130645	0.151748
330	0.985508	0.800135	0.001348	0.139327
360	0.983114	0.746821	0.001484	0.133625
390	0.980269	0.689296	0.001489	0.129261
420	0.976903	0.628096	0.001492	0.121766
450	0.972929	0.563583	0.001494	0.084954
480	0.968248	0.49602	0.001495	0.068314
510	0.962741	0.425647	0.001496	0.06393
540	0.956272	0.352766	0.001497	0.062885
570	0.948614	0.277875	0.001497	0.062639
600	0.940198	0.201911	0.001497	0.062582
630	0.931821	0.125022	0.001497	0.062568

Table G.4. Model sensitivity analysis data for maximum specific growth rate (continued)

Time (min)	$\mu_m = 0.0112 \text{ mg NO}_3/\text{mg X.min (-50\%)}$	$\mu_m = 0.0225 \text{ mg NO}_3/\text{mg X.min}$	$\mu_m = 0.0337 \text{ mg NO}_3/\text{mg X.min (+50\%)}$	Biomass Conc. = 6,000 mg/l
660	0.923931	0.053946	0.001498	0.062565
690	0.916756	0.016442	0.001498	0.062564
720	0.910384	0.013654	0.001498	0.062564
750	0.904819	0.013954	0.001498	0.062564
780	0.900018	0.0142	0.001498	0.062564
810	0.895915	0.014358	0.001498	0.062564
840	0.892432	0.014457	0.001498	0.062564
870	0.889493	0.01452	0.001498	0.062564
900	0.887022	0.014559	0.001498	0.062564
930	0.884952	0.014584	0.001498	0.062564
960	0.883222	0.014599	0.001498	0.062564
990	0.881778	0.014608	0.001498	0.062564
1020	0.880575	0.014614	0.001498	0.062564
1050	0.879572	0.014618	0.001498	0.062564
1080	0.878737	0.01462	0.001498	0.062564
1110	0.878041	0.014621	0.001498	0.062564
1140	0.87746	0.014622	0.001498	0.062564
1170	0.876974	0.014623	0.001498	0.062564
1200	0.876567	0.014623	0.001498	0.062564
1230	0.876224	0.014623	0.001498	0.062564
1260	0.875934	0.014623	0.001498	0.062564
1290	0.875688	0.014623	0.001498	0.062564

Table G.4. Model sensitivity analysis data for maximum specific growth rate (continued)

Time (min)	$\mu_m = 0.0112 \text{ mg NO}_3/\text{mg X.min (-50\%)}$	$\mu_m = 0.0225 \text{ mg NO}_3/\text{mg X.min}$	$\mu_m = 0.0337 \text{ mg NO}_3/\text{mg X.min (+50\%)}$	Biomass Conc. = 6,000 mg/l
1320	0.875477	0.014623	0.001498	0.062564
1350	0.875295	0.014623	0.001498	0.062564
1380	0.875136	0.014623	0.001498	0.062564
1410	0.874995	0.014623	0.001498	0.062564
660	0.923931	0.053946	0.001498	0.062565
690	0.916756	0.016442	0.001498	0.062564
1500	0.874651	0.014623	0.001498	0.062564
1530	0.874553	0.014623	0.001498	0.062564
1560	0.87446	0.014623	0.001498	0.062564
1590	0.87437	0.014624	0.001498	0.062564
1620	0.874282	0.014624	0.001498	0.062564
1650	0.874195	0.014624	0.001498	0.062564
1680	0.874108	0.014624	0.001498	0.062564
1710	0.87402	0.014624	0.001498	0.062564
1740	0.87393	0.014624	0.001498	0.062564
1770	0.873838	0.014624	0.001498	0.062564
1800	0.873742	0.014624	0.001498	0.062564
1830	0.873643	0.014624	0.001498	0.062564
1860	0.87354	0.014624	0.001498	0.062564
1890	0.873432	0.014624	0.001498	0.062564
1920	0.873319	0.014624	0.001498	0.062564
1950	0.8732	0.014624	0.001498	0.062564

Table G.4. Model sensitivity analysis data for maximum specific growth rate (continued)

Time (min)	$\mu_m = 0.0112 \text{ mg NO}_3/\text{mg}$ $X \cdot \text{min}^{-1} (-50\%)$	$\mu_m = 0.0225 \text{ mg NO}_3/\text{mg}$ $X \cdot \text{min}^{-1}$	$\mu_m = 0.0337 \text{ mg NO}_3/\text{mg}$ $X \cdot \text{min}^{-1} (+50\%)$	Biomass Conc. = 6,000 mg/l
1980	0.873075	0.014624	0.001498	0.062564
2010	0.872943	0.014624	0.001498	0.062564
2040	0.872805	0.014624	0.001498	0.062564
2070	0.872658	0.014624	0.001498	0.062564
2100	0.872504	0.014624	0.001498	0.062564
2040	0.872805	0.014624	0.001498	0.062564
2070	0.872658	0.014624	0.001498	0.062564
2100	0.872504	0.014624	0.001498	0.062564
2130	0.872341	0.014624	0.001498	0.062564
2160	0.872169	0.014624	0.001498	0.062564
2190	0.871987	0.014624	0.001498	0.062564
2220	0.871795	0.014624	0.001498	0.062564
2250	0.871592	0.014624	0.001498	0.062564
2280	0.871377	0.014624	0.001498	0.062564
2310	0.87115	0.014624	0.001498	0.062564
2340	0.87091	0.014624	0.001498	0.062564
2370	0.870656	0.014624	0.001498	0.062564
2400	0.870388	0.014624	0.001498	0.062564
2430	0.870104	0.014624	0.001498	0.062564
2460	0.869804	0.014624	0.001498	0.062564
2490	0.869487	0.014624	0.001498	0.062564
2520	0.869151	0.014624	0.001498	0.062564

Table G.4. Model sensitivity analysis data for maximum specific growth rate (continued)

Time (min)	$\mu_m = 0.0112 \text{ mg NO}_3/\text{mg}$ $X \cdot \text{min} (-50\%)$	$\mu_m = 0.0225 \text{ mg NO}_3/\text{mg}$ $X \cdot \text{min}$	$\mu_m = 0.0337 \text{ mg NO}_3/\text{mg}$ $X \cdot \text{min} (+50\%)$	Biomass Conc. = 6,000 mg/l
2550	0.868796	0.014624	0.001498	0.062564
2580	0.868421	0.014624	0.001498	0.062564
2610	0.868024	0.014624	0.001498	0.062564
2640	0.867604	0.014624	0.001498	0.062564
2670	0.86716	0.014624	0.001498	0.062564
2700	0.86669	0.014624	0.001498	0.062564
2730	0.866193	0.014624	0.001498	0.062564
2760	0.865667	0.014624	0.001498	0.062564
2790	0.865111	0.014624	0.001498	0.062564
2820	0.864522	0.014624	0.001498	0.062564
2850	0.8639	0.014624	0.001498	0.062564
2880	0.863237	0.014624	0.001498	0.062564
2910	0.862506	0.014624	0.001498	0.062564
2940	0.861757	0.014624	0.001498	0.062564
2970	0.861037	0.014624	0.001498	0.062564
3000	0.860371	0.014624	0.001498	0.062564

Table G.5. Model sensitivity analysis data for Monod half saturation constant

Time (min)	$K_s = 0.95 \text{ mg/l}$ (-50%)	$K_s = 1.90 \text{ mg/l}$	$K_s = 2.85 \text{ mg/l}$ (+50%)	Biomass Conc. = 6,000 mg/l
0	1	1	1	1
30	0.969461	0.982776	0.987398	0.98088
60	0.974581	0.98386	0.987091	0.978384
90	0.976375	0.982847	0.98512	0.958925
120	0.974974	0.979506	0.981131	0.915385
150	0.970053	0.973266	0.974477	0.828117
180	0.96079	0.963144	0.964126	0.671652
210	0.945764	0.947618	0.948539	0.42843
240	0.922512	0.924201	0.925259	0.259217
270	0.88864	0.890409	0.891741	0.182891
300	0.846385	0.848417	0.850116	0.151748
330	0.797664	0.800135	0.802315	0.139327
360	0.74372	0.746821	0.749617	0.133625
390	0.68535	0.689296	0.692874	0.129261
420	0.623051	0.628096	0.632657	0.121766
450	0.557129	0.563583	0.569374	0.084954
480	0.487775	0.49602	0.503345	0.068314
510	0.415138	0.425647	0.434887	0.06393
540	0.339403	0.352766	0.364397	0.062885
570	0.260027	0.277875	0.292491	0.062639
600	0.175779	0.201911	0.220278	0.062582
630	0.08932	0.125022	0.149998	0.062568

Table G.5. Model sensitivity analysis data for Monod half saturation constant (continued)

Time (min)	$K_s = 0.95 \text{ mg/l}$ (-50%)	$K_s = 1.90 \text{ mg/l}$	$K_s = 2.85 \text{ mg/l}$ (+50%)	Biomass Conc. = 6,000 mg/l
660	0.014588	0.053946	0.08563	0.062565
690	0.004576	0.016442	0.039204	0.062564
720	0.004802	0.013654	0.024523	0.062564
750	0.004957	0.013954	0.023292	0.062564
780	0.005057	0.0142	0.023535	0.062564
810	0.005122	0.014358	0.023779	0.062564
840	0.005162	0.014457	0.023942	0.062564
870	0.005188	0.01452	0.024044	0.062564
900	0.005204	0.014559	0.024108	0.062564
930	0.005214	0.014584	0.024147	0.062564
960	0.005221	0.014599	0.024171	0.062564
990	0.005225	0.014608	0.024187	0.062564
1020	0.005227	0.014614	0.024196	0.062564
1050	0.005229	0.014618	0.024202	0.062564
1080	0.00523	0.01462	0.024205	0.062564
1110	0.00523	0.014621	0.024207	0.062564
1140	0.005231	0.014622	0.024209	0.062564
1170	0.005231	0.014623	0.024209	0.062564
1200	0.005231	0.014623	0.02421	0.062564
1230	0.005231	0.014623	0.02421	0.062564
1260	0.005231	0.014623	0.02421	0.062564
1290	0.005231	0.014623	0.024211	0.062564

Table G.5. Model sensitivity analysis data for Monod half saturation constant (continued)

Time (min)	$K_s = 0.95 \text{ mg/l}$ (-50%)	$K_s = 1.90 \text{ mg/l}$	$K_s = 2.85 \text{ mg/l}$ (+50%)	Biomass Conc. = 6,000 mg/l
1320	0.005231	0.014623	0.024211	0.062564
1350	0.005231	0.014623	0.024211	0.062564
1380	0.005231	0.014623	0.024211	0.062564
1410	0.005231	0.014623	0.024211	0.062564
1440	0.005231	0.014623	0.024211	0.062564
1470	0.005231	0.014623	0.024211	0.062564
1500	0.005231	0.014623	0.024211	0.062564
1530	0.005231	0.014623	0.024211	0.062564
1560	0.005231	0.014623	0.024211	0.062564
1590	0.005231	0.014624	0.024211	0.062564
1620	0.005231	0.014624	0.024211	0.062564
1650	0.005231	0.014624	0.024211	0.062564
1680	0.005231	0.014624	0.024211	0.062564
1710	0.005231	0.014624	0.024211	0.062564
1740	0.005231	0.014624	0.024211	0.062564
1770	0.005231	0.014624	0.024211	0.062564
1800	0.005231	0.014624	0.024211	0.062564
1830	0.005231	0.014624	0.024211	0.062564
1860	0.005231	0.014624	0.024211	0.062564
1890	0.005231	0.014624	0.024211	0.062564
1920	0.005231	0.014624	0.024211	0.062564
1950	0.005231	0.014624	0.024211	0.062564

Table G.5. Model sensitivity analysis data for Monod half saturation constant (continued)

Time (min)	$K_s = 0.95 \text{ mg/l}$ (-50%)	$K_s = 1.90 \text{ mg/l}$	$K_s = 2.85 \text{ mg/l}$ (+50%)	Biomass Conc. = 6,000 mg/l
1980	0.005231	0.014624	0.024211	0.062564
2010	0.005231	0.014624	0.024211	0.062564
2040	0.005231	0.014624	0.024211	0.062564
2070	0.005231	0.014624	0.024211	0.062564
2100	0.005231	0.014624	0.024211	0.062564
2130	0.005231	0.014624	0.024211	0.062564
2160	0.005231	0.014624	0.024211	0.062564
2190	0.005231	0.014624	0.024211	0.062564
2220	0.005231	0.014624	0.024211	0.062564
2250	0.005231	0.014624	0.024211	0.062564
2280	0.005231	0.014624	0.024211	0.062564
2310	0.005231	0.014624	0.024211	0.062564
2340	0.005231	0.014624	0.024211	0.062564
2370	0.005231	0.014624	0.024211	0.062564
2400	0.005231	0.014624	0.024211	0.062564
2430	0.005231	0.014624	0.024211	0.062564
2460	0.005231	0.014624	0.024211	0.062564
2490	0.005231	0.014624	0.024211	0.062564
2520	0.005231	0.014624	0.024211	0.062564
2550	0.005231	0.014624	0.024211	0.062564
2580	0.005231	0.014624	0.024211	0.062564
2610	0.005231	0.014624	0.024211	0.062564

Table G.5. Model sensitivity analysis data for Monod half saturation constant (continued)

Time (min)	$K_s = 0.95 \text{ mg/l}$ (-50%)	$K_s = 1.90 \text{ mg/l}$	$K_s = 2.85 \text{ mg/l}$ (+50%)	Biomass Conc. = 6,000 mg/l
2640	0.005231	0.014624	0.024211	0.062564
2670	0.005231	0.014624	0.024211	0.062564
2700	0.005231	0.014624	0.024211	0.062564
2730	0.005231	0.014624	0.024211	0.062564
2760	0.005231	0.014624	0.024211	0.062564
2790	0.005231	0.014624	0.024211	0.062564
2820	0.005231	0.014624	0.024211	0.062564
2850	0.005231	0.014624	0.024211	0.062564
2880	0.005231	0.014624	0.024211	0.062564
2910	0.005231	0.014624	0.024211	0.062564
2940	0.005231	0.014624	0.024211	0.062564
2970	0.005231	0.014624	0.024211	0.062564
3000	0.005231	0.014624	0.024211	0.062564